



**Smaller, Smarter, Faster: The
Development and Application of
Microfluidic Devices to the Determination
of Phosphorus in Natural Waters**

By

Michaela Bowden

B.Sc. in Chemistry with German

*Thesis Submitted in Accordance with the Requirements for the
Degree of*

Doctor of Philosophy

To

Dublin City University

Supervisor: Dermot Diamond

Submission Date: February 2003

Declaration

I hereby certify that this material, which I now submit for assessment on the programme of study leading to the award of Doctor of Philosophy is entirely my own work and has not been taken from the work of others save and to the extent that such work has been cited and acknowledged within the text of my work.

Signature: Michaela Bowden
Michaela Bowden

ID No.: 95092579

Date: 22nd MAY 2003

Acknowledgements

I would like to take this opportunity to thank my family and friends who have stood by me and demonstrated incredible patience, understanding and cooperation through the good and difficult stages of my PhD. In particular, I must single out my parents for praise. They have instilled in me a self-belief that has lead me down this path in life. Throughout my time at the NCSR I have met and relied upon many people for many different reasons. Dermot has always been a source of encouragement and support. My lab group, both past (X150 / X152) and present members (SG03) have been, without exception, a pleasure to work alongside and a privilege to know. I have been fortunate enough to collaborate with two research groups in Denmark, namely the Mikroelektronik Centret (MIC) and Danfoss A/S. where I was warmly welcomed, encouraged and supported in my research endeavours.

I decided not to write a long-list of friends and colleagues whose input and support I have benefited from, for fear of omitting one vital name. Instead I believe that everyone I know and have known in the past three and a half years has, in some way, had an impact on my time at DCU and I thank you all.

Table of Contents

<i>Declaration</i>	ii
<i>Acknowledgements</i>	iii
<i>Table of Contents</i>	iv
<i>List of Abbreviations</i>	ix
<i>Abstract</i>	xii
<i>Introduction</i>	xiii
1 LITERATURE	1
1.1 Phosphates	2
1.1.1 Sampling and Storage of Orthophosphate-containing samples	4
1.2 Determination of Phosphorus	5
1.2.1 Colorimetric Detection	7
1.2.2 Flow Injection Analysis	8
1.3 Micro Systems Technology (MST)	10
1.4 Microfluidics	14
1.4.1 Flow	14
1.4.2 Pumping Mechanism	16
1.4.3 Silicon Microfabrication Techniques	19
1.4.4 Applications in Silicon and Glass Microsystems	21
1.4.5 Polymer Microtechnology	25
1.4.6 Polymer Materials	25
1.4.7 Polymer Microfabrication Techniques	29
1.4.8 Polymer Microsystem Applications	36
1.5 References	38
2 THE VANADOMOLYBDOPHOSPHORIC ACID (OR YELLOW) METHOD	48
2.1 Speciation of Phosphorus	50
2.2 Reagent / Stock Solution Preparation	52

2.3	Apparatus	55
2.4	Choice of Light Source	56
2.5	Calibration	58
2.6	Reaction Kinetics	62
2.6.1	Preliminary Experiment at Room Temperature	62
2.6.2	Experimental Set-up	63
2.6.3	Influence of Temperature on the Yellow Method Reaction	64
2.7	pH	68
2.7.1	Apparatus	69
2.7.2	pH of the Yellow Method Complex Solution	70
2.7.3	Modification of the pH of the Yellow Method Complex Solution	71
2.8	Fe(II) Interference	73
2.8.1	Sample Preparation	74
2.8.2	Experimental	74
2.9	Repeatability	77
2.10	Limits of Detection (LOD)	79
2.11	Lifetime Studies	81
2.12	Conclusion	83
2.13	References	84
3	APPLICATION OF THE YELLOW METHOD IN A MICROFLUIDIC MANIFOLD	86
3.1	Instrumental Set Up	88
3.1.1	Microfluidic Chip Holder	91
3.1.2	Pumping Unit	93
3.1.3	Micro-dispensing Syringes	94
3.1.4	Valve Fluid Control	94
3.1.5	Reservoirs	95
3.1.6	Tubing and Interconnects	95

3.1.7	Waste Collection and Disposai	96
3.2	Optical Detection	97
3.2.1	UV-LED	97
3.2.2	Portable Spectrometer	98
3.2.3	Optical Fibres	99
3.3	Flow Regime	100
3.4	Calibration Study	102
3.4.1	Microfluidic Chip Layout	102
3.4.2	Preliminary Analysis with Malachite Green Dye	104
3.4.3	Yellow Method Analysis	106
3.5	Kinetic Study in the Microfluidic Manifold	111
3.5.1	Microfluidic Manifold	112
3.5.2	Kinetic Measurements in the Microfluidic Manifold	114
3.6	Repeatability	117
3.7	Reproducibility	119
3.7.1	Reproducibility of a Standard 4 mgL ⁻¹ PO ₄ ³⁻ - P sample	119
3.7.2	Long-term Reproducibility of the Yellow Method Calibration	121
3.8	Signal-to-Noise Ratio	123
3.9	Limits of Detection (LOD)	125
3.10	Comparison of the Yellow Method in the Microfluidic and Conventional System	127
3.10.1	Calibration Comparison	127
3.10.2	Molar Extinction Coefficient of the Yellow Phosphate Complex	130
3.11	Conclusion	133
3.12	References	133
4	REAL APPLICATIONS OF THE YELLOW METHOD IN MICROFLUIDIC SYSTEMS	135

4.1	River Samples	138
4.2	Sampling and Storage	138
4.3	Locations	139
4.3.1	Broadmeadow River	140
4.3.2	Santry River	141
4.3.3	River Ward	141
4.4	Validation of the Microfluidic System for Real Sample Analysis	141
4.5	Sample Analysis	144
4.5.1	Study of the Broadmeadow River	144
4.5.2	Study of Clonshaugh Bridge on the Santry River	148
4.5.3	Real Sample Analysis of the River Ward	151
4.6	Application of the Yellow Method in an Industrial Prototype Integrated Microfluidic System (MicroChem Project)	153
4.7	Industrial Prototype	154
4.8	IP Chip Layout	157
4.9	Experimental Procedure	159
4.10	Preliminary analytical measurements	161
4.11	Calibration	165
4.12	Unknown analysis	167
4.13	Conclusion	169
4.14	References	170
5	THE DESIGN, FABRICATION AND APPLICATION OF A POLYMER MICROFLUIDIC MANIFOLD	172
5.1	Microfluidic Chip and Holder Design	174
5.2	CO₂ Laser Technique	176

5.2.1	Laser Ablation	177
5.2.2	Fabrication of Micron-sized Structures	180
5.2.3	Order of Ablation	183
5.3	Scanning Electron Microscope (SEM) Analysis	186
5.4	Chip Integration	190
5.5	Bonding	192
5.6	Leak-free Microfluidic Interconnects	195
5.7	Experimental	196
5.7.1	Microfluidic System	196
5.7.2	Optical Detection	198
5.8	Analytical Results	201
5.8.1	Validation of Polymer Microfluidic Chip	201
5.8.2	Real Sample Analysis	206
5.9	Conclusion	212
5.10	References	212
6	CURRENT STATUS AND FUTURE WORK	214
6.1	Polymer Microfluidic Manifold Fabrication	215
6.1.1	Hot Embossing	215
6.1.2	Choice of Polymer	219
6.2	Pumping	223
6.2.1	Preliminary Flow-rate Measurements	224
6.2.2	Sampling	227
6.2.3	Remote Sensing	228
6.2.4	Packaging	230
6.3	Conclusion	232
6.4	References	232

List of Abbreviations

μ CP	Microcontact Printing
μ TAS	Miniaturised Total Analysis Systems
μ TM	Microtransfer Molding
AM	Atomic Mass
ASE	Advanced Silicon Etching
BOD	Biochemical Oxygen Demand
BR	Butadiene Rubber
CAD	Computer-aided Design
CE	Capillary Electrophoresis
COC	Cycloolefin Copolymer
CVD:	Chemical Vapour Deposition
DIP	Dissolved Inorganic Phosphorus
DNA	Deoxyribonucleic Acid
DO	Dissolved Oxygen
DOP	Dissolved Organic Phosphorus
DRIE	Dry Reactive Ion Etching
DRP	Dissolved Reactive Phosphorus
EOF	Electroosmotic Flow
EPA	Environmental Protection Agency
EU	European Union
FIA	Flow Injection Analysis
FL	Focal Length
GC	Gas Chromatography
GSM	Global System for Mobile Communication
HPLC	High Performance Liquid Chromatography
IC	Ion Chromatography
IP	Industrial Prototype
IR	Infrared
ISE	Ion Selective Electrode
LED	Light Emitting Diode

LIGA	Lithographie, Galvanik und Abformung
LOD	Limit of Detection
LPCVD	Low Pressure Chemical Vapour Deposition
MEMS	Micro Electro Mechanical Systems
MIMIC	Micromolding in Capillaries
MST	Microsystems Technology
MW	Molecular Weight
PDMS	Polymethyl Disiloxane
PE	Polyethylene
PEEK	Polyether Etherketone
PES	Polyether Sulfone
PMMA	Polymethyl Methacrylate
PP	Polypropylene
PS	Polystyrene
PTFE	Polytetrafluoroethylene
PU	Polyurethane
PVC	Polyvinyl Chloride
PVDF	Polyvinylidene Fluoride
RE	Relative Error
REM	Replica Molding
RF	Radio Frequency
RNA	Ribonucleic Acid
RSD	Relative Standard Deviation
SAE	Spark Assisted Etching
SAMIM	Solvent-Assisted Micromolding
SBR	Styrene Butadiene Rubber
SEM	Scanning Electron Microscopy
SSR	Sum of the Square Residual
TAS	Total (Chemical) Analysis Systems
TCD	Thermal Conductivity Detector
TDP	Total Dissolved Phosphorus
T _g	Glass Transition Temperature
Topas®	Thermoplastic Olefin Polymer of Amorphous Structure
TP	Total Phosphorus

TPE
TPO
TPU
UV-LED

Thermoplastic Polyethylene
Thermoplastic Polyolefins
Thermoplastic Polyurethane
Ultra-Violet Light Emitting Diode

Abstract

The development of a miniaturised microfluidic instrument for monitoring phosphorus in natural waters from the optimisation of the chemistry through to the fabrication of the microfluidic manifold in polymeric materials is presented. The research initially was concerned with optimising the yellow colorimetric method for a phosphate determination and its transferral to a Si-etched microfluidic chip configuration. This simple method employs one reagent mixed in a 1:1 ratio with an orthophosphate-containing sample to produce a yellow colour absorbing strongly below 400nm.

A stopped flow approach is used which, together with the very rapid kinetics and simple reagent stream, enables a very uncomplicated microfluidic manifold design to be adopted. The working wavelength was 380nm, which coincided with the peak output of a recently developed UV-LED narrow bandwidth light source. The limit of detection for the yellow method is $0.2 \text{ mgL}^{-1} \text{ PO}_4^{3-} - \text{P}$ with a linear range from 0 - $50 \text{ mgL}^{-1} \text{ PO}_4^{3-} - \text{P}$ possible. The reaction time at room temperature is less than 3 minutes, which means up to 20 samples / hour can be analysed.

The next stage in the research involved applying the results obtained in the Si-etched microfluidic chips to the design and fabrication of a microfluidic manifold in polymer materials. Chips were made by a combination of microfabrication techniques including a CO_2 laser ablation, hot embossing and micromilling. Transferring the technology to a polymeric platform required a whole new set of experiments to be undertaken. The key issues addressed were multiple layer alignment, optical detection, bonding of polymeric materials; the provision of leak-free fluidic interconnects to external tubing and reproducible analytical measurements.

Introduction

Phosphorus is essential for plant and animal species in natural waters. It is typically present in the form of phosphate, of which the inorganic orthophosphate form is the most stable state. Phosphate concentrations are predominantly influenced by human interference and this type of over-enrichment is commonly referred to as cultural Eutrophication.

Spectrophotometric methods based on colorimetric detection have been widely applied to the determination of orthophosphate. There are two basic procedural steps to consider when water samples are being analysed for phosphorus, the conversion of the target phosphorus to dissolved orthophosphate and the colorimetric detection of the dissolved orthophosphate fraction. The vast majority of methods employ the molybdenum blue method, which is ideal for visual titrations, because of the deep blue coloured complex formed. It is also suitable for colorimetric measurements based on conventional tungsten filament sources because the molybdenum blue complex absorbs in the 650 - 700 nm region of the visible spectrum.

There are many examples of Flow Injection Analysis (FIA) for the determination of phosphates. These typically involve the molybdenum blue method, and with these macro-bench systems, the approach works well. However the transfer of this method to a miniaturised, field-deployable system is difficult for several reasons. Firstly ascorbic acid has limited stability, and therefore limits the overall lifetime of the reagent cocktail used and secondly the generation of the blue colour is accompanied by the formation of a fine precipitate, which would rapidly block the small dimensions of the microfluidic channels. The blue complex formed can also be problematic due to its tendency to coat the inner walls of the vessel through which it is pumped. Clearly therefore, the blue method cannot meet the key target requirement of one-year autonomous functioning for future miniaturised environmental monitoring instruments.

An alternative approach known as the 'yellow' or vanadomolybdophosphoric acid method has become a more viable option. This colorimetric technique involves the

formation of a yellow coloured heteropoly acid, vanadomolybdophosphoric acid, whereby ammonium molybdate, $(\text{NH}_4)_6\text{Mo}_7\text{O}_{24}\cdot 7\text{H}_2\text{O}$ is reacted with ammonium metavanadate, NH_4VO_3 under acidic conditions. The combined reagent and sample containing orthophosphate react to form the $(\text{NH}_4)_3\text{PO}_4\text{NH}_4\text{VO}_3\cdot 16\text{MoO}_3$ complex, resulting in a distinct yellow colour arising from strong absorbance below 400 nm. The reagent is very stable and no precipitation occurs during the reaction or in storage. Batches of this reagent have been used continuously in our laboratory for over one year with no significant loss in performance.

Laminar flow dominates in microfluidic channels, and while reagent / sample mixing can be achieved through incorporation of customised mixing chambers, a stopped-flow approach has been adopted to take advantage of the rapid diffusion occurring in narrow channels and to keep the microfluidic manifold as simple as possible. Through miniaturisation, flow-rates can be vastly reduced compared to conventional FIA systems. For example, at a flow rate of $1 \mu\text{L} / \text{min}$ the reagent consumption is less than 500 mL / year for continuous operation.

The goal of the research was to produce devices capable of functioning autonomously in the field for over one year that generate minimum waste and require minimal maintenance (12 months maintenance-free) due to low-powered operation and excellent reagent stability. If these microsystems are configured to work in a "sleep mode" (1 measurement / day), reagent consumption ($10 \mu\text{L} / \text{measurement}$) will be dramatically reduced (less 10 mL / year). The project's long-term goal was to develop a remote, autonomous device, which could be positioned on any water body (river, lake, wastewater facility, agricultural site etc.) and would be automated to carry out periodic analyses. The analytical data would then be retrieved and transmitted to a web-based program via GSM-communications. The distribution and use of wireless sensing devices would allow rapid detection and location of pollution, with consequent miniaturisation of associated damage to the environment and identification of offenders. The ability to dynamically track trends would facilitate both early warning of emerging problems on a longer scale and the effect of remedial strategies.

In order to achieve this the prototype system must be small, environmentally compatible, robust, inexpensive to own and operate, and capable of providing

reliable analytical information over extended periods of autonomous operation. At present a number of the key issues in realising the project goal have been achieved and are presented in this thesis including the optimisation of the yellow method chemistry, the implementation of the yellow method in an integrated microfluidic manifold, the analysis of real samples and the design and fabrication of a new polymeric microfluidic manifold with two microfabrication techniques, CO₂ laser ablation and hot embossing.

1 LITERATURE

1.1 Phosphates

Phosphorus is one of the most basic nutrients required by all organisms to exist. Naturally occurring phosphorus is rare, can only be found in certain rocks, soils and organic material, and amounts to about only 0.12 % in the lithosphere. It readily forms bonds with organic matter and soil particles, which accounts for why there are low concentrations naturally occurring. However, it is its extensive inclusion in fertilisers, and other chemicals from human activity, which cause the problems.

Small amounts of phosphorus are found in many sources and are a necessity for several different processes. In the human body it is vital for muscle contraction and bone formation, which involves the building of a tricalcium phosphate complex. In agriculture, common fertilisers contain calcium dihydrogen phosphate, $\text{Ca}(\text{H}_2\text{PO}_4)_2$.

Phosphorus is essential for aquatic life playing a pivotal role in growth development in natural waters [1]. Phosphorus exists in a particulate or dissolved form. The dissolved matter is of both the organic and inorganic variety [2]. Phosphorus (P), in water and / or wastewater, is typically present in the form of a phosphate (PO_4^{3-}), which can be divided into three major categories, the orthophosphates, the condensed phosphates (pyro-, meta-, poly-), and the organic phosphorus compounds (see Table 1-1). When natural conditions apply to any water body, phosphate concentrations, calculated as hydrogen phosphate ions, are almost always less than 0.1 mgL^{-1} . However, most water bodies are affected by human interference. Wherever phosphorus is the growth-limiting nutrient in the water body, it is usually a combination of raw or untreated wastewater, agricultural runoff and / or industrial waste, which stimulate the growth of microorganisms in excess quantities, which ultimately leads to the process known as Eutrophication. The importance of measuring phosphorus levels in aquatic bodies relates to the role phosphorus has in Eutrophication, and photosynthetic and decomposition processes.

Table 1-1 Phosphorus forms typically found in water / wastewater

Cause	Compound	Formula
Fertiliser	Superphosphate	$\text{Ca}(\text{H}_2\text{PO}_4)_2$
Scale Preventative	Hydroxyapatite	$3\text{Ca}_8(\text{PO}_4)_2 \cdot \text{Ca}(\text{OH})_2$
Hard Water Treatment	Hexametaphosphate	$\text{Na}_6\text{P}_6\text{O}_{18} / (\text{NaPO}_3)_6$
Commercial Plasticiser	Triphenyl Phosphate	$(\text{C}_6\text{H}_5)_3\text{PO}_4$
Additive in Petrol	Tricresyl Phosphate	$(\text{Cresyl})_3\text{PO}_4$
Pesticides	Parathion, Malathion, Ethion, Thimet	Organophosphates

Eutrophication is a process rapidly accelerated by human activity causing excessive growth of nutrients in lakes, rivers or other water bodies. Shallow lakes or rivers with very slow flow are the most susceptible to Eutrophication. This growth depends upon the amount of phosphorus and nitrate available. The outcome is that huge quantities of algae and aquatic plants grow, then die and are subsequently decomposed by bacteria, which in turn exhausts the dissolved oxygen supply in the water, causing large scale fish kills. Scum lying on the water surface and the stench of decomposing algae, i.e. hydrogen sulphide gas, indicate that the body of water is in an advanced stage of Eutrophication.

Phosphate concentrations are influenced predominantly by human interference. Wastewater effluent, in the form of body waste and food residues, contributes strongly to levels of phosphate present in surface waters. Detergents, fertilisers, animal waste, industrial discharge and potable water treatment also extensively promote an increase in phosphate concentration [3].

If an excess of orthophosphate is present, rapid algal growth leads to so-called "blooms", which release toxic fumes into the environment [4]. When algae die bacteria systematically decompose them, which sequentially exhausts all oxygen reserves. With deficient oxygen supply life cannot be sustained and large fish kills transpire. This overkill enrichment of water with nutrients can be exclusively attributed to human intrusion, and is accordingly referred to as cultural Eutrophication, which has been the case in recent years in Ireland where water pollution has become a major cause for concern [5-9].

1.1.1 Sampling and Storage of Orthophosphate-containing samples

Sampling Preparation

The simplest form of sampling is filtration, whereby the water sample containing the target analyte is filtered through a membrane filter of specific pore size. The choice of filter is based on the purity of the sample required, the size of the particulate matter and the dimensions of the tubing / channels the sample is introduced into. Filtration through a 0.45 μm pore diameter membrane filter separates dissolved from suspended forms of phosphorus. This is a convenient and reproducible method of making a gross distinction between dissolved and suspended particulate. Membrane is preferred to depth filtration because it consistently separates particulate matter based on size. Pre-filtration through a glass fibre filter can be undertaken, although it is not strictly necessary.

Types of storage

When water samples are stored numerous processes can occur that greatly affect the composition of the phosphorus fraction therein. Ideally samples should be analysed directly after collection to minimise changes in phosphorus concentrations over time. However there are five or six key factors that determine how effective a storage technique is. These include filtration, sample composition, material composition and pre-treatment of container, light sensitivity, storage temperature and duration of storage.

Whether a sample is filtered or not is significant in terms of how long a sample can then be stored before phosphorus concentration becomes unstable or is affected by biological activity in the sample. When measuring reactive phosphorus water samples need to be filtered through 0.45 μm filter paper immediately upon collection to avoid exchange of particles in the storage container. Filtration is carried out to remove bacteria, plankton and suspended solid, which can affect nutrient concentrations, but colloidal particulate matter can still affect the nutrient balance. It has been reported in the literature that there is a significant loss of

phosphorus concentration, if samples are stored unfiltered. Filtration eliminates particles that can absorb phosphorus, and bacteria that utilise phosphorus to leach onto glass surfaces [10-11].

The type of sample to be analysed can have many different chemical and biological compositions. There are several main types of sample including seawater, freshwater, groundwater, estuarine, potable and wastewater. The acidity (or pH) of the sample influences the type of phosphorus complexes that can form. Phosphorus has a habit of adsorbing onto container walls due to bacterial processes, so the choice of storage vessel is critical; more specifically the material from which the vessel is composed of and any pre-treatment the material is subjected to. Some typical materials used are glass, polyethylene, polypropylene and polycarbonate and the most common pre-treatments involve washing the storage vessel with either deionised water or dilute acid followed by rinsing in deionised water. All containers absorb a quantity of phosphorus. Plastic containers rinsed in dilute acid have shown less adsorption [11]. Samples stored in the dark, at either room temperature or under refrigeration, have limited algal growth. Photosynthesis, which also decreases the phosphorus concentration in a sample, is impeded in the dark [3].

1.2 Determination of Phosphorus

There are a variety of analytical methods for the determination of phosphate, some of which are shown in Table 1-2.

Table 1-2 Popular Techniques employed in Phosphorus Analysis

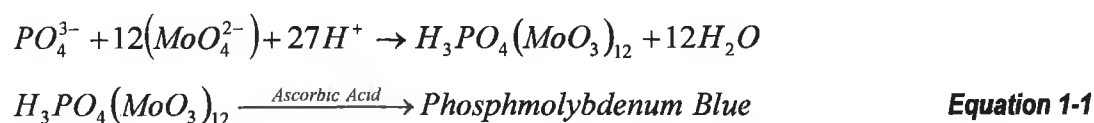
Technique	Method
Spectrophotometric	Atomic Emission, Colorimetry, Fluorescence
Electrochemical	Potentiometry, Enzyme Electrode, Voltammetry
Separation	Ion Chromatography, Capillary Electrophoresis, HPLC

Spectrophotometric methods based on colorimetric chemistry are possibly the easiest and most frequently used analytical methods in a chemical laboratory.

There are two general procedural steps when considering the spectrophotometric analysis of phosphorus:

1. The conversion of the target phosphorus form to dissolved orthophosphate.
2. The colorimetric detection of dissolved orthophosphate [12].

There are numerous colorimetric methods reported in the literature, including the heteropoly blue, stannous chloride, ascorbic acid, malachite green and the vanadomolybdophosphoric acid method. The most common of these is based on the formation of 12-molybdophosphoric acid from phosphate and molybdate in acid solution and subsequent reduction to a heteropoly blue compound, often referred to as molybdenum blue as shown in Equation 1-5 [13-14].



The reduction product above absorbs in the wavelength region of 650-700nm and is known as "molybdenum blue". Also there is a "heteropoly blue" product absorbing in the 820-830nm region, both of which were coined by Boltz and Mellon [15]. This method is recommended for phosphate analysis in water samples because it is selective, detecting phosphate in the low concentration region of 0.01-10 mgL⁻¹, with a minimum detectable concentration of 0.01 mgL⁻¹ phosphorus [16]. There are at least five other colorimetric methods of determination involving, 2-amino-4-chlorobenzenethiol, chloranilate and carminic acid.

Many spectrophotometric techniques are merely variations on the blue method theme, utilising a diverse group of reducing reagents, ranging from ascorbic acid and potassium antimonyl tartrate [17], to stannous chloride and glycerol [18], all producing the same intense blue colour detectable at either 650nm or 800nm. Because all these reagents are employed in the reduction step of the colorimetric reaction they are not stable in solution for long periods of time.

Another consideration is the implementation of a completely alternative technique. A wide variety of techniques and methods are described in the literature, but several stand out as being of particular relevance to this study. Determinations

based on Flow Injection Analysis (FIA) are of prime importance considering the integrated microfluidic device design. A thorough account of FI techniques and applicability to micro devices is given in Section 1.2.2.

Other techniques of secondary interest are chromatographic and electrochemical approaches. By implementing a chromatographic method orthophosphate can be separated according to its relative affinity for a mobile and / or stationary phase. Ion Chromatography (IC) is most commonly used, but can be slow and relatively insensitive. Often trace enrichment techniques are required for the detection of low levels of phosphate [19]. Capillary Electrophoresis (CE) offers quick separations at the expense of sensitive measurement; however in recent years high ionic strength matrices have proved successful in lowering the limit of detection of CE systems by introducing on-capillary pre-concentration [20].

Electrochemically, a number of potentiometric methods have been cited in the literature. These involve direct measurements using phosphate electrodes and indirect via lead, calcium, or cadmium ion selective electrodes (ISE's), although lack of sensitivity in the former and poor selectivity in the latter greatly undermine the techniques [21]. Amperometric techniques involve either measuring orthophosphate as phosphomolybdate or using enzyme electrodes, whereby orthophosphate generates H_2O_2 , which is then, measured amperometrically, resulting in both high specificity and good sensitivity [22].

There are several other techniques worth mentioning that are currently under-utilised or being developed including enzymatic and X-ray fluorescence ion pair and radioactivation analysis [23].

1.2.1 Colorimetric Detection

Vanadomolybdophosphoric Acid (Yellow) Method

An alternative method, in preference over the molybdenum blue method, is the standard yellow method (vanadomolybdophosphoric acid method). This colorimetric technique involves the formation of a heteropoly complex, the yellow

vanadomolybdophosphoric acid, whereby ammonium molybdate, $(\text{NH}_4)_6\text{Mo}_7\text{O}_{24}\cdot 7\text{H}_2\text{O}$ is reacted with ammonium metavanadate NH_4VO_3 , under acidic conditions [24]. The reagent formed and a sample containing orthophosphate react to form the above-mentioned heteropoly acid, $(\text{NH}_4)_3\text{PO}_4\text{NH}_4\text{VO}_3\cdot 16\text{MoO}_3$, resulting in a distinct yellow colour. The orthophosphate concentration is directly proportional to the colour intensity of the yellow complex created.

The Beer-Lambert law is an empirical expression, which relates to the variation in the intensity of light as it passes through an absorbing medium, and is written as:

$$\log \frac{I}{I_0} = A = \epsilon c l \quad \text{Equation 1-2}$$

where I_0 is the incident intensity, I is the intensity after passage through a sample of length l [cm], and c [mol L⁻¹] is the molar concentration of an absorbing sample. The molar absorption coefficient is denoted by the symbol, ϵ [cm⁻¹ mol⁻¹ L] and refers to the sample at the frequency of the incident light. The absorbance of a sample is represented by the dimensionless quantity, A .

1.2.2 Flow Injection Analysis

Flow injection analysis (FIA) is a technique involving the injection of a liquid sample into a moving non-segmented flowing carrier stream [25]. The sample zone or plug, as it passes through a coil, disperses on-route to a detector. Ruzicka developed the first FIA system and described it in its simplest form to consist of four major components, a pump, an injection port, a mixing coil and a flow-through detector. The pumping unit drives the flow through the system. The small, well-defined aliquot of a liquid sample is injected into a carrier stream at an injection port. The sample plug then disperses in the carrier stream as it passes through a mixing coil, of specific dimensions, depending on the speed of the reaction of the sample in the carrier stream. As the reaction reaches completion the dispersed sample plug arrives at the flow-through detector, where it is analysed. The data from the detector is usually in the form of a sharp peak where the height is directly proportional to the concentration of the analyte.

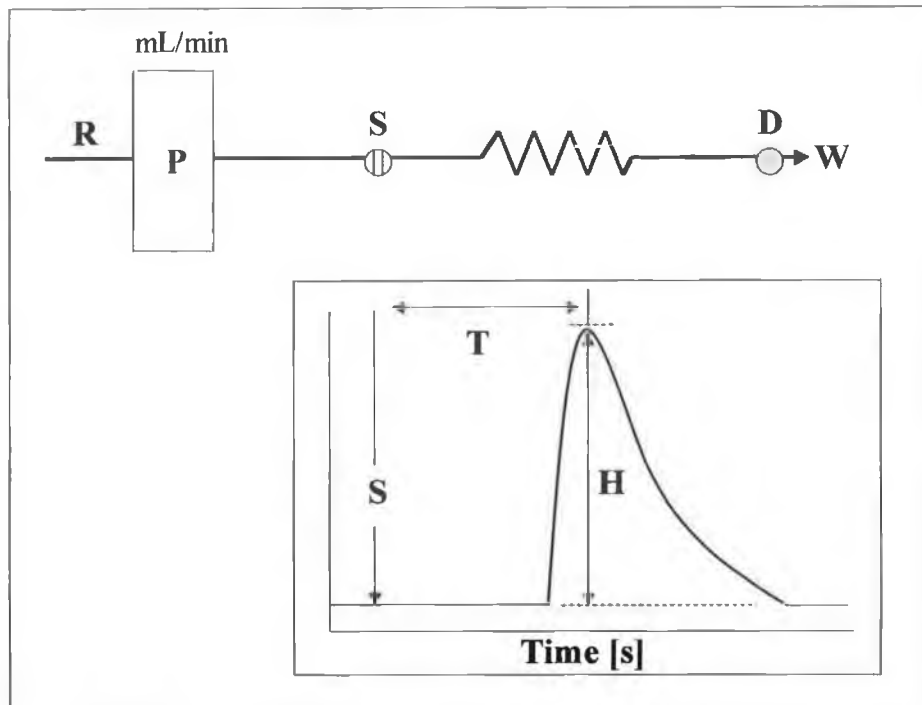


Figure 1-1 Schematic of a simple FIA system and recorded sample plug

Nowadays FIA is as well established as a spectrometric or titrimetric determination. In Figure 1-1 the simple FIA system is represented schematically and the expected recorded signal is given, where R, is reagent stream, P is pump, S is sample, D is detector, W is waste, T is time and H is peak height [25].

In short, FIA is a very reproducible technique, which is relatively simple, thus facilitating high sample throughput and easy adaptability to automation. FIA has been frequently applied to the determination of phosphorus and techniques have been reported for a large number of water bodies. Benson and Mc Kelvie carried out an extensive optimisation and validation of a flow injection (FI) procedure for dissolved reactive phosphorus (DRP) in wastewater, followed by an on-line automation of the entire process. The FI procedure employed a colorimetric reaction, the formation of molybdophosphoric acid and its subsequent reduction to molybdenum blue with tin(II)chloride [26]. Tin(II)chloride was chosen as the reductant because of its long-term stability in solution. The wavelength maximum for this method is the 690-700 nm range compared to 882 nm when ascorbic acid is used, therefore an improvement in sensitivity was achieved when the transmittance was recorded using a solid-state photometer and a red LED (λ_{\max} 635 nm) [27]. Following the validation study the method was applied to an on-line

automated procedure. In its favour the system showed good reliability, low operational costs, a reduction in reagent consumption and minimal maintenance requirements. The data was retrieved and wirelessly transmitted via a radio-frequency communications link and the results compared favourably with a validated laboratory method [28].

Janse et al. also optimised an FIA method for the determination of phosphate using the same method as Benson and McKelvie with the outstanding difference being that Janse's study wasn't specifically targeted at wastewater determinations. Performance characteristics such as peak height, peak width, signal-to-noise ratio and the correlation coefficient of the calibration graph were assessed. Experimental parameters such as injection volume, tube diameter, pump rates, coil lengths, concentrations of reagents and temperature were analysed. Considering the number of variables to be optimised a factorial experimental system was designed to limit the number of experiments necessary to achieve an improved system optimisation [29]. FIA has been applied to more unusual colorimetric determinations involving Rhodamine B and phosphomolybdate, resulting in detection limits reported in the ppb range [30]. Another method boasting ppt phosphate trace determinations is based on the formation of the coloured ion formed between molybdophosphate and Malachite Green at a wavelength of 627 nm. This method utilised small volumes of sample solutions, an organic solvent (Methyl Cellosolve) and a tiny membrane filter for collection of the molybdophosphate with Malachite Green. The trace level determinations are possible by sample filtration through a cellulose nitrate membrane filter under suction [31].

Other noteworthy papers describe the determinations of phosphate in wastewater, surface waters and seawater [32-35].

1.3 Micro Systems Technology (MST)

All quantitative chemical analyses performed in a laboratory involve many procedural steps, where the measurement of the analyte of interest is but one of

many [36]. Typical analytical procedures usually involve a minimum of five steps including:

1. Collection and introduction of a representative sample of the analyte of interest
2. Pre-treatment of the sample, i.e. filtration, dissolution, dilution
3. Separation of the analyte or masking of interfering species
4. Measurement of the analyte
5. Evaluation and interpretation of the results

More accurate and reproducible measurements are achieved by adhering to these steps, however the process can be very time-consuming and labour-intensive [37]. In the early eighties Prof. H. Michael Widmer coined the term "Total (chemical) Analysis System" or TAS, for short. The concept, in its simplest form, was based on the automation of chemical analyses with bench-scale instrumentation [38]. Automation speeds up processes, limits human involvement and is achieved by the optimisation of flow system designs to facilitate more efficient manipulation and sample analysis. The first TAS-type instrument constructed by Widmer et al. was designed to be easily controllable and portable. The first step in realising a fully automated system was to incorporate the sample handling and treatment procedures into a flow system [39-40]. The major advantages of the system included high sensitivity, specificity for trace substances, versatility and a robustness when performing field measurements. The prototype integrated analysis system operated continuously performing one to ten analyses per hour and the automation had a number of steps including calibration, trace enrichment and a gas chromatographic (GC) separation. Firstly a sample was taken and pre-treated, secondly a separation was performed and detected and thirdly the data was processed and converted to either an acoustic or optical signal, which indicated a sample had surpassed a critical concentration limit.

TAS-based instruments were widely recognised as a step forward and generated huge interest. By the late eighties Andreas Manz, a colleague of Widmer's, probed the theoretical implications of miniaturising TAS instruments, which lead to the frequently-used terminology "Micro Total Analysis System (μ TAS)" [41]. The continuous monitoring of the concentration levels of many chemical species, pioneered by Widmer, had become increasingly important in multiple disciplines

including biotechnology, process control and the environmental and medical sciences [42]. Although TAS instruments were multipurpose systems capable of producing highly reproducible and precise measurements, analysis times were still lengthy. It was proposed that μ TAS be defined in terms of both a chemical sensor and a TAS. The simplest definition of μ TAS is a TAS, where the sampling and pre-treatment steps are performed in immediate proximity to the point of detection. μ TAS not only concerned itself with automation of multiple functions, but with the physical integration of two or more of these functions on one platform.

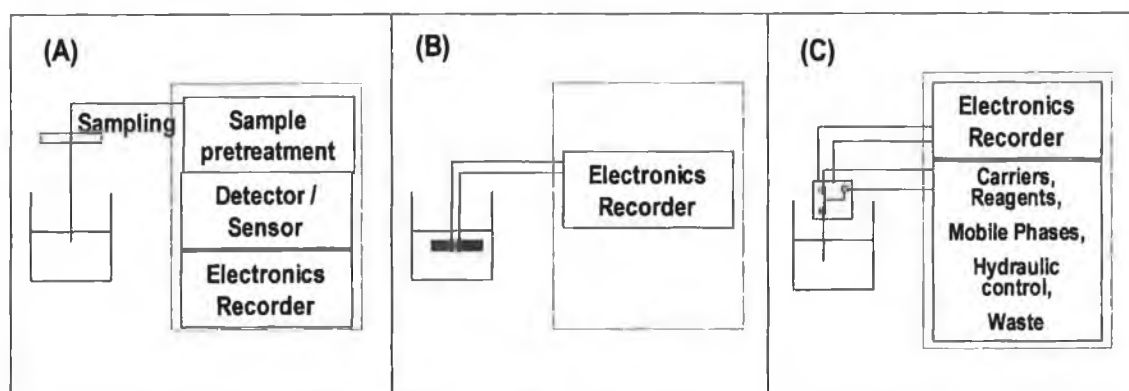


Figure 1-2 The relationship between a TAS (A), an ideal chemical sensor (B) and a miniaturised TAS, μ TAS (C) [43]

In Figure 1-2(C) the μ TAS with multiple functions taking place on a platform differs from the TAS in Figure 1-2(A) in terms of distance the sample has to travel before it is detected. In Figure 1-2(B) the sensor selectively interacts with the sample to the exclusion of all interfering species. The μ TAS resembles the chemical sensor with the added benefit of complete control of the process from start to finish.

Flow Injection analysis (FIA) has been instrumental in the development of, initially, TAS and then μ TAS. Coupling FIA with separation methods like gas / liquid chromatography or capillary electrophoresis resulted in very powerful, robust TAS instruments. Some early examples included a gas-chromatograph-based monitor for trace analysis in air, a high-speed capillary electrophoresis detection method for high performance liquid chromatography (HPLC) and an on-line glucose analyser for bioprocess control [39, 44-45]. Chromatography and electrophoresis were first introduced to the concept of miniaturisation, when particles of micrometer dimensions were used to pack columns to achieve improved separation efficiency.

The advantages of utilising micro columns were a reduction in waste generation, lower cost, increased speed of analysis and an overall improvement in the analytical performance of the system.

To achieve μ TAS, micro fabrication techniques had to be developed and perfected. The fabrication of three-dimensional micro devices was based on micromachining. In the last twenty years many devices including micro-valves, -pumps and -flow sensors have been developed in silicon and have since been integrated into miniaturised chemical and biochemical analysis systems. Integration of micro flow devices enhances precise liquid handling and stricter flow control [46-47]. μ FIA systems based on micro flow systems have been successfully fabricated and have demonstrated the usefulness of a combination of partly integrated and discrete components [48].

The concept of miniaturisation, as has been demonstrated, can be described and defined in a multitude of ways, with the most popular definitions including Microsystems Technology (MST), miniaturised Total Analysis Systems (μ TAS), Lab-on-a-Chip and MicroElectroMechanical Systems (MEMS). To properly define the field of miniaturisation it is best to quote the key instigators in this emerging technology. There are many conflicting opinions in the literature and because the field is still very much in a growth stage there is no one absolute definition that encompasses all aspects of miniaturisation. In general terms μ TAS is most frequently used in Europe, whereas the Americans favour MEMS because the technology has its foundation in the fabrication of semi-conductor micro devices made of silicon [49].

As shown in Table 1-3 microfluidic systems have a diverse applicability [50]. Microfluidics is the central technology in the four key areas of development (see Table 1-3) miniaturised analytical systems, biomedical devices, tools for chemistry and biochemistry and systems for fundamental research.

Table 1-3 Potential Applications of Microfluidic devices

Key Research Fields	Applied Areas
Miniaturised Analytical Systems	Genomics / Proteomics Chemical / Biological Warfare defense Clinical analysis High throughput screening Environmental monitoring
Biomedical Devices	Implantable devices
Tools for Chemistry	Small-scale organic synthesis Sample preparation Amplification of nucleic acids
Systems for Fundamental Research	Fluid flow studies Chemical reactions Biomimetic systems Microdosing systems

1.4 Microfluidics

Microfluidics, as a field of study, represents the behaviour of fluids in small sized channels and, as a topic, is a very important consideration in the design of microelements used in miniaturised systems [51-52]. Greenwood and Greenway described the important role fluid manipulation techniques play in the development of miniaturised microfluidic devices [53]. Because of the micron-sized dimensions of devices, volumes are small, which means there are fewer molecules to begin with, even at a reasonable concentration. Conserving each molecule in micro-devices is of utmost importance and can only be achieved through good sample handling and minimal dispersion of all processes that take place on-chip [54].

1.4.1 Flow

In standard FIA sample plugs are injected into a flowing carrier stream to which reagent(s) are added at various stages and reaction takes place in a coil before detection. In a coil of reduced cross-section, the flow is no longer turbulent. Laminar flow dominates in sub-millilitre systems. In reducing the size of the coil convective effects are minimised and transport distances shortened, thus making molecular diffusion the major mixing mechanism.

Laminar flow can be described as a series of parallel layers, or lamina, moving at different velocities. A flow is said to be laminar if the viscosity is high, the velocity is low and the length scale is small [55].

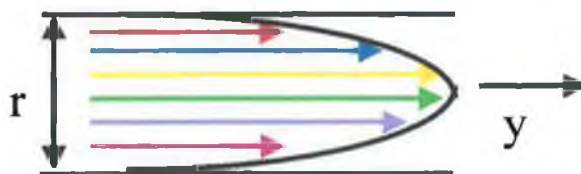


Figure 1-3: Pressure-driven laminar flow with coloured arrows indicating well-defined streamlines [56]

Diffusion is the process by which matter is transported from one part of a system to another as a result of random molecular motions. It is generally a product of intermolecular collisions rather than turbulence or bulk transport. Diffusion is the only available mixing option under laminar flow conditions, unless a mixing chamber is specifically introduced. Mass transport by diffusion occurs 100 times faster in a microfluidic device, that has dimensions 10-fold smaller than a conventional bench FI instrument [57]. The mass transport by diffusion can be determined in a fluidic system by calculating the Reynolds number using Equation 1-3. The Reynolds number (Re) is a dimensionless quantity associated with how smooth the flow of a fluid is. The friction associated with each layer leads to viscosity. A critical velocity is reached as the fluid flow-rate increases and the nature of the flow becomes turbulent, forming eddy currents and vortices [58]. Reynolds numbers are calculated by;

$$Re = \frac{DV\rho}{\mu} \quad \text{Equation 1-3}$$

where D is the internal diameter of the tube or channel [m], V is the fluid velocity [ms^{-1}], ρ is the fluid density [kgm^{-3}] and μ is the fluid viscosity [$kgm^{-1}s^{-1}$]. Flow is deemed laminar when the Reynolds number does not exceed 2000. Thus diffusion dominates mixing processes below this value.

Poiseuille's Law describes flowing fluids in channels. For laminar flow, the volume flow-rate is given by the pressure difference divided by the viscous resistance.

$$V = \Delta P \pi r^4 t / 8 \eta L$$

Equation 1-4

where V is the volume of injected analyte [ml], ΔP [bar] is the pressure difference across the channel, r is the channel radius [m], t is the injection time [s], η is the viscosity of the fluid [$\text{kgm}^{-1}\text{s}^{-1}$] and L is the length of the channel connecting reservoir and manifold [m]. Consequently, Poiseuille's Law also shows the dependence of the volume flow-rate on the radius and the length of the channel.

The dispersion of the sample plug increases with the square root of the distance travelled through a tube, decreases with decreasing flow-rate and decreases with increasing temperature rates [59]. Variations in channel width introduce a skew to the flow profile and the deeper the channel the greater the dispersion. Etch depth of channel plays a prominent role in behaviour of dispersion in fluids. Generally it can be shown that decreasing the depth of the channel leads to a lower dispersion of the sample plug, which is a recognised prerequisite in a microsystem. Dispersion is a negative effect; and therefore it is desirable to keep dispersion effects small because this in turn increases the number of plugs per unit time that can be generated. To reduce dispersion, the residence time in the channel has to be extended. This is accomplished by curtailing the flow-rate and by minimising the channel dimensions.

To comply with all the many elements important in the design of an optimum micro fluidic chip for a given application, ultimately a balance between low dispersion, low flow-resistance and short reaction time must be realised [60].

1.4.2 Pumping Mechanism

Pumping systems for microfluidic analysis have tended to be either electrokinetic or pressure-driven techniques. Electrokinetic pumping has been the basis of most micro-device pumping schemes. However systems with off-chip pneumatic or hydrodynamic pumping combined with on-chip channels have solved many issues relating to sample loading and mixing materials.

Pressure-driven Flow

In pressure-driven systems frictional forces at the solid-liquid interface at the walls of the channels, result in a substantial drop in pressure, which lowers the flow-rate leading to laminar parabolic flow profiles as shown in Figure 1-4. An outcome of laminar flow is that the flow velocity is highest in the middle of the channel and approaches zero at the walls.

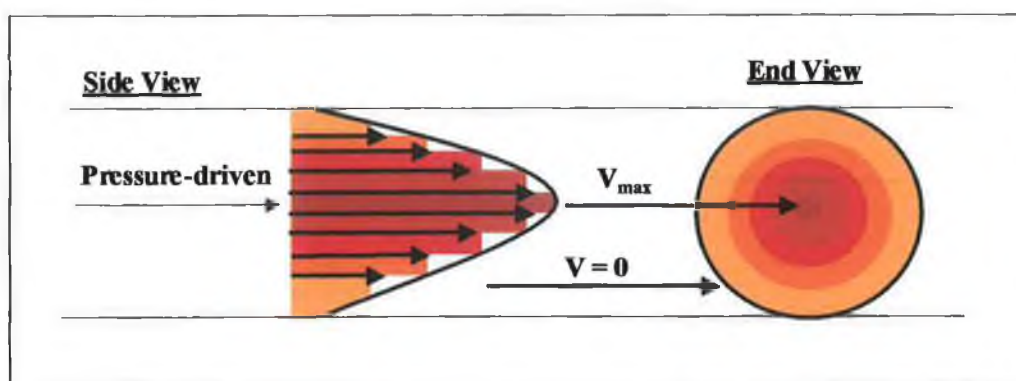


Figure 1-4 Schematic of pressure-driven parabolic flow in a micron-sized cylindrical channel

There are several disadvantages in using pressure-driven flow for a μ TAS, including high back pressure due to the small channel dimensions, and parabolic flow profiles, which can cause band-broadening and sample dilution [61].

Electrokinetic Flow

Electrokinetic flow enables fluids to be transported through fluidic networks. This is achieved by ensuring that the potential drop is across the sample fluid, so that the bulk solvent flow is towards the cathode, where at a single point downstream, detection can take place [62]. Electrokinetic flow is dependent on three phenomena the electrical insulation properties of the substrate materials, the occurrence of Joule heating when a field is applied across a fluid-filled channel and the generation of bulk solvent flow towards the cathode from surface charges on the walls of microchannels.

A lot of time, money and effort has gone into developing multiple elements that can be incorporated into a lab-on-a-chip device, a key issue being sample and reagent mixing. Under electrokinetic flow reagents are mixed by applying a specific potential across the channel, which depends upon the channel geometry and the properties of the material inside the channel(s) [63]. Electrokinetic flow is the most commonly used pumping mechanism for microfluidic devices and can be broken into two types, electroosmotic (EOF) and electrophoretic flow. To date, EOF has been the most frequently used flow method used in microfluidic separations due to the ease with which a flow is generated [64]. A cross-section flow profile, of EOF, is shown in Figure 1-5.

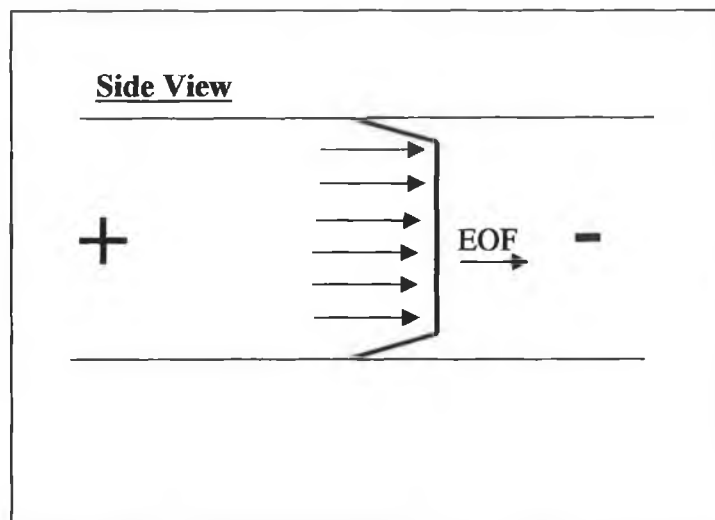


Figure 1-5 Cross-section electrokinetic flow profile

In electrically driven microfluidic systems, the driving force of the EOF is uniformly distributed along the length of the micro-channel. There is no pressure drop and the flow velocity is uniform across the channel diameter, except very close to the wall.

Many studies have been predominantly based on electrokinetic fluid pumping, in particular, due to the simple experimental procedures required to achieve EOF [64]. EOF requires no moving parts and has a minimal back pressure, also at relatively low electric field strengths; electroosmotic ability is the main process. Very little analyte separation occurs in miniaturised systems with EOF at field strengths of $80 - 300 \text{ V cm}^{-3}$ [65].

1.4.3 Silicon Microfabrication Techniques

The fabrication of micro devices in silicon has its foundations in the microelectronics industry. The field is often referred to as planar fluidic chip technology and uses a number of well-established and accepted techniques. Primarily the planar surface they were referring to was silicon, although glass has become increasingly important for chromatographic systems and plastics and ceramics have more recently come to the fore [66-68]. Silicon was frequently used for many reasons. It can be produced to high levels of purity and crystalline perfection, and because of the high demand is a relatively cost efficient material. Silicon is atomically flat, has yield strength greater than steel, has excellent mechanical and chemical properties and can be micro machined on the order of a few nanometers [69].

There are four main processes, which concern themselves with silicon fabrication, which are film deposition, photolithography, etching and bonding. Film deposition is required to generate the desired dimensions of the microstructures to be fabricated. By depositing various materials like metals, inorganic oxides and polymers by either spin coating, thermal oxidation, chemical vapour deposition (CVD) or sputtering techniques dimensions from a few micrometers down to several nanometres can be achieved. Photolithography involves generating a pattern of geometric shapes on a photosensitive material known as a photoresist. The design is defined by dark regions on the glass mask and can be transferred to the photoresist by UV, X-ray or e-beam light. Etching involves the transfer of structures to underlying films and substrates of the mask and comes in two forms, dry and wet. By wet etching the mask is submerged in a solution, which will etch only the structure in the desired material and not the other exposed to the etch solution. Dry etching is achieved in partially or fully ionised gaseous environments (plasma etching). Finally bonding is necessary to assemble the fabricated structures into a coherent device. Silicon-silicon, silicon-oxide and silicon-glass bonding are the most common. Due to the planarity of the materials bonding leads to fusion and a perfectly tight seal. In Figure 1-6 the fabrication process is schematically shown.

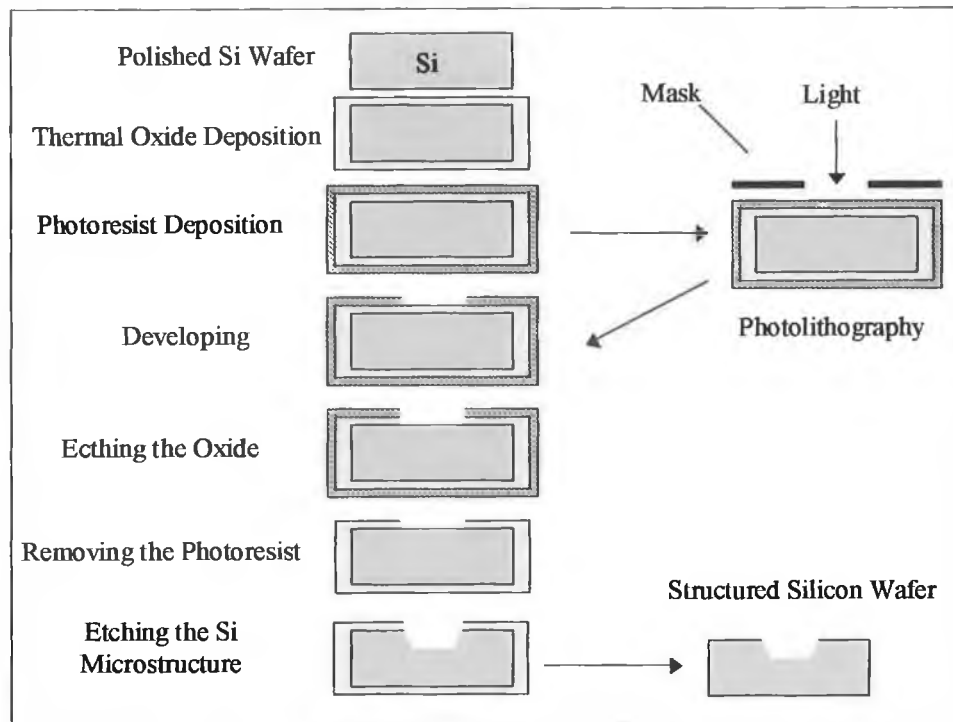


Figure 1-6 A simplified schematic of the basic processes involved in the fabrication of a silicon wafer

A major benefit of micro machining is the reproducibility that can be achieved in manufacturing. Silicon wafers can yield hundreds, if not thousands of individual chips.

At present, typical, well-defined micro-fluidic sensors combine conventional pump and valve technology with a more progressive approach of integrating the mixing, reaction and optical detection of liquids in a microchip [70]. Traditionally, glass and / or silicon are the predominant materials employed in the design of microchips for continuous flow systems. This is primarily due to their excellent physical, electrical and optical properties. A three-layered wafer usually consisting of an anodically bonded Pyrex / silicon / Pyrex sandwich forms the foundation of these integral microchips [71]. Anodic bonding is considered a desirable choice for protecting the device from the working environment and / or merging the device with auxiliary functions. Anodic bonding brings a glass and silicon wafer into contact using an electrostatic attraction, which forces covalent bonding on the surface of both materials [72]. The 400 μm thick Si layer (Silicon/Oxide/Silicon) is protectively coated by deposition of silicon nitride to the surface by a lower-pressure chemical vapour process (LPCVD) to combat corrosion [73]. Channels, inlet through-holes

and an optical cuvette on the Si wafer are predominantly etched by a dry reactive ion etching (DRIE) or by an advanced silicon etching (ASE) process. After which, all three layers of the wafer must be correctly aligned to ensure interconnection of all the fluidic components. When they are precisely positioned the layers are bonded and referred to as wafer stacks, which are then ready for application purposes.

Wafers consisting solely of three glass layers have similarly been developed. These wafers employed fusion, instead of, anodic bonding, and also applied photolithographic and wet etching techniques for the etching of the micro fluidic channels of the inner glass. Since DRIE hasn't yet advanced enough to be applied to a glass interface, spark assisted etching (SAE) was chosen for the drilling of the optical cuvette with much success, resulting in improved sensitivity capabilities due to extended optical path length. Glass microfluidic chips have shown enhanced performance over the above-described Si wafer in areas such as long-term chemical stability of the device since glass is less prone to corrosion than silicon, and lower sample dispersion due to the SAE etch technique employed in the drilling of the optical cuvette [59]

1.4.4 Applications in Silicon and Glass Microsystems

Shockley, Bardeen and Brattain of Bell Telephone Laboratories received the Nobel Prize in 1948 for developing electrical switches based on semiconductor properties [74]. With the advance of materials such as silicon and germanium, the advent of integrated circuits became a rapidly developing research field, with outstanding contributions, over the last 50 years, that included:

1. Sensor Membranes milled in silicon by Honeywell Inc. [75]
2. Anodic Bonding of Glass by G. Wallis, D. Pommerantz [72]
3. Stanford University's gas chromatography system on a wafer in 1979 [76]
4. Automotive absolute pressure sensors for pollution control in the early 80's [77]
5. Single-use, silicon, micromachined blood pressure sensors [77]
6. Coulometric acid-base titration systems in 1985 [78]

7. Silicon based Micro pumps in 1988 [79]
8. Inception of μ -TAS concept by Ceiba-Geigy GmbH in 1990 [80]
9. On-Chip DNA sequencing utilising capillary gel electrophoresis in 1998 [81]
10. Ultra low cost disposable plastic chips like the hydrostatic pressure-driven microfluidic detector card commercially available as an evaluation kit at Micronics Inc.

The Stanford gas chromatograph was the first chemical analytical technique that was miniaturised and is still considered a marvel even by today's standards. Terry et al. built a miniature gas analysis system based on the standard principles of gas chromatography. The system was made of silicon and fabricated using photolithography and chemical etching techniques. The design layout consisted of a sample injection valve and a 1.5 m-long separating capillary column and detection was via thermal conductivity. The entire capillary column and GC-system fit on a 5 cm-diameter silicon wafer, which was a three-fold downsize scaling, when compared to bench instrumentation available at the time. The sample injection component was based on the principle that the injected gas sample must only be milliseconds in duration and nanolitres in volume. In order to achieve this a simple, solenoid-actuated diaphragm valve was fabricated. The thermal conductivity detector (TCD) was chosen for the speedy response, simple design and robustness. It was also integrated onto the miniature system and coupled to the silicon wafer via the sensing element, a nickel film resistor. There were six major integrated components in the system. These were carrier gas output, interconnect through holes to the micro valve on the backside of the wafer, sample gas input. Sample gas output and carrier gas vent to extern. To demonstrate the system's capability simple measurements were made with an oscilloscope to produce a chromatogram. The first sample to be analysed was a mixture of nitrogen, pentane and hexane and eluted peaks for all three gases were obtained.

There has also been commercial production of clever devices like the piezo pressure-sensor, ink-jet nozzles and airbag sensors, based on microsystems technology [82]. Two clever devices, which were micro machined in silicon, are types of pressure sensors. The first was introduced in the eighties by the automobile industry to control car emission levels. The second was a blood pressure sensor for hospital operating rooms. Because of the high demand (20

million / year) manufacturing is cheap and devices are single-use, which drastically reduces the chance of infection. These highly specific cases have changed the face of the micro machining industry into a self-sufficient, growth sector, with vast opportunities [77]. The next phase of marketable devices can be sub-divided into several major categories:

1. Analytical devices for predominantly environmental applications
2. Biochemical devices for on-chip synthesis, integrated protein digestion, drug discovery
3. DNA sequencing and assays
4. Biomedical Diagnostics
5. Capillary electrophoresis, ion chromatography
6. Molecular biological applications [43]

Chip designs are both varied and complex, and can perform an assortment of applications, which have or are in the process of being employed. For example, integrating sample preparation and separation via on-chip immunoassay has been demonstrated, a GC based chip-CE system has recently been commercially introduced by Shimadzu, and even DNA sequencing has been performed on-chip using capillary gel electrophoresis [83,84]. The latter development has particularly generated increased attention in developing chips capable of multi-tasking in the more complex fields of drug discovery, proteomics, and the most promising area of synthesis on a chip, which could ignite the whole microfluidic industry.

In 2000 Sanders and Manz reviewed the current crop of hot topics in terms of genomic and proteomic analysis [85]. Genomics involves the characterisation of all the genes of an organism, whereas proteomics deals with identification and characterisation of all proteins in a cell. By combining both fields revolutionary steps towards complete biological understanding have begun [86]. Genomic analysis can be performed with a microarray-based system [87] or by separations based on CE, which are dealt with next. Proteomic analysis can be carried out by both methods also. The CE chips have, in particular, been adapted for use in immunoassays [88-90].

Microfluidic chips have been employed in biomedical sensor systems, which are commercially available from companies, such as Orchid Biosciences, Agilent

Technologies and Caliper Technologies. Currently the most successful MEMS products on the market include disposable blood pressure sensors, pressure sensors for engines, air bag accelerometers, inkjet printer heads and magnetic heads for computer hard drives [91-92].

The development and fabrication of microfluidic devices in glass and quartz has taken place at almost the same pace as silicon microtechnology. This is primarily due to the suitability of glass and quartz materials to the miniaturisation of capillary electrophoresis (CE). Initially silicon substrates were used in the microfabrication of CE devices [93-95]. It was envisioned that upon miniaturisation and automation the robustness, flexibility and overall dynamic control for the user, would be improved [42]. CE systems predominantly employ electroosmotic flow to manipulate fluids in microchannels, silicon fabrication afforded researchers a tried and tested material with which to work [93]. Devices were fabricated by standard lithographic and bulk-machining methods and the channels sealed by anodic bonding with a glass cover plate. The development of miniaturised CE devices has been favoured over chromatographic separations because an applied voltage is easier to implement across the terminals of microchannels [96].

Glass or quartz-based CE microfluidic devices can facilitate high-voltage applications, which make them more versatile substrate materials than silicon for separations. Although silicon was traditionally the material of choice, it was never the most suitable for separations because of the limitations associated with its semi-conductor properties and the fact that it is not transparent at wavelengths typically chosen for optical detection [93]. Planar glass plates were patterned photolithographically and chemically etched with primarily fluorescence detection being employed [97-98]. With chip design improvements absorbance detection was made possible [99]. Slater and co-workers also reported electrochemical detection for on-chip CE separations [100]. Indirect amperometric detection was utilised in the separation of high-sensitivity DNA restriction fragments and polymerase chain reaction (PCR) product sizing [101]. Numerous DNA fragments and PCR product sizing separations in miniaturised CE systems have been reported in the literature [102-]. To date biological applications have been the driving force behind the development and fabrication of glass and quartz microfluidic devices. In the future polymer materials will have an invested role to

play in separation systems because of the wider choice of physical, chemical, thermal and electrical properties available to suit specific applications.

Glass and quartz have also been used as the primary substrate material in a number of microfluidic devices for the determination of nitrate, nitrites and orthophosphate in aqueous environmental samples. Haswell et al. first reported a μ FIA manifold for the determination of orthophosphate in 1995 [105]. The determination was based upon a colorimetric reaction in a microfluidic chip with the flow being driven by electroosmotic pumping. The chip was fabricated photolithographically and wet etched to produce the desired micron-scale channel dimensions [106]. Haswell and co-workers have also been involved in a number of other environmental determinations with μ FIA chips [107-108].

1.4.5 Polymer Microtechnology

There is an increasing demand for the establishment of microfabrication technologies for the microstructuring of polymers that are equivalent to existing microfabrication technologies for the manufacturing of silicon or glass-based microsystems [109]. Polymers provide an alternative substrate to silicon and glass and have the advantage of being less expensive, easier to manipulate than silica-based substrates and have a wide range of properties to suit a given application [110]. Microfluidic systems fabricated in polymers are increasingly finding applications as analytical systems, biomedical devices and tools for both chemistry and biochemistry [50].

1.4.6 Polymer Materials

The word polymer comes from Greek with a literal translation "many (poly) parts (meros)". A polymer is a long molecule consisting of many small repeat units known as monomers. Polymers are predominantly structures made up of carbon, hydrogen and oxygen and sometimes containing silicon, sulphur, chlorine and fluorine. Polymers are macromolecular substances with a high molecular mass [111]. They are formed when monomer units react to form linear or three-dimensional chains by a process known as polymerisation. When a monomer

reacts with a like monomer unit to form a chain the structure is called a homopolymer. When two monomer units are reacted the structure is known as a copolymer.

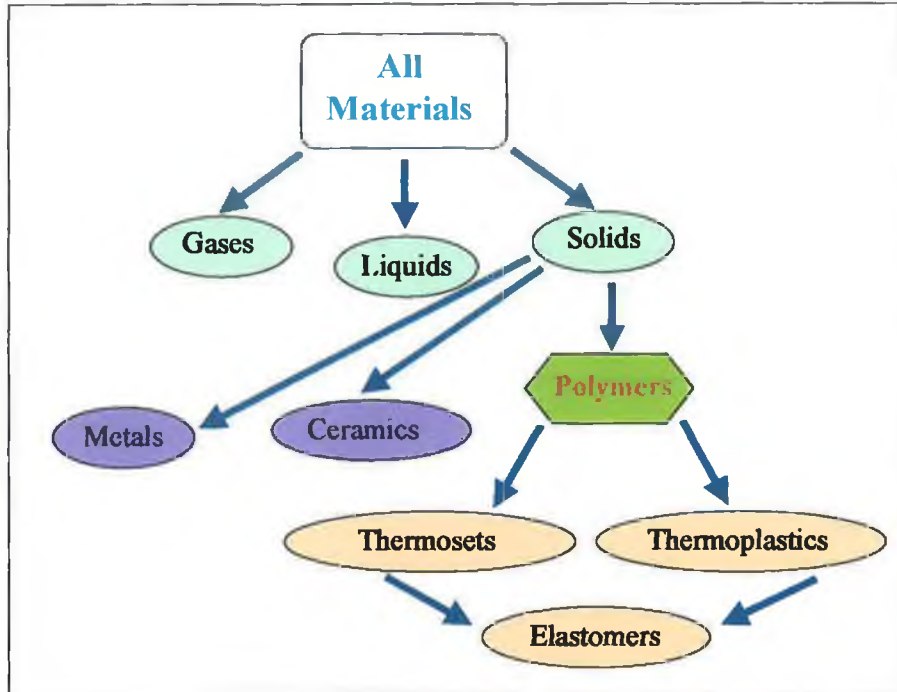


Figure 1-7 Polymer position in the table of materials

The basic properties that a polymer material exhibits are derived from their molecular structure. Polymers are broadly classified into three categories as shown in Figure 1-7 as thermoplasts, thermosets and elastomers (rubbers).

All polymers are classified as either thermoplastic or thermoset. The third group, i.e. elastomers, are grouped based upon their physical properties rather than their chemical nature and can be either thermoplastic or thermoset.

Thermoplastics can be defined as materials that have similar properties of a viscous liquid, when heated, and can be repeatedly cooled and re-heated. The most commonly used thermoplastics are polyethylene (PE), polypropylene (PP), polyvinyl chloride (PVC) and polystyrene (PS), which, between them, account for 85 % by volume of the world plastics consumption [112].

Thermosets are polymers that undergo a chemical change to build molecular weight and viscosity. They are set or cross-linked with heat, which means the reaction is non-reversible under heating. The three most common types of thermosets are epoxy, polyester and polyurethane.

Elastomers are rubber like polymers that were the first plastics to be researched and developed for commercial use. Natural rubber was first discovered in the gum resin of trees in the South African jungle and was used as a waterproofing fabric. Elastomers are either thermoplastic or thermoset. Thermoset elastomers are formed by vulcanisation, where sulphur (~ 4%) is added to the polymer blend when heated. The sulphur produces cross-links that make the rubber stiffer and harder. Examples of common thermoset elastomers are butadiene rubber (BR), styrene-butadiene rubber (SBR), polyurethane (PU) and silicone [113]. Thermoplastic elastomers are formed by copolymerisation of two or more monomer units. One of the monomers has soft amorphous characteristics, the other hard, crystalline features resulting in rubber-like polymers similar to the vulcanised plastics. Examples of thermoplastic elastomers include thermoplastic urethane (TPU), thermoplastic elastomers (TPE) and thermoplastic olefins (TPO).

There are a multitude of polymeric materials that are commercially available, which can be used for any specific microfluidic application [111]. These materials have a diverse range of properties, which can be categorised under the main headings presented in Table 1-4.

Depending upon the desired application a material can be selected that most suits the analysis. There are many well-known and routinely-used polymer materials that can be used to fabricate microfluidic devices and be applied to numerous analyses. Perhaps the most frequently used polymer materials in microfluidics are Polymethyl Methacrylate (PMMA) and Polydimethyl Siloxane (PDMS).

Table 1-4 Table of typical properties highlighting the diversity of polymer materials

Polymer Properties	
<u>Physical</u>	Density Refractive Index % Transmission UV Resistance /Oxidation Water Absorption Flammability
<u>Chemical</u>	UV Degradation Chemical Resistivity Chemical Solubility Chemical Premeability
<u>Mechanical</u>	Hardness Elasticity Plasticity Energy Capacity Stress Strain Tensile Strength Stiffness
<u>Thermal</u>	Thermal Stability Glass Transition Temperature Melting Point Specific Heat Capacity
<u>Electrical</u>	Insulation Conductivity Dielectric Strength Resistivity

PMMA is also commonly referred to as Perspex. Acrylic is a general term used to describe a large family of polymers. PMMA is an amorphous, transparent and colourless thermoplastic that is hard and stiff. It has good abrasion and UV resistance and excellent optical clarity but poor low temperature, fatigue and solvent resistances. Thin films of PMMA are normally made from impact-modified grades, which incorporate a small portion of elastomer, in order to improve their flexibility. PMMA is ideal for laser ablation because it is not easily melted and it has a high absorptivity at the lasers operating wavelength of 10.6 μm . PMMA has a glass transition temperature, T_g , of 105 $^{\circ}\text{C}$, at which the amorphous polymer changes from a glass to an elastomer / rubber.

PDMS is an elastomer that is also commonly known as silicone rubber and consists of repeating units $\text{—O—Si(CH}_3\text{)}_2\text{—}$. PDMS has a very low T_g of -123 $^{\circ}\text{C}$, which means it is a liquid at room temperature and is commercially available from

Dow Corning (Sylgard 184 Kit, Silicon Elastomer, Dow Corning, Wiesbaden, Germany). The PDMS comes as a two-part kit containing a liquid silicon rubber base and a catalyst or curing agent. PDMS is excellent for the fabrication of microfluidic devices for a number of reasons including [50]:

1. Micron-scale features are highly reproducible by replicate molding
2. Optical transparency down to a wavelength of 280 nm, which means detection via UV / Vis absorbance and fluorescence is possible
3. Low temperature curing
4. Reversible sealing to itself and many other materials by making molecular contact on the surface
5. Surface chemistry can be manipulated and controlled with ease [114]
6. Conformation to smooth, non-planar surfaces
7. Demolds easily without damaging micron-sized features of the mold or the microfluidic device.

1.4.7 Polymer Microfabrication Techniques

There are many new techniques cited in the literature, which are fast becoming standard practice in the fabrication of microfluidic systems in polymers. There are several, general, microfabrication techniques for polymer materials that stand out, which include laser ablation, soft lithography, injection molding and hot embossing.

Two types of polymer microfabrication techniques exist, namely direct techniques, whereby single devices are fabricated individually and replication techniques, whereby a master structure is used to form the structure in a polymer material. Laser ablation (1) falls into the category of direct techniques [115-116]. Soft lithography (2) injection molding (3) and hot embossing (4) fall into the latter category, which has the commercial focus of the polymer microfabrication field [109]. Both injection molding and hot embossing produce two-dimensional plastic wafers with micro-structures in the surface and sometimes, depending on the size and scale of the features, one mold can be inter-changeable between the two techniques.

For the replication techniques a master must be created. These masters can be fabricated in silicon, therefore a wide range of fabrication technologies are available, for example silicon micromachining, laser ablation, mechanical micromachining or LIGA (Lithographie, Galvanik und Abformung, meaning "replication"). LIGA was developed by the Karlsruhe Research Centre in Germany [117]. The LIGA process combines synchrotron radiation lithography, galvanofforming, and plastic molding, which results in the mass production of microstructures with high aspect ratio and great structural height [118].

Laser Ablation

In the simplest terms, laser ablation is the interaction of laser energy with the surface of a substrate resulting in material removal [119]. The process of laser ablation relies upon the absorption of laser photons by the sample material. Ultrafast lasers have been developed, which incorporate a multi-photon absorption that can ablate more material, even those normally transparent at the laser wavelength [119].

There are numerous lasers currently available commercially, that have contributed to the development of micron-sized devices in polymer materials including carbon dioxide lasers, solid-state lasers, eg. Nd:YAG, titanium sapphire, copper vapour lasers, diode lasers and Excimer lasers.

There are two ways in which micromachining can be carried out with lasers, by direct writing and mask projection [115]. The former method is used for solid-state lasers and the latter for Excimer lasers. Direct writing is a simple technique only requiring a sample material and the beam motion to generate features. It utilises inexpensive optical components, interfaces with CAD software packages and replicate designs for rapid prototyping. Its limitations include the limited range of features and shapes, which can be ablated and the small working field that can be ablated at one time [120]. Mask projection is a more flexible technique, which can produce many types of structures and has high precision and quality in the fabricated features. Mask projection can be used to mimic a direct writing technique and can ablate larger surface areas. The disadvantages are that projection optics are relatively expensive compared to those for direct writing and

the biggest issue is the need to have a high-quality mask designed, which can make the various shapes and features required for the design. Laser instruments incorporating the direct ablation approach and the indirect mask projection are shown schematically in Figure 1-8.

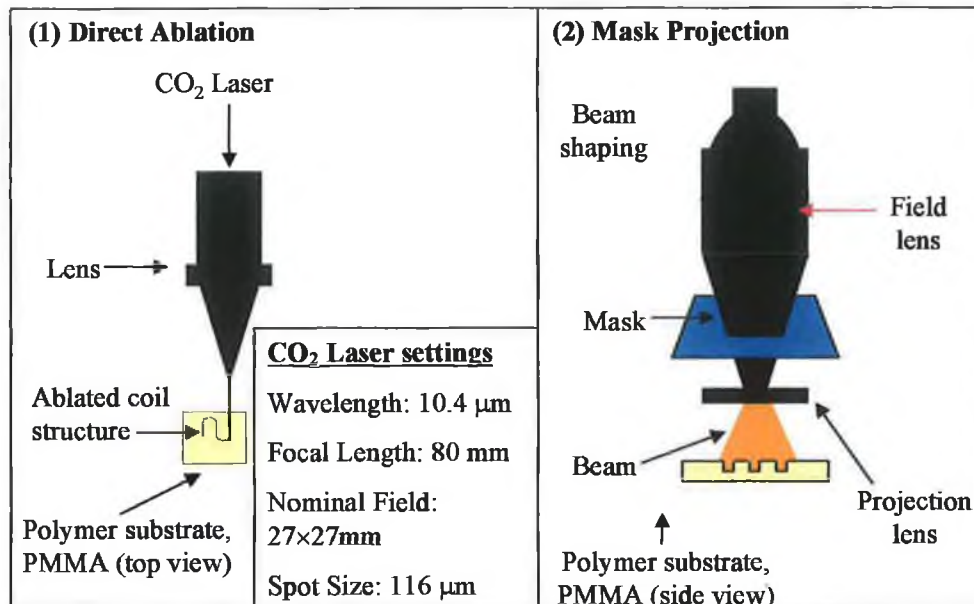


Figure 1-8 Schematic showing the two modes of laser ablation; direct writing (1) and mask projection (2)

The CO₂ laser instrument is shown with direct focussing, whereby the laser can be focused to a very small spot size. In the case of an Excimer laser the mask shape dictates the shape of the beam, and therefore it need not be focussed to a spot size because it is multimode and spatially incoherent [121].

Soft Lithography

Soft Lithography is based on self-assembly and replica molding to fabricate nano- and micro-scale features and channels [122]. Soft Lithography involves the use of an elastomeric stamp with patterned relief structures on its surface to make features, which have dimensions between 30 nm and 100 μm. There have been a number of ways in which the soft lithography technique can be achieved including microcontact printing (μCP), replica molding (REM), microtransfer molding (μTM), micromolding in capillaries (MIMIC) and solvent-assisted micromolding (SAMIM)

[123-128]. PDMS is the most frequently used elastomer for soft lithographic microfabrication, although others such as polyurethanes and polyimides can also be used [129]. PDMS is the most popular choice because of its range of properties, which can be attributed to the inorganic siloxane backbone and organic methyl groups attached to silicon [130].

The simple soft lithographic process for PDMS is shown in Figure 1-9. The master is fabricated using a similar technique to those employed in silicon microfabrication, like photolithography, micromachining or electron beam ablation. An example of a master is the photo polymerisation of the photoresist SU 8, which involves exposure of the photoresist to UV light [131]. The unexposed photoresist is washed away, leaving a wafer with micron-sized features protruding from the surface [132]. The master, when complete, is exposed to a vapour, for example, $\text{CF}_3(\text{CF}_2)_6(\text{CH}_2)\text{SiCl}_3$, for approx. 30 min. The elastomeric stamp or mold can then be prepared by a process known as cast molding, which requires the liquid elastomer to be poured over the master, then heated to elevated temperatures to form a solid, which can be peeled from the master and contains micron-sized features [133].

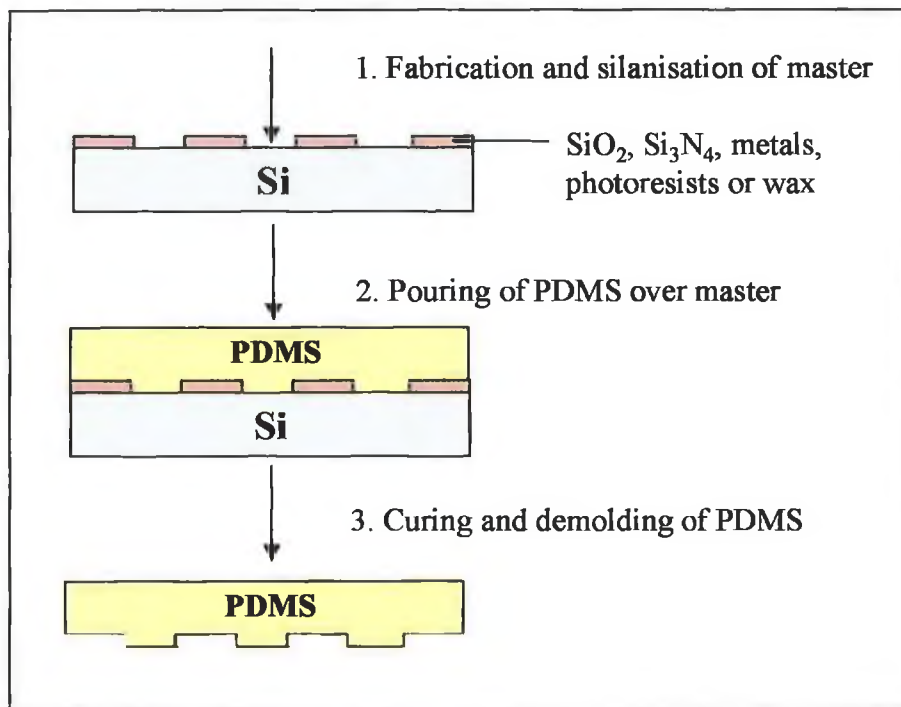


Figure 1-9 Schematic of the three basic processes for the fabrication of micro-sized features in PDMS by soft lithography

Soft Lithography is a technique that was developed to enable the rapid reproduction of prototype microfluidic devices. Elastomeric PDMS, when used as a stamp, has been shown to be very durable with no visible degradation in excess of 50 uses over a period of several months [122]. The advantages of PDMS as a material for fabrication of micro-scale devices have, previously, been described in Section 1.4.4: Polymer Materials. Now the challenges are dealt with, specifically in terms of soft lithographic techniques. The three major disadvantages of PDMS are due to shrinkage, elasticity and softness.

Upon curing PDMS shrinks by approx. 1 %, and can be easily re-swelled by organic solvents like hexane and butane, which means they aren't suitable for microfluidic applications where strong organic solvents are a necessary requirement. The elastic property of PDMS and its thermal expansion mean that dimension accuracy across a large surface area is harder to achieve. The softness of PDMS has a knock-on effect on the aspect ratio of features made in the PDMS. If low and high limitations in aspect ratio are breached the PDMS will deform and defects will be found in the microfabricated features. Delamarche et al. determined that aspect ratios should be maintained within 0.2 and 2 if defect-free stamps of molds are to be fabricated [134].

Injection Molding

Injection molding is a method to obtain molded products by injecting plastic materials molten by heat into a mold and then cooling and solidifying them. The method is suitable for large production of small-scale complex features in plastics [135]. The process of injection molding has four primary steps clamping, injection, cooling and removal of products.

An instrument that can perform all four steps is known as an injection molder (see Figure 1-10). The injection molder consists of two parts, the clamping unit and the injection unit. The former is used to open and / or close a die and for the ejection of fully formed parts. The latter melts the plastic material by heating and injects the molten plastic into a mold. A mold is a hollow metal block, which molten plastic is injected into to form a certain fixed shape. The molten plastic is delivered to the

mold via a sprue and fills cavities by way of runners and gates. The mold is opened after the cooling process and the ejector rod of the injection molding instrument pushes the ejector of the mold to further eject moldings / fully formed parts.

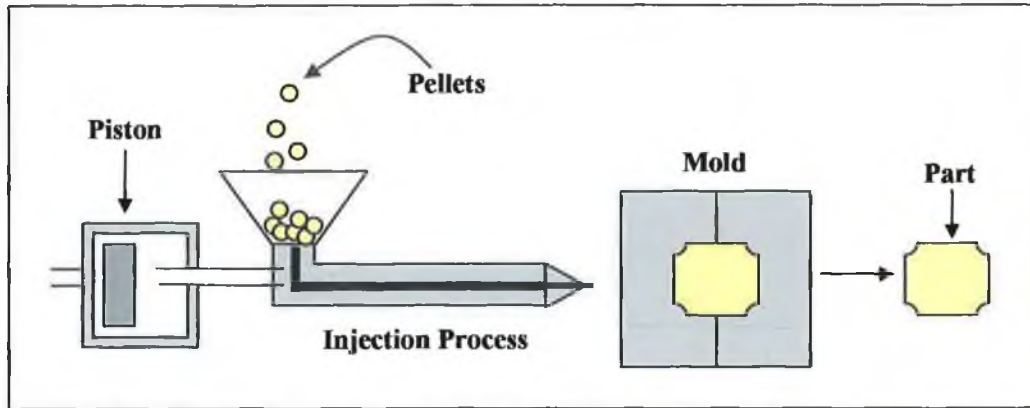


Figure 1-10 Schematic of Injection Molding Instrumentation

The three main molding conditions, which have to be optimised for each polymer material and corresponding design, are cylinder temperature, injection speed and mold temperature.

The cylinder temperature is usually set to above the T_g of the polymer being melted. The injection speed involves setting the speed at which the sprue injects the molten plastic and also the distance the molten plastic is injected from, i.e. how far the piston is from the mold. By altering these conditions the appearance, dimensions and mechanical properties can be optimised [135].

Hot Embossing

Polymer hot embossing is a procedure whereby an inverse of a master is created and molded in a polymer material through heat and pressure [136]. Hot embossing is the process to press a mold into a pre-fabricated semi-finished plastic product that is located on a substrate under vacuum as shown in Figure 1-11 [137]. There are three major stages in the process, which are heating, molding and demolding.

The process takes place at a temperature that ensures sufficient flow-ability of the plastic material. In Figure 1-11 the master replication mold contains the protruding micron-scale features and the substrate is the polymer material into which these features are being pressed. After the mold has been pressed, the plastic material is cooled down to a temperature, which provides for a sufficient strength, so that the micro-constructed plastic material can be demolded [138].

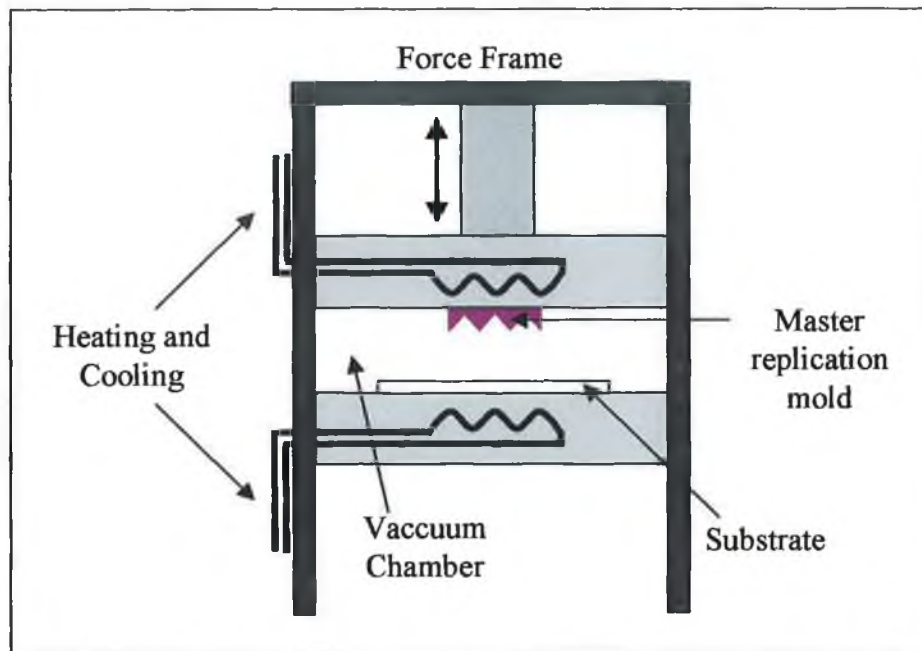


Figure 1-11 Schematic of the basic components of a hot embossing instrument

Hot embossing is superior to the technique of injection molding for a number of reasons. During the hot embossing molding process small deformation rates mean low velocities (molten material), which results in very fine structures without deformations occurring. Also internal stresses in the molded plastic material are minimal compared to injection molding because the whole process is conducted close to the thermal equilibrium, i.e. tool and substrate are heated to a similar temperature prior to molding, whereas with injection molding the molten plastic is injected into a cold mold [110]. The main process conditions, such as molding forces and temperatures, can be more rigidly controlled resulting in the fabrication of microstructures with very thin, unstructured carrier layers [139]. Although recently it has been demonstrated that microfluidic channels can be made from a silicon mask by imprinting at room temperature. It was demonstrated that with a greater applied force (450-2700 psi) between the tool and substrate, in a hydraulic

press, microfluidic channels can be imprinted into the polymer material and it need not be heated to its glass transition temperature [140].

Hot embossing is probably the most powerful instrument of those mentioned, for the fabrication of multiple replicates of polymer microstructures. However the quality of the master tool dictates the quality of the finished polymer structure [109, 141].

1.4.8 Polymer Microsystem Applications

As discussed polymers can be machined using a range of different microfabrication techniques creating high-quality microfluidic systems at a low cost and in volume [111]. The next topic of interest is how easily these polymeric devices can be applied to real chemical and biological processes.

PDMS has proved to be a most useful material for the fabrication of microfluidic separation systems; in particular, the development of capillary electrophoresis (CE) chips [110]. PDMS is an excellent material for electrokinetic and pressure pumping because the polymers surface can be charged and microfluidic devices fabricated in PDMS and sealed irreversibly can withstand very high pressures. In 1997 Effenhauser et al. reported the first miniaturised CE system fabricated in PDMS [142]. The system was used to separate fragments of DNA from fluorescently labelled peptides. Whitesides et al. went on to further develop CE chips with a variety of microfabrication techniques to perform separations and analyses of amino acids, DNA fragments and peptide charge ladders [143]. Miniaturised CE chips fabricated in PMMA have also been reported by Ford et al. by X-ray lithography [144]. These CE chips were fabricated in PMMA with a fibre-optic-based laser-induced fluorescence detector for the restriction analysis of double-stranded DNA, which can be used in the fields forensics, genotyping and restriction mapping.

PDMS is said to have a poorly defined EOF [145]. By utilising different fabrication techniques, for example laser ablation, new materials can be exploited in the design of CE chips. For example Girault and co-workers fabricated CE chips in a number of materials including polystyrene (PS), polycarbonate (PC), polyvinyl

chloride (PVC) and polymethyl methacrylate (PMMA) by a laser photoablation technique [115,146]. Newer polymer materials, such as parylene and Zeonor, which have not been commercially available that long have also been applied to the CE-MS analysis of small organic molecules [147-148]. The biocompatibility of polymers, in particular PDMS, has meant that numerous biological applications have been found in the literature including microfabricated cell sorters, microfluidic chips for the patterning of cells and proteins and for the sizing and sorting of DNA fragments [149-154].

A range of other devices and microfluidic networks have been developed with polymer materials and successfully applied to applications other than separations [155-156, 143]. Examples include a cell-based biosensor, which was developed to analyse electro-active cells that have been exposed to irritants [157]. Non-biological applications include a microfluidic switch and a liquid core waveguide [158-159]. A microfluidic device, fabricated by a novel technique, solid-object printing, was reported by Whitesides and co-workers [160]. PDMS has excellent chemical and physical properties that make a versatile polymer material in terms of fabrication of microfluidic devices. PDMS is a good platform for components such as glass capillaries, silicone tubing, optical fibres and electronic devices, which facilitate flow control in the form of valves [161], pumps [162], mixers [163] and switches [164] encapsulated in microfluidic devices. A plethora of further applications of PDMS-based microfluidic devices can be found in the literature [165-168] and have been reviewed by Mc Donald et al. [169].

Lab-on-a-chip style polymer devices are being developed and introduced to the market by companies such as Caliper Technologies Corp. in California, who are particularly interested in enzyme and cell-based assays, and the analysis of DNA and RNA [170].

Surface modification of polymer substrates will play an integral role in the further development, understanding and application of polymer microfluidic devices [171]. The multitude of polymer materials commercially available and under development means that surface modification protocols are not as well understood as the chemical modification of glass or quartz. There are numerous ways in which polymer materials can be chemically altered on the surface and a key focus for many research groups is the development of routine, simple well-defined surface

modification techniques [172]. Pugmire et al. used an Excimer laser to fabricate microfluidic channels in PMMA under different atmospheres, causing changes in the surface characteristics of the polymer, which had a knock-on effect on the electroosmotic mobility through the microfluidic channels [173]. During laser ablation many reactive species are formed at the surface and in the gas phase. The interaction of these reaction products with the walls of the microfluidic channels results in a different chemical functionality at the surface compared to the bulk polymer itself [174]. As previously shown EOF is commonly used to manipulate fluids in micro-channels and EOF mobility is directly proportional to the fixed charge that the channel wall possesses [175]. Ultimately by fine-tuning the surface characteristics of the polymer material, during the laser ablation process, the electroosmotic flow can be controlled and made more reliable resulting in more reproducible measurements.

1.5 References

- 1 A.E. Greenberg, A.D. Eaton, L.S. Cleseri, *Standard Methods for the Examination of Water and Wastewater*, Phosphorus 4500-P, 18th Ed., ASPH, Washington, DC, USA, 1992, 166-181.
- 2 E.M. Thurman, *Organic Geochemistry of Natural Waters*, Martinus Nijhoff, Dr. W. Junk (Eds.), Dordrecht, The Netherlands, 1985, 497.
- 3 I.D. McKelvie, D.M.W. Peat, P.J. Worsfold, *Anal. Proc. Anal. Comm.*, 1995, **32**, 437-445.
- 4 Article, "Strong Tendency to Bloom Formation", *The Irish Times*, 5th January 2000, 2000, <http://www.ireland.com/newspaper/archive/>
- 5 Article, "Water Quality", *The Irish Times*, 20th May 2000, 2000, <http://www.ireland.com/newspaper/archive/>
- 6 Article, "Water Quality in Three Rivers Dramatically Worse", *The Irish Times*, 14th March 2000, 2000, <http://www.ireland.com/newspapers/archive/>
- 7 Article "EU to sue Ireland over Drinking Water Quality", *The Irish Times*, 15th May 2000., 2000, <http://www.ireland.com/newspapers/archive/>
- 8 Article, "Ireland not Implementing Directives within Deadlines", *The Irish Times*, 15th July 2000, 2000, <http://www.ireland.com/newspapers/archives/>

-
- 9 Article, "EU name the Three Irish Cities in its Wastewater List", *The Irish Times*, 21st March 2001, 2001, <http://www.ireland.com/newspapers/archives/>
- 10 L.A. Clementson, S. Wayte, *Water Research*, 1992, **26**, 1171.
- 11 D. Lambert, W.A. Maher, I. Hogg, *Water Research*, 1992, **26**, 645.
- 12 MicroChem: - A Miniaturised Industrial Chemical Sensing System, Work Package 5 report (unpublished), 1998, EU 5th Framework, No. BRP-CT98-0787.
- 13 W. Wieman, J. Beukenkamp, *Treatise on Analytical Chemistry*, I.M. Kolthoff, P.J. (Eds.), Wiley, New York, 1961, **5**, 317-402.
- 14 L.C.W. Baker, G. Foster, W. Tan, F. Scholnick, T.P. McCutcheon, *J. Am. Chem Soc.*, 1955, **77**, 2136.
- 15 D.F. Boltz, M.G. Mellon, *Ind. Eng. Chem. Anal. Ed.*, 1942, **19**, 873.
- 16 D.F. Boltz, M.G. Mellon, *Ind. Eng. Chem. Anal. Ed.*, 1948, **29**, 749.
- 17 G.P. Edwards, A.H. Molof, R.W. Schneeman, *J. Amer. Water Works Assoc.*, 1965, **57**, 917.
- 18 O. Sletten, C.M. Bach, *J. Amer. Water Works Assoc.*, 1961, **53**, 1031.
- 19 P.R. Haddad, P.E. Jackson, *Ion Chromatography: Principles and Applications*, Elsevier Science Publishers BV, Amsterdam, The Netherlands, 1990, 776.
- 20 M. van den Hoop, J.J. van Staden, *J. Chromatography A*, 1997, **770**, 321-328.
- 21 S.A. Glazier, M.A. Arnold, *Anal. Chem.*, 1988, **60**, 2540.
- 22 T. Yao, N. Kobayashi, T. Wasa, *Anal. Chim. Acta*, 1990, **238**, 339.
- 23 T.R. Crompton, *Comprehensive Water Analysis, Volume 1: Natural Waters*, Elsevier Applied Science, New York, USA, 1992, 524.
- 24 G. Mission, *Chemiker-Ztg.*, 1908, **32**, 633.
- 25 J. Ruzicka, *Anal. Chem.*, 1983, **55**, 1040A.
- 26 R.L. Benson, Y.B. Truong, I.D. Mc Kelvie, B.T. Hart, *Wat. Res.*, 1996, **30**, 1959.
- 27 P.J. Worsfold, J.R. Clinch, H. Casey, *Anal. Chim. Acta*, 1987, **197**, 43.
- 28 R.L. Benson, Y.B. Truong, I.D. McKelvie, B.T. Hart, G.W. Bryant, W.P. Hilkmann, *Water Research*, 1996, **30**, 1965.
- 29 T.A.H.M. Janse, P.F.A. Van der Wiel, G. Kateman, *Anal. Chim. Acta*, 1983, **155**, 91.
- 30 F. Mas, J.M. Estella, V. Cerda, *Water, Air, and Soil Pollution*, 1990, **52**, 360.

-
- 31 S. Motomizu, J.P. Susanto, M. Oshima, *Anal. Sci.*, 1995, **11**, 156.
- 32 H. Abderrazak, M. Dachraoui, B. Lendl, *Analyst*, 2000, **125**, 1211.
- 33 M. Aoyagi, Y. Yasumasa, T. Himeo, *J. Flow Injection Anal.*, 1992, **9**, 47.
- 34 D.J. Malcolme-Lawes, K.H. Wong, *Analyst*, 1990, **115**, 65.
- 35 K.S. Johnson, R.L. Petty, *Anal. Chem.*, 1982, **54**, 1185.
- 36 N. Graber, H. Lüdi, H.M. Widmer, *Sens. Actuators B*, 1990, **1**, 239 – 243.
- 37 A. Manz, D.J. Harrison, E. Verpoorte, J.C. Fettinger, A. Paulus, H.M. Widmer, *J. Chrom. B*, 1992, **513**, 253–258.
- 38 H.M. Widmer, J.F. Erard, G. Grass, *Intern. J. Environ. Anal. Chem.*, 1984, **18**, 1 –10.
- 39 J. Ruzicka, E.H. Hansen, *Flow Injection Analysis*, 2nd Ed., John Wiley and Sons, New York, USA, 1988.
- 40 M. Valcarel, M.D. Luque de Castro, *Flow Injection Analysis: Principles and Applications*, John Wiley and Sons, New York, USA, 1987.
- 41 E. Verpoorte, A. Manz, H. Ludi, A.E Bruno, F. Maystr, B. Krattiger, H.M. Widmer, *Sens. Actuators B*, 1992, **6**, 66-70.
- 42 A. Manz, J.C. Fettinger, E. Verpoorte, H. Lüdi, H.M. Widmer, D.J. Harrison, *Trends Anal. Chem.*, 1991, **10**, 144 – 149.
- 43 E. Verpoorte, *Introduction to Microfluidics for Chemical Applications*, Workshop Micro Chem. Sys., University of Hull, Hull, UK, July 2001, 2001.
- 44 M. Garn, P. Cevey, M. Gisin, C. Thommen, *Biotechnol. Bioeng.*, 1989, **34**, 423.
- 45 C.A. Monnig, J.W. Jorgenson, *Anal. Chem.*, 1991, **63**, 802.
- 46 T.S.J. Lammerink, M. Elwenspoek, J.H.J. Fluitman, *Proc. IEEE Workshop*, Salt Lake City, USA, 1993, 254-259.
- 47 V. Gass, B.H. van der Schoot, N.F. de Rooij, *Technical Digest, IEEE Transducers*, 1993, 1048.
- 48 A. van den Berg, P. Bergvald, *Proc. 2nd Int. Symp. MicroTAS*, Kluwer, The Netherlands, 1995, 181.
- 49 *Lab-on-a-Chip: The Revolution in Portable Instrumentation*, 2nd Ed., Technical Insights, Englewood, N.J., USA, 1997.
- 50 J. Cooper Mc Donald, D.C. Duffy, J.R. Anderson, D.T. Chiu, H. Wu, O.J.A. Schueller, G.M. Whitesides, *Electrophoresis*, 2000, **21**, 27-40.

-
- 51 S. Shojij, *Topics in Curr. Chem.*, 1998, **194**, 163.
- 52 P. Gravesen, J. Branbjerg, O.S. Jensen, *J. Micromech. Microeng.*, 1993, **3**, 169.
- 53 P.A. Greenwood, G.M. Greenway, *Trends in Anal. Chem.*, 2002, **21 (11)**, 726.
- 54 N.A. Polsen, M.A. Hayes, *Anal. Chem.*, 2001, **73**, 315A.
- 55 S. Thompson, *Analysis of a flat plat in laminar flow: Basic equations and solutions*, ME 673, San Diego State University, 1999,
<http://thermal.sdsu.edu/profs/Bhattacharjee/sooby/classes/f99/me673f99/sthompson/slides/conclusion.html>
- 56 I. Levine, *Physical Chemistry*, 2nd Ed., Mc-Graw-Hill, 1983.
- 57 M. Fremantle, *Science*, 2000, **77**, 27-36.
- 58 Electronic Library, Reynolds Number, Infonautics Corporation,
<http://www.encyclopedia.com/articlesnew/39531.html>
- 59 A. Daridon, V. Fascio, J. Lichtenberg, R. Wütrich, H. Langen, E. Verpoorte, N.F. de Rooij, *Fresenius J. Anal. Chem.*, 2001, **371**, 261-269.
- 60 J.P. Krog, H. Dirac, B. Fabius and Peter Graveson, A. Dairdon, Jan Lichtenberg, Elisabeth Verpoorte and Nico F. de Rooji, G. Pennarum-Thomas, M. Sequeira and D. Diamond, M. Denninger, O. Geschke and J. Kutter, S. Horowitz, C. Strec, P. Charles, L. Cognet, *Proc. Micro TAS '00*, Micro Total Analysis Systems 2000, Enschede, Netherlands, 2000, A. van den Berg, W. Olthuis, and P. Bergveld (Eds.), Kluwer Academic Publishers: Dordrecht, Netherlands, 2000, 419-422.
- 61 S.F.Y. Li, *Capillary Electrophoresis*, Elsevier, New York, USA, 1994.
- 62 D.J. Harrison, P.G. Galvina, *Sens. Actuators B*, 1993, **10**, 107-116.
- 63 S.C. Jacobsen, T.E. Mc Knight, J.M. Ramsey, *Anal. Chem.*, 1999, **71**, 4455-4459.
- 64 P.D.I. Fletcher, S.J. Haswell, V.N. Paunov, *Analyst*, 1999, **124**, 1273.
- 65 S.J. Haswell, *Analyst*, 1997, **122**, 1R.
- 66 J.S. Danel, G. Delapierre, *J. Micromech. Microeng.*, 1991, **1**, 187.
- 67 E.W. Becker, W. Erfeld, P. Hagman, A. Maner, D. Münchmeyer, *Microelec. Eng.*, 1986, **4**, 35.
- 68 J. Knapp, G. Andrae, D. Petersohn, *Sens. Actuators A*, 1990, **23**, 1080-1089.
- 69 A. Manz, *Chimia*, 1996, **50**, 140 - 143.

-
- 70 A. Daridon, M. Sequeira, G. Pennarun-Thomas, J. Lichtenberg, E. Verpoorte, D. Diamond, N.F. de Rooij, *Proc. Eurosensors XIV*, Copenhagen, Denmark, 2000, 815-818.
- 71 Supplied by Steffen Horowitz, Gesellschaft fur Silizium-Mikrosysteme (GeSim) mbH, Rossendorfer Technologie Zentrum, Grossermannsdorf, Dresden, Germany.
- 72 G. Wallis, D.I.J. Pomerantz, *Appl. Phys.*, 1969, **40**, 3946.
- 73 O. Geschke, M. Denninger, P. Telleman, and J.P. Kutter, *Protective Coatings in Microfluidic Systems*, Pittcon 2000, New Orleans, USA, 2000 (poster presentation).
- 74 J. Bardeen, W.H. Brattain, *Phys. Rev.*, 1948, **74**, 230-233
- 75 M. Mehregany, A.S. Dewa, *Part I: MEMS Overview, Introduction to MicroElectroMechanical Systems and the Multiuser MEMS Processes*, MCNC Short Course Handbook, CASE Western Reserve University, Cleveland, OH, USA, 1993, <http://isu.iisc.ernet.in/~deena/mems/partI/TOC.html>
- 76 S.C. Terry, J.H. Jerman, J.B. Angel, *IEEE Trans. Electron. Dev.*, ED-26, 1979, 1880.
- 77 G.T.A. Kovacs, K. Petersen, M. Albin, *Anal. Chem.*, 1996, **68**, 407A.
- 78 B. van der Schoot, P. Bergveld, *Sens. Actuators B*, 1985, **8**, 11.
- 79 H. van Lintel et al, *Sens. Actuators B*, 1988, **15**, 153-167.
- 80 A. Manz, N. Graber, H.M. Widmer, *Sens. Actuators B*, 1990, **1**, 244-248
- 81 R.A. Mathies, P.C. Simpson, A.T. Woolley, *Proc. MicroTAS '98*, Banff, Alberta, Canada, 1998, 1-7.
- 82 J.van Kuijk, *Numerical Modeling of Flows*, Ph.D. Thesis, University of Twente, The Netherlands, ISBN 90-9010395-3, 1997.
- 83 A.T. Woolley, D. Hadley, P. Landre, A.J. de Mello, R.A. Mathies, M.A. Northrup, *Anal. Chem.*, 1996, **68**, 4081.
- 84 M.S. Ibrahim, R.S. Lofts, P.B. Jahrling, E.A. Henchal, V.W. Weedn, M.A. Northrup, P. Gelgrader, *Anal. Chem.*, 1998, **70**, 2013-2017.
- 85 G.H.W. Sanders, A. Manz, *Trends Anal. Chem.*, 2000, **19(6)**, 364-378.
- 86 C.Ashton, *Chem. Ind.*, 1999, 422.
- 87 R.F. Service, *Science*, 1998, **282**, 396.

-
- 88 F. von Heeren, E. Verpoorte, A. Manz, W. Thormann, *Anal. Chem.*, 1996, **68**, 2044.
- 89 N. Chiem, D.J. Harrison, *Anal. Chem.*, 1997, **69**, 373-378.
- 90 L.B. Koutny, D. Schmalzing, T.A. Taylor, M. Fuchs, *Anal. Chem.*, 1996, **68**, 18.
- 91 A.K. Deisingh, *Analyst*, 2003, **128**, 9-11.
- 92 J. De Gaspari, *Mech. Eng.*, 2002, **38**.
- 93 D.J. Harrison, P.G. Glavina, *Sens. Actuators B*, 1993, **10**, 107-116.
- 94 C.S. Effenhauser, G.J.M. Bruin, A. Paulus, *Electrophoresis*, 1997, **18**, 2203.
- 95 C.L. Colyer, T. Tang, N. Chiem, D.J. Harrison, *Electrophoresis*, 1997, **18**, 1733.
- 96 J.P. Kutter, *Trends Anal. Chem.*, 2000, **19(6)**, 353-363.
- 97 D.E. Raymond, A. Manz, H.M. Widmer, *Anal. Chem.*, 1994, **66**, 2858-2865.
- 98 S.C. Jacobsen, R Hergenröder, L.B. Koutny, J.M. Ramsey, *Anal. Chem.*, 1994, **66**, 1114-1118.
- 99 Z. Liang, N. Chiem, G. Ocvirk, T. Tang, K. Fluri, D.J. Harrison, *Anal. Chem.*, 1996, **68**, 1040-1046.
- 100 J.M. Slater, E.J. Watt, *Analyst*, 1994, **119**, 2303-2307.
- 101 A.T. Woolley, K. Lao, A.N. Glazer, R.A. Mathies, *Anal. Chem.*, 1998, **70**, 684-688.
- 102 J. Khandurina, S.C. Jacobson, L.C. Waters, R.S. Foote, J.M. Ramsey, *Anal. Chem.*, 1999, **71**, 1815-1819.
- 103 Y. Shi, P.C. Simpson, J.R. Scherer, D. Wexler, C. Skibola, M.T. Smith, R.A. Mathies, *Anal. Chem.*, 1999, **71**, 5354.
- 104 L.C. Waters, S.C. Jacobson, N. Krouchtina, J. Khandurina, R.S. Foote, J.M. Ramsey, *Anal. Chem.*, 1998, **70**, 5172-5176.
- 105 R.N.C. Daykin, S.J. Haswell, *Anal. Chim. Acta*, 1995, **313**, 155-159.
- 106 G.N. Doku, S.J. Haswell, *Anal. Chim. Acta*, 1999, **382**, 1-13.
- 107 P.H. Petsul, G.M. Greenway, S.J. Haswell, *Anal. Chim. Acta*, 2001, **428**, 155-161.
- 108 G.M. Greenway, S.J. Haswell, P.H. Petsul, *Anal. Chim. Acta*, 1999, **387**, 1-10.

-
- 109 O. Rötting, W. Rpkke, H. Becker, " Polymer Microfabrication Technologies", *Business Briefing: Future Drug Discovery, Technology and Services*, Mildendo GmbH, Jena, Germany (<http://www.mildendo-fluidics.com>), 2001, 1-6.
- 110 L. Martynova, L.E. Locascio, M. Gaitan, G.W. Kramer, R.G. Christensen, W.A. Mac Crehan, *Anal. Chem.*, 1997, **69**, 4783-4789.
- 111 A. de Mello, *Lab Chip*, 2002, **2**, 31N.
- 112 N.G. Mc Crum, C.P. Buckley, C.B. Bucknall, *Principles of Polymer Engineering*, Oxford University Press, New York, USA, 1998, Chap. 8.2, 326.
- 113 J. Greene, Elastomeric (Rubber) Material, California State University, Chico, California, USA, 10th December 1999, 1999, <http://www.csuchico.edu/~jgreene/itec041/m41-ch09/sld001.htm>
- 114 Y. Xia, E. Kim, X.-M. Zhao, J.A. Rogers, M. Prentiss, G.M. Whitesides, *Science*, 1996, **273**, 347-349.
- 115 M.A. Roberts, J.S. Rossier, P. Bercier, *Anal. Chem.*, 1997, **69 (11)**, 2035-2042.
- 116 P. Renaud, H. van Lintel, M. Heuschkel, L. Guenin, *Proc. Micro-TAS' 98*, Micro Total Analysis Systems, Banff, Canada, 1998, 17-22.
- 117 A. Both, W. Bacher, M. Hecke, K.-D. Müller, R. Ruprecht, M. Stohrmann, *Microsystem Tech.* 2, 1998, 104-108.
- 118 E.W. Becker, W. Ehrfeld, P. Hagmann, A. Maner, D. Münchmeyer, *Microelec. Eng.*, 1986, **4**, 35-56.
- 119 M. Gower, N. Rizvi, "Applications of Laser Ablation to Microengineering", 2000, Exitech Ltd., Oxford, UK.
- 120 N. Rizvi, *Proc. Microeng. '99*, Congress for Microsystems and Precision Engineering, Stuttgart, Germany, 1999, 161-168.
- 121 N. Rizvi, *Symp. On Design Test and μ Fab. Of MEMS and MOEMS*, 1999, SPIE, Paris, France, **3680**, 546-552.
- 122 Y. Xia, G.M. Whitesides, *Annu. Rev. Mater. Sci.*, 1998, **28**, 153-184.
- 123 Y. Xia, G.M. Whitesides, *Langmuir*, 1997, **13**, 2059-2067.
- 124 X.-M. Zhao, Y. Xia, G.M. Whitesides, *J. Mater. Chem.*, 1997, **7**, 1069-1074.
- 125 X.-M. Zhao, Y. Xia, G.M. Whitesides, *Adv. Mater.*, 1996, **8**, 420-424.
- 126 Y. Xia, E. Kim, G.M. Whitesides, *J. Am. Chem. Soc.*, 1996, **118**, 5722-5731.
- 127 E. Kim, Y. Xia, X.-M. Zhao, G.M. Whitesides, *Adv. Mater.*, 1997, **9**, 651-654.

-
- 128 D. Qin, Y. Xia, G.M. Whitesides, *Adv. Mater.*, 1996, **8(11)**, 917-919.
- 129 A. Kumar, G.M. Whitesides, *Appl. Phys. Lett.*, 1993, **63**, 2002-2004.
- 130 S.J. Clarson, J.A. Semlyen, *Siloxane Polymers*, 1993, Prentice Hall, Englewood Cliffs, New Jersey, USA.
- 131 S. Brettain, K. Paul, X.-M. Zhao, G.M. Whitesides, *Physics World*, 1998, **11**, 31-36.
- 132 Y. Xia, G.M. Whitesides, *Angew. Chem. Int. Ed. Engl.*, 1998, **37**, 550-575.
- 133 H.C. Haverkorn, P.E.J. Legierse, G.E. Thomas, *Phillips Tech. Rev.*, 1982, **40**, 287-297.
- 134 E. Delamarche, H. Schmid, H.A. Biebuyck, B. Michel, *Adv. Mater.*, 1997, **9**, 741-746.
- 135 R.M. Mc Cormick, R.J. Nelson, M.G. Alonso-Amigo, D.J. Benvegno, H.H. Hooper, *Anal. Chem.*, 1997, **69**, 2626-2630.
- 136 T. Kenny, M. Tang, P. Griffin, *Natl. Nanofab. Users Network*, 2001, Stanford Nanofabrication Facility, 62-63.
- 137 H. Becker, U. Heim, *Sens. Actuators A*, 2000, **83(1-3)**, 130-135.
- 138 M. Hecke, W. Bacher, K.D. Muller, *Microsystem Tech.*, 1998, **4**, 122-124.
- 139 R.W. Jaszewski, H. Schrift, J. Gobrecht, P. Smith, *Microelec. Eng.*, 1998, **41 / 42**, 575-578.
- 140 J. Xu, L. Locascio, M. Gaitan, C.S. Lee, *Anal. Chem.*, 2000, **72**, 1930-1933.
- 141 H. Becker, W. Dietz, P. Dannberg, *Proc. Micro-TAS' 98*, Micro Total Analysis Systems, Banff, Canada, Kluwer Academic Publishers, Dordrecht, Netherlands, 1998, 253-256.
- 142 C.S. Effenhauser, G.J.M. Bruin, A. Paulus, M. Ehrat, *Anal. Chem.*, 1997, **69**, 3451-3457.
- 143 D.C. Duffy, J. Cooper Mc Donald, O.J.A. Schueller, G.M. Whitesides, *Anal. Chem.*, 1998, **70**, 4974-4984.
- 144 S.M. Ford, B. Kar, S. Mc Whorter, J. Davies, S.A. Soper, M. Klopff, G. Calderon, V. Saile, *J. Microcol. Sep.*, 1998, **10(5)**, 413-422.
- 145 Y. Liu, J.C. Fanguy, J.M. Bldesoe, C.S. Henry, *Anal. Chem.*, 2000, **72**, 5939-5944.
- 146 Z. Wu, N. Xanthopoulos, F. Reymond, J.S. Rossier, P. Bercier, H. Girault, *Electrophoresis*, 2002, **23**, 782-790.

-
- 147 L Licklider, X.-Q. Wang, A. Deasi, Y.-C. Tai, T.D. Lee, *Anal. Chem.*, 2000, **72**, 367.
- 148 J. Kameoka, H.G. Craighead, H. Zhang, J. Henion, *Anal. Chem.*, 2001, **73**, 1935-1941.
- 149 E. Delamarche, A. Bernard, H. Schmid, B. Michel, H. Biebuyck, *Science*, 1997, **276**, 779-781.
- 150 S. Liu, Y. Shi, W.W. Ja, R.A. Mathies, *Anal. Chem.*, 1999, **71**, 566-573.
- 151 A.Y. Fu, C. Spence, A. Scherer, F.H. Arnold, S.R. Quake, *Nat. Biotechnol.*, 1999, **17**, 1109-1111.
- 152 A.T. Woolley, R.A. Mathies, *Anal. Chem.*, 1995, **67**, 3676-3680.
- 153 H.P. Chou, C. Spence, A. Scherer, S.R. Quake, *Proc. Natl. Acad. Sci. USA*, 1999, **96**, 11-13.
- 154 S. Takayama, J. Cooper Mc Donald, E. Ostuni, M.N. Laing, P.J.A. Kenis, R.F. Ismagilov, G.M. Whitesides, *Proc. Natl. Acad. Sci. USA*, 1999, **96**, 5545-5548.
- 155 M.A. Burns, et al, *Science*, 1998, **282**, 484-487.
- 156 H. Becker, C. Gärtner, *Electrophoresis*, 2000, **21**, 12-26.
- 157 B.D. De Busschere, D.A. Borkholder, G.T.A. Kovacs, *Solid State Sens. Actuator Workshop*, 1998, Hilton Head, SC, USA, 358-362.
- 158 J.A. Schueller, X.-M. Zhao, G.M. Whitesides, S.P. Smith, M. Prentiss, *Adv. Mater.*, 1999, **11**, 37-41.
- 159 D.C. Duffy, O.J.A. Schueller, S.T. Brittain, G.M. Whitesides, *J. Micromech. Microeng.*, 1999, **9**, 211-217.
- 160 J. Cooper Mc Donald, M.L. Chabiny, S.J. Metallo, J.R. Anderson, A.D. Stroock, G.M. Whitesides, *Anal. Chem.*, 2002, **74**, 1537-1545.
- 161 D.J. Beebe, J.S. Moore, Q. Yu, R.H. Liu, M.L. Kraft, B.-H. Jo, C. Devadoss, *Proc. Natl. Acad. Sci. USA*, 2000, **97**, 13488-13493.
- 162 J.R. Anderson, J.C. Mc Donald, H.A. Stone, G.M. Whitesides, *Anal. Chem.*, 2002, (submitted for publication).
- 163 A.D. Stroock, S.K.W. Dertinger, A. Adjari, I. Mezic, H.A. Stone, G.M. Whitesides, *Science*, 2002, **295**, 647-651.
- 164 R.F. Ismagilov, D. Rosmarin, P.J.A. Kenis, D.T. Chiu, W. Zhang, H.A. Stone, G.M. Whitesides, *Anal. Chem.*, 2001, **73**, 4682-4687.
- 165 J.C. Mc Donald, S.J. Metallo, G.M. Whitesides, *Anal. Chem.*, 2001, **73**, 5645-5650.

-
- 166 E. Eteshola, D. Leckband, *Sens. Actuators B*, 2001, **72**, 129-133.
- 167 J. Gao, J. Xu, L.E. Locascio, C.S. Lee, *Anal. Chem.*, 2001, **73**, 2648-2655.
- 168 Y. Jiang, P.-C. Wang, L.E. Locascio, L.P. Lee, *Anal. Chem.*, 2001, **73**, 2048-2053.
- 169 J.C. Mc Donald, G.M. Whitesides, *Acc. Chem. Res.*, 2002, **35(7)**, 491-499.
- 170 A.R. Kopf-Sill, *Micro-TAS '00*, A. van den Berg (Eds.), Kluwer Academic Publ., 2000, 233-238.
- 171 B. Vaidya, S.A. Soper, R.L. Mc Carley, *Analyst*, 2002, **127**, 1289-1292.
- 172 A.C. Henry, T.J. Tutt, M. Galloway, Y.Y. Davidson, C.S. Mc Whorter, S.A. Soper, R.L. Mc Carley, *Anal. Chem.*, 2000, **72**, 5331-5337.
- 173 D.L. Pugmire, E.A. Wadell, R. Haasch, M.J. Tarlov, L.E. Locascio, *Anal. Chem.*, 2002, **74**, 871-878.
- 174 T.J. Johnson, D. Ross, M. Gaitan, L.E. Locascio, *Anal. Chem.*, 2001, **73**, 3656-3661.
- 175 D. Figeys, D. Pinto, *Anal. Chem.*, 2000, **72**, 330A.

2 The Vanadomolybdophosphoric Acid (or Yellow) Method

Phosphorus is a nutrient required by all organisms. Inorganic phosphorus is found predominantly in the form of phosphates with orthophosphate being the most stable form. Wastewater effluent, food residues, detergents, fertilisers, animal waste, industrial discharge and drinking water treatment all contribute significantly to phosphate levels in natural waters [1]. Spectrophotometric methods, based on colorimetric detection have been widely applied for the determination of orthophosphate. Almost all wet chemical assays of phosphate are based on the well-known molybdenum blue method, which is ideal for visual titrations, because of the deep blue coloured complex formed. It is also suitable for colorimetric measurements based on tungsten filament sources because the molybdenum blue complex absorbs in the 650 - 700 nm region of the visible spectrum. However this approach will not transfer easily to a miniaturised format for several important reasons. Ascorbic acid is used in the reduction step of the formation of the molybdenum blue complex. In the presence of ascorbic acid the reagent tends to form a finely dispersed precipitate and the ascorbic acid itself is only stable for a restricted time period. This makes the blue method very unattractive not only because the precipitate could rapidly block the narrow microfluidic channels, but also from the point of view of meeting the target of one-year autonomous functioning for future miniaturised environmental monitoring instruments.

However, the yellow method (vanadomolybdophosphoric acid method) has recently become an attractive alternative. This colorimetric technique involves the formation of a heteropoly acid, yellow vanadomolybdophosphoric acid, whereby ammonium molybdate, $(\text{NH}_4)_6\text{Mo}_7\text{O}_{24}\cdot 7\text{H}_2\text{O}$, is reacted with ammonium metavanadate, NH_4VO_3 , under acidic conditions [2]. The combined reagent and sample containing orthophosphate react to form the above-mentioned heteropoly acid, $(\text{NH}_4)_3\text{PO}_4\text{NH}_4\text{VO}_3\cdot 16\text{MoO}_3$, resulting in a distinct yellow colour arising from strong absorbance below 400 nm. The reagent has been stored for approx. 18 months in a brown glass vessel in the dark. No precipitation has been noted to date. In this chapter the yellow method is examined and the chemical reagent is shown to have a lifetime in excess of one year with no significant loss in performance.

2.1 Speciation of Phosphorus

Phosphorus fractions have been extensively named and categorised, the following is a brief description of the most significant fractions to be measured. Phosphorus in natural waters and sediment occurs predominantly as orthophosphate, but also as organic and condensed phosphates with various different molecular weights.

The most frequently analysed phosphorus quantities are total phosphorus (TP) and dissolved reactive phosphorus (DRP), because they are relatively easy to determine [3]. The total phosphorus content is comprised of both dissolved and suspended entities, the former is defined as the fraction that is still present after filtration through a 0.45 μm membrane filter.

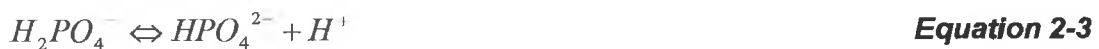
The total dissolved phosphorus (TDP) fraction is made up of dissolved inorganic phosphorus (DIP), which is a combination of the orthophosphate and condensed phosphates fractions, and the dissolved organic phosphorus (DOP). The DOP partially hydrolyses to orthophosphate when reacted with acidic molybdate, which is used in the standard blue method for the determination of orthophosphate. The term dissolved reactive phosphorus (DRP) describes the measurable orthophosphate concentration in a water body.

Orthophosphate determinations are important benchmarks in measuring the "bioavailable" dissolved phosphorus concentration for the process of photosynthesis [4]. There are three different forms of orthophosphate ions present in water. The pH of the water body determines which form is prevalent.

The Henderson-Hasselbach equation defines the pH of a solution of a conjugate acid-base pair in terms of the dissociation constant of the weak acid and the equilibrium concentrations of the acid and its conjugate base. pK_a values can be related to pH values by using Equation 2-1, where $[\text{A}^-]$ is the molar concentration of the salt (dissociated species) and $[\text{HA}]$ is the concentration of the undissociated acid. When the concentration of the salt and acid are equal, the pH of the system equals the pK_a of the acid [5].

$$pH = pK_a + \log \frac{[A^-]}{[HA]} \quad \text{Equation 2-1}$$

When $pK = pH$, then $[HA]$ is equal to $[A]$. Values of pK_a yield quantitative information concerning acid strength; very strong acids being characterized by undefined pK values, semi-strong acids being characterized by small pK_a values: and weak acids being characterized with larger pK_a values. In the three equations 2-3, 2-4 and 2-5 the dissociation of o-phosphoric acid is given. The pK_a values are also tabulated in Table 2-1.



The dissociation constants or pK_a values for o-phosphoric acid are shown in Table 2-1.

Table 2-1 Dissociation Constants of o-Phosphoric Acid

Phosphoric Acid	pKa1	pKa2	pKa3
H_3PO_4	$H_2PO_4^-$	HPO_4^{2-}	PO_4^{3-}
2.13	7.2	12.36	

The ion PO_4^{3-} doesn't naturally occur in water. It is nearly always a mixture of HPO_4^{2-} and $H_2PO_4^-$ that is found. Therefore in all analyses orthophosphate concentrations are reported in terms of hydrogen phosphate ions [6]. The distribution curves are also given for the three species of phosphorus based on the pH of the solution in Figure 2-1, where alpha, α is the fraction of any species in relation to the total concentration at a given pH. The three pK_a values are determined from Equation 2-1 and are given in Table 2-1. In Figure 2-1 the three intersecting points on the distribution curve correspond to the pK_a values of 2.13, 7.2 and 12.36 for pK_a 1, 2 and 3 respectively.

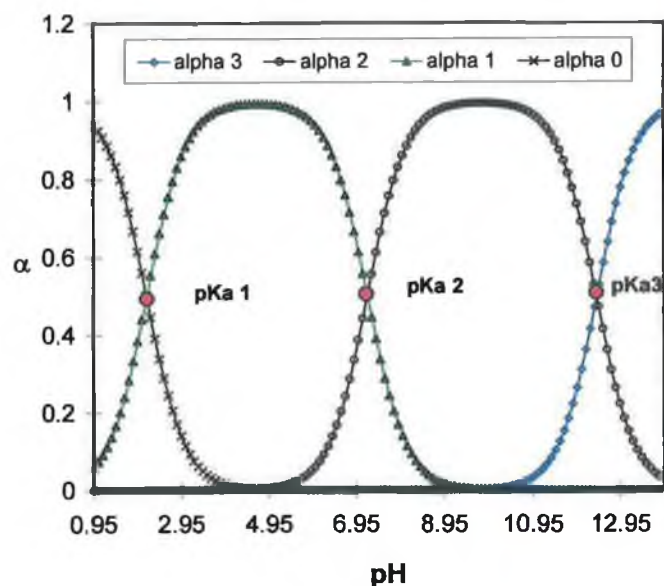


Figure 2-1 Distribution curves for the speciation of phosphorus*

2.2 Reagent / Stock Solution Preparation

The yellow complex has a three-component composition. All chemicals were of analytical-reagent grade and the solutions were prepared with double deionised water. Ammonium molybdate, $(\text{NH}_4)_6\text{Mo}_7\text{O}_{24}\cdot 4\text{H}_2\text{O}$, ammonium metavanadate, NH_4VO_3 , and potassium dihydrogen phosphate, KH_2PO_4 , were obtained from FLUKA Chemicals (Sigma-Aldrich Ireland Ltd., Tallaght, Dublin 24, Ireland). Hydrochloric acid (37% wt. in water) was obtained from Aldrich (same as FLUKA Chemicals). The relative quantities used are shown in Table 2-2.

Table 2-2 Components of the yellow method combined reagent

Component	Structure	Aliquot
Ammonium molybdate	$(\text{NH}_4)_6\text{Mo}_7\text{O}_{24}\cdot 4\text{H}_2\text{O}$	7.143 g/L
Ammonium metavanadate	NH_4VO_3	0.357 g/L
Conc. Hydrochloric acid (37%)	HCl	95 ml

* Amended from literature; D. Diamond, V.H.A. Hanratty "Spreadsheet Applications in Chemistry using Microsoft Excel", Wiley Interscience, USA, 1997.

Milli-Q water was used throughout the analysis. It was taken from the Millipore Milli-Ro Plus 30 system. The water purification system includes two purification steps to produce distilled quality water.

1. The ammonium metavanadate was dissolved in 300 ml of deionised water by heating to boiling, cooled and then 95 ml of conc. HCl was added.
2. The ammonium molybdate was dissolved in 300 ml of deionised water with vigorous shaking
3. Both mixtures were added to a 1 L volumetric flask and made up to the mark with deionised water.

In the case of the orthophosphate-containing sample, potassium dihydrogen phosphate, $K_2H_2PO_4 \cdot 7H_2O$ was placed in a glass Petrie dish and dried in an oven for 3 hours at $80^\circ C$ (M.W. after drying: 136.09 g / mol). A 50 mgL^{-1} P (A.M.: 31 g / mol) stock solution was prepared by addition of 219.5mg of the anhydrous salt to a 1L volumetric flask. Then 10ml of 4M sulphuric acid, H_2SO_4 , was added and made up to the mark with deionised water. The 4M sulphuric acid aids the preservation of the stock solution. From the 50 mgL^{-1} P stock solution, a series of standards over the concentration range 0 – 50 mgL^{-1} were prepared.

The yellow method complex was prepared by mixing the combined reagent and the orthophosphate-containing sample in a 1:1 ratio. All orthophosphate contained within an aqueous sample, upon reaction with the reagent, is converted to phosphorus, and is denoted as PO_4^{3-} - P. 25 ml standard solutions were prepared by dilution as shown in Table 2-3 and mixed with 25 ml of reagent to resulting in the formation of the heteropoly complex.

For all the conventional 1 cm cuvette analyses described in this chapter the yellow heteropoly complex was prepared, as described above, prior to the absorbance measurement. All analytical measurements were made in triplicate to verify reproducibility, unless otherwise stated.

Table 2-3 Dilution factors in the preparation of the standard and sample solutions

Conc. $\text{PO}_4^{3-}\text{-P}$ [mgL^{-1}]	Vol. $50 \text{ mgL}^{-1} \text{ P}$ [ml]	Vol. dist. H_2O [ml]
0	0	25
0.5	0.25	24.75
1	0.5	24.5
2.5	1.25	23.75
5	2.5	22.5
10	5	20
20	10	15
25	12.5	12.5
30	15	10
40	20	5
50	25	0

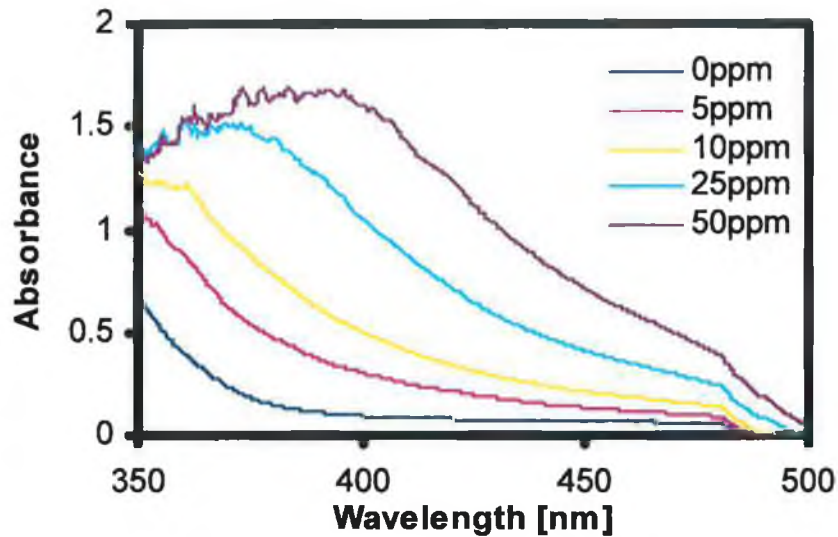


Figure 2-2 Typical UV spectrum of the yellow vanadomolybdophosphoric acid complex over the concentration range $0 - 50 \text{ mgL}^{-1} \text{ PO}_4^{3-}\text{P}$ with a tungsten-halogen lamp as source

The absorbance spectra of a selection of $\text{PO}_4^{3-}\text{-P}$ samples between $0 - 50 \text{ mgL}^{-1}$ over the wavelength range of $350 - 500 \text{ nm}$ are shown in Figure 2-2. It is evident that the complex absorbs strongly below a wavelength of 425 nm , peaking between approx. $375 - 400 \text{ nm}$.

2.3 Apparatus

Analysis was carried out in a conventional 1-cm cuvette in a system based on the schematic in Figure 2-3.

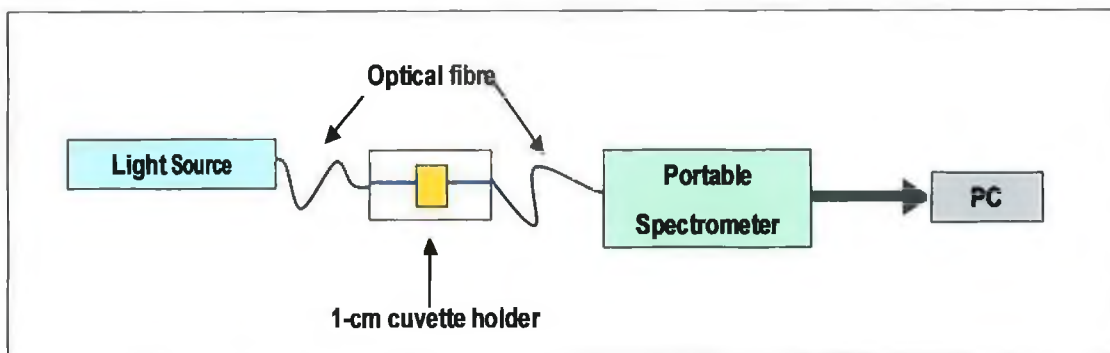


Figure 2-3 Schematic of the conventional bench system for the 1-cm cuvette measurements

A range of light sources was initially tested to find the most suitable one that provided the best light intensity below 400 nm. The four light sources assessed were:

1. A tungsten-halogen lamp (Model: LS-1, Ocean Optics B.V., Duiven, The Netherlands)
2. A deuterium lamp (Model: DH2000, Avantes, Soerense Zand, The Netherlands)
3. A blue LED (Model: GaN LED, Nichia Corp., Tokushima, Japan)
4. A UV-LED (Model: NSHU-550E, Nichia Corp., Tokushima, Japan)

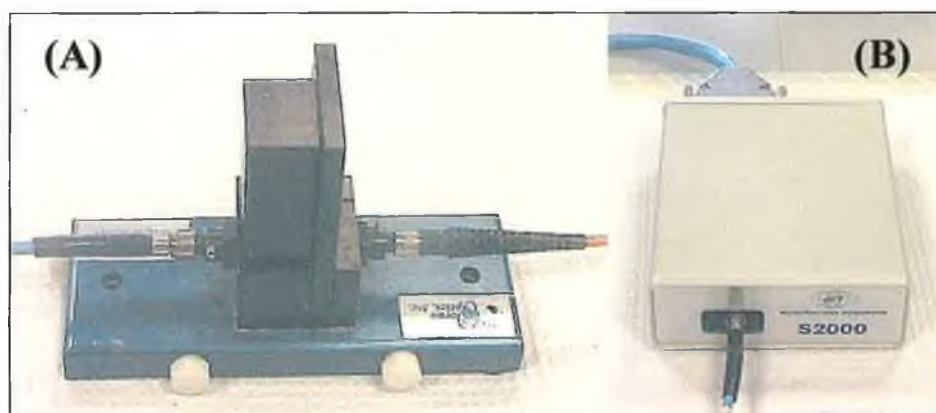


Figure 2-4 Photograph of the 1-cm cuvette holder (A) and the portable spectrometer (B) by Ocean Optics

A 1 cm quartz cuvette was used for all measurements (Model: Z27, 665-0, Sigma-Aldrich Ireland Ltd., Dublin, Ireland). It was secured in a portable holder with a black aluminium cover (Model: CUV-UV / CUV-Cover), which eliminated all ambient light and blocked the light path when taking dark current measurements (Figure 2-4 (A)). The conventional set up comprised a portable S-2000 mini-spectrometer (Figure 2-4 (B)) with accompanying software, the OOIBase₃₂ Program, all of which were obtained from Ocean Optics (Ocean Optics B.V., Duiven, The Netherlands). Light was transmitted from the lamp through the cuvette holder to the spectrometer via optical fibres (Edmund Optics Ltd., York, UK). The spectrometer was connected to a PC via a ribbon cable, and an I/O card (National Instruments, Newbury, Berkshire, UK) was used to retrieve data from the spectrometer.

2.4 Choice of Light Source

Initially the intensity of each light source was measured over the wavelength range 335 – 1000 nm. The integration time was set as 50 ms with a boxcar smoothing of 20. Initially the challenge presented with using the yellow method was the fact that the yellow complex absorbed strongly below 400 nm and commonly employed sources did not emit strongly in this region.

The tungsten-halogen lamp is a small, portable lamp with a wavelength range of 300 – 900 nm requiring a 12V DC battery supply. Although the tungsten-halogen lamp does emit light in the lower UV range, the broadband source has poor intensity where the yellow complex absorbs as shown in Figure 2-5. This, coupled with the large power supply necessary to generate light, makes it a less than ideal source for the application.

The emission range of the deuterium lamp is marginally more suited to the yellow complex than the tungsten-halogen lamp. The intensity of the light is better below 400 nm as shown in Figure 2-5. However the same problem applies to the deuterium as the tungsten-halogen source.

The gallium nitride, GaN-LED emits a pale blue / violet light. The GaN-LED is a broadband source, which has a peak output in the 428 – 430 nm spectral region and an energy bandgap of approx. 3.4 V. Again the light intensity below 400 nm wasn't sufficient as shown in Figure 2-5. The only benefits of incorporating this LED in the optical detection compared to a conventional light source, are the lower power required to generate the light, typically 3 – 3.5 V and the small size of the device.

It wasn't until Nichia invented the UV-LED however that an ideal light source became available for the yellow method. The UV-LED is a narrowband source with the peak output of λ_{\max} 375 nm with a 10° divergence. It has an energy bandgap of ca. 3.9 V and requires a battery of approx. 4 V [7].

The emission spectra of the four light sources were compared over the desired wavelength region for yellow method analysis of 330 – 430 nm. Clearly it is shown in Figure 2-5 that the UV-LED has the strongest emission spectrum below 400nm. This, coupled with its minimal power consumption and its compact, portable size make it a superior choice to both its conventional counterparts and other LED's, such as the blue GaN LED.

However, there was a more convincing reason why the UV-LED was chosen as the most suitable light source for yellow method analysis. The emission data for all four light sources and the absorbance data of a PO_4^{3-} - P sample of 50 mgL^{-1} concentration, were normalised and plotted on the same scale using Sigma Plot software. The good coherence of the UV-LED with the absorbance spectrum of the heteropoly complex is demonstrated in Figure 2-5.

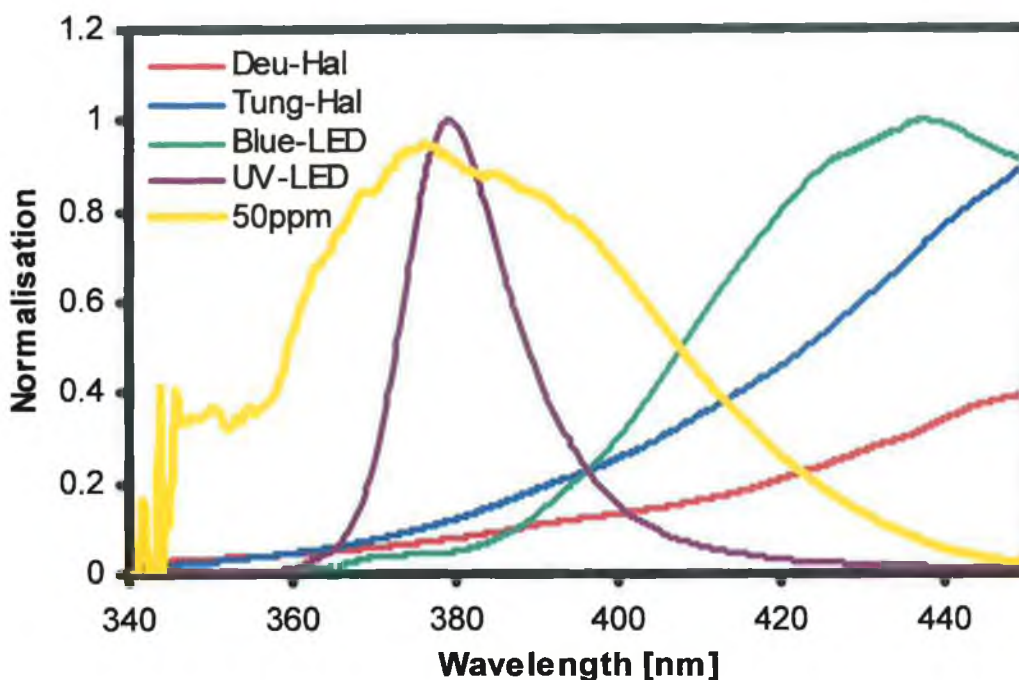


Figure 2-5 Normalised plot showing the UV-LED as the most suitable light source for measuring the absorbance of the yellow complex of a $50 \text{ mgL}^{-1} \text{PO}_4^{3-} - \text{P}$

The UV-LED was chosen as the most suitable light source for the yellow method. To prove that this was the case and to demonstrate the chemical stability of the method a linearity study was undertaken.

2.5 Calibration

A calibration study was carried out with the Nichia UV-LED as the light source. A set of standard solutions was prepared from the 50 mgL^{-1} stock (Section 2.1) by dilution over the concentration range $0 - 50 \text{ mgL}^{-1} \text{P}$. Each 25 ml standard was then mixed with 25 ml of the combined reagent in a 50 ml volumetric flask and the sample was left to stand to allow the reaction to reach completion at room temperature for approx. 5 min. The sample was then poured into the 1 cm cuvette ready for analysis. Absorbance measurements for each sample were made in triplicate.

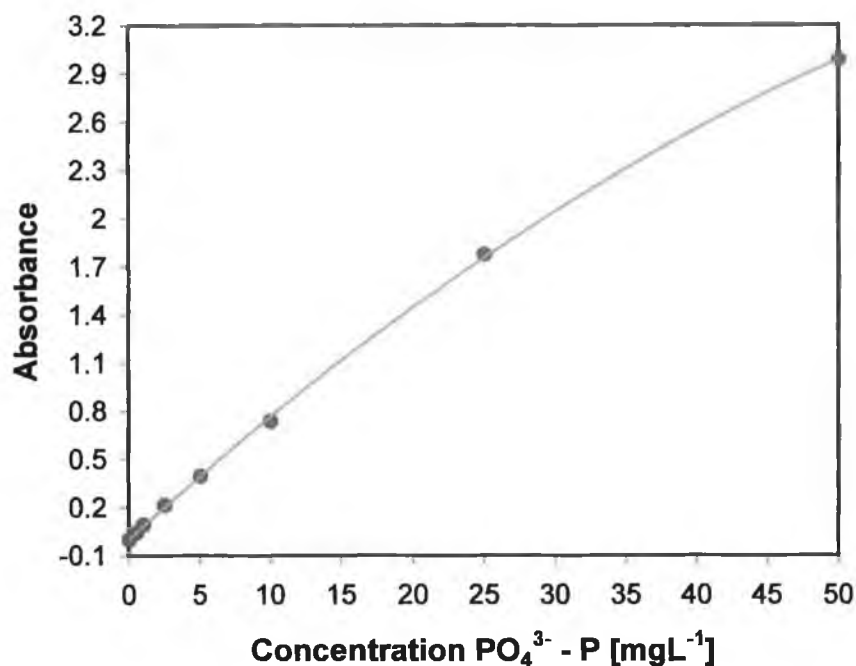


Figure 2-6 Calibration plot with the UV-LED light source over the concentration range 0 - 50 mgL^{-1} $\text{PO}_4^{3-} - \text{P}$ at a wavelength of 380 nm

The average absorbance calculated from the triplicate measurements was plotted against the concentration $\text{PO}_4^{3-} - \text{P}$ over the range 0 – 50 mgL^{-1} as shown in Figure 2-6. Error bars were included ($n = 3$ replicates), although the data points representing each calibration standard on the plot mask them. This was due to the good reproducibility of the repeat measurements (% RSD < 1.3 % for every point, see Table 2-4).

Beer's Law is not obeyed at 50 mgL^{-1} as there is a small deviation from linearity as is shown in Figure 2-6. This can be explained by closer examination of the absorbance spectra (see Figure 2-5) from 0 – 50 mgL^{-1} . Above a wavelength of 430 nm linearity is obeyed over the whole range, however the sensitivity is lower in this range. To ensure the most sensitive measurement for implementation in a microfluidic chip with a 25-fold decrease in optical path length, 380 nm was the best choice for all analyses.

The slope of the line, m , was calculated as $0.0605 \pm 2 \times 10^{-10}$ (RSD: 0.3815 %), from which the molar absorptivity, ϵ , was estimated as 8129.11 ± 31.55 (RSD: 0.38 %).

It has already been demonstrated that the peak output of λ_{\max} 375 nm from the UV-LED is in good agreement with the maximum absorbance of the yellow complex in the UV spectrum. The calibration demonstrated the sensitivity and highly reproducible data achieved when the UV-LED light source was employed.

Table 2-4 Calibration data for the UV-LED calibration over the concentration range 0 – 50 mgL⁻¹ PO₄³⁻ - P at a wavelength of 380 nm

Conc. PO ₄ ³⁻ -P [mgL ⁻¹]	Run 1	Run 2	Run 3	Average	Std. Dev.	% RSD
0	0.0000	0.0000	0.0000	0.0000	0.0000	0.0000
0.5	0.0450	0.0440	0.0450	0.0447	0.0006	1.2926
1	0.0940	0.0940	0.0950	0.0943	0.0006	0.6120
2.5	0.2170	0.2150	0.2150	0.2157	0.0012	0.5354
5	0.3950	0.3990	0.3970	0.3970	0.0020	0.5038
10	0.7370	0.7360	0.7390	0.7373	0.0015	0.2072
25	1.7780	1.7760	1.7760	1.7767	0.0012	0.0650
50	2.9790	3.0000	2.9810	2.9867	0.0116	0.3881

After establishing that the UV-LED was a good choice of light source for the yellow method and showing that the calibration yielded a linear correlation between the absorbance and the concentration over the range 0 – 50 mgL⁻¹ PO₄³⁻ - P, the sensitivity of the absorbance measurement with the UV-LED at a range of wavelengths was assessed. The five wavelengths were 380, 390, 400, 420 and 430 nm. This particular region of the UV-Vis spectrum was chosen to coincide with the absorbance spectrum of the complex formed via the yellow method. This also determined whether 380 nm was a suitable choice as the working wavelength for the yellow method.

As shown in Figure 2-7 five calibrations with the UV-LED light source were undertaken at wavelengths of 380, 390, 400, 420 and 430 nm. The calibration at 380 nm was taken from Figure 2-6. The other four calibrations were carried out at the same time over the concentration range 0 – 50 mgL⁻¹ PO₄³⁻ - P using the same P standard solutions as is given in Table 2-5. The absorbance of a 50 mgL⁻¹ PO₄³⁻ - P standard was over threefold greater at 380 nm than at 430 nm. For obvious

reasons 380 nm was chosen as the working wavelength for all the analytical measurements referred to in this thesis.

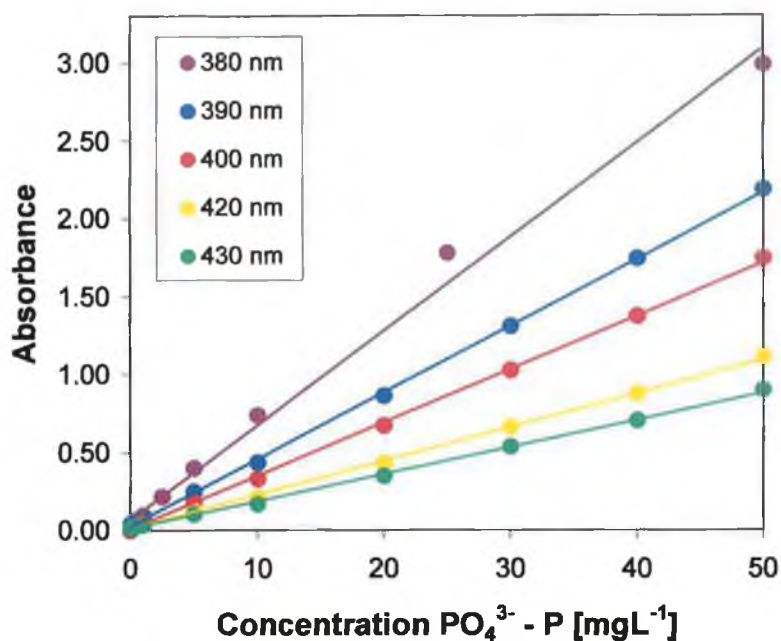


Figure 2-7 Comparison calibration plots of absorbance versus concentration PO_4^{3-} - P for the concentration range 0 – 50 mgL^{-1} with a UV-LED light source at 5 different wavelengths

Based on these results the decision to use 380 nm as the working wavelength throughout this research, with the UV-LED as a light source, was made.

Table 2-5 Absorbance measurements made over the concentration range 0 – 50 mgL^{-1} PO_4^{3-} - P with the UV-LED as a light source to compare the calibrations made at 5 different wavelength

Conc. PO_4^{3-} P [mgL^{-1}]	380nm	390nm	400nm	420nm	430nm
0	0.0000	0.0391	0.0236	0.0240	0.0228
0.3	N/A	0.0540	0.0349	0.0309	0.0284
0.5	0.0447	0.0581	0.0358	0.0299	0.0261
1	0.0943	0.0778	0.0525	0.0407	0.0348
2.5	0.2157	N/A	N/A	N/A	N/A
5	0.3970	0.2471	0.1856	0.1259	0.1033
10	0.7373	0.4331	0.3301	0.2089	0.1670
20	N/A	0.8617	0.6698	0.4305	0.3457
25	1.7767	N/A	N/A	N/A	N/A
30	N/A	1.3081	1.0262	0.6600	0.5324
40	N/A	1.7414	1.3718	0.8780	0.7019
50	2.9867	2.1832	1.7421	1.1086	0.8952

2.6 Reaction Kinetics

The rate of the chemical reaction of the yellow method reagent and an orthophosphate containing sample was important to investigate in order to estimate how quickly a measurement could be made, i.e. how high the sample turnaround / hour would be. It was also important in terms of this research project that the chemistry of the yellow method was fully investigated and optimised and then successfully translated to a microfluidic manifold.

2.6.1 Preliminary Experiment at Room Temperature

The assumption of 1st order for the kinetic reaction of an orthophosphate sample with the combined reagent to form a heteropoly complex was initially investigated at room temperature in the conventional system (Figure 2-3) as shown in Figure 2-8. The first absorbance spectrum was captured immediately (after ~ 0.5 s) followed by repeated acquisitions over the wavelength range 360 - 550 nm being measured every 10 s for 3.5 min. The Figure 2-8 inset plots absorbance versus time, which corresponds to the absorbance measured for each spectrum at a wavelength of 380 nm.

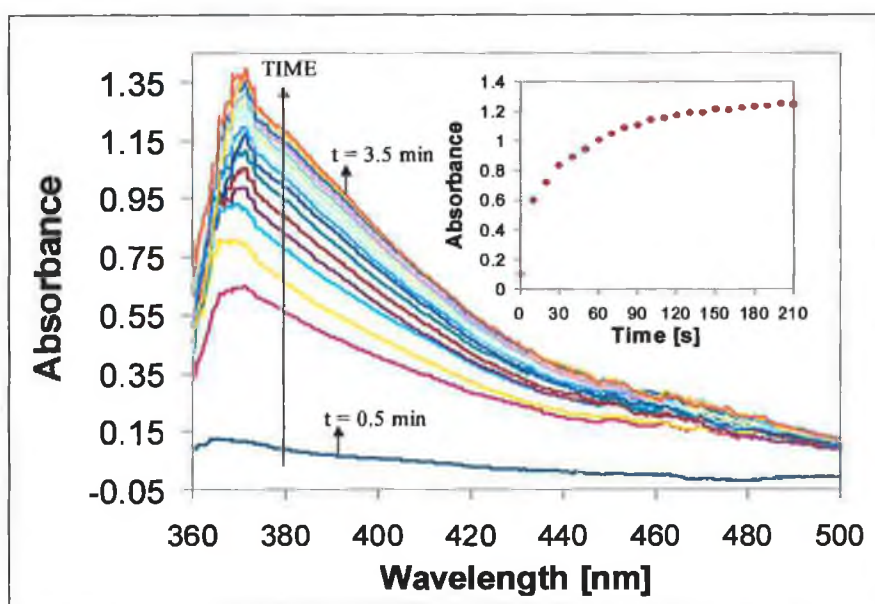


Figure 2-8 The absorbance response over time as a 20 mgL⁻¹ PO₄³⁻ standard and the acidic reagent react to form the PO₄³⁻ - P heteropoly complex at room temperature (INSET: The average absorbance versus time at 380 nm)

Establishing that the reaction rate was 1st order involved carrying out a more controlled experiment. The temperature at which the yellow method reaction takes place has to be stable and continuously monitored and the data acquisition rate increased. In order to achieve this a new thermal set up was designed and fabricated.

2.6.2 Experimental Set-up

The new temperature apparatus comprising a portable mini-spectrometer (Model S2000) with accompanying software, the OOIBase₃₂ Program, a tungsten-halogen source (Model LS1) and a 1 cm cuvette holder (Model CUV-UV), all of which were obtained from Ocean Optics Inc. (Ocean Optics B.V., Duiven, The Netherlands) was assembled. Light was transmitted from the lamp through the cuvette holder to the spectrometer via optical fibres (Edmund Optics Ltd., York, UK). The spectrometer was connected to a laptop PC via a ribbon cable, and a DAQ-700 I/O card (National Instruments, Newbury, Berkshire, UK) was used to retrieve data from the spectrometer. In time-based acquisition mode, spectra were acquired at fixed time intervals, which allowed the user to monitor the change in complex absorbance as a function of time. For analyses at elevated temperatures a heated control box was purpose-built to house the 1 cm cuvette and holder and a simple LabView program controlled the temperature changes. In Figure 2-9 the inside of the box is shown on the right hand side and the lid on the left. Inside the box **A**, depicts the reservoir for the reagent, **B**, the reservoir for the orthophosphate-containing sample and **C**, the cuvette holder with a 1 cm cuvette positioned on top of the heating mat. In the lid of the box **D** represents the sample injection port, **E** is where the temperature probe is attached and **AI** and **BI** are two through holes to the reservoirs for the sample and the reagent respectively for refilling the injection syringes.

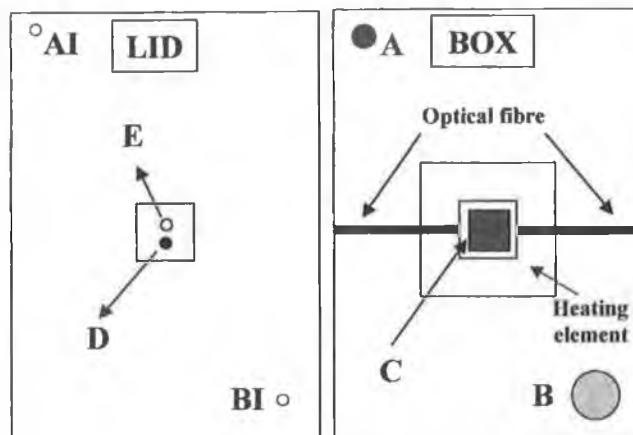


Figure 2-9 Schematic of temperature-control box within which the kinetic experiments were performed over the temperature range 22 – 55 °C

2.6.3 Influence of Temperature on the Yellow Method Reaction

The temperature study was carried out at 5 °C intervals over the temperature range 25 – 50 °C. The yellow method reaction gave a good fit to the 1st order model. For the purpose of this study a 1st order model was set up in a Microsoft Excel spreadsheet. The Solver tool in Microsoft Excel fits the real analytical data to an ideal model for a 1st order kinetic reaction [8-9].

$$x - a_0(1 - e^{-K_A t}) \quad \text{Equation 2-5}$$

The residual of the ideal model data and the real analytical data was calculated, along with the squared residual and the sum of the squared residual (SSR). In order to interpret whether the reaction is 1st order, the Solver tool fits the model to the real data so that the value for the SSR is minimised. K_A , a_0 and x (Equation 2-5) are set as variables and change accordingly, when new data is introduced to the spreadsheet. K_A is the rate of the reaction for a given temperature and the time constant can be calculated, as $1/K_A$ and the sum of a_0 and x equal the maximum absorbance of the complex when the reaction has reached completion.

In Figure 2-10 the average kinetic profiles recorded at each temperature were plotted against each other showing the dependence of the rate of reaction on the temperature. However the absorbance of the 10 mgL⁻¹ PO₄³⁻ - P sample should theoretically be the same, irrespective of the temperature at which the experiment

is being carried out at. It was shown that although the absorbance at each temperature showed good repeatability (RSD: < 6.5 %) the overall reproducibility of the experiment was not as good. The average absorbance of the 10 mgL⁻¹ PO₄³⁻ - P sample over the temperature range 25 – 50 °C was 0.5923 ± 0.0783 (RSD: 13.2230 %). There are a number of possible explanations for the poor reproducibility:

1. The injection syringe containing the PO₄³⁻ sample volume wasn't accurately and reproducibly refilled prior to each experiment
2. The reagent contained in the 1-cm cuvette wasn't accurately measured out
3. The 1-cm cuvette is not ideal for ensuring efficient mixing and reacting of the reagent and sample

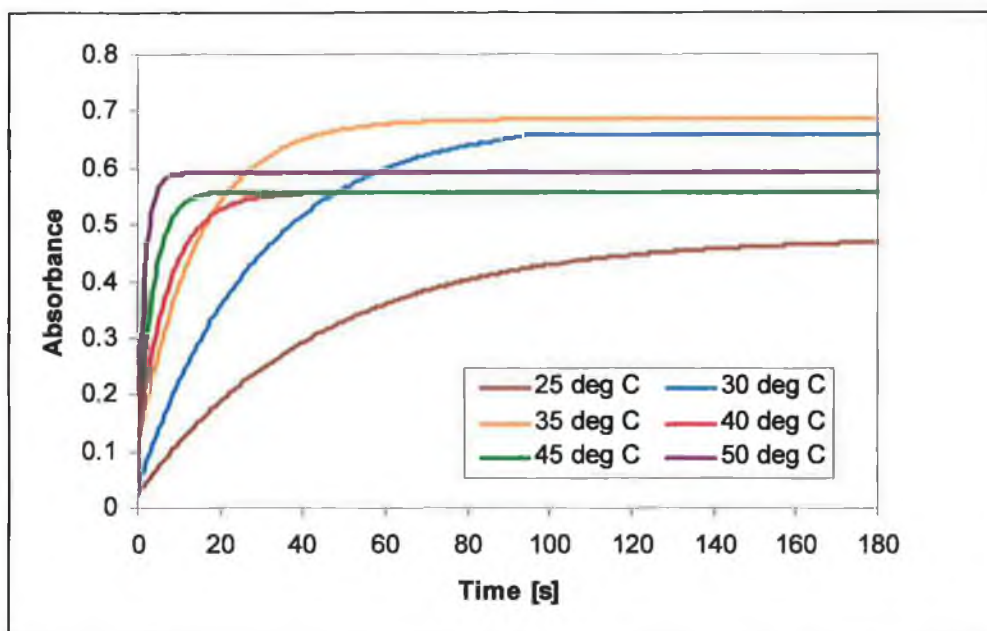


Figure 2-10 Comparison of the kinetic profile of the yellow method reaction over the temperature range 25 – 50 °C at the working wavelength of 380 nm

In conclusion the major finding of the bench analysis was that the reaction rate for the yellow method was very fast, and that by ramping the temperature up the reaction time could be significantly reduced to several seconds, which was a critical factor when considering an experimental design for a microfluidic manifold, and the overall analytical strategy. However, the uncertainty associated with the injection technique, the variation in the volume of injected sample and the whole issue of efficient mixing in the cuvette influenced the quality of the data obtained. Despite

this, the rapid acquisition of the data led to well-defined exponential increases in the absorbance as expected. All the data was successfully fitted to the 1st order model. Real-time trials were performed in triplicate at each temperature interval and an average value for the rate constant was calculated for a 1st order reaction as documented in Figure 2-6.

Table 2-6 Values for the rate constant, *k*, over the temperature range 25 – 50 °C at a wavelength of 380 nm

Temperature [°C]	k 1 [s ⁻¹]	k 2 [s ⁻¹]	k 3 [s ⁻¹]	Aver k [s ⁻¹]	Std. Dev.	% RSD
25	0.0189	0.0258	0.0227	0.0225	0.0034	15.1703
30	0.0417	0.0307	0.0279	0.0335	0.0073	21.7309
35	0.0579	0.0713	0.0883	0.0725	0.0152	21.0115
40	0.1324	0.1174	0.1414	0.1304	0.0121	9.2870
45	0.2022	0.3894	0.2823	0.2913	0.0939	32.2355
50	1.1192	1.2277	1.9800	1.4423	0.4688	32.5050

It was clear that the repeatability of the measurement at each temperature wasn't good with the lowest relative deviation of 9.2870 % being calculated for the analysis at 40 °C. There was too much room for human error with the kinetic experiments carried out in the conventional 1-cm cuvette and the temperature at which the reaction was taking place was not accurately enough recorded. The temperature reading from the LabView software referred to the ambient temperature in the box and not to the solution contained within.

The relationship between the rate at which a reaction proceeds and its temperature is determined by the Arrhenius equation. This dependence described by the well-known Arrhenius equation in its standard form is shown in equation 2-6 and an integrated form as in Equation 2-7. The Arrhenius equation is used to show the effect of a change in temperature on the rate constant and therefore the rate of the reaction.

$$k = Ae^{\frac{-Ea}{RT}} \quad \text{Equation 2-6}$$

$$a \ln k = \ln A - \frac{Ea}{RT} \quad \text{Equation 2-7}$$

In equation 2-6 the rate constant, *k*, is the product of a pre-exponential factor, *A*, which has identical units to *k* (s⁻¹ for 1st order), and the exponential factor, e^{-Ea/RT},

comprised of absolute temperature, T (K), gas constant, R ($\text{kJmol}^{-1}\text{K}^{-1}$) and the activation energy, E_a (kJmol^{-1}). The activation energy of a reaction is the amount of energy needed to initiate the reaction and it dictates the temperature-dependence of the rate constant. The pre-concentration factor, also known as the frequency or steric factor, is a term, which includes factors like the frequency of collisions and their orientation. It varies slightly with temperature, although not much and is often assumed to be a constant across a small temperature range. E_a and A can be estimated by plotting $\ln k$ vs. $1/T$ from Equation 2-7. It is generally accepted that the rates of reactions with large activation energies are highly influenced by changes in temperature [10].

The average of $\ln k$ was plotted in Figure 2-11 versus the absolute temperature over the range 25 – 45 °C. In order to determine the correlation of the data to linearity, the average of the R^2 value ($n = 3$; linear plots) was calculated as 0.9629 ± 0.0245 (2.5436 %).

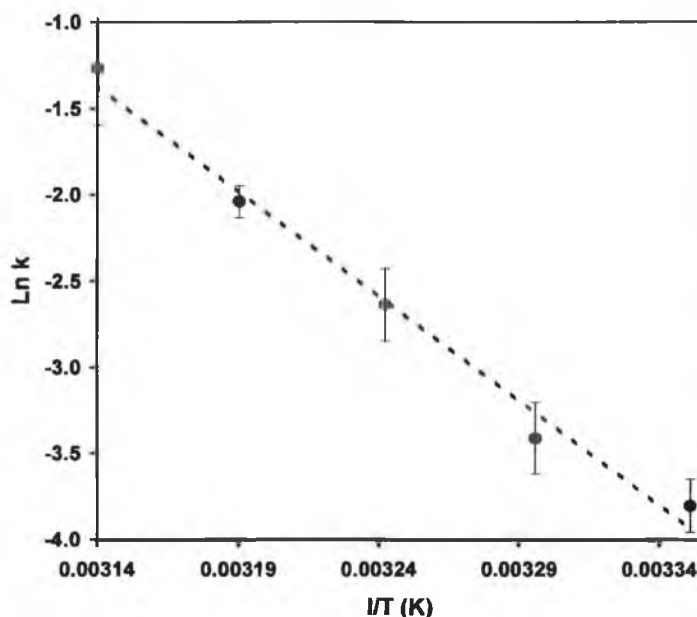


Figure 2-11 Arrhenius plot of average $\ln k$ versus $1/T$ for the three runs performed in a conventional 1-cm cuvette over the temperature range 25 – 45 °C

The pre-concentration factor, a_0 was calculated as the intercept of the line of the equation and the slope of the line as $-E_a/R$, where R is the gas constant and has a value of $8.3415 \text{ kJmol}^{-1}\text{K}^{-1}$. The activation energy, E_a , and the pre-concentration

factor, A, were calculated as $101362 \text{ kJmol}^{-1} \pm 6029 \text{ kJmol}^{-1}$ (RSD: 5.95 %) and $36.97 \text{ kJmol}^{-1} \pm 2.42 \text{ kJmol}^{-1}$ (RSD: 6.55 %) respectively.

In summary, as the temperature exceeded 45°C the data became less reliable and harder to reproduce. The reasons for this included the fast kinetics, the injection method and the non-uniformity of the heating within the thermal box. There were also limitations in the spectrometer software, which hindered the number of acquisitions that could be made every second. However, data for higher temperatures was not strictly necessary for the application of the yellow method to the monitoring of wastewater and drinking water for phosphorus. Temperatures at a wastewater plant, during most treatments, usually do not exceed the range $30 - 40^{\circ}\text{C}$, and if the method is applied to drinking water, then the temperatures are significantly lower again. Thus the results presented here within the range $22 - 50^{\circ}\text{C}$ provide relevant information on the reaction rates for this particular application.

2.7 pH

The acidity or alkalinity of a solution is important in terms of speciation of the analyte of interest, in this case phosphate. Phosphorus is present in various forms in aqueous solution depending on the pH of the sample. As described in Chapter 1 (Section 1.1.2) there are three pK_a values representing three different phosphate forms, PO_4^{3-} , HPO_4^{2-} and $\text{H}_2\text{PO}_4^{-}$. In order to determine in which form the orthophosphate is present when the sample is reacted with the reagent, the pH of the sample was measured. A further study of the change in absorbance based on pH was investigated. A large range of $0.6 - 10$ pH was analysed.

The aim of this experiment was to establish that the pH of the yellow heteropoly complex solution formed was stable for the concentration range $0 - 50 \text{ mgL}^{-1} \text{ PO}_4^{3-}$ - P and then to observe the effect a change in the pH of the reagent has on the physical and chemical composition of the heteropoly complex solution. To measure the pH of the yellow heteropoly solution, 20 ml of reagent were reacted with 20 ml of an orthophosphate-containing standard in a volumetric flask. When the reaction was finished, in ca. 3 min, the pH of the solution was measured. For the pH adjusted samples the method was slightly varied, whereby 20 ml of reagent

was measured into a 400 ml beaker containing a magnetic stirrer. The glass pH electrode was then fitted just below the surface of the solution. A 1 M NaOH solution was used to alter the pH of the reagent by drop-wise addition. The pH of the reagent was modified over the pH range 0.6 – 10 with the pH being adjusted in 1-pH unit increments. 20 ml of a 2.5 mgL^{-1} P sample was then added to the solution and the colorimetric reaction reached completion in approx. 3 min. After which the pH of the yellow complex solution was measured.

2.7.1 Apparatus

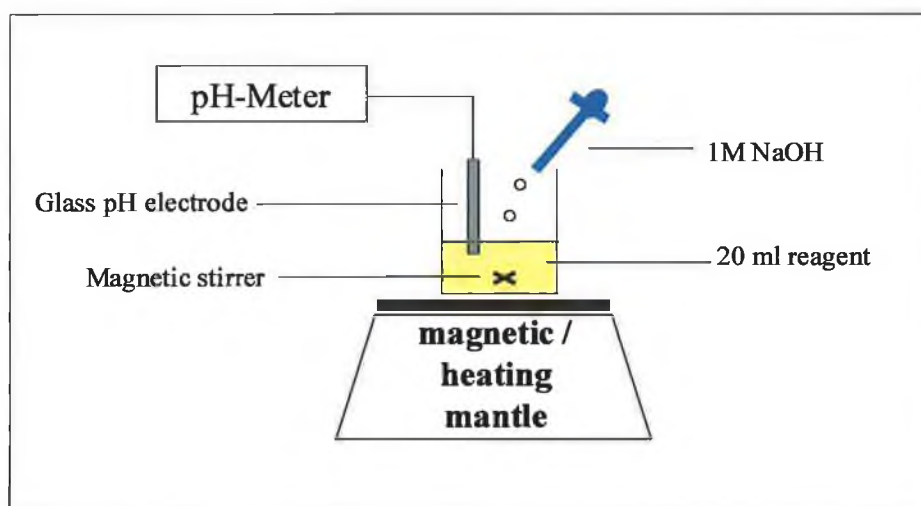


Figure 2-12 Schematic of the apparatus utilised in the pH study of the yellow vanadomolybdophosphoric acid complex at a wavelength of 380 nm at room temperature

The instrumental set up consisted of a pH glass electrode to record the change in pH as the 1 M NaOH solution was added as shown in Figure 2-12. The glass electrode was connected to a pH-meter (Model: 691 pH Meter, Metrohm Ireland Ltd., Tallaght, Dublin 24, Ireland), which measured the signal. A magnetic stirrer and a magnetic / heating mantle were used to keep the reagent at a constant flux whilst the 1 M NaOH solution and then the orthophosphate containing sample were added. The absorbance spectra were obtained with the portable spectrometer as shown schematically in Figure 2-3.

2.7.2 pH of the Yellow Method Complex Solution

The pH of the heteropoly complex solution was measured over the linear range of 0 – 50 mgL⁻¹ PO₄³⁻ - P. A series of standards, 0, 5, 10, 25 and 50 mgL⁻¹ were prepared and the pH of each measured in triplicate.

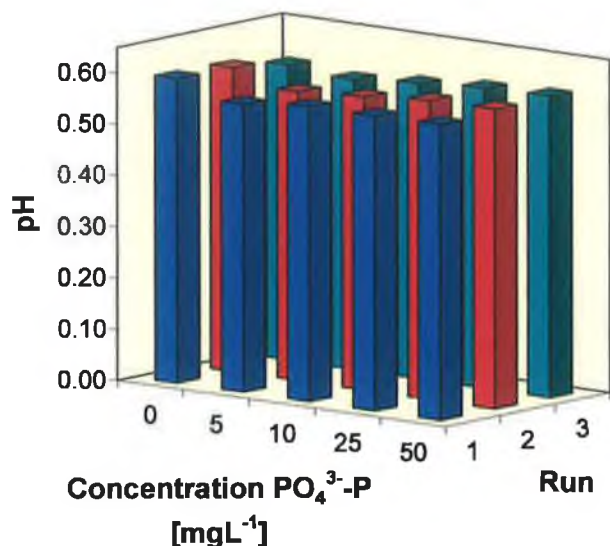


Figure 2-13 Triplicate measurements of pH for each PO₄³⁻ - P sample over the concentration range 0 – 50 mgL⁻¹ at the working wavelength of 380 nm

The results of this study are illustrated in Figure 2-13. The initial impression was that the yellow heteropoly complex is very acidic, remaining below pH 0.6 for the entire linear range.

Table 2-7 Average pH measurements made over the concentration range 0 – 50 mgL⁻¹ PO₄³⁻ - P at the working wavelength of 380 nm

Conc. PO ₄ ³⁻ - P [mgL ⁻¹]	0	5	10	25	50
Run 1	0.5940	0.5620	0.5750	0.5750	0.5770
Run 2	0.5930	0.5640	0.5720	0.5830	0.5850
Run 3	0.5760	0.5660	0.5760	0.5850	0.5880
Average pH	0.5877	0.5640	0.5743	0.5810	0.5833
Std. Dev.	0.0101	0.0020	0.0021	0.0053	0.0057
% RSD	1.7214	0.3546	0.3624	0.9108	0.9748

From the histogram the variance in pH over the linear range is visibly very small. From the data in Table 2-7 the pH of the yellow complex, without a pH adjustment, was calculated as 0.5781 ± 0.0099 (RSD: 1.7069 %), which was the average of the fifteen absorbance measurements over the concentration range 0 – 50 mgL⁻¹. The average absorbance didn't exceed a relative standard deviation of 1.8 % for the whole concentration range.

2.7.3 Modification of the pH of the Yellow Method Complex Solution

The pH was adjusted in increments of 1-pH unit over the range 0.6 - 10. An absorbance spectrum was traced for each pH-adjusted sample and the experiment was performed in triplicate with the average absorbance versus wavelength being plotted in Figure 2-14, over the range 330 – 420 nm, which is the region where the yellow complex absorbs most strongly. The raw data (~ 1400 data points / pH measurement) used to produce the absorbance spectra was treated to a moving average calculation for n= 20 data points, which resulted in the smooth plot.

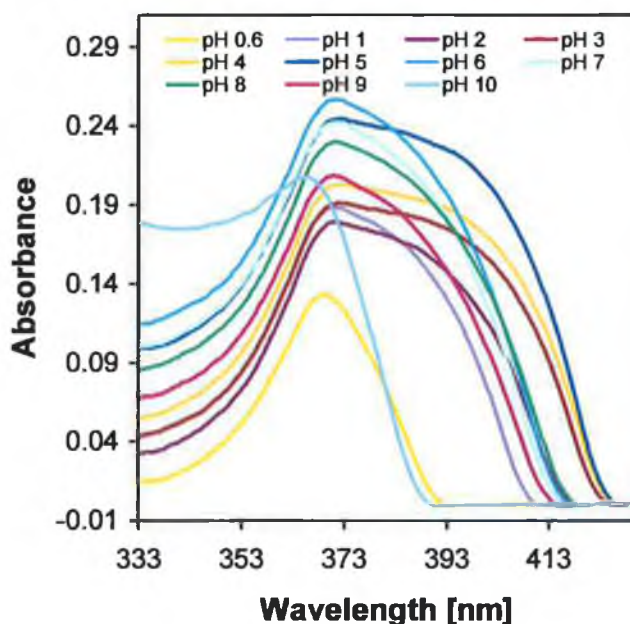


Figure 2-14 Plot of change in absorbance spectrum of 10mgL⁻¹ PO₄³⁻ - P yellow heteropoly complex for the pH range of 0.65 – 10 over the wavelength range 330 – 420 nm

The pH experiment was performed in triplicate and the results are shown in Table 2-8. At each adjusted pH (pH 1 – 10) the reproducibility of the measurement was excellent with an overall relative standard deviation of less than 1.8 % for each pH measurement.

Table 2-8 Absorbance measurements made in triplicate at 380 nm over the pH range 0 – 10

pH	1	2	3	Aver. Abs.	Std. Dev.	% RSD
0.6	0.1135	0.1145	0.1125	0.1135	0.0010	0.8811
1	0.1650	0.1670	0.1650	0.1657	0.0012	0.6970
2	0.1620	0.1630	0.1620	0.1623	0.0006	0.3557
3	0.1870	0.1900	0.1900	0.1890	0.0017	0.9164
4	0.1990	0.1980	0.1970	0.1980	0.0010	0.5051
5	0.2450	0.2440	0.2440	0.2443	0.0006	0.2363
6	0.2420	0.2420	0.2440	0.2427	0.0012	0.4758
7	0.2310	0.2290	0.2290	0.2297	0.0012	0.5028
8	0.2060	0.2070	0.2050	0.2060	0.0010	0.4854
9	0.1960	0.1940	0.1950	0.1950	0.0010	0.5128
10	0.1510	0.1500	0.1460	0.1490	0.0026	1.7757

A histogram depicting the change in absorbance as the pH changed is shown in Figure 2-10.

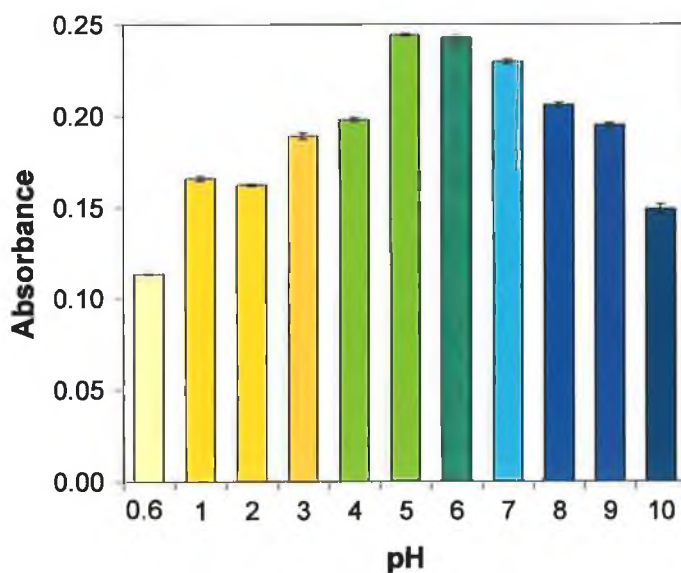


Figure 2-15 Histogram depicting the average change in pH from 0.65 – 10 of the $10\text{mgL}^{-1} \text{PO}_4^{3-}$ - P complex at the working wavelength of 380 nm

The histogram is colour-coded in accordance with the colour changes that were observed at each pH, where an absorbance measurement was made. The colour of the yellow method complex solution changed from pale yellow (pH ~1) to dark blue (pH ~ 10) as the pH was increased. Under very acidic conditions the complex was relatively stable from pH 0.96 up to a pH value of 3. Between pH 3 - 6 the complex changed slowly from orange to green. At a pH of 7 the complex was turquoise in colour.

However it was also noted that the colour of the solution was not stable at this pH and a rapid colour change to dark blue took place between pH 8 – 10. By altering the pH of the reagent the yellow complex solution was chemically altered, so even though the absorbance was highest at pH 6, the chemical stability of the solution was not satisfactory. The chemical stability was good in the acidic range between a pH of approx. 1 - 3.

There were two important findings of the pH investigation:

1. The pH of the orthophosphate heteropoly complex is very stable over the linear concentration range 0 – 50 mgL⁻¹.
2. When the pH of the reagent is adjusted to result in a sample pH > 4, the solution is unstable.

The drop-wise addition of 1M NaOH can reduce the lifetime of the reagent by forming a precipitate. Both long-term chemical stability and a precipitate-free reagent are vital for the yellow methods implementation in a microfluidic manifold, which will be discussed in greater detail in Chapter 3. By altering the pH of the solution the chemical stability is compromised and the reagent doesn't fit the long-term goals set for the project.

2.8 Fe(II) Interference

In the limited literature available relating to the vanadomolybdophosphoric acid method, there are references leading to Fe²⁺ as an interfering ion in aqueous

samples [11,12]. The purpose of this study was to demonstrate that although Fe^{2+} does interfere in the reaction, it only does so when present in high concentrations.

2.8.1 Sample Preparation

A 1L stock solution of $300 \text{ mgL}^{-1} \text{ Fe}^{2+}$ ion was prepared with 1.4735 g of the anhydrous FeSO_4 salt (M.W.: 152 g / mol). From the $50 \text{ mgL}^{-1} \text{ P}$ stock solution, a series of standards over the concentration range 0 – 50 mgL^{-1} were prepared. In total ten standard solutions were prepared. Each calibration standard was spiked with 150 mgL^{-1} of the interfering ion. 5 ml of each sample was mixed with 5 ml of the reagent and allowed to react at room temperature for 5 min ensuring the reaction had reached completion prior to making an absorbance at 380 nm.

2.8.2 Experimental

A UV-LED was used as the light source for the experiment and again a working wavelength of 380 nm was selected. The absorbance of each sample was measured in triplicate, the results of which were plotted against the concentration $\text{PO}_4^{3-} - \text{P} / 150 \text{ mgL}^{-1} \text{ Fe}^{2+}$ over the concentration range 0 – 50 mgL^{-1} as shown in Figure 2-16. The same concentration range that was employed in the calibration study described in Section 2.4 was applied here to highlight the level of interference the Fe^{2+} has on the yellow method.

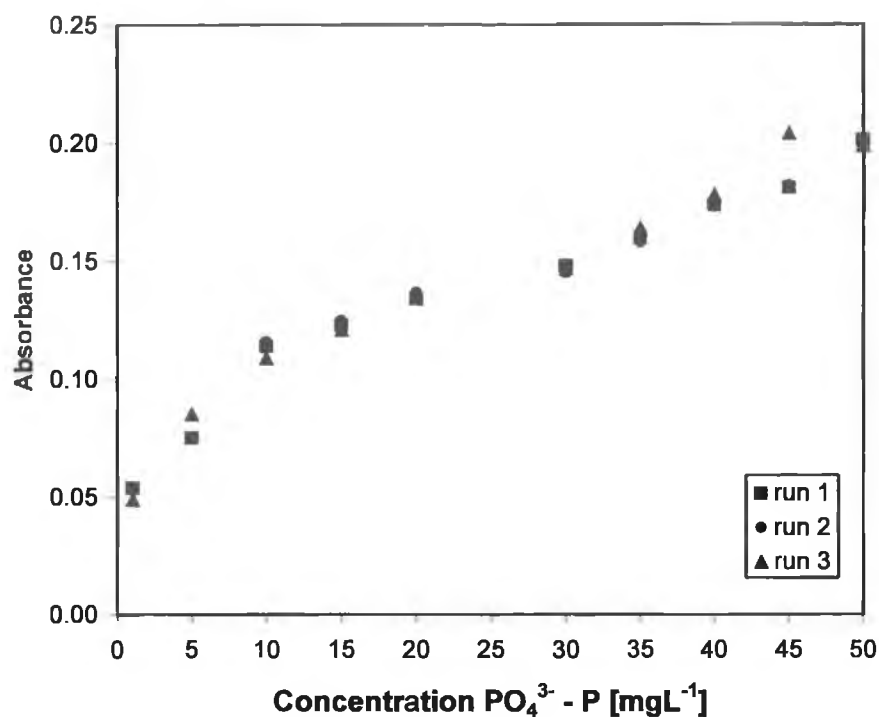


Figure 2-16 Triplicate calibration of absorbance versus concentration $\text{PO}_4^{3-} - \text{P}$ spiked with $150 \text{ mgL}^{-1} \text{Fe}^{2+}$ over the concentration range $0 - 50 \text{ mgL}^{-1}$ at a working wavelength of 380 nm

Deviations from linearity were evident in all three plots with poor R^2 values being calculated as 0.9437, 0.9290 and 0.9505 for run 1, 2 and 3, respectively.

The absorbance data taken at a wavelength of 380 nm over the concentration range $0 - 50 \text{ mgL}^{-1} \text{PO}_4^{3-} - \text{P}$ spiked with $150 \text{ mgL}^{-1} \text{Fe}^{2+}$ interfering ion are tabulated in Table 2-9. When the concentration of Fe^{2+} , present in an orthophosphate-containing sample, exceeded 150 mgL^{-1} , a discolouration of the solution occurred. Instead of a yellow solution forming when the reagent was added, a pale "green-blue" solution resulted. The average absorbance yielded reasonable reproducibility ($n = 3$) and the overall relative standard deviation of all samples was less than 6.1 %.

Table 2-9 Triplicate measurements for the calibration over the concentration range 0 – 50 mgL⁻¹ PO₄³⁻ - P spiked with 150 mgL⁻¹ Fe²⁺ interfering ion

Conc. PO ₄ ³⁻ -P [mgL ⁻¹]	Run 1	Run 2	Run 3	Average	Std. Dev.	% RSD
1	0.0540	0.0530	0.0490	0.0520	0.0022	4.1543
5	0.0750	0.0750	0.0850	0.0783	0.0047	6.0179
10	0.1140	0.1160	0.1090	0.1130	0.0029	2.6052
15	0.1230	0.1250	0.1210	0.1230	0.0016	1.3276
20	0.1340	0.1370	0.1350	0.1353	0.0012	0.9216
30	0.1480	0.1450	0.1470	0.1467	0.0012	0.8504
35	0.1600	0.1580	0.1640	0.1607	0.0025	1.5526
40	0.1740	0.1730	0.1780	0.1750	0.0022	1.2344
45	0.1810	0.1820	0.2040	0.1890	0.0106	5.6161
50	0.2010	0.1990	0.1990	0.1997	0.0009	0.4722

The linearity of the plot was questionable with an R² value of 0.9411 ± 0.0110 (RSD: 1.1677 %) being computed, although the reproducibility of the data was good.

The extent to which an excess of Fe²⁺ ion present in an orthophosphate sample can affect the sensitivity of the yellow method was assessed. The calibration carried out with the standards spiked with 150 mgL⁻¹ Fe²⁺ interfering ion was compared with a previous standard calibration (Figure 2-6) and plotted in Figure 2-17. Both calibrations were performed with the same portable spectrometer as described in Section 2.2.

The interference of Fe²⁺ at concentrations in excess of 150 mgL⁻¹ was such that nearly a 6-fold decrease in sensitivity resulted. For example, the average absorbance of a 50 mgL⁻¹ PO₄³⁻ - P without the presence of any Fe²⁺ was 2.9867 ± 0.0116 (RSD: 0.3881 %, see Table 2-4), compared with 0.1997 ± 0.0009 (RSD: 0.4722 %). The absorbance when the Fe²⁺ interfering ion was present was lower by a factor of approx. 15 compared to the regular absorbance without any Fe²⁺ present.

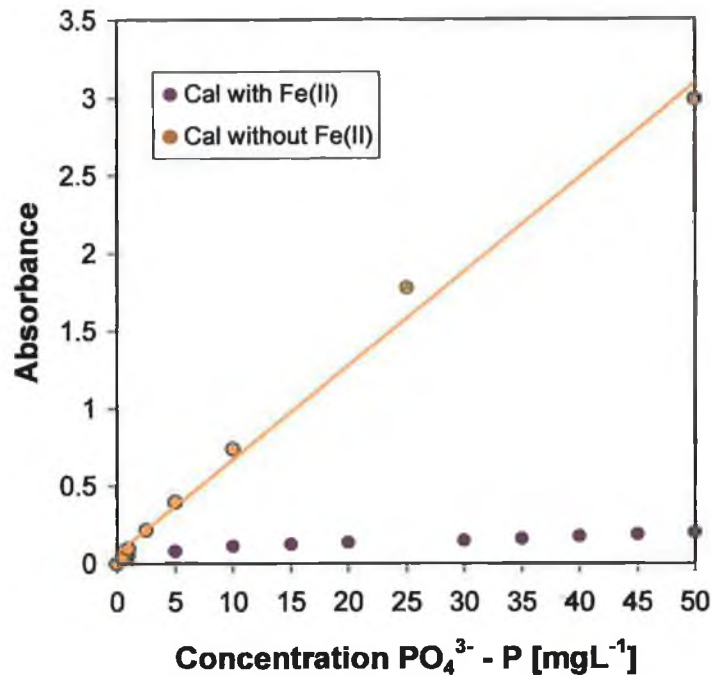


Figure 2-17 Comparison of the average $\text{PO}_4^{3-} - \text{P}$ concentration, with and without $150 \text{ mg}^{-1} \text{ Fe}^{2+}$ as an interfering ion, over the range $0 - 50 \text{ mgL}^{-1}$

When an excess of Fe^{2+} ions ($\geq 150 \text{ mgL}^{-1}$) are present in an orthophosphate-containing sample a reaction occurs, which converts the Fe^{2+} ions to Fe^{3+} ions, which is distinguished by a discoloration of the sample (“green-blue”). High concentrations of Fe^{2+} ions are not often found in water bodies, so the extent of interference is not a major problem.

2.9 Repeatability

A 4 mgL^{-1} standard was prepared from the 50 mgL^{-1} P stock solution. 5 ml of the 4 mgL^{-1} sample was reacted with 5 ml of the reagent and allowed to stand for 5 min at room temperature to ensure the reaction had reached completion. Again a UV-LED was the chosen light source for the absorbance measurements and the working wavelength was 380 nm. The absorbance of the $4 \text{ mgL}^{-1} \text{ PO}_4^{3-} - \text{P}$ was measured in triplicate and the simple experiment was replicated fifteen times.

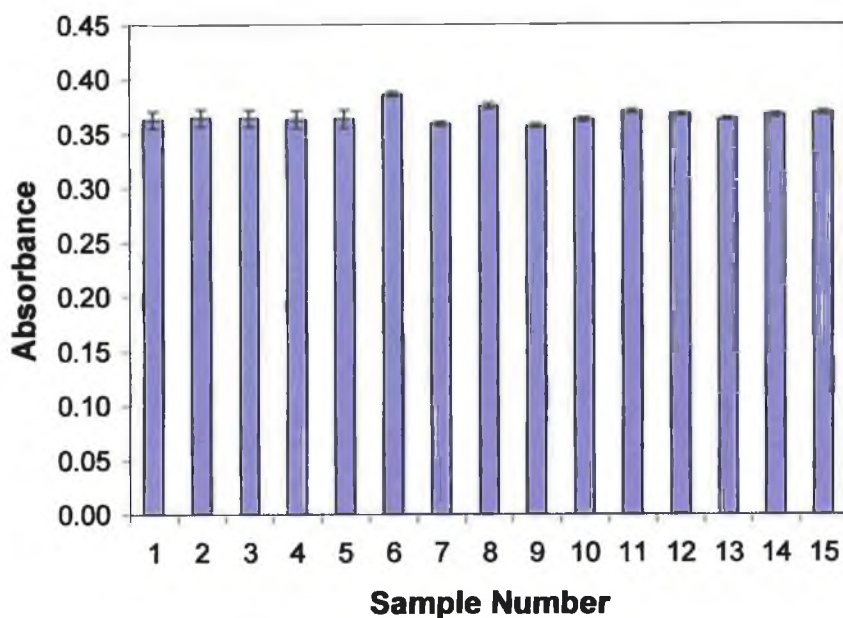


Figure 2-18 Repeat absorbance measurements of the $4 \text{ mgL}^{-1} \text{ PO}_4^{3-} - \text{P}$ complex at the working wavelength of 380 nm

The histogram in Figure 2-18 depicts the excellent repeatability in measurement of a 4 mgL^{-1} sample. Error bars are included for $n = 3$.

Table 2-10 Triplicate absorbance measurements recorded for a $4 \text{ mgL}^{-1} \text{ PO}_4^{3-} - \text{P}$ complex at the working wavelength of 380 nm

Sample	Abs. $4 \text{ mgL}^{-1} \text{ PO}_4^{3-} - \text{P}$	Std. Dev.	% RSD
1	0.3630	0.0080	2.2039
2	0.3650	0.0080	2.1918
3	0.3640	0.0080	2.1978
4	0.3633	0.0085	2.3408
5	0.3637	0.0085	2.3387
6	0.3860	0.0020	0.5181
7	0.3590	0.0020	0.5571
8	0.3753	0.0025	0.6705
9	0.3570	0.0020	0.5602
10	0.3630	0.0020	0.5510
11	0.3700	0.0020	0.5405
12	0.3677	0.0015	0.4155
13	0.3633	0.0015	0.4204
14	0.3670	0.0020	0.5450
15	0.3690	0.0020	0.5420

From the data displayed in Table 2-10 the relative standard deviation was less than 2.4 % for all 15 absorbance measurements. The average absorbance of the 4 mgL⁻¹ PO₄³⁻ - P for the fifteen runs was calculated as 0.3664 ± 0.0070 (RSD: 1.9102 %).

2.10 Limits of Detection (LOD)

It was important to assess the lowest possible concentration of orthophosphate ion that could be detected in an aqueous sample. From the literature it was cited as 0.2 mgL⁻¹ PO₄³⁻ - P as a benchmark for the yellow method [13]. To estimate the LOD of the method a calibration was performed plotting absorbance against PO₄³⁻ - P over the concentration range 0 – 5 mgL⁻¹. 100 ml of a 5 mgL⁻¹ P standard was prepared from the 50 mgL⁻¹ PO₄³⁻ stock solution by dilution (5 ml 50 mgL⁻¹ P stock / 100 ml H₂O). From this a series of standards were prepared with particular attention to the 0 – 1 mgL⁻¹ concentration range.

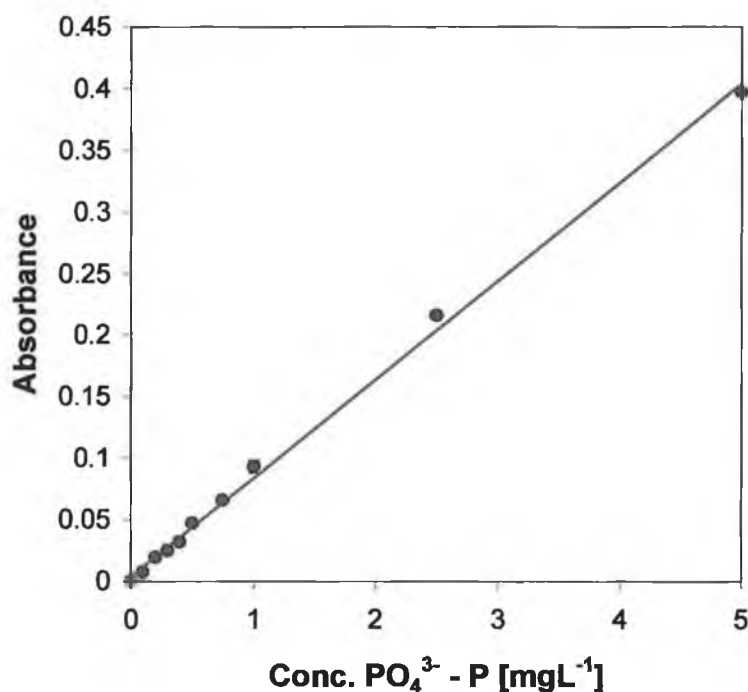


Figure 2-19 Calibration plot of absorbance versus concentration PO₄³⁻ - P over the range 0 – 5 mgL⁻¹ at a working wavelength of 380 nm

Triplicate absorbance measurements were taken for each sample, the average of which was plotted against concentration $\text{PO}_4^{3-} - \text{P}$ over the range 0 – 5 mgL^{-1} at a wavelength of 380 nm with the UV-LED as light source. The results of which are displayed graphically in Figure 2-19 and statistically in Table 2-11. Error bars were included for $n=3$ replicates. The reproducibility was fairly good (RSD: < 5.4 % for each data point). The calibration was linear over the concentration range with an R^2 value of 0.9974 ± 0.0007 (RSD: 0.0702 %) being calculated as the average of the three calibrations (see Table 2-11).

Table 2-11 Absorbance measurements over the concentration range 0 – 5 mgL^{-1} $\text{PO}_4^{3-} - \text{P}$ at a working wavelength of 380 nm

Conc. $\text{PO}_4^{3-} - \text{P}$ [mgL^{-1}]	1	2	3	Aver. Abs.	Std. Dev.	% RSD
0	0.0000	0.0000	0.0000	0.0000	0.0000	0.0000
0.1	0.0072	0.0076	0.0078	0.0075	0.0003	4.0554
0.2	0.0189	0.0190	0.0190	0.0190	0.0001	0.3044
0.3	0.0247	0.0247	0.0248	0.0247	0.0000	0.1168
0.4	0.0320	0.0321	0.0319	0.0320	0.0001	0.3125
0.5	0.0471	0.0476	0.0466	0.0471	0.0005	1.0616
0.75	0.0654	0.0655	0.0657	0.0655	0.0002	0.2331
1	0.0895	0.0910	0.0989	0.0931	0.0051	5.4224
2.5	0.2170	0.2150	0.2150	0.2157	0.0012	0.5354
5	0.3950	0.3990	0.3970	0.3970	0.0020	0.5038

The limit of detection of the yellow method measured in the conventional system was calculated from Equation 2-8.

$$LOD = 3 sd$$

Equation 2-8

The LOD was calculated by multiplying the standard deviation (sd) of the baseline absorbance by 3 ($n = 60$ data points, frequency of measurement: 1 data point / sec). The baseline absorbance was recorded for distilled water as $3.57 \times 10^{-4} \pm 2.77 \times 10^{-6}$ (RSD: 0.7764 %). The average concentration was calculated from the equation of the line as 0.0023 ± 0.0011 (RSD: 4.8795 %), which resulted in a LOD of $0.0687 \pm 0.0034 \text{ mgL}^{-1}$ (% RSD 4.8793 %). In practice the reproducibility of the measurement was hindered below a concentration of $0.1 \text{ mgL}^{-1} \text{ PO}_4^{3-} - \text{P}$.

2.11 Lifetime Studies

The assessment of the reagent lifetime was a critical factor for field deployable instruments along with consumption of reagents (minimal). To demonstrate that this has been achieved two different batches of reagent prepared months apart were analysed over a 10-week period. The results from the two batches were compared with each other to show that:

1. The reagent was chemically stable / precipitate-free
2. There was no loss in sensitivity in the measurement over time

The highest concentration standard of 50 mgL^{-1} was chosen for the study because any deviations from reproducibility for each weekly measurement would be easily observed. Two 10 ml aliquots of a 50 mgL^{-1} P stock solution were each mixed with 10 ml of both reagent batches. Both reagent batches were prepared as per the method described in Section 2.1. The first batch was prepared in December 1999 and was labelled reagent 1. The second batch was made in April 2001 and was accordingly named reagent 2.

The 10-week experiment was carried out in the period September to December 2001, which meant that at the start of the study reagent 1 and reagent 2 were 20 months and 4 months old, respectively. Each measurement of absorbance for both reagent 1 and reagent 2 analyses was performed in triplicate and the average of which is presented graphically in Figure 2-20. The data for reagent 1 and 2 is also given in Table 2-12.

Error bars were included for each weekly analysis for $n = 3$ repeat measurements. For reagent 1 the average absorbance data in Table 2-12 exhibited good accuracy over the 10-week period with a relative standard deviation of less than 2.6 % for each weekly measurement. The overall average absorbance for the 10 weeks was calculated as 2.3723 ± 0.1111 (RSD: 4.6827 %).

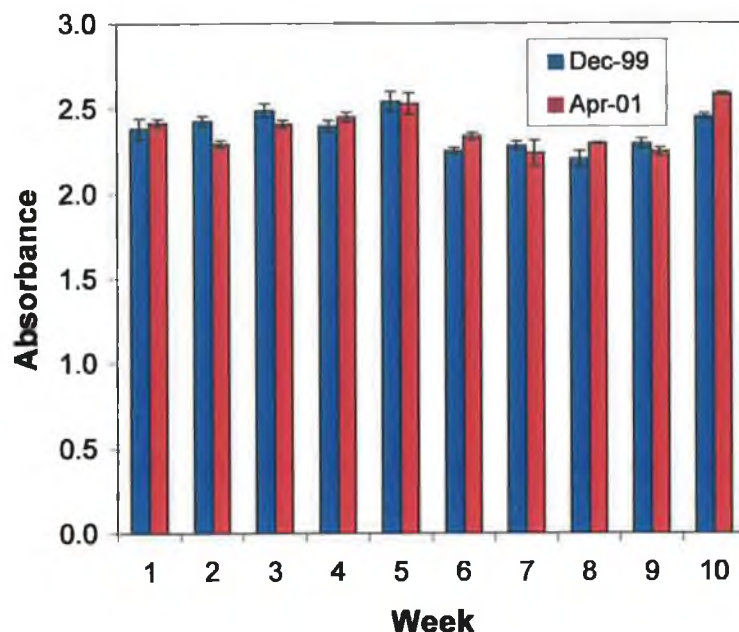


Figure 2-20 Histogram comparing the weekly absorbance of a $50 \text{ mgL}^{-1} \text{ PO}_4^{3-} - \text{P}$ sample with both reagent batches at 380 nm

Error bars were included in Figure 2-20 for each weekly analysis for $n = 3$ replications for reagent batch 2 also. The average absorbance data of reagent 2 in Table 2-12 had a relative standard deviation of less than 3.3 % for each weekly measurement over the 10-week period. The overall average absorbance for the 10 weeks was calculated as 2.3811 ± 0.1182 (RSD: 4.9659 %).

Table 2-12 Absorbance measurements made with a $50 \text{ mgL}^{-1} \text{ PO}_4^{3-} - \text{P}$ from reagent batch 2 over a 10-week period

Reagent Batch	Dec-99			Apr-01		
	Aver. Abs.	Std. Dev.	% RSD	Aver. Abs.	Std. Dev.	% RSD
Week 1	2.3822	0.0616	2.5870	2.4175	0.0219	0.9053
Week 2	2.4295	0.0285	1.1722	2.2933	0.0200	0.8735
Week 3	2.4900	0.0387	1.5559	2.4103	0.0195	0.8091
Week 4	2.3975	0.0336	1.4029	2.4515	0.0281	1.1463
Week 5	2.5433	0.0568	2.2316	2.5307	0.0629	2.4871
Week 6	2.2512	0.0185	0.8198	2.3392	0.0199	0.8508
Week 7	2.2825	0.0247	1.0841	2.2400	0.0736	3.2835
Week 8	2.2035	0.0497	2.2550	2.2967	0.0036	0.1575
Week 9	2.2920	0.0281	1.2261	2.2465	0.0252	1.1235
Week 10	2.4515	0.0163	0.6652	2.5853	0.0076	0.2929

A third fresh reagent batch was prepared and the absorbance of a 50 mgL⁻¹ PO₄³⁻ - P was taken in triplicate resulting in a value of 2.4130 ± 0.0729 (RSD: 3.0215 %). The result was compared with both reagent 1 and 2. Experimental concentrations were calculated from the equation of the line of a new calibration made with reagent batch 3, the results of which are shown in Table 2-13.

Table 2-13 Comparison of the results from the three reagent batches

Reagent Batch	Aver. Abs.	PO ₄ ³⁻ -P Conc. [mgL ⁻¹]	Std. Dev.	% RSD	% RE
Dec-99	2.3723	47.8624	2.2218	4.6420	4.2752
Apr-01	2.3811	48.0380	2.3649	4.9229	3.9240
Feb-02	2.4317	49.0495	0.3522	0.7181	1.9010

The average concentration was calculated as 47.8624 ± 2.2218 mgL⁻¹ PO₄³⁻ - P (RSD: 4.6420 %) and 48.0380 ± 2.3649 mgL⁻¹ PO₄³⁻ - P (RSD: 4.9229 %), for reagent 1 and 2, respectively. The relative error for reagent 1 and 2 was also calculated as 4.2752 and 3.9240 %, respectively. The two reagent batches were then compared to the February 2002 batch. The absorbance recorded for the third batch was marginally higher than the other two and the trend showed that over time the sensitivity decreased slightly. However the relative error remained less than 4.3 % two years after the batch was made up. Initially the main aim was to find a reagent that would be chemically stable for 1 year. The results here show that the lifetime of the yellow method reagent can be extended to even longer than that (> 2 years to date).

2.12 Conclusion

In this chapter the optimisation and chemical stability of the yellow colorimetric method for the determination of phosphorus in aqueous samples has been demonstrated. Variables such as pH of the heteropoly acid complex (Figure 2-13) and the interference of Fe²⁺ ions (Figure 2-17) were addressed. A validation study of the yellow method was made, which included the investigation of the following parameters, linearity (Figure 2-6), repeatability (Table 2-10), sensitivity of measurement (Figure 2-7), and long-term reagent stability (Table 2-13) was carried

out. The kinetic response of the yellow method reagent and an ortho-phosphate containing sample was also investigated and the reaction was shown to be rapid reaching completion within 3 min at room temperature (Figure 2-8). The validation was a success and the method was then implemented in a determination of phosphorus in a microfluidic manifold, the results of which are presented in Chapter 3.

2.13 References

- 1 I.D. Mc Kelvie, D.M.W. Worsfold, *Anal. Proc.*, 1995, **32**, 437-445.
- 2 G. Mission, *Chem.-Ztg.*, 1908, **32**, 633.
- 3 I.D. Mc Kelvie, B.T. Hart, T.J. Cardwell, R.W. Catrall, *Talanta*, 1993, **40**, 1981.
- 4 J.B Cotner, R.G. Wetzel, *Limnol. Oceanogr.*, 1992, **37**, 232.
- 5 P.W. Atkins, *Physical Chemistry*, 5th Ed., Oxford University Press, 1994.
- 6 W. Fresenius, K.E. Quentin, W. Schneider (Eds.), *Water Analysis*, Springer-Verlag, 1997, 239-240.
- 7 "High Power Can Type UV-LED", Nichia Product Guide, Model: NSHU590E Narrow Directivity, Nichia Chemical Industries Ltd., Tokushima 774, Japan, 2001 (Cat. No.: 98617).
- 8 D. Diamond, V.C.A. Hanratty, *Spreadsheet Applications in Chemistry using Microsoft Excel*, Wiley Interscience, New York 1997.
- 9 P. Kane and D. Diamond, *Talanta*, 1997, **44**, 1847-1858.
- 10 P.W. Atkins, *Concepts in Physical Chemistry*, Oxford Chemistry Guides, 1995.
- 11 D.F. Bolt, M.G. Mellon, *Anal. Chem.*, 1948, **29**, 749.
- 12 R.E. Kitson, M.G. Mellon, *Ind. Eng. Chem., Anal. Ed.*, 1944, **16**, 379.

-
- 13 A.E. Greenberg, A.D. Eaton, L.S. Cleseri, "*Standard Methods for the Examination of Water and Wastewater*", 4500-P Phosphorus, 18th Edit., ASPH, Washington, DC, USA, 1994, 166 – 181.

3 Application of the Yellow Method in a Microfluidic Manifold

Progress in the development of a miniaturised microfluidic instrument for monitoring phosphorus in natural waters and wastewater is presented in this chapter. The yellow colorimetric method for phosphate analysis has been transferred to a microfluidic system. This simple method employs one reagent mixed in a 1:1 ratio with a sample to produce a yellow colour absorbing strongly below 400nm. A stopped flow approach was used which, together with the very rapid kinetics and simple reagent stream, enabled a very uncomplicated microfluidic manifold design to be employed. The working wavelength was 380 nm to coincide with the peak output of a recently developed UV-LED narrow bandwidth light source. The aims of the microfluidic analysis were to:

1. demonstrate the reproducibility and control possible in the microfluidic manifold
2. reproduce the limit of detection ($0.2 \text{ mgL}^{-1} \text{ PO}_4^{3-} - \text{P}$) and the dynamic linear range ($0 - 50 \text{ mg}^{-1} \text{ PO}_4^{3-} - \text{P}$) for the yellow method achieved in the conventional set-up.
3. show significant improvement in chemical consumption and waste generation when the scale was reduced
4. highlight the integration of multiple components into a simple device
5. decrease the power requirement, size and the cost of making reproducible analytical measurements
6. promote the need for developing small-scale devices capable of operating autonomously in-situ.

The reaction time at room temperature was less than 3 min, which meant about 20 samples / hour could theoretically be analysed. Another important feature of the application of the yellow method was the chemical stability of the reagent and the long-term function of the method in the microfluidic manifold. The reagent lifetime has been shown in Chapter 2 to be stable for a minimum of one year. Multiple calibrations have been performed in the microfluidic system over a 12-month period showing only minimal loss in performance and a $4 \text{ mgL}^{-1} \text{ P}$ standard was analysed in the microfluidic manifold on a weekly basis with a relative standard deviation of less than 2.3 %.

The successful implementation of the yellow method in the microfluidic manifold is the first major stepping stone in this research. The ultimate goal is to develop a

polymeric microfluidic device capable of functioning, autonomously for one year without maintenance and with less than 500 ml waste generation / year.

3.1 Instrumental Set Up

The microsystem had more components than the conventional set-up, the microfluidic manifold being the principle element of the system. The other key components were the pump, light source, spectrometer, microchip holder, valve-control and sample / storage reservoirs. In Figure 3-1 a simplified schematic of the instrumentation is given. The system consisted of a Harvard PHD 2000 syringe pump (Antec Leyden BV, The Netherlands) fitted with a syringe holder (designed by Danfoss A/S, Nordborg, Denmark) securing the borosilicate glass 3.3 (DURAN[®]) syringes in position (Innovative Labor Systeme (ILS), Dresden, Germany). The syringes were connected to the microchip holder by PEEK tubing. Valves labelled **(v1)** and **(v2)** were positioned between the syringes and the microchip, controlling the flow from the reservoirs for refilling, and from the syringes for injecting. **(v1)** controls the sample flow and **(v2)** the reagent. The reservoirs labelled **(r1)** and **(r2)** were connected to the valves **(v1)** and **(v2)** and contained the sample and the reagent respectively. The third reservoir, **(r3)**, was for the waste collection from the chip, after it passed through the waste channel. The microchip holder was designed to facilitate fluidic interconnections in silicon chips with flow channels. The novel concept encompassed wedging the microchip between two rigid plates. The top layer was fabricated in Perspex, and was fastened with 4 locator screws for alignment. The chip was aligned to holes in the bottom layer, which connected to the syringe pump via PEEK tubing. On the microchips underside interconnection holes were spaced 4.6 mm apart in an array. These aligned with holes of similar dimension in the bottom layer of the holder. Chips are typically 23 by 14 mm in size, which equated to a 5 × 3 array of fluidic inlets. The holder orifices were sunken to accommodate o-rings, which provided leak-free interconnects to the external PEEK tubing. The o-rings were of a soft black polymer material with an outer diameter of 2 mm and inner diameter of 0.8 mm (Apple Rubber Product Inc., New York, USA) and the yellow PEEK tubing had an outer diameter of 1.6 mm and an inner diameter of 0.0178 mm (UpChurch Scientific Ltd., England).

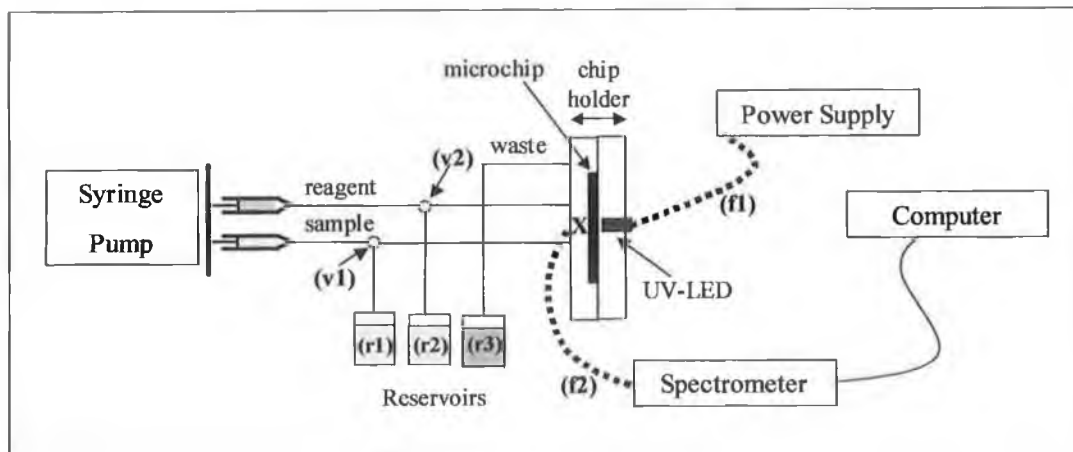


Figure 3-1 Schematic of the microfluidic system including all components

The Ocean Optics S2000 spectrometer (Ocean Optics Inc., Florida, USA) with OOIBase₃₂ software was chosen because of its portability and good sensitivity. The optical detection was incorporated into the microfluidic chip holder (Model: NSHU-590E, Nichia Europe B.V., Hornweg 18, 1045 AR Amsterdam, The Netherlands). This was made possible due to the small dimensions of the UV-LED (6.2 mm × 4.7 mm) and an optical fibre with an outer diameter of 2.8 mm and a core of inner diameter, 240 μm. The UV-LED was embedded in the top Perspex lid of the microchip holder. The hole in the Perspex layer was positioned directly above the optical cuvette hole. The UV-LED was then aligned in the hole, where it was secured a fixed distance of 1.8 mm from the surface of the microchip. An electrical cable connected the UV-LED to its power supply, which is shown as **(f1)** in Figure 3-1. The portable spectrometer was connected to the microchip via the aforementioned optical fibre **(f2)**, which was fitted to the bottom layer of the microchip holder at the point **X**.

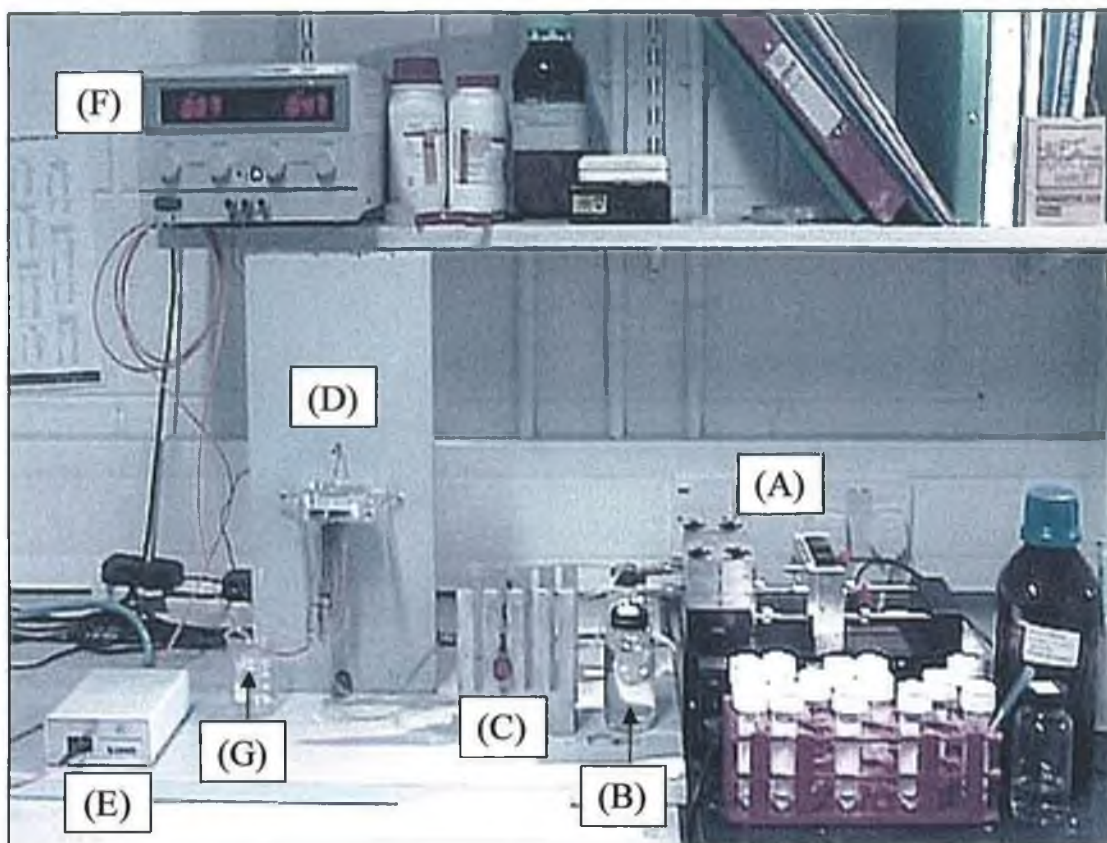


Figure 3-2 Photograph of the microfluidic system

In Figure 3-2 a photograph of the microfluidic set-up is shown with the key components labelled (A) → (G), where:

- (A) is the pumping unit with the syringe holder attached
- (B) is the 100 ml reservoir storage bottle for the refilling of syringes with the reagent and respective orthophosphate-containing sample.
- (C) is the two valves for the manual control of the movement of fluid
- (D) is the microfluidic chip encased in its Perspex holder with the UV-LED embedded in the top, and the optical fibre in the bottom, lid.
- (E) is the portable spectrometer
- (F) is the power supply for the UV-LED
- (G) is the point of outflow and collection of the waste solution

Each component is subsequently described in more detail stating its function, operation, capabilities and limitations.

3.1.1 Microfluidic Chip Holder

The chip holder is mounted on a platform to ensure no movement as is shown in the photograph in Figure 3-3.



Figure 3-3 Side profile of the microfluidic chip holder including interconnects and optical detection

In Figure 3-3 the microchip holder is shown secured in its stand, which consists of two parts the ring labelled 1 and the upright, labelled 2. The microchip holder fits into the 7.4 cm-diameter ring and is secured in place by three pins of 6 mm diameter positioned on its perimeter. The upright is screwed down onto a 1m x 0.4 m wooden table. The upright is also made of wood with dimensions 10 cm x 30 cm. There are two holes spaced 5 cm apart, which are located on the upright board, which facilitate the attachment of the ring. These holes, which are also found in the ring, are aligned with the upright. Two screws of 8 cm length were used to hold the microchip holder in place. The sample and reagent lines are labelled as S and R respectively and the waste reservoir is also shown in Figure 3-3.

The microfluidic chip is secured between two blocks of Perspex, the top layer is of transparent polymethyl methacrylate (PMMA) and houses the light source, the bottom is for the transfer of optical data via fibre optics to the spectrometer and promotes leak-free fluidic interconnects.

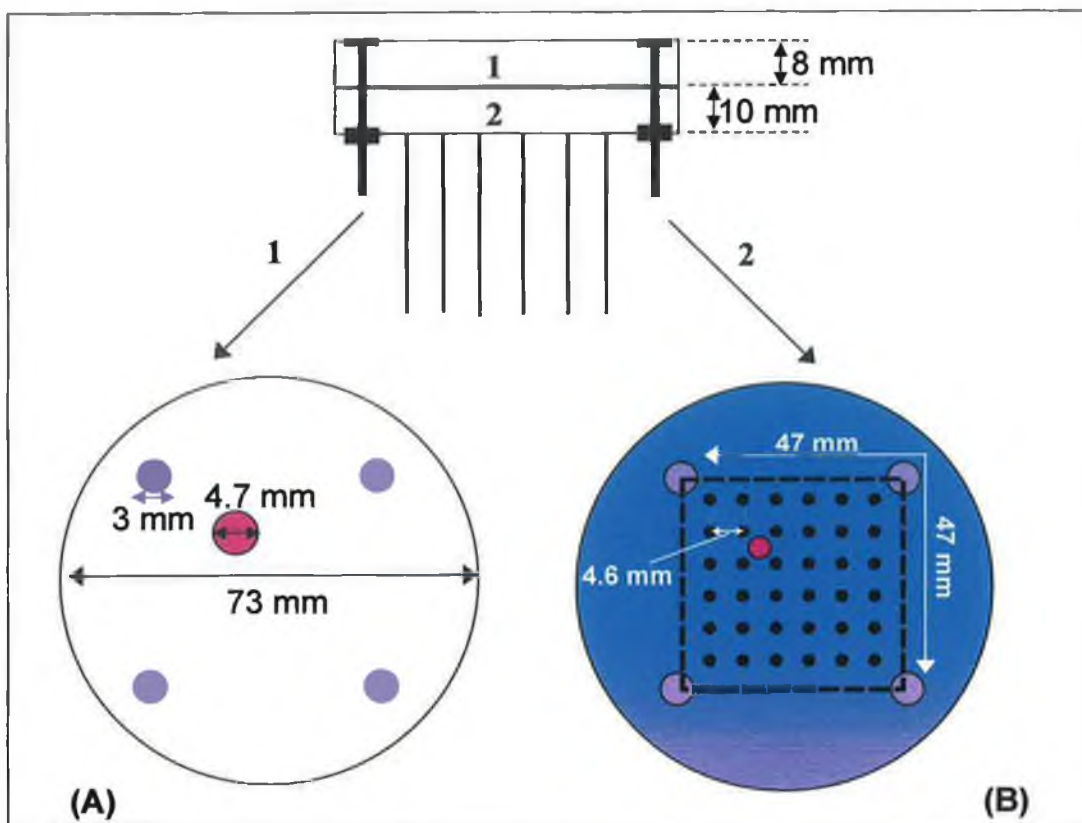


Figure 3-4 Schematic showing the design and layout of the top (A) and bottom (B) layers of the silicon microfluidic chip holder

In Figure 3-4 the holder is shown as consisting of two layers, the top, 1, and the bottom, 2. When opened out the layout of the top layer is labelled as (A) and the bottom as (B). The top layer was 8 mm thick and of optically clear PMMA. The red circle of 4.7 mm diameter indicates the position and diameter of the hole to house the UV-LED. The UV-LED was of 6.2 mm length and lay 1.8 mm from the surface of the microchip, when inserted in position. There are 4 alignment holes of 3 mm diameter in both layers, whereby 3 mm diameter nuts and bolts are used to fasten the two parts together and the entire diameter of the holder is 73 mm.

The bottom layer of the holder is more complicated in design. The fluid is pumped onto the fluidic channels of the chip via the 1 mm interconnecting holes shown in figure 3-4 (B). The silicon microfluidic chips fabricated for this research were 23×15 mm, of which the backside, interconnection holes are spaced 4.6 mm apart in an 6×6 hole array, align with holes of similar dimensions in the holder. The holder orifices are sunken to accommodate o-rings, which promote leak-free flow. The

microfluidic chip is fitted into the holder ensuring the optical cuvette is aligned over the 2 mm diameter hole for the optical fibre connection.

3.1.2 Pumping Unit

The Harvard PHD syringe pump was initially chosen for its micro-dispensing capabilities. For a 250 μL syringe the nominal flow-rate range is between 0.05 μL / hr and 47.5 mL / hr [1]. The manipulation of precise micro doses of fluid was further promoted by the addition of a Danfoss (purpose-built) syringe holder¹, which not only held syringes of all sizes in place but also allowed multiple syringes to be refilled and used simultaneously. The holder could securely clamp up to fourteen syringes, two on the bottom and six in each of the next two rows as shown in Figure 3-5. The holder consisted of two parts. The first controlled the movement of the needle of the syringe. The syringe end was secured in a groove in the holder and as the pump moved the syringe was refilled / injected with fluid. The second part consisted of three layers, which held each individual syringe in place by a teeth pattern that kept the component tight and compact. Four screws were used to maintain the tight fit.

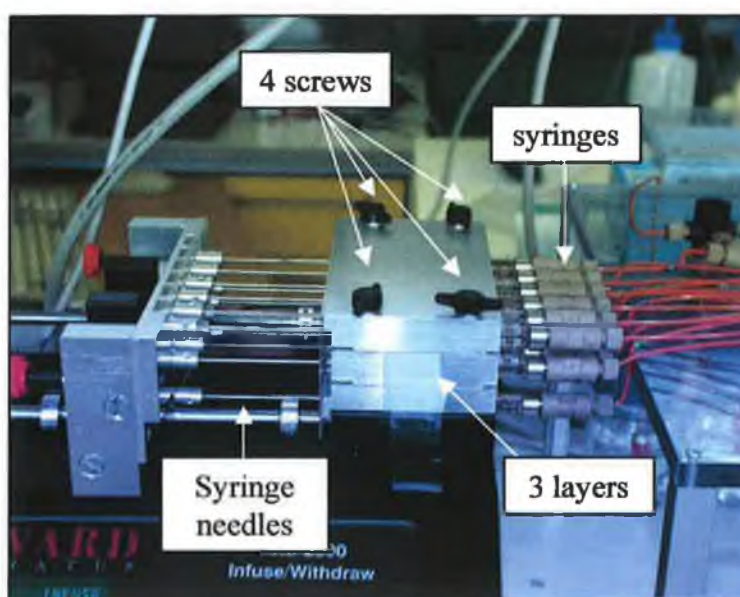


Figure 3-5 Syringe pump fitted with metal holder containing up to 14 syringes

¹ Fabricated by Danfoss A/S, Nordborg, DK-3640, Denmark, www.danfoss.dk

Typically only two syringes, for the reagent and orthophosphate sample, were needed. The syringe holder was initially designed for a more complex colorimetric method for the determination of aluminium in wastewater, which had three reagents alone. The two syringes were positioned on opposite sides of the holder. This was done to maintain a balanced flow between the reagent and the sample across the microfluidic chip. In this way the stoichiometric ratio of 1:1 for the yellow method reaction was preserved.

3.1.3 Micro-dispensing Syringes

In Figure 3-6 a photograph of the micro-syringe (Innovative Labor Systeme (ILS), Mittelstrasse, Stützerbach, Germany) utilised to pump fluid from reservoir to chip is shown. The micro-syringes shell was made of borosilicate glass and the needle of stainless steel with a volume of 250 μL and a diameter of 2.3 mm. When the pump was operated in refill mode the piston moved backwards pulling the syringes in the holder back also. The syringes were filled from the reservoir bottles via the yellow PEEK tubing. When inject mode was selected the pump piston moved forwards and the syringes dispensed fluid through the PEEK tubing network onto the microfluidic chip.

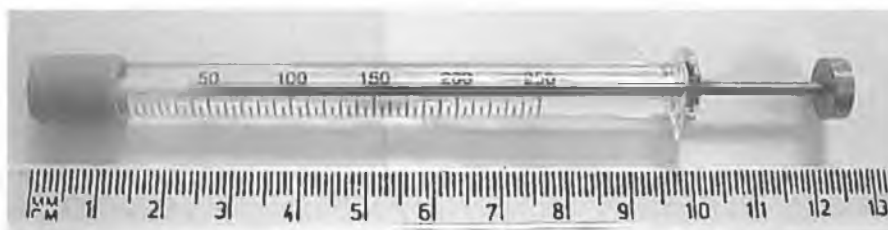


Figure 3-6 Photograph of a 250 μL syringe for the transportation of fluid from the reservoirs onto the microfluidic manifold

3.1.4 Valve Fluid Control

The valves were made of stainless steel with rubber external covers for easy manual use. Leak-free connections to the pump and microfluidic manifold were made with PEEK tubing and ferrules. Two valves were required for the control of the reagent and the sample respectively. By switching the valves 90° in a clockwise direction a flow from the syringes onto the microfluidic chip or from the

reservoirs to the syringes was achieved. The valves were controlled manually, which proved important when optimising the flow-rate for analysis.

3.1.5 Reservoirs

The reservoirs were 250 ml, acid-washed, brown, glass bottles with screw-top lids. 1mm diameter holes were drilled in the lids so that the FIA tubing could fit through and be submerged in the solution within. The reservoirs were used to store the reagent and the orthophosphate sample. The reservoirs were interchangeable, i.e. they could easily be removed and replaced. The low volumes of reagent and sample required for the microfluidic analysis meant that once the reagent bottles were filled they could be used over extended periods of time.

3.1.6 Tubing and Interconnects

PEEK and FIA peristaltic tubing were both incorporated in the flow system. The yellow PEEK (Model: 1536L, UpChurch Scientific, Anachem Ltd., Luton, Bedfordshire, UK) tubing is a hard, rigid polymer material with an outer diameter of 1.6 mm and an inner diameter of 175 μm . The PEEK tubing connects the syringes to the valves and from the valves to the microfluidic chip. The microchip holder was fitted with PEEK tubing, which is connected to the rest of the system as shown in Figure 3-7. There are three channels to consider, the reagent, the sample and the waste channel. A union with two ferrules was used to make the interconnection (Model: P-702, UpChurch Scientific, Anachem Ltd., Luton, Bedfordshire, UK). The peristaltic tubing was a soft, polymer material. It was therefore used for its flexibility to transfer fluid through the reservoir lid for the refilling the syringes and from the waste outlet to the waste reservoir.

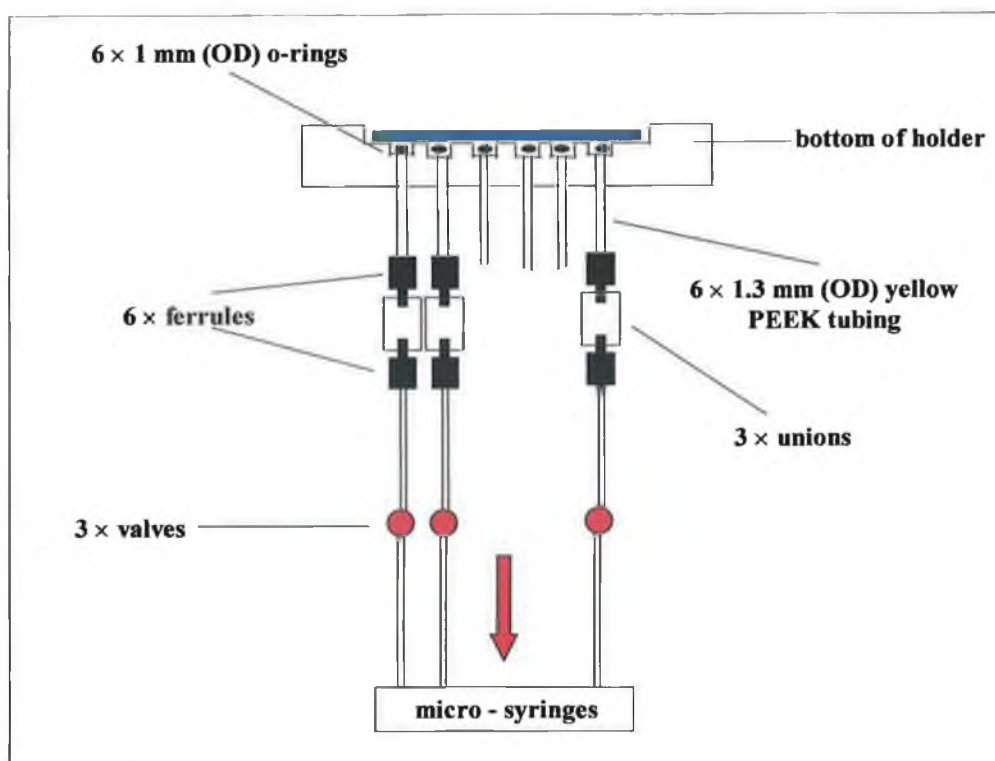


Figure 3-7 Schematic highlighting how leak-free flow is achieved at the tubing / microfluidic manifold interface resulting using quick release, finger-tight ferrules and o-rings

The o-rings of inner and outer diameters of 0.55 mm and 1 mm respectively were composed of black rubber. They were placed in the sunken holes of the bottom layer of the holder in Figure 3-7. The PEEK tubing inserted in the holder lies flush with the bottom of the sunken orifices. The force exerted on the o-rings when the microchip is aligned in the holder and tightened with the screws promotes leak-free fluidic interconnects.

3.1.7 Waste Collection and Disposal

The waste was collected in a similar bottle to that for the storage of the reagent and the sample. Because the flow-rate is minimal and the amount of waste generated is negligible, the waste jar does not need to be disposed frequently. The waste solution must first be diluted with water and then flushed down the sink with the tap running.

3.2 Optical Detection

There were many limitations placed on the optical detection with respect to the yellow method, because the complex absorbed strongly below 400 nm. As shown in chapter 2 conventional lamps such as the tungsten-halogen and the deuterium lamp, although emitting light in the range of interest, had a poor intensity.

3.2.1 UV-LED

A photograph and schematic of the UV-LED are shown in Figure 3-8 on the left and right respectively. The photograph shows the low purplish-blue glow emitted by the LED and the plastic tubing to protect the soldered parts. In the schematic the dimensions of the UV-LED are documented indicating the small size of the device.

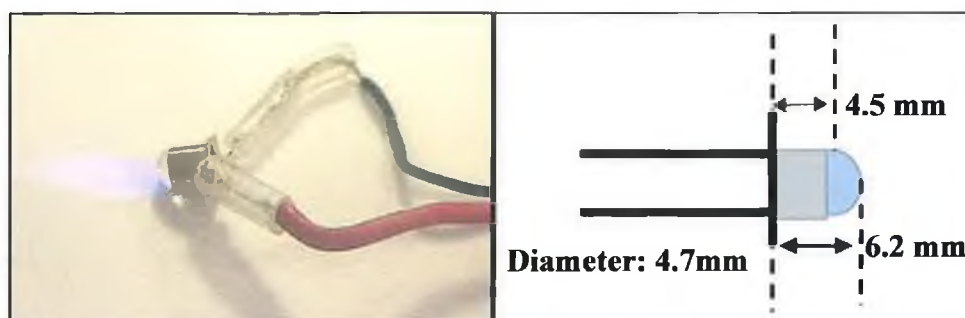


Figure 3-8 Illumination of a UV-LED and its dimensions

It wasn't until the advent of the UV-LED that a suitable source became available. However the UV-LED has proven to be ideal for the yellow method for a multitude of reasons:

1. ***Small size:*** compact, improvement in overall scale of the instrumentation
2. ***Low power consumption:*** 9V battery (Model: Duracell PP3, Farnell, FEC(Ireland) Limited, Dublin, Ireland), approx. 1000 microfluidic measurements (of 5 min duration) can be taken when the UV-LED is operated in sleep mode, whereby the battery is switched on for the time it takes to make a measurement rather than running continuously.

$$P_{(UV-LED)} = 0.06 W$$

$$P_{(9V Battery)} = 4.95 W hr$$

$$\Rightarrow \frac{4.95 W hr}{0.06 W} = 82.5 hr \text{ (continuous operation)}$$

$$\cong 1000 \text{ measurements}$$

* where P is the power [Watts]

3. Suitability to the colorimetric method: 380 nm working wavelength near the λ_{max} for the lamp emission spectrum and the yellow complex absorbance spectrum
4. Simplicity: Very easy to use, assemble and incorporate in system
5. Integration into a microfluidic manifold: embedded in the top layer of the microfluidic chip holder with optimum sensitivity being achieved
6. Cost efficient: LED's are cheap, particularly when bought in bulk

3.2.2 Portable Spectrometer

The portable spectrometer shown in Figure 3-9 has dimensions of 14.2 (L) mm \times 10.5 (W) \times 4.1 (H) mm. The optical signal was transported via an optical fibre from the optical cuvette to the spectrometer and the data was then transferred to a PC via an electric cable, where the signal was converted to an optical quantity using the spectrometer software.

With the OOIBase₃₂ software all analytical measurements were made in absorbance mode with the exception of the emission spectra of the light sources, which were taken as an intensity-based measurement.

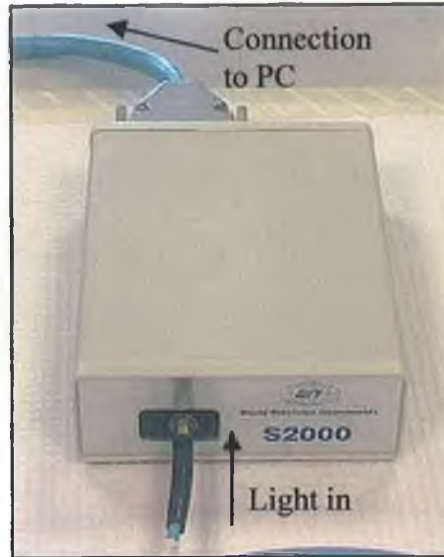


Figure 3-9 Picture of the S-2000 portable spectrometer manufactured by Ocean Optics

3.2.3 Optical Fibres

In Figure 3-10 the optical fibre is shown as a photograph (A) and a schematic of the propagation of light through a fibre (B).

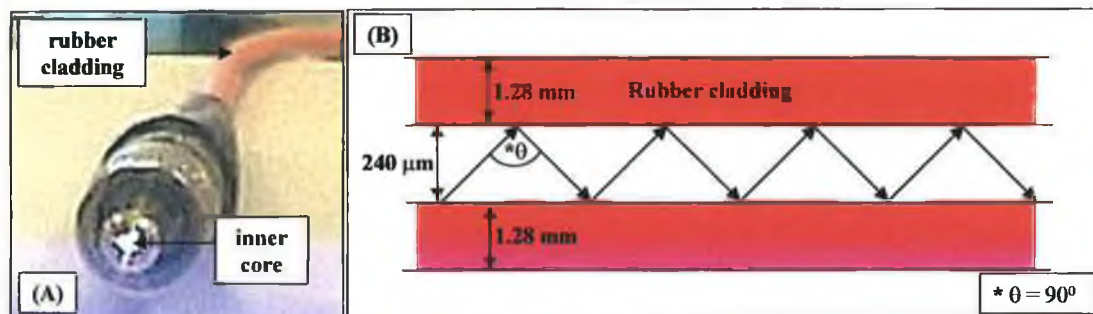


Figure 3-10 Optical fibre with inner diameter of $240\ \mu\text{m}$ illuminated by a tungsten-halogen light source (A) and the side profile of the light propagation through the optical fibre (B)

The photograph on the left shows the small spot size of the optical fibre that has to be correctly aligned to the optical cuvette to ensure maximum light is transmitted to the spectrometer for detection. To show how small the spot size actually is a tungsten-halogen lamp was attached at the opposite end. On the right the schematic shows how the light propagates as a wave with a 61° angle of incidence. The inner core consists of acrylic polymer (polymethyl methacrylate)

and is sheathed with a thin layer of fluoropolymer, which has a lower refractive index than the fibre core itself.

The optical fibre lay flush with the bottom of the microchip holder in direct contact with the bottom of the microfluidic chip. An optical fibre of inner core diameter 240 μm and outer diameter of 2.2 mm was chosen to best suit the micro-cuvette of 200 μm diameter.

3.3 Flow Regime

At first a continuous mode was considered to be the most likely flow regime. At very slow flow-rates of circa 1 $\mu\text{L} / \text{min}$ in a long meandering micro-channel, laminar flow dominates. Firstly the reagent and sample are introduced into separate micro-channels, at a fixed point both channels converged and the reagent and sample mix by diffusion. The reaction time is approx. 3 min for the yellow method, which means that if a flow-rate of 1 $\mu\text{L} / \text{min}$ is used the reaction coil volume has to be greater than or equal to 3 μL to ensure the reaction has reached completion. The resulting sample plug passes over the optical cuvette for detection. The continuous flow regime was tricky to optimise, so considering the rapid kinetics of the yellow method the idea of employing a stopped flow was investigated.

An advantage of implementing a stopped flow regime was the replacement of the long meandering coil chip layout with a far simpler t-junction microfluidic design. The stopped flow method also facilitates sampling when a micro-dialysis sampling unit is attached to the microfluidic manifold. Reaction kinetics can also be monitored in the micro-cuvette under stopped flow.

Under stopped flow conditions very small volumes of fluid were required, which resulted in less reagent consumption and decreased waste generation. Unlike with continuous flow in microfluidic channels, very low flow-rates were not necessary. The reproducibility of the flow-rate wasn't an issue, as long as the two pumps for

the reagent and sample operated in tandem, so that accurate on-chip mixing took place.

The sample and the reagent were still introduced via two separate micro-channels. However at the t-junction, where the two channels converged there was no need for a long reaction channel. The straight channel was less than 1 mm in length, which equated to a 5-fold reduction in the volume of the microfluidic chip. The whole chip could be filled very quickly and the flow stopped to make a measurement. Instead of the reaction happening somewhere along the reaction coil, to produce a moving sample plug, it was monitored in the optical cuvette, where the end point of the reaction could be seen in real-time. When the reaction had reached completion and a steady-state signal recorded, the flow was switched on again and the microfluidic chip was refilled again as the sample was pumped to the waste collection bottle. The reaction time was approx. 3 min at room temperature, which meant that sample turnaround was typically 18 - 20 samples / hour. Other advantages of a stopped flow method were the decrease in power consumption of the light source and the pump under stopped flow because the system need only be on when a measurement is required. The power consumption is less of an issue in the laboratory set-up, but is critical when considering the design for a robust system capable of operating in-situ for extended periods of time, maintenance-free.

The stopped flow regime was optimised for the microfluidic manifold. Both the sample and the reagent were passed through the chip simultaneously at a total flow rate of 1 μL / min for approx. 1 min or until a stable signal was observed. An integration time of 300 ms provided a good signal-to-noise ratio at a reasonably fast data acquisition rate. When the flow was stopped diffusional mixing took place rapidly and the yellow heteropoly complex was formed in the optical cuvette. When the flow was re-started, the complex was flushed to waste and the signal returned to its original baseline.

3.4 Calibration Study

The yellow method has been successfully investigated in a 1-cm cuvette set-up. The microfluidic chip has a micro-cuvette of 400 μm path length, which is twenty five times smaller than the conventional system. The application and suitability of the yellow method in a microfluidic measurement was examined in this chapter. A linear correlation of absorbance versus concentration would be a clear indication that the yellow method could be adapted to a microfluidic system. The sensitivity of the analytical measurement in the microfluidic manifold was also assessed.

3.4.1 Microfluidic Chip Layout

The chip was fabricated using the dry reactive ion etching (DRIE) technique resulting in a three-layered wafer of Pyrex/Silicon/Pyrex [2]. The 400 μm thick silicon layer is protectively coated by deposition of silicon nitride to the surface by a low-pressure chemical vapour process (LPCVD) to combat corrosion [3]. And an advanced silicon etching (ASE) process is used to etch the optical cuvette. After which, all three layers of the chip must be correctly aligned to ensure interconnection of the fluidic components. When the wafer is anodically bonded, it is known as a wafer stack [4, 5]. Anodic bonding is desirable for protecting the chip from the working environment.

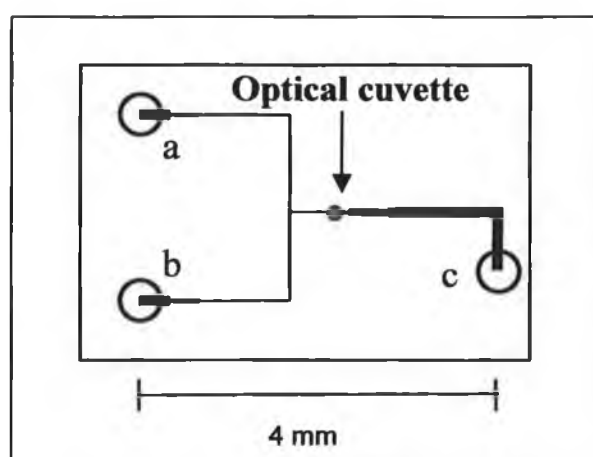


Figure 3-11 Microfluidic chip layout utilised for the stopped flow measurement

The chip layout in Figure 3-11 was utilised in the stopped flow measurements made for the linearity study. The inlets for the reagent and the sample were labelled, as a and b, respectively, the waste outlet as c and the optical cuvette was positioned as marked in the schematic. The inlet / outlet holes were 200 μm in diameter. The t-junction channel layout had a width of 80 μm and a depth of 120 μm , whereas the waste channel was wider, resulting from a tapering of the channel from 200 – 280 μm over a 1 mm distance, to discourage air bubbles from lodging over the optical cuvette. The optical cuvette itself had a depth of 400 μm , which was the path length for the measurement as defined by Beers Law.

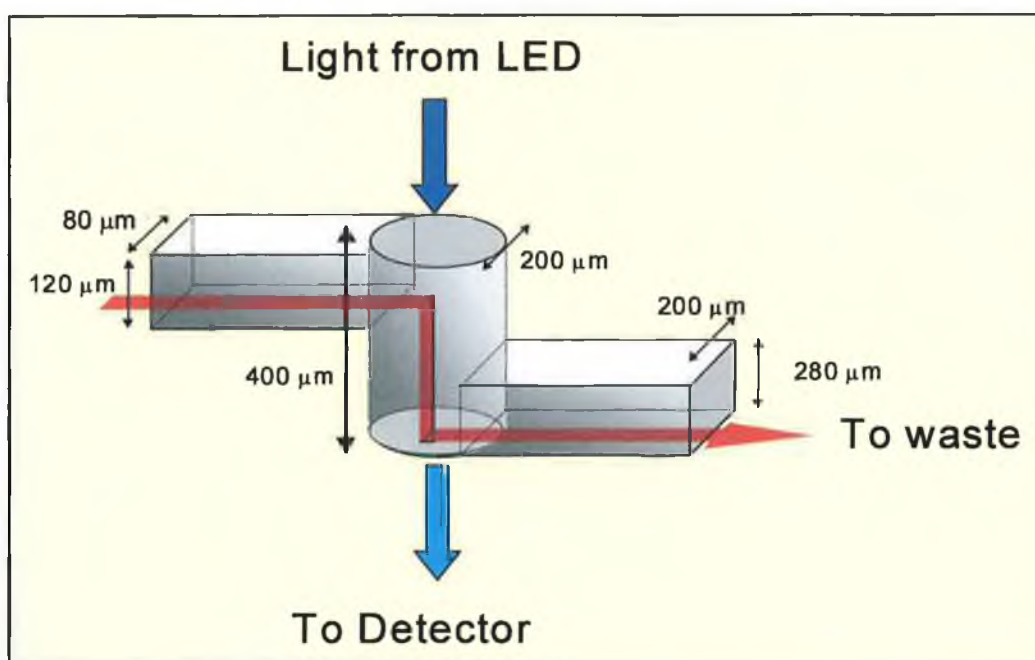


Figure 3-12 Schematic indicating the flow from and to the optical cuvette of the microfluidic manifold [6]

In Figure 3-12 the design of the optical cuvette in the silicon layer is shown. The flow path is indicated by the red arrow, whereby the fluid comes in from the top and passes out through the bottom, which shows that the silicon wafer is etched on both sides, with the inlets and microfluidic channel on one side and the waste channel on the opposite. The double-sided microfluidic design is sandwiched between two Pyrex plates each of 1 mm thickness by anodic bonding as previously mentioned.

3.4.2 Preliminary Analysis with Malachite Green Dye

Initial experiments in the microfluidic manifold were based on the absorbance of the Malachite Green dye in the micro-cuvette. Malachite Green was primarily chosen because of its intense blue colour. Even if the measurement weren't sensitive, at least a signal would be observed, to indicate that the microfluidic chip was functioning correctly.

A series of standards were prepared over the concentration range 0 – 182.5 mgL⁻¹ and triplicate measurements of each standard were performed. From the well-known absorbance spectrum of Malachite Green the wavelength range investigated was 620 – 650 nm. The analysis was carried out at three different wavelengths 620, 635 and 650 nm. A standard tungsten-halogen lamp as described in the conventional analysis was utilised (see Chapter 2, Section 2.4). The intensity signal from the tungsten-halogen lamp in the mid-UV range is good.

The microfluidic system set-up as described from Figure 3-1 was utilised, with a few minor adjustments. The reservoirs, instead of containing the yellow method reagent and the orthophosphate sample, were substituted for distilled water and a standard Malachite Green dye of known concentration. A continuous flow method was implemented with a flow-rate of 1 µL / min chosen for the analysis. A baseline was captured at an integration time of 500 ms with the distilled water. When a stable baseline signal was achieved (within 2 min) the valve controlling the dye was switched from flow-to-reservoir to flow-to-microfluidic chip. After several seconds a large jump in the absorbance signal was observed. The signal quickly reached a maximum height and a stable plateau was realised. This stable signal or plug maximum was recorded for 1 min. Then the valves were alternated with the distilled water flowing across the microfluidic chip and the dye back to the reservoir jar. The signal returned to the initial baseline position and the cycle was repeated in triplicate.

The absorbance of each calibration standard was calculated as the average of the plug maximum ($n = 30$ data points) less the baseline signal average ($n = 30$ data points). The calibration was carried out in triplicate at the three wavelengths. In Figure 3-13 the average absorbance ($n = 3$) versus the dye concentration over the range 0 – 182.5 mgL⁻¹ at the three wavelengths 620, 635 and 650 nm is plotted.

By comparing the three plots the optimum wavelength for measuring the absorbance of the Malachite Green dye was determined. As the wavelength was decreased, the sensitivity of the measurement increased. This was a result of the best coherence of the tungsten-halogen lamps emission spectrum and the wavelength maximum (620 nm) of the dye.

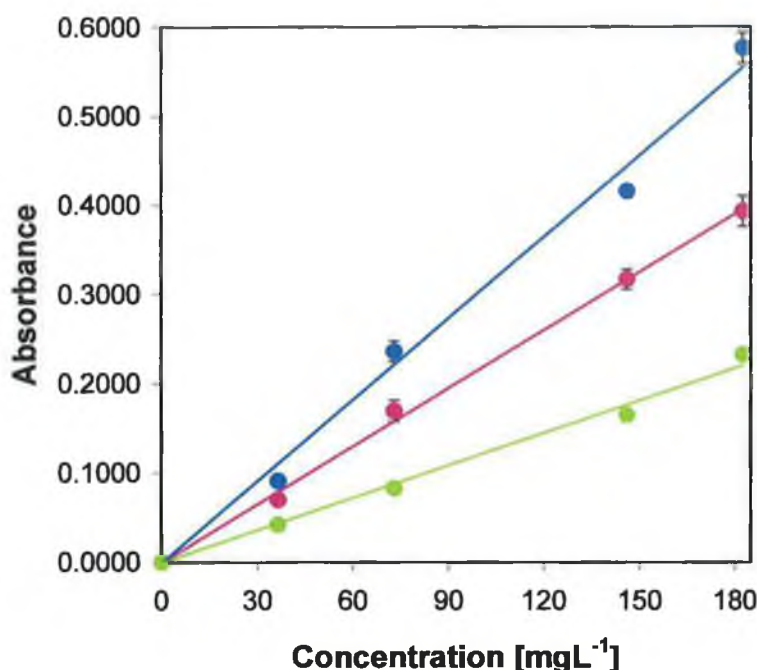


Figure 3-13 Comparison of calibration plots of dye concentration versus absorbance over the concentration range 0 – 182.5 mgL⁻¹ at the three wavelengths of 620, 635 and 650 nm

Table 3-1 Average absorbance of the Malachite Green dye measured at three wavelengths 620, 635 and 650 nm

Conc. PO ₄ ³⁻ - P[mgL ⁻¹]	0	5	10	25	50
620 nm					
Average Absorbance	0	0.0912	0.2359	0.4156	0.5766
Std.Dev.	0	0.0027	0.0114	0.0074	0.0175
% RSD	0	2.9444	4.8424	1.7781	3.0312
635 nm					
Average Absorbance	0	0.0698	0.1692	0.3170	0.3927
Std.Dev.	0	0.0038	0.0121	0.0112	0.0174
% RSD	0	5.4085	7.1575	3.5214	4.4292
650 nm					
Average Absorbance	0	0.0421	0.0828	0.1643	0.2319
Std.Dev.	0	0.0022	0.0021	0.0030	0.0029
% RSD	0	5.1847	2.5946	1.8335	1.2339

Error bars were included and an RSD value of less than 7.2 % (n = 3) was calculated highlighting the reproducibility of all three data sets. All three calibrations satisfied the criteria for linearity with R^2 values of 0.9911 ± 0.0047 (RSD: 0.4707 %), 0.9962 ± 0.0035 (RSD: 0.3535 %) and 0.9918 ± 0.0032 (0.3180 %). The average absorbance values measured at the three wavelengths are shown in Table 3-1.

The basic purpose of carrying out a calibration study with a strong dye like Malachite Green was to discover firstly whether an analytical measurement could even be made in the microfluidic manifold. Having clearly demonstrated that it was possible, a number of issues were addressed, which were of aid, when considering the yellow method measurement, including:

1. The erosion of the silicon chips was expedited by strongly alkaline solutions
2. The use of an intensely coloured dye in the system leads to coatings of the micro-channel walls and the optical cuvette, impeding accurate measurement of the analyte of interest
3. The use of unstable reagents, i.e. reagents that precipitate, in the microfluidic manifold leads to blockages in the narrow conduits

The Malachite Green calibration in the microfluidic manifold was exactly as would have been seen in a conventional system with good reproducibility demonstrated in the preliminary results.

3.4.3 Yellow Method Analysis

The heteropoly acid complex, of concentration $\text{PO}_4^{3-} - \text{P}$, formed during the yellow method reaction has been shown to be extremely acidic ($\text{pH} < 1$), so the lifetime of the silicon chip was not affected by erosion, i.e. the chip is only eroded by very basic solutions. The long-term chemical stability of the reagent also meant that a blockage arising from precipitate formation was not a problem. The yellow method heteropoly complex was not an intense colour like that of a dye. In fact the yellow colour was quite weak in comparison to the Malachite Green dye, which posed a number of challenges in terms of optical detection. However, coating of the

microfluidic chips inner walls and optical cuvette was not experienced. To maintain the clean conditions within the microfluidic chip a mild acidic solution (0.1 M HCl) was prepared. Any grit or stains were simply removed by pumping a small amount of the acidic solution through the chip. By gentle heating of the solution prior to injection onto the chip the cleaning process was completed within minutes. The cleaning of the microfluidic chip was performed on a twice-daily basis (pre- and post-analysis).

Calibration Study of pre-mixed PO_4^{3-} - P complex

The first experiment undertaken was the investigation of the sensitivity of the yellow complex measurement in the microfluidic manifold. Calibration standards over the concentration range 0 – 50 mgL^{-1} were prepared from the stock solution and reacted with the reagent to form the PO_4^{3-} - P samples. Each pre-mixed PO_4^{3-} - P sample was analysed as described for the Malachite Green study with distilled water utilised to generate a baseline signal.

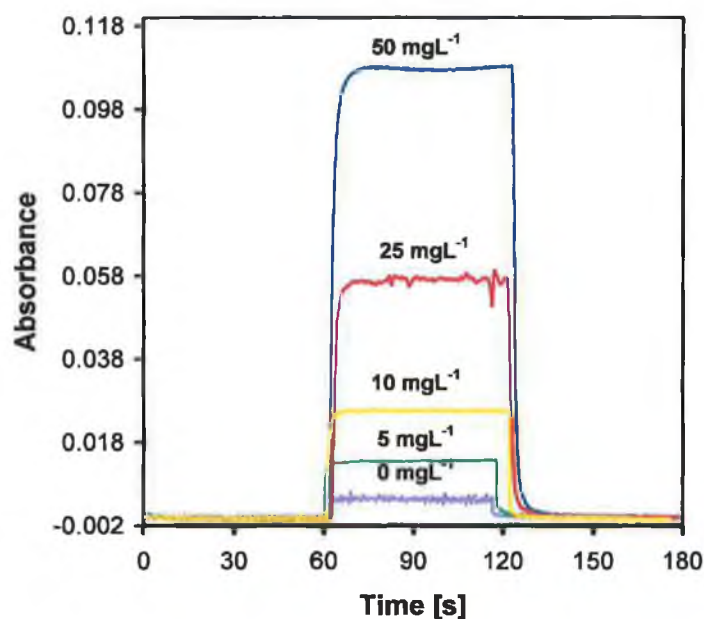


Figure 3-14 Real-time plug injections made over the concentration range 0 –50 mgL^{-1} PO_4^{3-} - P at a working wavelength of 380 nm

The sample plugs shown in Figure 3-14 were recorded in real-time. Each plug shown was the average signal ($n = 3$) calculated at each concentration. The plug max average and the baseline average were calculated for $n = 30$ data points.

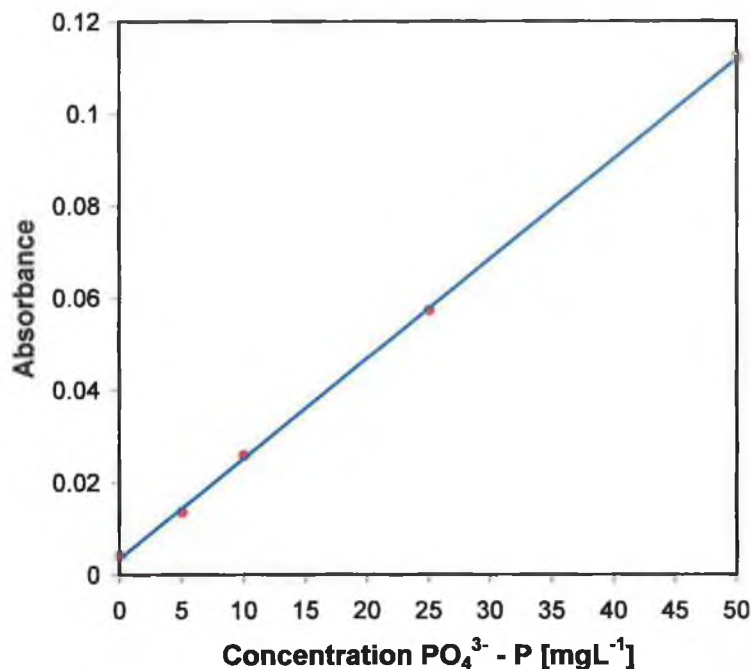


Figure 3-15 Average plot of absorbance versus concentration of $PO_4^{3-} - P$ over the concentration range $0 - 50 \text{ mgL}^{-1}$ at a working wavelength of 380 nm

The average absorbance was then plotted versus the $PO_4^{3-} - P$ concentration over the range $0 - 50 \text{ mgL}^{-1}$ at a wavelength of 380 nm as shown in Figure 3-15

Error bars were included ($n=3$ replicates), although the data points representing each calibration standard on the plot mask them. This was due to the fine reproducibility of the repeat measurements ($\% \text{ RSD} < 2.6 \%$ for every point, see Table 3-2). The slope of the line, m , was calculated as $0.0022 \pm 2.9104 \times 10^{-11}$ ($\text{RSD}: 1.3230 \times 10^{-5} \%$). The R^2 value for the calibration of the pre-mixed yellow heteropoly acidic complex was calculated as $0.9998 \pm 5.8000 \times 10^{-5}$ ($\text{RSD}: 5.8000 \times 10^{-3} \%$).

Table 3-2 Triplicate measurements of the absorbance of the PO_4^{3-} - P complex over the concentration range 0 – 50 mgL^{-1} at a working wavelength of 380 nm

Conc. [mgL^{-1}]	1	2	3	Aver. Abs.	Std. Dev.	% RSD
0.0000	0.0043	0.0041	0.0041	0.0042	0.0001	2.6011
5.0000	0.0136	0.0136	0.0138	0.0136	0.0001	0.7887
10.0000	0.0257	0.0260	0.0261	0.0259	0.0002	0.6651
25.0000	0.0573	0.0573	0.0574	0.0573	0.0001	0.1123
50.0000	0.1130	0.1121	0.1115	0.1122	0.0008	0.6786

Calibration Study of the on-line mixed PO_4^{3-} - P complex

Firstly a reference baseline was measured with deionised water at a total flow-rate of 1 μL / min for 1 min. For this stage of the calibration study the reagent and orthophosphate standard were reacted along the microfluidic channel (Figure 3-11) and in the optical cuvette.

For the purpose of this analysis a stopped flow method was employed. Both the sample and the reagent were passed through the chip simultaneously at a total flow rate of 1 μL / min for 1 min. When the flow was stopped diffusional mixing took place rapidly because of the narrow width of the short, mixing channel and the two solutions then reacted to form the yellow heteropoly complex. The reaction was complete when a steady state signal was observed. The flow was then restarted and at a rate of 1 μL / min laminar flow again dominated and the whole process was repeated in triplicate. The resulting injection plugs are shown in Figure 3-16.

Averages for the baseline and the plug maximum were calculated ($n=30$ data points). The absorbance was calculated by subtracting the averaged water baseline from the averaged plug maximum. The average absorbance of each sample was plotted against PO_4^{3-} - P concentration over the range 0 – 50 mgL^{-1} at a wavelength of 380 nm in Figure 3-17 and the results tabulated in Table 3-3. Error bars were included for $n = 3$ replicates.

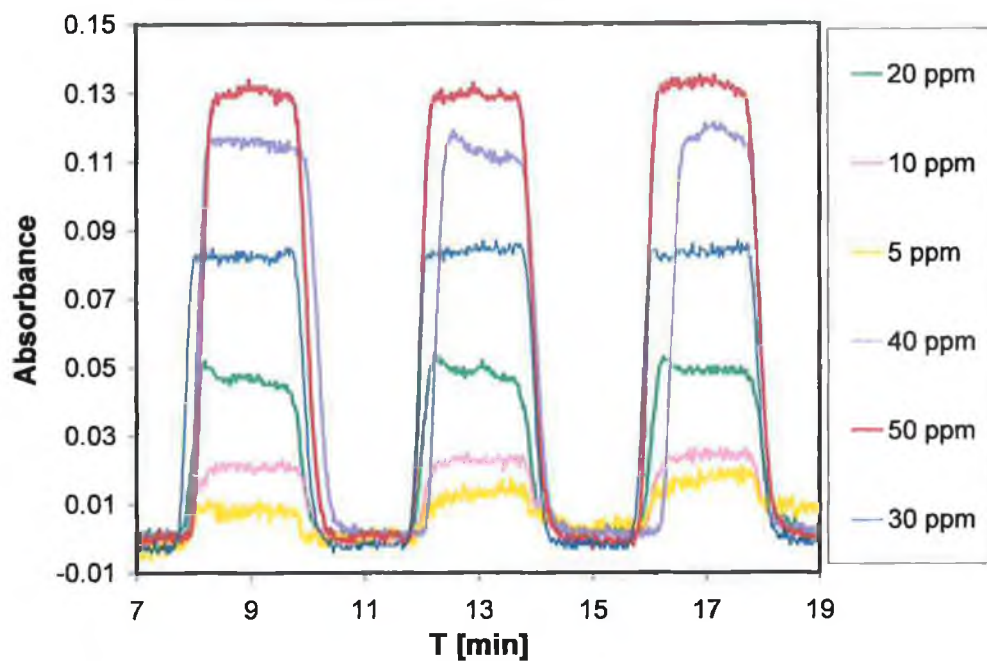


Figure 3-16 Multiple injection plugs over the concentration range 0–50 $\text{PO}_4^{3-} - \text{P}$ mgL^{-1} under stopped flow conditions at a working wavelength of 380 nm

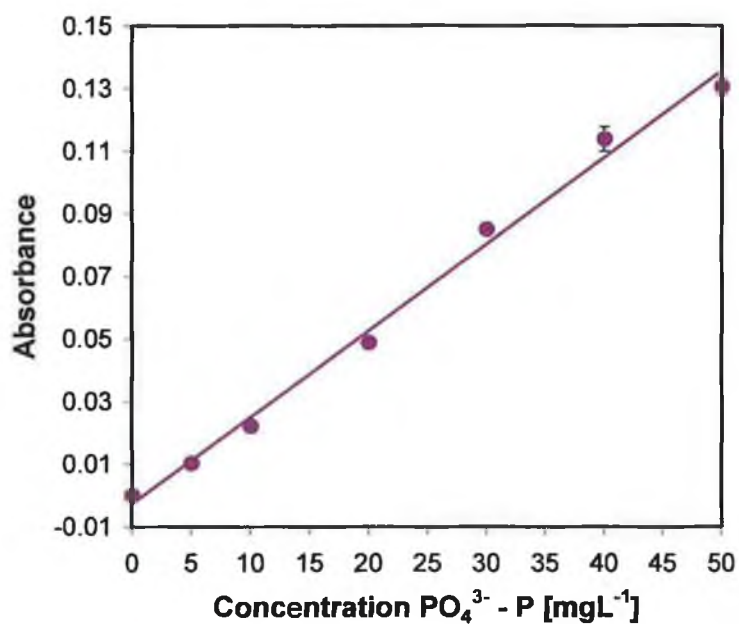


Figure 3-17 On-line calibration of absorbance versus concentration $\text{PO}_4^{3-} - \text{P}$ over the concentration range 0–50 mgL^{-1} at a working wavelength of 380 nm

The average slope and R^2 values were calculated from the triplicate measurements as $0.0028 \pm 4.1159 \times 10^{-11}$ (RSD: 1.4699×10^{-6} %) and 0.9929 ± 0.0023 (RSD:

0.2313 %) respectively. A correlation coefficient of the absorbance data from the on-line to the pre-mixed samples was calculated as 0.9924 ± 0.0015 (RSD: 0.1506 %).

Table 3-3 Triplicate measurements of absorbance over the concentration range 0 – 50 PO_4^{3-} - P mgL^{-1} at a working wavelength of 380 nm

Conc. [mgL^{-1}]	1	2	3	Aver. Abs.	Std. Dev.	% RSD
0	0.0000	0.0000	0.0000	0.0000	0.0000	0.0000
5	0.0105	0.0101	0.0103	0.0103	0.0002	1.8554
10	0.0211	0.0224	0.0231	0.0222	0.0010	4.5617
20	0.0482	0.0495	0.0489	0.0489	0.0006	1.2917
30	0.0852	0.0856	0.0845	0.0851	0.0005	0.6042
40	0.1156	0.1095	0.1166	0.1139	0.0038	3.3725
50	0.1298	0.1283	0.1334	0.1305	0.0026	2.0092

3.5 Kinetic Study in the Microfluidic Manifold

Reaction kinetics can be monitored in a controlled environment under laminar flow in a microfluidic manifold. Improved control of the reaction conditions results in more accurate estimates of rate constants, from room temperature up to 45°C. Microfluidic chips offer fundamental advantages over conventional bench measurements for the investigation of reaction kinetics, in particular, the reduction in reagent/sample volumes and the control over mixing processes. For example, small volumes of reagents are easily heated and cooled, and mixing can be extremely rapid in narrow channels.

Quick sample turnaround is universally regarded as one of the major advantages of conventional FIA. However, FIA instruments are still relatively large in size, when compared with microfluidic systems. Typically in conventional FIA the temperature is controlled by a thermostat bath and the reaction is carried out in a jacketed flow cell. This type of temperature control is very slow and it can take several hours just to increase the temperature by several degrees, which increases the analysis time required per sample drastically. Comparing this to the method employed in this microsystem, sample turnaround is approximately 1 hour, for a kinetics study that involves multiple temperature settings. This is due to the fact that the temperature

can be stepped up/down in a matter of seconds because of the tiny volumes involved and the efficient heat gain/loss arising from the high surface volume to bulk ratio, and the availability of novel materials such as optically transparent heating pads that are easily integrated into microfluidic manifolds.

3.5.1 Microfluidic Manifold

The system (see Figure 3-18) comprised a Harvard PHD 2000 syringe pump (Antec Leyden BV, the Netherlands) fitted with a syringe holder (Danfoss A/S, Nordborg, Denmark) securing the borosilicate glass 3.3 (DURAN®) syringes in position (Innovative Labor Systeme, Mittelstasse 37, Germany). The syringes were connected to the microchip and holder, by 1/8" PEEK tubing. Valves labelled (v1) and (v2) were positioned between the syringes and the microchip, controlling the flow from the reservoirs for refilling, and from the syringes for injecting. (v1) controlled the sample flow and (v2) the reagent-line. The reservoirs labelled (r1) and (r2) were connected to the valves (v1) and (v2) and contained the sample and the reagent, respectively. The third reservoir, (r3), was for the waste collection from the chip, after the yellow solution has passed through the waste channel.

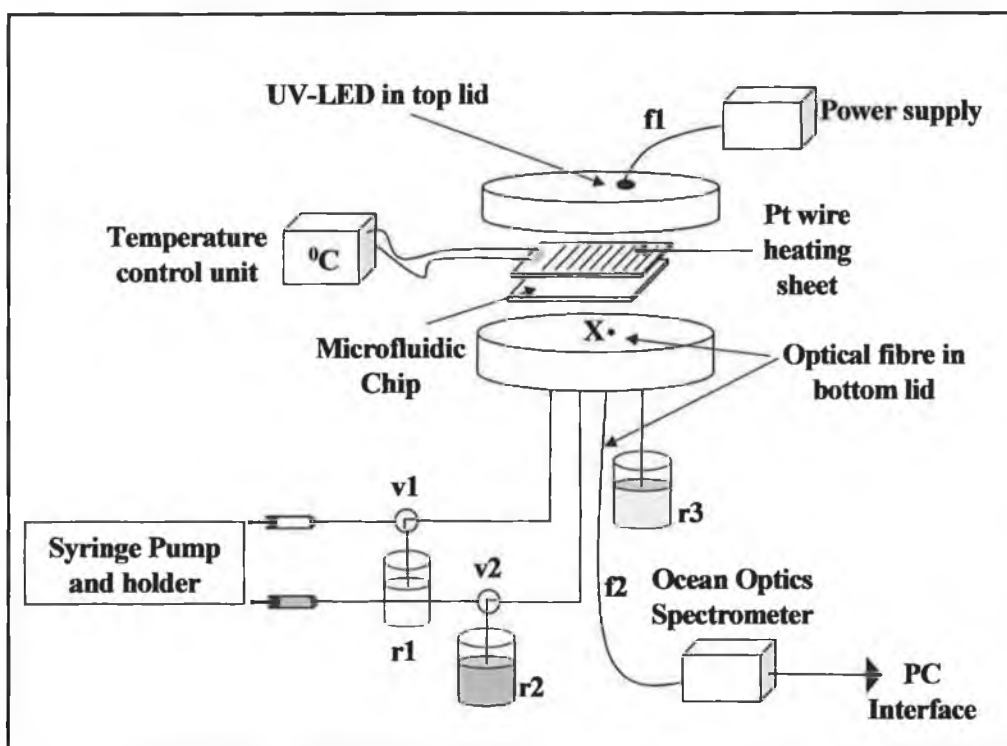


Figure 3-18 Schematic diagram of the microfluidic system, incorporating the temperature system

The microchip holder was designed to facilitate fluidic interconnections and optimise optical alignment. The novel concept encompassed sandwiching the microchip between two rigid plates. The top layer was made of Perspex, and was fastened with 4 locator screws for alignment. The chip was aligned to holes in the bottom layer, which connected to the syringe pump via PEEK tubing. Chips were typically 23 by 23mm in size. On the microchip underside interconnection holes were spaced 4.6mm apart in an array. These aligned with holes of similar dimension in the bottom layer of the holder. The holder orifices were sunken to accommodate o-rings (Apple Rubber Products, Inc., USA) that provided leak-free interconnects to the external PEEK tubing (Anachem Ltd., Luton, Bedfordshire, UK)[7]. The Ocean Optics S2000 spectrometer with OOIBase₃₂ software was chosen because of its portability and sensitivity.

Another important component was the UV-LED (NSHU-590E model, Nichia Corporation, Tokushima, Japan), which was embedded in the microchip holder. Signals from the spectrometer were integrated over 50 ms at the working wavelength of 380 nm. An electrical cable connected the UV-LED, which requires 48 mW of energy, to its power supply shown in Figure 3-18 as (f1). The portable spectrometer was connected to the microchip via an optical fibre (f2), which was fixed to the bottom layer of the microchip holder at the point X [8]. In an optimised system this could be replaced with a photodiode element or equivalent low power integrated optical detector.

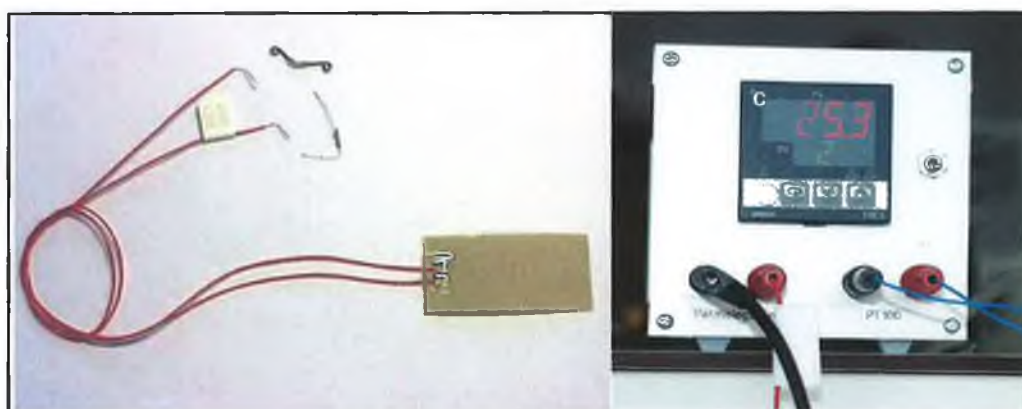


Figure 3-19 Heating foil and temperature control unit utilised throughout the kinetic experimentation

The Thermal-Clear™ transparent heating pad as photographed in Figure 3-19 (Minco Products, Inc., Minnesota, USA) was affixed to the topside of the glass cover plate of the microfluidic chip and thus sandwiched between the chip and the top Perspex lid of the chip holder. The heating pad consisted of a micro-thin fine resistive, wire element, typically 0.02 mm in diameter, sandwiched between layers of optical grade polyester, which acted as an insulator. The operating temperature range for the heating pad was 55 – 120°C with a minimum light transmission of 82 % over the visible spectrum. The heating pad dimensions were 40 mm (length) by 25 mm (width) by 0.25 mm (thickness), which fit well with the dimensions of the microfluidic chip holder. The heating pad required a 24 V DC supply and was regulated by a temperature control unit (CT14 model, also by Minco Products, Inc.).

3.5.2 Kinetic Measurements in the Microfluidic Manifold

By decreasing the flow-rate in small increments, on-line monitoring of the kinetics of the yellow method in a controlled environment was achieved. With an estimated dead volume of 0.115 µl for the microfluidic pathway, the time delay (and hence the position on the reaction profile) from mixing to arrival at the optical cuvette was controlled. In one run at 25 °C the flow-rate was varied from 20 to 0.08 µL/min and the time delay was estimated from Equation 3-1, where T is time (min), V is the chip volume (µl) and Q is the total flow-rate (µl /min). A series of time delays were calculated for flow rates in the specified range.

$$T = V/Q$$

Equation 3-1

For this temperature study, the development of the yellow heteropoly complex was monitored every 5 °C over the temperature range 22 - 45°C. Six temperatures were chosen over the range and the experiments were carried out in triplicate at each temperature increment. The measurement parameters throughout the kinetic investigation were set as follows, an integration time of 100 ms, a working wavelength of 380nm, a time acquisition program of 4000 acquisitions, with one every 0.5 sec. The acquisition cycle could be manually stopped, when the relevant information was gathered, so the total analysis time was dependent on the

temperature and flow-rate selections. Preliminary experiments were carried out at room temperature, $22.5\text{ }^{\circ}\text{C} \pm 0.5^{\circ}\text{C}$, providing basic information with which to investigate the entire temperature range.

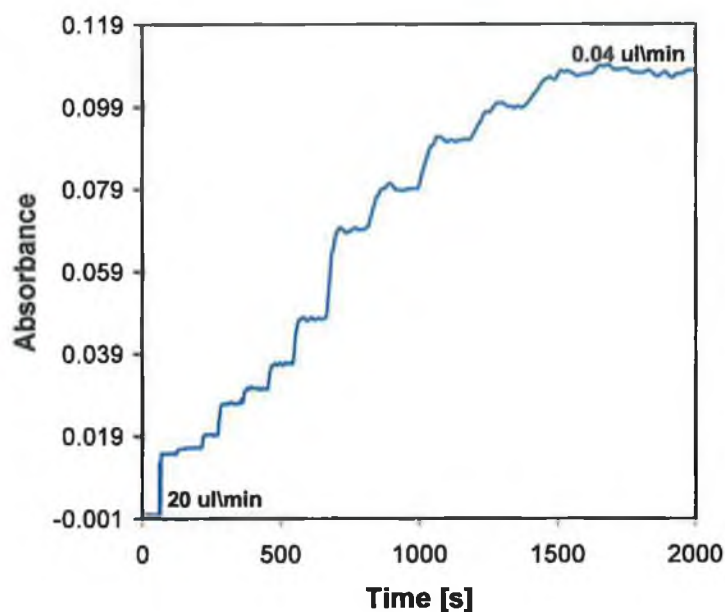


Figure 3-20 Stepwise sequence resulting from reducing the flow-rate in increments to capture kinetic data at specific time intervals of the reaction

The data was captured continuously as the flow-rate was decreased in increments and an average of each step on the real-time plot was calculated. The step shape, which represents the increase in absorbance to a steady state as the flow-rate decreases, is shown in Figure 3-20. Each step corresponds to a decrease in the flow rate, which enables the integrated optical cuvette to 'see' a point further along the kinetic curve.

The triplicate measurements performed at room temperature were plotted against each other in real-time as depicted in Figure 3-21. From the graph it was evident that the room temperature analysis yielded 3 reproducible kinetic curves with a minimum divergence in trend observed for run 1 (pink) after 80 s, resulting in a lower maximum absorbance of the complex at the end point of the reaction.

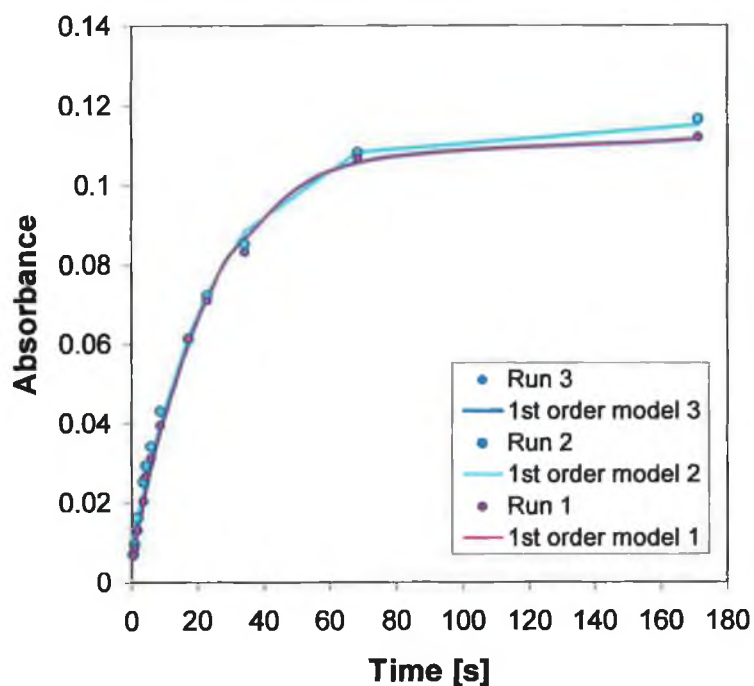


Figure 3-21 Kinetic plot for real-time data captured at 23 °C (room temperature) fitted to the 1st order model measured at 380 nm in the microfluidic manifold

However the average absorbance for the 50 mgL⁻¹ PO₄³⁻ - P complex was calculated as 0.1135 ± 0.0027 (RSD: 2.3379 %).

Table 3-4 Rate of Reaction data over the temperature range 22 – 45 °C at a working wavelength of 380 nm

Temp. [°C]	k1 [s ⁻¹]	k2 [s ⁻¹]	k3 [s ⁻¹]	Aver. k [s ⁻¹]	Std. Dev.	% RSD
25	0.0490	0.046	0.0495	0.0493	0.0003	0.6086
30	0.0973	0.1017	0.0971	0.0987	0.0026	2.6501
35	0.1545	0.1568	0.1459	0.1524	0.0056	3.7741
40	0.2609	0.2512	0.2509	0.2544	0.0057	2.2367
45	0.3337	N/A	N/A	0.3337	N/A	N/A

The rate constant was calculated over the temperature range 23 – 45 °C and in accordance with the kinetic theory increased with increasing temperature as shown in Table 3-4. When the rate constant was compared with the conventional system values the results showed that the experiments in the microfluidic manifold more accurately monitored the kinetics of the yellow method reaction. This was because of the controlled environment and the temperature stability for each measurement.

An RSD of ca. 4 % was calculated for the whole range compared with an RSD of ca. 33 % for the conventional system.

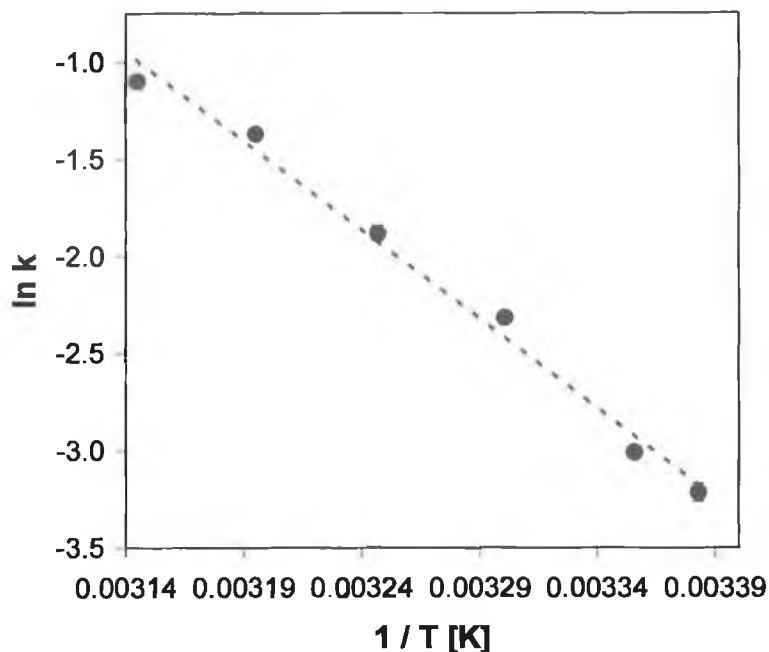


Figure 3-22 Calibration plot of $\ln k$ versus absolute temperature over the temperature interval 298 – 318 K at a working wavelength of 380 nm obtained with the microfluidic system

A linear Arrhenius plot showed that the rate of reaction is dependent on the temperature at which the reaction was proceeding. The average data for the three runs is plotted in Figure 3-22 with an R^2 value of 0.9906 ± 0.0040 (RSD: 0.3995 %). Error bars ($n = 3$) were included, but due to the good reproducibility of the data are masked by the data symbol on the graph. From the results the Arrhenius parameters, A and E_a were calculated as $40.16 \text{ kJmol}^{-1} \pm 1.54 \text{ kJmol}^{-1}$ (RSD: 3.84 %) and $106816 \text{ kJmol}^{-1} \pm 3910 \text{ kJmol}^{-1}$ (RSD: 3.7 %) respectively.

3.6 Repeatability

The repeatability of the measurement technique was excellent. In Figure 3-23 five repeat injections of a $4 \text{ mgL}^{-1} \text{ PO}_4^{3-}$ - P sample are shown.

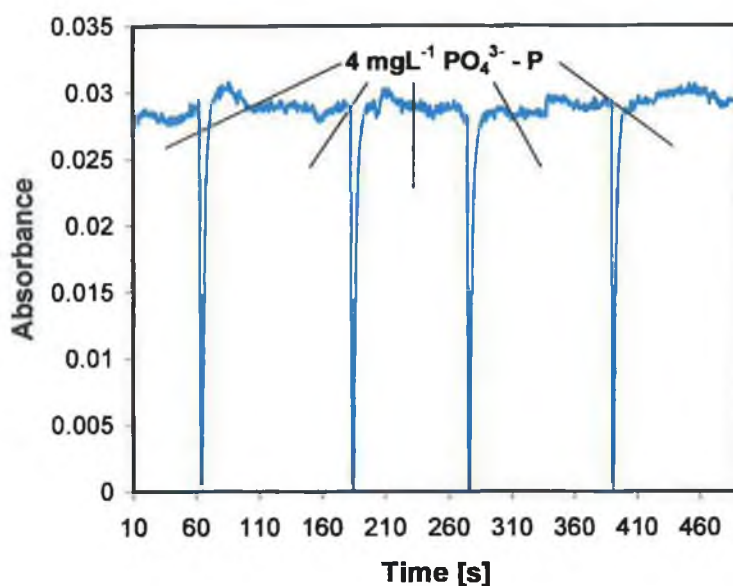


Figure 3-23 Repeatable plug injections of a $4 \text{ mgL}^{-1} \text{ PO}_4^{3-} - \text{P}$ sample in the microfluidic manifold at a working wavelength of 380 nm

The 4 mgL^{-1} standard was prepared by dilution of the 50 mgL^{-1} P stock solution (See Chapter 2, Section 2.1) and the $\text{PO}_4^{3-} - \text{P}$ complex was formed on-line in the microfluidic manifold under stopped flow conditions. Having already established that the signal returned to the same baseline position after each measurement, only one baseline was recorded at the beginning. Thus the time required to make 15 repeat measurements was quicker because as soon as the pump was restarted and the signal returned to the baseline, the pump was stopped and the next measurement made. The results presented in Table 3-5 are the average absorbance ($n = 30$ data points) for each plug. Each value has been subtracted from the same average baseline, rather than from a specific baseline taken prior to each measurement as has previously been described.

Table 3-5 15 repeat absorbance measurements of a 4 mgL⁻¹ PO₄³⁻ - P sample at a working wavelength of 380 nm

Plug	Abs.	Std. Dev.	% RSD
1	0.0064	0.0003	4.2309
2	0.0065	0.0002	3.4984
3	0.0067	0.0002	2.9439
4	0.0071	0.0002	3.3028
5	0.0069	0.0003	3.9814
6	0.0066	0.0004	5.5363
7	0.0068	0.0003	4.3543
8	0.0067	0.0003	3.8819
9	0.0076	0.0002	2.9900
10	0.0073	0.0003	4.3963
11	0.0070	0.0002	2.8597
12	0.0076	0.0003	3.3813
13	0.0064	0.0002	3.3163
14	0.0067	0.0003	4.6515
15	0.0071	0.0004	5.0226

The measurement of the 4 mgL⁻¹ PO₄³⁻ - P complex was repeated fifteen times with a RSD of typically ca. 5 % or less for the entire run. The average absorbance of the 4 mgL⁻¹ PO₄³⁻ - P for the fifteen runs was 0.0069 ± 0.0004 (RSD: 5.5546 %).

3.7 Reproducibility

It was very important to demonstrate that the reproducibility of the analytical measurement in the microfluidic manifold was better than that in the conventional system.

3.7.1 Reproducibility of a Standard 4 mgL⁻¹ PO₄³⁻ - P sample

Again a 4 mgL⁻¹ sample was prepared for the reproducibility study. Weekly absorbance values were measured in triplicate in the microfluidic manifold over a 2-month period and the average absorbance along with error bars for n = 3 were plotted as a histogram shown in Figure 3-24.

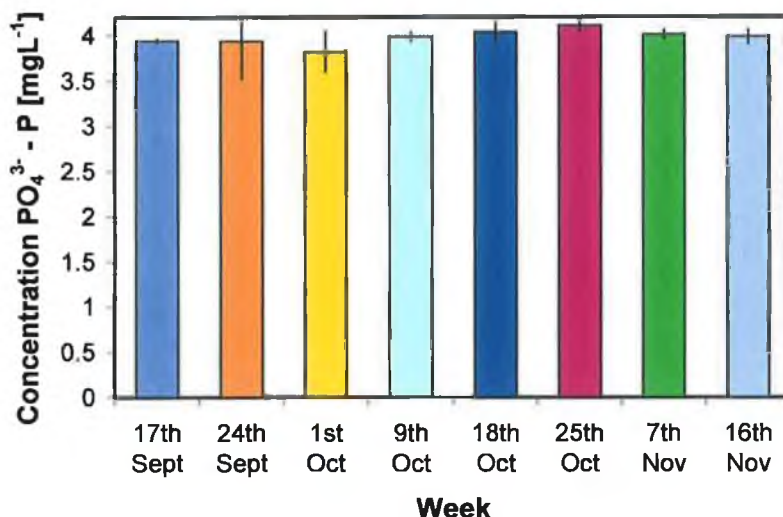


Figure 3-24 Weekly absorbance measurements made under stopped flow conditions in the microfluidic manifold for a sample of $4 \text{ mgL}^{-1} \text{ PO}_4^{3-} - \text{P}$ concentration at a working wavelength of 380 nm

A calibration was performed at the beginning of the study over the concentration range $0 - 50 \text{ mgL}^{-1} \text{ PO}_4^{3-} - \text{P}$. Eight measurements over the 2-month period were carried out. The absorbance values were then converted to a concentration based on the equation of the line for the linear plot, the results of which are shown in Figure 3-7. The relative error of the measured compared to the actual concentration was calculated as less than 4.7 % for the eight repeat measurements (see Table 3-6).

The average concentration of the eight measurements was calculated as 3.9797 ± 0.0846 (RSD: 2.1253 %) with a relative error of 0.5070 % when compared with the actual concentration of $4 \text{ mgL}^{-1} \text{ PO}_4^{3-} - \text{P}$.

Table 3-6 Weekly absorbance measurements of a 4 mgL⁻¹ PO₄³⁻ - P sample at a working wavelength of 380 nm

Week Ending	1	2	3	PO ₄ ³⁻ -P [mgL ⁻¹]	Std. Dev.	% RSD	% RE
17th Sept	3.9351	3.9659	3.9247	3.9419	0.0214	0.5433	1.4742
24th Sept	4.2462	4.1082	3.4598	3.9381	0.4199	10.6623	1.5729
1st Oct	3.8139	3.6001	4.0546	3.8229	0.2274	5.9473	4.6338
9th Oct	3.9402	3.9724	4.0464	3.9863	0.0545	1.3662	0.3432
18th Oct	4.0323	4.1496	3.9387	4.0402	0.1057	2.6157	0.9959
25th Oct	4.0636	4.0781	4.1946	4.1121	0.0718	1.7463	2.7257
7th Nov	4.0505	3.9509	4.0355	4.0123	0.0537	1.3382	0.3067
16th Nov	4.0792	3.9222	3.9506	3.9840	0.0837	2.0997	0.4015

3.7.2 Long-term Reproducibility of the Yellow Method Calibration

Standard calibrations as described previously were undertaken sporadically over a 1-year period, the results of which are shown in Figure 3-25. The samples were made with the same reagent batch solution. Six independent calibrations were carried out on different microsystems using the same batch of reagent, which was prepared in September 2000, i.e. one month prior to the first calibration. However, even though the analyses were carried out on different systems the same microfluidic chip layout was used. The first calibration was made in November 2000, where eight standards were analysed (0, 1, 5, 10, 15, 25, 40 and 50 mgL⁻¹), the second in February 2001 with five standards (0, 5, 10, 25 and 50 mgL⁻¹) etc.. In Figure 3-25 the six calibrations are plotted showing the highly comparable results obtained.

The major aim of this analysis was to emphasise the excellent chemical stability of the reaction over long periods of time (at least 1 year) and to demonstrate the extended lifetime of the yellow method reagent batch, compared to other reagent cocktails reported in a variety of different colorimetric methods for the determination of phosphate [9-12].

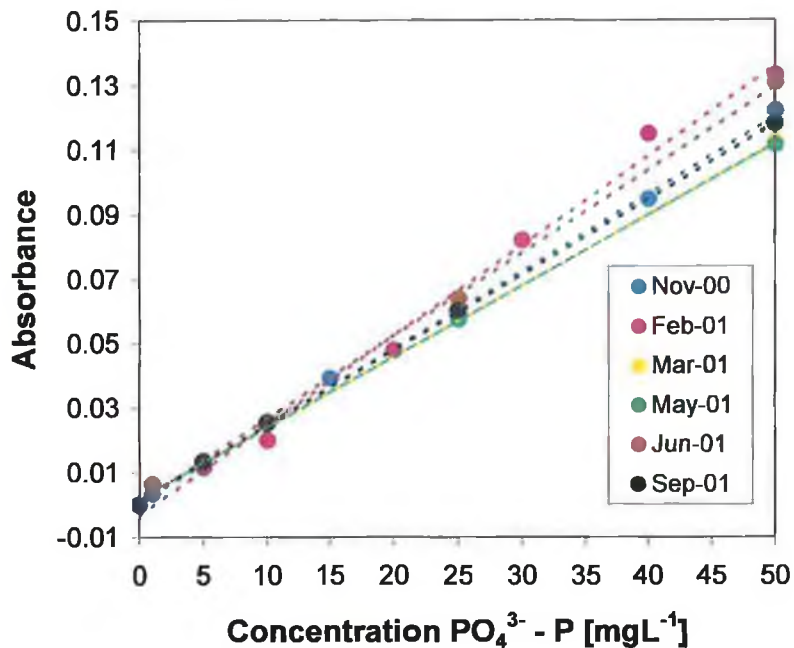


Figure 3-25 Comparison of multiple calibrations of absorbance versus concentration $\text{PO}_4^{3-} - \text{P}$ for a concentration range 0 – 50 mgL^{-1} over a 12 month period [13]

Different standard solutions within the 0 – 50 mgL^{-1} were prepared. However, in order to plot the average calibration for the 12-month period the standard solutions common to all 6 calibrations were used namely 0, 5, 10, 25 and 50 mgL^{-1} . The average absorbance versus the concentration $\text{PO}_4^{3-} - \text{P}$ was plotted in Figure 3-25 resulting in a perfect linear correlation with an R^2 value of 1 ± 0.0027 (RSD: 0.2750 %). The average results of which are displayed in Table 3-7. Error bars ($n = 3$) were included on the plot and the reproducibility of the data with the yellow method for a 1-year period was good with a RSD of less than 7.6 % ($n = 3$).

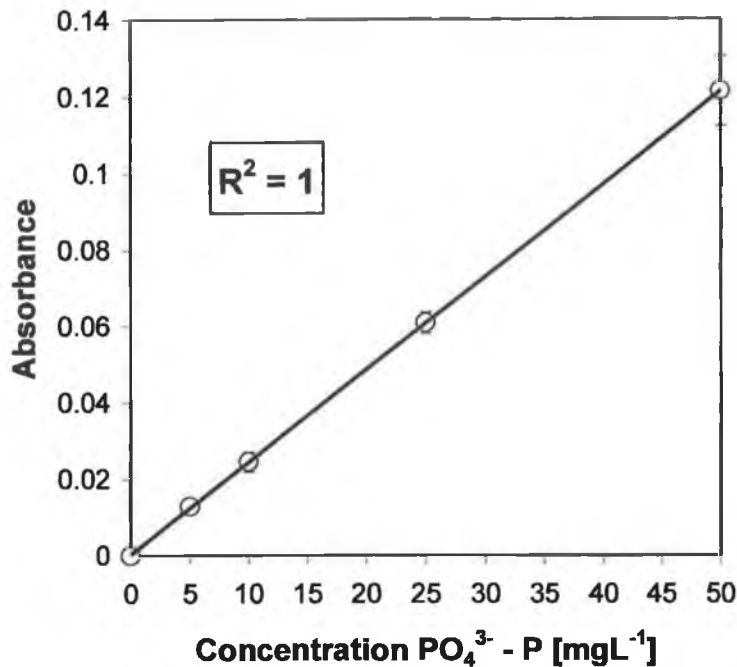


Figure 3-26 Calibration plot of absorbance versus concentration $PO_4^{3-} - P$ over the concentration range 0 – 50 mgL^{-1} representing the average data accumulated over a one year period

Table 3-7 Average absorbance data acquired over a 12-month period with a concentration range of 0 – 50 mgL^{-1} $PO_4^{3-} - P$ and a working wavelength of 380 nm

Conc. $PO_4^{3-} - P$ [mgL^{-1}]	Aver. Abs.	Std. Dev.	% RSD
0	0	0	0
5	0.012925	0.000946	7.322678
10	0.024533	0.00255	10.39518
25	0.060901	0.002737	4.49466
50	0.121281	0.00914	7.536605

3.8 Signal-to-Noise Ratio

Noise can be described as the random fluctuations of an analytical instrument measured as the standard deviation of the signal [14]. The signal is the average value, in this case absorbance, of the output of the portable spectrometer used. The signal to noise ratio (SNR) was calculated for the microfluidic measurements made with the portable spectrometer from Equation 3-1, where S is the signal, N is

the noise, S_{aver} is the average of the signal and ΔS is the standard deviation of the signal.

$$\frac{S}{N} = 5 S_{aver} / \Delta S \quad \text{Equation 3-2}$$

In order to calculate the SNR, an absorbance signal for a $5 \text{ mgL}^{-1} \text{ PO}_4^{3-} - \text{P}$ was recorded in real-time at a total flow-rate, Q_{TOTAL} , of $1 \mu\text{L} / \text{min}$. The stable baseline was captured for 1 min at an integration time of 300 ms and the raw data was treated with a moving average for $n = 25$ data points.

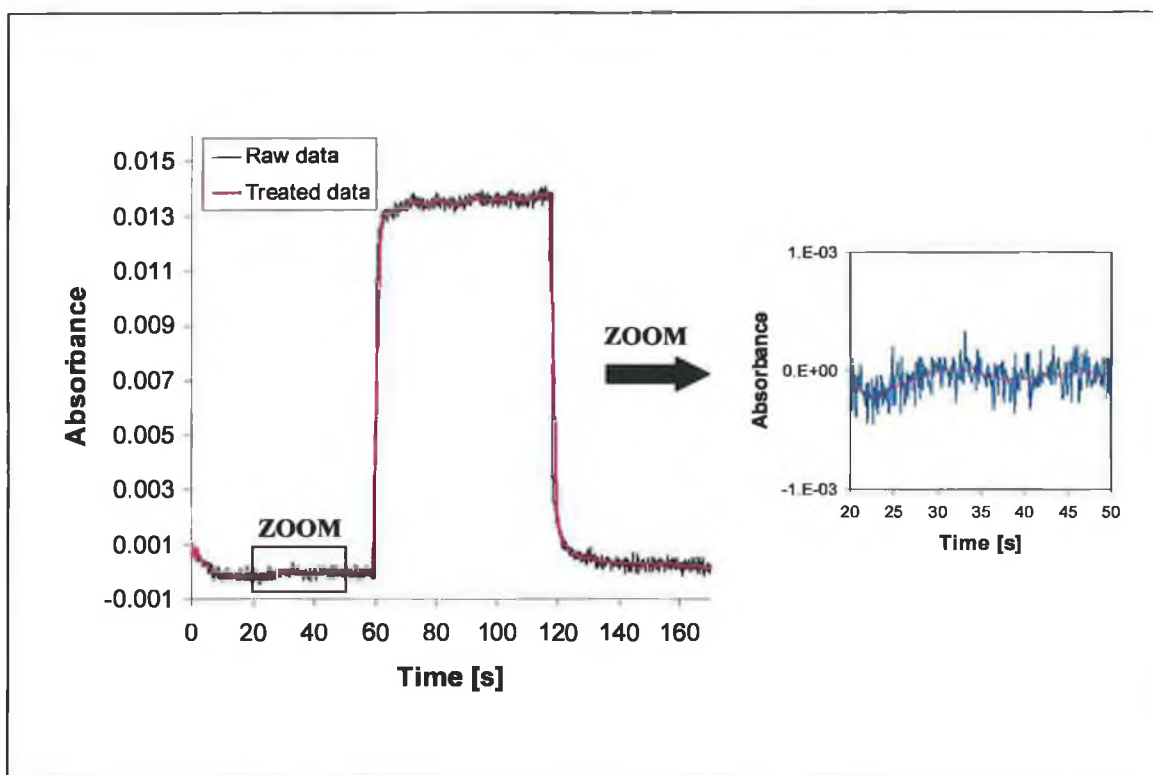


Figure 3-27 Real-time plug of $5 \text{ mgL}^{-1} \text{ PO}_4^{3-} - \text{P}$ with raw and treated data with inset of baseline signal ($n = 300$) for SNR determination

The raw and treated signals are shown in Figure 3-27 over the timescale 0 – 160 s. The average absorbance of the baseline signal ($n = 300$ data points) was calculated for the raw and treated data as 3.90×10^{-4} and 1.54×10^{-4} respectively.

The SNR for each data set was calculated and tabulated in Table 3-8. A signal to noise ratio of 3:1 is often quoted as the required minimum for an analytical instrument.

Table 3-8 Signal-to-Noise ratio calculated from the baseline signal recorded in the microfluidic manifold

Data	S_{aver}	ΔS	S/N
Raw	0.000390	0.000130	15.05
Treated	0.000154	0.000062	12.51

From the results it was evident that the raw and treated data were well above the theoretical threshold, with the raw data having a better SNR than the treated. All the data presented in this chapter has been treated with a moving average of $n = 25$ data points and all average values are determined for $n = 30$ data points.

3.9 Limits of Detection (LOD)

The limits of detection for the yellow method has been experimentally investigated in the conventional system, as described in Chapter 2, to be typically ca. $0.1 \text{ mgL}^{-1} \text{ PO}_4^{3-} - \text{P}$. The aim of this experiment was to experimentally determine the LOD of the yellow method in the microfluidic system and to compare the LOD with that achieved in the conventional set up (Chapter 2, Section 2.8).

The determination of the LOD was calculated by applying Equation 3-2 (where sd is the standard deviation) to the standard deviation of the baseline for the noise. Distilled water was pumped across the microfluidic chip and a stable baseline signal was plotted as absorbance versus time at a rate of 10 data points / s.

An average absorbance for the baseline signal was determined for $n = 30$ data points and the standard deviation of the signal was calculated. The absorbance of the baseline signal was measured in triplicate and determined as $1.29 \times 10^{-4} \pm 1.93 \times 10^{-6}$ (RSD: 1.4949 %).

$$LOD = 3 \text{ } sd$$

Equation 3-3

The standard deviation of each baseline was multiplied by three, which resulted in a value of $3.87 \times 10^{-4} \pm 5.78 \times 10^{-6}$ (RSD: 1.4949 %).

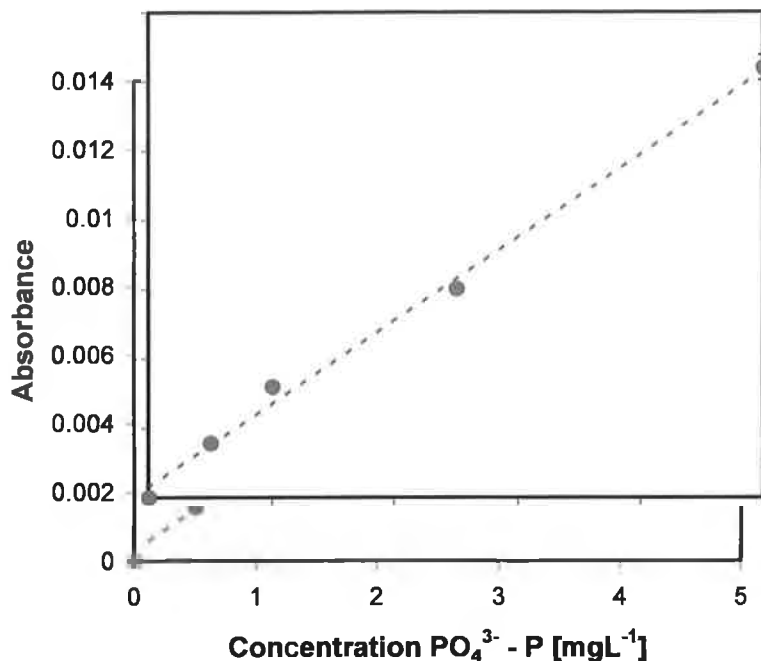


Figure 3-28 Calibration plot of concentration $PO_4^{3-} - P$ versus absorbance over the concentration range $0 - 5 \text{ mgL}^{-1}$ at a working wavelength of 380 nm

For the LOD study the lower end of the concentration range for the yellow method, $0 - 5 \text{ mgL}^{-1}$, was investigated. Five standard solutions, 0, 0.5, 1, 2.5 and 5 mgL^{-1} , were prepared from the 50 mgL^{-1} P stock. The experimental conditions were the same as described previously.

Triplicate plug injections under stopped flow were made for each sample. The average plug maximum ($n = 30$ data points) was subtracted from the baseline average. The resulting absorbance was plotted versus the $PO_4^{3-} - P$ concentration over the range $0 - 5 \text{ mgL}^{-1}$ at a wavelength of 380 nm . Error bars were included but due to the good reproducibility (RSD < 3.5 % for all triplicate measurements) of the data they are masked by the point symbols in Figure 3-28.

Table 3-9 Triplicate absorbance measurements made over the concentration range 0 – 5 mgL⁻¹ PO₄³⁻ - P at a working wavelength of 380 nm

Conc. PO ₄ ³⁻ -P [mgL ⁻¹]	1	2	3	Abs.	Std. Dev.	% RSD
0.0	0.0000	0.0000	0.0000	0.0000	0.0000	0.0000
0.5	0.0016	0.0016	0.0015	0.0016	0.0000	2.1069
1.0	0.0033	0.0032	0.0031	0.0032	0.0001	3.3075
2.5	0.0061	0.0060	0.0059	0.0060	0.0001	1.0510
5.0	0.0123	0.0128	0.0121	0.0124	0.0004	2.9515

From Figure 3-28 it was clear that the linearity is maintained in the low concentration range for the yellow method with an R² value 0.9954 ± 0.0008 (RSD: 0.0842 %) and the slope of 0.0024 ± 0.0001 (RSD: 2.3727 %) being comparable with that of the larger range of 0 – 50 mgL⁻¹ PO₄³⁻ - P.

The sensitivity of the yellow method in the microfluidic manifold at lower concentrations was better than that achieved in the conventional set-up. From the equation of the line from the calibration the LOD was determined to be 0.0361 mgL⁻¹ ± 0.0024 mgL⁻¹ (RSD: 6.6653 %).

3.10 Comparison of the Yellow Method in the Microfluidic and Conventional System

3.10.1 Calibration Comparison

The final analytical study performed in the microfluidic manifold was to validate the yellow method by comparing calibrations from the microfluidic and conventional systems. Three calibrations were carried out over the concentration range 0 – 50 mgL⁻¹ PO₄³⁻ - P at a wavelength of 380 nm. 5 standards were prepared (0, 5, 10, 25 and 50 mgL⁻¹) from the 50 mgL⁻¹ PO₄³⁻ stock solution. One calibration was made in the microfluidic manifold, where the optical path length was 400 μm. The other two calibrations were carried out in the conventional system, where two different optical cuvettes of path length 1 mm and 1 cm were used.

The microfluidic calibration was made under stopped flow as previously described, whereby the orthophosphate-containing sample was mixed on-line with the reagent. For both conventional calibrations 5 ml of both the sample and the reagent were measured into a 10 ml volumetric flask and left for approx. 5 min at room temperature to allow the PO_4^{3-} - P complex to develop. The three calibrations were carried out in triplicate, with the results being plotted in Figure 3-29.

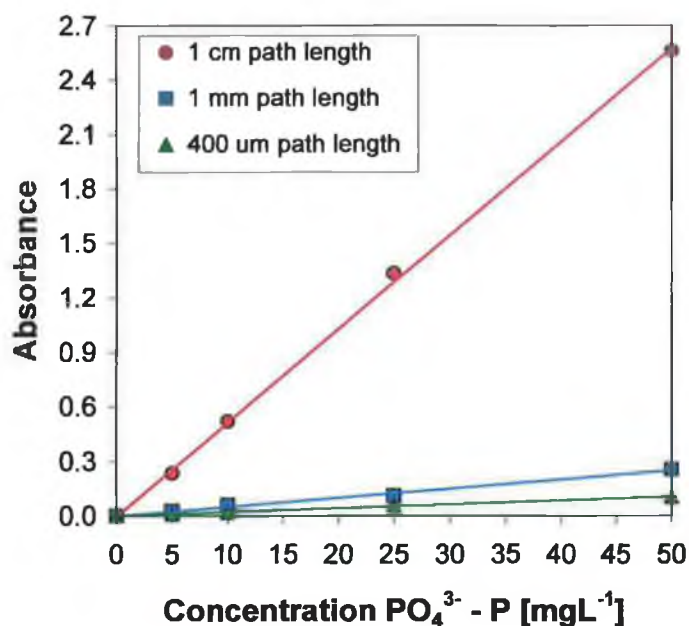


Figure 3-29 Linear plot of absorbance versus concentration PO_4^{3-} - P over the range 0 – 50 mgL^{-1} for three path lengths of 400 m, 1 mm and 1 cm at a wavelength of 380 nm

The results achieved in the microfluidic manifold were compared with those in the conventional system in order to investigate the relative accuracy and sensitivity [15].

Table 3-10 Absorbance data used to compare the three path lengths over the concentration range 0 – 50 mgL^{-1} measured at a wavelength of 380 nm

Conc. PO_4^{3-} -P [mgL^{-1}]	1 cm	1 mm	400 um	Average	Std. Dev.	% RSD
0	0.0000	0.00000	0.0000	0.0000	0.0000	0.0000
5	0.2334	0.26969	0.2382	0.2471	0.0162	6.5735
10	0.5173	0.57019	0.5359	0.5411	0.0185	3.4170
25	1.3316	1.11506	1.3299	1.2588	0.1094	8.6936
50	2.5597	2.54704	2.6929	2.5999	0.0739	2.8409

The comparison was made possible by multiplying the absorbance data from both the microfluidic and the 1 mm cuvette analyses by a factor based on the differing optical path lengths associated with the three systems. The 400 μm micro-cuvette has a path length, which is twenty five times smaller than that of the 1 cm cuvette and the 1 mm cuvette has a path length that is ten times that of the 1 cm cuvette. As a consequence the microfluidic data was multiplied by twenty-five, and the 1 mm data was multiplied by ten, the results of which are documented in Table 3-10.

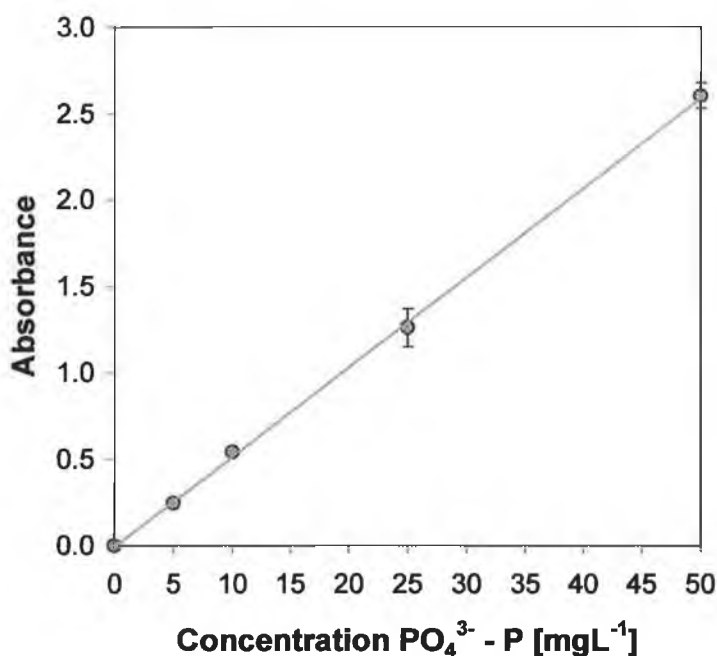


Figure 3-30 Average absorbance of the normalised data for the three path lengths versus the concentrations over the range 0 – 50 mgL^{-1} at a wavelength of 380 nm

In Figure 3-30 the average absorbance was calculated and plotted against $\text{PO}_4^{3-} - \text{P}$ concentration over the range 0 – 50 mgL^{-1} at the working wavelength of 380 nm. The slope of the line, m , was determined as 0.0518 ± 0.0021 (RSD: 4.0678 %) and the R^2 value was calculated to be 0.9995 ± 0.0034 (RSD: 0.3452 %). The three sets of data with different optical path lengths were assessed to gauge the accuracy of the measurement. Theoretically a 25-fold factor decrease in optical path length would result in a 25-fold decrease in absorbance signal. When the absorbance measurements made in the microfluidic system were compared with

the conventional 1 cm cuvette values the 25-fold decrease was evident. The validation of this is shown in Table 3-11, where the original absorbance 1 cm cuvette values were divided by their corresponding value in the microfluidic system and the resultant factor was tabulated. From the table three factors are shown relating to the change in optical path length from the microsystem to the 1 mm cuvette (2.5-fold), the 1 mm cuvette to the 1 cm cuvette (10-fold) and the microsystem to the 1 cm cuvette (25-fold). The average factor decrease for each experiment was calculated as 2.4889, 9.9315 and 24.3712 respectively. The relative error was estimated for the calculated factors compared to the theoretical factors as less than 2.6 % for all three experiments (see Table 3-11).

Table 3-11 Validation that the calibrations performed over different path lengths in different instrumentation are comparable

Conc. PO ₄ ³⁻ -P [mgL ⁻¹]	400 μm → 1 mm	10 mm → 1 cm	400 μm → 1 cm
5	2.8333	8.6581	24.5313
10	2.6612	9.0745	24.1494
25	2.0965	11.9432	25.0387
50	2.3647	10.0499	23.7655
Average	2.4889	9.9315	24.3712
Std. Dev.	0.3254	1.4625	0.5438
% RSD	13.0755	14.7262	2.2313
% RE	0.4423	0.6854	2.5151

This simple study showed that measurements in the microfluidic system were highly comparable with those in both the 1 mm and 1 cm as would be expected with any good analytical technique. The fact that even though the optical cuvette in the microfluidic system was twenty five times smaller than that of the conventional set up, the results were still excellent. This was very encouraging, when considering the next step, to design and fabricate a replicate microfluidic manifold in a polymeric material.

3.10.2 Molar Extinction Coefficient of the Yellow Phosphate Complex

To our knowledge, the molar absorptivity for the vanadomolybdophosphoric acid (Phosphate complex formed with the yellow method, see Chapter 2, Section 2.1) has not been reported in the literature, so there were two main reasons why it is

presented here. The first reason was to establish a value for the molar absorptivity and the second, to show that the microfluidic system measurements were comparable with the bench results.

Two calibrations were chosen to compare the bench and microfluidic systems respectively. The calibrations were plotted as absorbance versus concentration in mgL^{-1} . From Beer's Law the molar absorptivity was calculated using SI units, i.e. the molarity of the sample is required. In Table 3-12 the conversion of the concentration from parts per million [mgL^{-1}] to Molarity [moles / Liter] is given.

Table 3-12 Conversion of concentration units from parts per million [mgL^{-1}] to Molarity [moles / L]

Conc. $\text{PO}_4^{3-}\text{-P}$ [mgL^{-1}]	Concentration [M]
0	0.0000
0.5	3.6740E-06
1	7.3481E-06
2.5	1.8370E-05
5	3.6740E-05
10	7.3481E-05
25	1.8370E-04
50	3.6740E-04

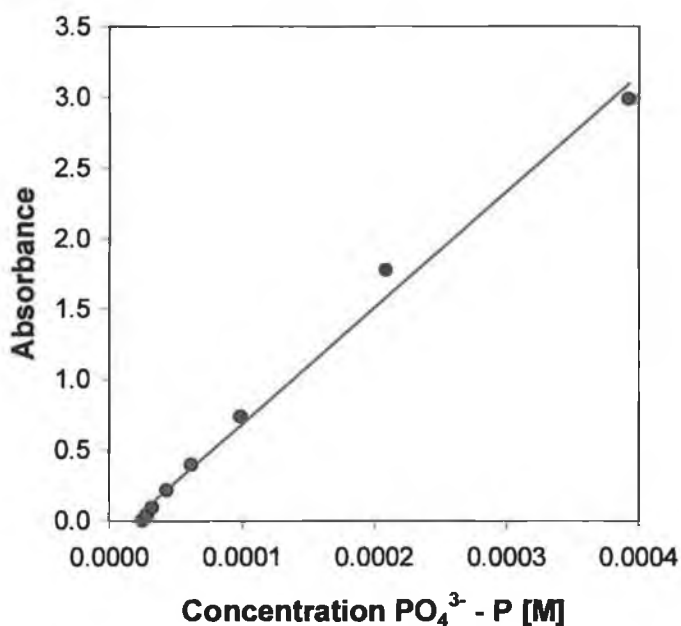


Figure 3-31 Linear plot of absorbance versus $\text{PO}_4^{3-}\text{-P}$ concentration [M] over the range 0 – 50 mgL^{-1} for the conventional system at the working wavelength of 380 nm

In Figure 3-31 the linear plot of absorbance versus PO_4^{3-} - P concentration [M] at a wavelength of 380 nm is plotted for the conventional system. For an optical path length of 1 cm, the molar absorptivity was directly calculated from the slope as $8382.24 \text{ L mol}^{-1} \text{ cm}^{-1} \pm 64.053 \text{ L mol}^{-1} \text{ cm}^{-1}$ (RSD: 0.77 %).

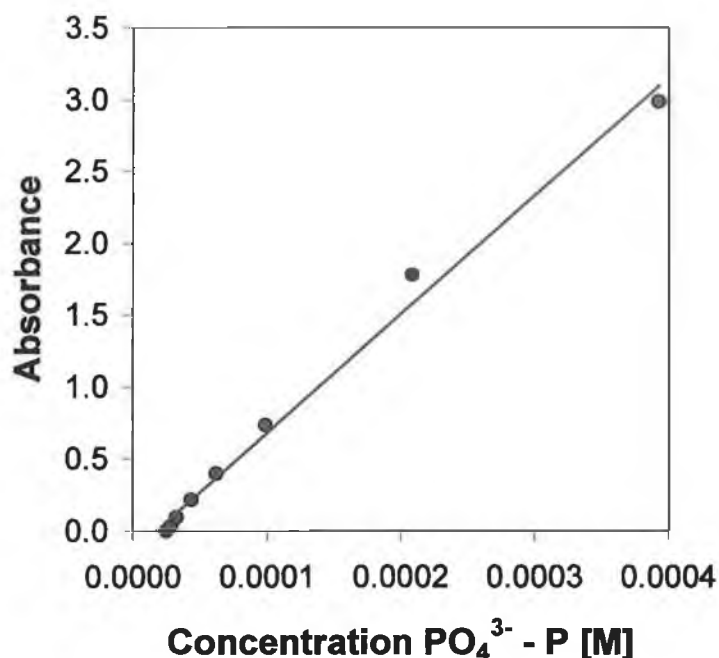


Figure 3-32 Linear plot of absorbance versus PO_4^{3-} - P concentration [M] over the range $0 - 50 \text{ mgL}^{-1}$ for the microfluidic manifold at the working wavelength of 380 nm

In Figure 3-32 the linear plot of the absorbance versus the PO_4^{3-} - P concentration at a wavelength of 380 nm in the microfluidic manifold is plotted. To determine the molar absorptivity for an optical path length of $400 \mu\text{m}$, the slope was multiplied by twenty-five and estimated to be $8482.56 \text{ L mol}^{-1} \text{ cm}^{-1} \pm 31.39 \text{ L mol}^{-1} \text{ cm}^{-1}$ (RSD: 0.37 %). The molar absorptivity for both systems was, as expected, highly comparable.

3.11 Conclusion

The microfluidic system was optimised for the successful implementation of the yellow method. The microfluidic manifold was first used for preliminary testing of a strong absorbing dye, Malachite Green. An extensive validation of the yellow method was carried out to include linearity, repeatability, reproducibility, limits of detection, reagent lifetime, long-term microsystem stability and the signal-to-noise ratio. The calibration data for the microfluidic manifold and conventional system were compared by:

1. plotting the calibrations from both on the same scale
2. calculating the molar absorptivity of the phosphate complex for both systems

A stopped flow regime was adopted for the analysis to great effect, which resulted in lower reagent consumption and waste generation. The stopped flow also facilitated the use of a simple T-junction microfluidic layout for all measurements rather than a complex, meandering reaction coil synonymous with continuous flow measurements.

3.12 References

- 1 "PHD 2000 Syringe Pump Series User's Manual", Harvard Apparatus Inc., Massachusetts, USA, 1999, 43.
- 2 A. Daridon, M. Sequeira, G. Pennarun-Thomas, J. Lichtenberg, E. Verpoorte, D. Diamond, N.F. de Rooij, *Proc. Eurosensors XIV*, 2000, 815 – 818.
- 3 O. Geschke, M. Denninger, P. Telleman, J.P. Kutter, *Pittcon*, 2000, New Orleans, USA (poster presentation).
- 4 M. Madou, *Fundamentals of Microfabrication*, CRC Press LLC, Florida, USA, 1997, 53-87.
- 5 N. Maluf, *An Introduction to MicroElectroMechanicalSystems Engineering*, Artech House Inc., Boston, USA, 2000, 51-71.

-
- 6 M. Sequeira, M. Bowden, E. Minogue, D. Diamond, *Talanta*, 2002, **56**, 355 – 364.
- 7 J.P. Krog, H. Dirac, Birgit Fabius, P. Graveson, A. Daridon, J. Lichtenberg, E. Verpoorte, N.F. de Rooij, G. Pennarun-Thomas, M. Sequeira, D. Diamond, M. Denninger, O. Geschke, J.P. Kutter, S. Howitz, C. Strec, P. Charles and L. Cognet, *Micro Total Analysis Systems 2000: Proc. μ TAS Symp.*, Kluwer Academic Publishers: Dordrecht, 2000, 419-422.
- 8 M. Bowden, M. Sequeira, P. Gravesen, J.P. Krog, D. Diamond, *Analyst*, 2002, **127**, 1-4.
- 9 D.F. Boltz, M.G. Mellon, *Ind. Eng. Chem., Anal. Ed.*, 1942, **19**, 873.
- 10 G. Mission, *Chemiker-Ztg.*, 1908, **32**, 633.
- 11 G.P. Edwards, A.H. Molof, R.W. Schneeman, *J. Amer. Water Works Assoc.*, 1965, **57**, 917.
- 12 O. Sletten, C.M. Bach, *J. Amer. Water Works Assoc.*, 1961, **53**, 1031.
- 13 M. Bowden, D. Diamond, *Sens. Actuators B, Spec. Ed.*, "Europt(r)ode VI", Manchester, 2003, **90(1-3)**, 170-174.
- 14 D.A. Skoog, D.M. West, F.J. Holler, *"Fundamentals of Analytical Chemistry"*, 7th Edit., 1996.
- 15 M. Bowden, M. Sequeira, P. Gravesen, J.P. Krog, D. Diamond, *J. Environ. Monit.*, 2002, **5**, 767-771.

4 Real Applications of the Yellow Method in Microfluidic Systems

Phosphorus is essential for aquatic life playing a pivotal role in growth development of natural waters. It readily forms bonds with organic matter and soil particles, which accounts for the low concentrations naturally occurring. However, phosphorus (P) in the form of a phosphate (PO_4^{3-}) is much more abundant. Phosphates are predominantly found as orthophosphates, a nutrient vital to plant growth. Plants, such as algae, require small amounts of orthophosphates to grow. If an excess of orthophosphate is present rapid algal growth leads to blooms. When algae die bacteria systematically decompose them, which sequentially exhausts all oxygen reserves [1]. With deficient oxygen supply life cannot be sustained and large fish kills transpire. This overkill enrichment of water with nutrients can be exclusively attributed to human intrusion, and is accordingly referred to as cultural Eutrophication.

Cultural Eutrophication has many sources, with those of major significance being wastewater effluent, detergents, fertilisers, drinking water treatment and human, animal and industrial waste to name but a few. Sewage effluent from wastewater treatment plants often fails to meet standard criteria set by environmental agencies and industrial waste frequently contains unacceptable levels of phosphorus. Agricultural waste, in the form of over-enriched soils and surface run-off from farms has increasingly been earmarked as the key contributor to phosphate-levels in rivers and lakes

In recent years the consequences of high nutrient levels in river and wastewater have become a key environmental issue within the EU with a major emphasis being placed on nutrient concentrations in sensitive regions [2]. Sensitive areas are categorised in several ways including:

1. Natural fresh water bodies that are eutrophic or which in the near future will become eutrophic
2. Stagnant lakes and streams with poor water exchange
3. Surface freshwaters intended for the abstraction of drinking water
4. Areas requiring further treatment to fulfil the Council Directives.

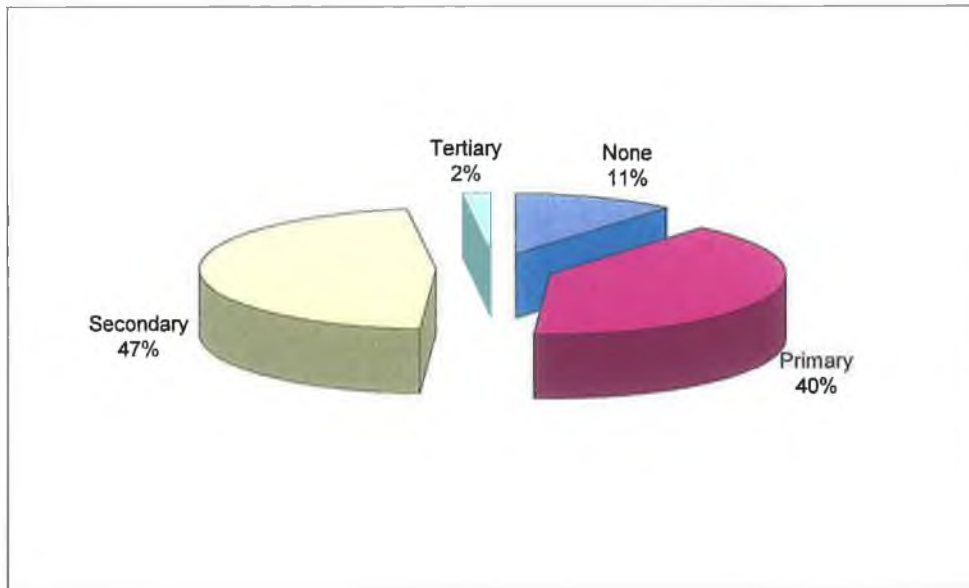


Figure 4-1 Percentage of sewerage schemes in each treatment category

The treatment of wastewater in Ireland is shown as a pie chart in Figure 4-1 [3-4]. The chart shows that only 2 % of all wastewater in Ireland is tertiary treated to remove phosphorus and nitrogen, which is a poor statistic compared to many other European countries.

The Irish Environment Protection Agency (EPA) is the governmental body that implements the national strategies to combat water pollution. The Irish EPA publishes annual reports on the national water quality based on the environmental monitoring they undertake throughout the year [5-7]. The Irish EPA has devised water quality assessment techniques and a classification system based on the biological and chemical results [8]. The classification is defined and shown for the nutrient phosphorus in Table 4-4 (see Section 4.4, page 145).

With this table as a guide sampling locations on a water body can be given a classification, which is indicative of the quality of the water at that point. This table is not the definitive guide, but it provides a basic definition for the water quality.

4.1 River Samples

Water samples were taken from three river sources, the Broadmeadow, the Santry and the Ward River. All three rivers are located in greater Dublin area and are within 1 hours driving distance from Dublin City University (DCU), where the National Centre for Sensor Research (NCSR) is located. Eight sampling locations along the Broadmeadow were selected and the concentration of phosphorus was measured. One location, the Clonshaugh Bridge, on the Santry River was chosen, where weekly sampling took place over a two-month period. With respect to the River Ward one sample was taken and the repeatability of the measurement in the microfluidic manifold was assessed. From the Broadmeadow River results information about the phosphorus concentration of the entire river was gathered, whereas in the case of the Santry River the sampling location with the highest concentration of phosphorus was repeatedly assessed to observe fluctuations in concentration and to interpret the cause of such changes. All samples were mixed on-chip with the yellow method reagent under stopped flow conditions in the microfluidic manifold and all samples were analysed in triplicate.

4.2 Sampling and Storage

River samples were collected in a 100 ml acid-washed, brown-glass flask. The flask was previously soaked in a 0.1 M HCl bath for 24 hours. The flask was then rinsed thoroughly and filled to overflowing with deionised water. On-site the initial sample was collected in a plastic container, which was attached to a rope and thrown into the middle of the river, where it was deepest. From this 10 ml aliquots were extracted into a plastic disposable syringe and passed through a 45 μm membrane filter. The filtered sample was transferred to the 100 ml acid-washed brown flask and the sampling was repeated until it was filled to overflowing. When the storage vessel was completely filled and sealed with a screw-top cap, the threat of degradation due to aeration was minimised. This is important when considering that river samples must be transported back to the laboratory and analysed in less than two hours because after which the orthophosphate becomes bio-available and leaches onto the glassware [9]. Post-analysis, the sample jars

were rinsed and refilled with deionised water and stored until the next sampling date.

4.3 Locations

Every two years the Irish EPA publishes a "State of the Environment" report, of which a sub-section deals solely with water pollution. Nutrient levels are monitored nationally and an extensive list of sampling locations is given. For the purpose of this study the sampling sites were restricted to the greater Dublin area, so that samples could be transported back to the lab for analysis in under two hours.

In the case of the first experiment a river was selected, where samples were taken at specific sampling locations along that river to develop a basic understanding of the complex changes in phosphorus concentrations from source to mouth. When selecting a river, the Broadmeadow flowing from the northwest of Dublin to the East coast, just north of the city was chosen for a number of reasons including:

1. the landscape through which the river runs, which is initially agricultural, then densely-populated and finally industrial
2. the high levels of phosphorus reported by the Irish EPA for all sampling locations along the Broadmeadow river [4]
3. the proximity of the river to the laboratory for rapid, accurate measurement

The criteria for the second sampling location differed from those of the Broadmeadow River. The second experiment involved only one sampling point on a river, where extremely high phosphorus levels had been reported. The Santry River was chosen, with the Clonshaugh Bridge location as the point for repeat sampling, because again the river was not only close to the university, but phosphorus concentrations were extremely high. Samples were collected on a weekly basis over a two-month period. From the results temporal changes in phosphorus were observed.

4.3.1 Broadmeadow River

The source of the Broadmeadow River is located in a predominantly agricultural region. The forked source of the Broadmeadow converges quickly and the first population densities, before the convergence, are the towns of Ratoath and Ashbourne as shown in Table 4-1. There are a total of four towns ranging in population density from small to medium-scale through which the river flows. The mouth of the river is located at the Malahide estuary, where there are a number of contributing discharges to the river including the towns of Swords and Malahide, a small-scale industrial estate and the Swords wastewater treatment facility for the region.

Table 4-1 EPA locations on the River Broadmeadow

Number	Sampling Locations	Discharges
1	Ratoath Bridge	Agricultural / Domestic
2	Ashbourne	Domestic
3	0.5 km o/s Ashbourne	Domestic / Agricultural
4	Milltown Bridge	Agricultural
5	Fieldstown House	Agricultural
6	Lispopple Bridge	Agricultural / Domestic
7	Lissenhall Bridge	Domestic / Industrial
8	Malahide Estuary	Industrial / Domestic

On the map in Figure 4-1 the sampling locations are clearly marked and labelled 1 – 8. The NCSR laboratory is located approx. 30 min by car from the furthest sampling point on the Broadmeadow River at Ratoath Bridge.

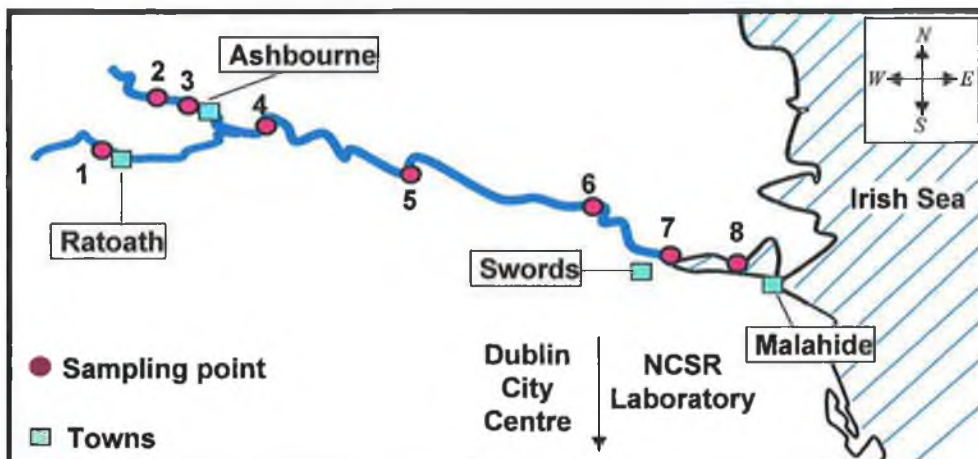


Figure 4-2 Map of the Broadmeadow River highlighting the sampling locations

4.3.2 Santry River

The Santry River is much smaller in length, but lies in a very densely populated suburb with a large industrial estate. The river flows through a completely urban landscape. Its source is located in Ballymun, which has an extremely high population density and flows east through the large Clonshaugh industrial estate, with heavy population densities along its entire course and several large factories along its banks, including Cadburys and Tayto Crisps before it enters the Irish Sea. Phosphorus levels are a combination of industrial and domestic effluent in the case of the Santry River compared with primarily the agricultural run-off (with small industrial / domestic discharge) for the Broadmeadow River.

4.3.3 River Ward

The Chapelmidway sampling location is located on the River Ward. The region is predominantly agricultural, which indicates that the phosphorus content is probably reasonably high and a result of run-off from farming in the form of fertilisers, slurry etc. and domestic waste. Also poor maintenance of septic tanks results in effluent leakages, which run into rivers completely untreated.

4.4 Validation of the Microfluidic System for Real Sample Analysis

Initially the measurements of orthophosphate concentration carried out in the microfluidic manifold were validated against an Ion Chromatography (IC) method. Ion exchange chromatography with suppressed conductivity detection was chosen as the reference method. PO_4^{3-} standards, prepared from a $50 \text{ mgL}^{-1} \text{ PO}_4^{3-}$ stock solution (6.59 g KH_2PO_4 in 1 litre), were passed through an anion exchange column (Dionex Ionpac® AS17 4 x 250 mm analytical column with Dionex Ionpac® AG17 4 x 50 mm guard column). The mobile phase was 50 % NaOH and the eluent was passed through a suppresser after separation. At a flow-rate of $1.4 \mu\text{l}/\text{min.}$, a $75 \mu\text{l}$ volume of the PO_4^{3-} standard was injected onto the column and

eluted out at approx. 6 min. The results of a validation study are provided in Table 4-2 showing the concentration and corresponding triplicate peak area measurements.

Table 4-2 Ion Chromatography reference calibration data over the concentration range 0 – 150 mgL⁻¹ PO₄³⁻

Conc. PO ₄ ³⁻ [mgL ⁻¹]	1	2	3	Aver. Peak Area [μS]	Std. Dev.	% RSD
0	0.0000	0.0000	0.0000	0.0000	0.0000	0.0000
1	0.2495	0.2439	0.2465	0.2466	0.0028	1.1363
5	1.5807	1.5938	1.5712	1.5819	0.0113	0.7173
10	3.6999	3.5442	3.6767	3.6403	0.0840	2.3075

In Figure 4-3 the linear plot of the averaged peak area versus the PO₄³⁻ concentration over the range 0 – 10 mgL⁻¹ PO₄³⁻. The error bars are almost completely masked by the plotted points due to good reproducibility of the data yielding a relative standard deviation of less than 2.3 % for all the calibration. The slope and the R² value were calculated as 0.3659 ± 0.0079 (RSD: 2.1456 %) and 0.9954 ± 0.0016 (RSD: 0.1624 %) respectively.

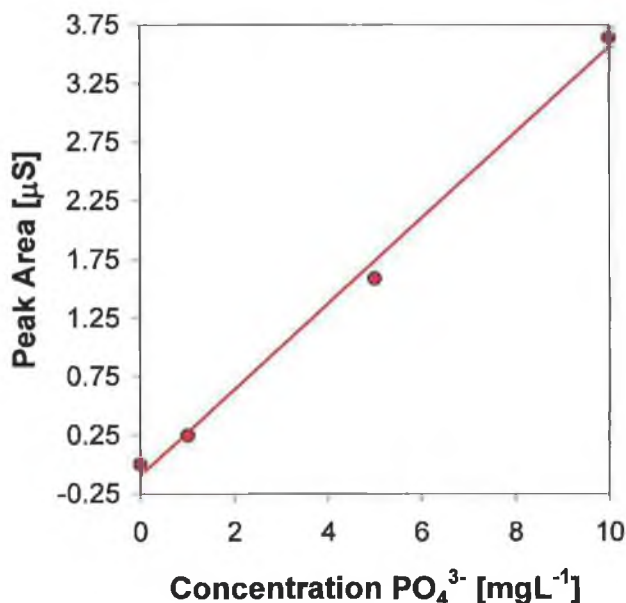


Figure 4-3 Linear plot of absorbance versus PO₄³⁻ concentration over the range 0 – 10 mgL⁻¹ at the working wavelength of 380 nm by ion chromatography

The calibration data over the concentration range 0 – 10 mgL⁻¹ PO₄³⁻ - P for the microfluidic system and the ion chromatography were compared. In order to make the comparison the experimental concentrations of each of the standards were calculated from the equations, Equation 4-1 and 4-2. The true concentration was given as PO₄³⁻ - P so the ion chromatographic measurements had firstly to be converted from PO₄³⁻ to P and then inserted into the equation of the line as shown in Equation 4-1.

$$y = 0.1194x - 0.0314$$

Equation 4-1

In Table 4-3 the results are tabulated side by side and are highly comparable. A real sample, taken at Lissenhall Bridge on the Broadmeadow River, was analysed on both systems and the experimental concentration calculated as 1.1421 ± 0.0360 (RDS: 3.1529 %) and 1.1244 ± 0.0196 (RDS: 1.7406 %) for the IC and the microfluidic system respectively. On the whole the repeatability was slightly better for the IC method, but the relative error for the experimental concentration compared to the true concentration was superior for the microfluidic system than the IC.

Table 4-3 Validation of the microsystem values with the results obtained from an Ion Chromatographic determination

True Conc.	Ion Chromatography				Microfluidic System			
	Mean	Std. Dev.	% RSD	% RE	Mean	Std. Dev.	% RSD	% RE
1	0.9372	0.0077	0.8172	6.2768	1.0721	0.0583	5.4339	7.2079
5	4.5865	0.0310	0.6762	8.2700	5.1266	0.0976	1.9040	2.5326
10	10.2120	0.2296	2.2481	2.1199	9.8511	0.0825	0.8377	1.4888
Lissenhall Br.	1.1421	0.0360	3.1529	N/A	1.1244	0.0196	1.7406	N/A

Overall the comparison of both methods was good, which indicated that the microfluidic system was a valid way of analysing real samples, capable of repeatable and reproducible measurement. The microfluidic system also is much smaller in size than a bench-scale instrument like the IC instrument requiring less power, having more integrated features and consuming less reagents and producing less waste. At present the integrated features include a light source

(UV-LED), sample delivery, a sample and reagent reaction channel, a micro-sized cuvette for optical detection and reagent and waste storage reservoirs.

4.5 Sample Analysis

Every sample collected in this study was filtered on-site and measured in triplicate in the microfluidic manifold in less than two hours to ensure that the orthophosphate analyte hadn't begun to leach out of the water sample. The absorbance of each sample was recorded under stopped flow conditions on the microfluidic chip over the optical cuvette. The average absorbance was calculated as the average of the plug maximum (n = 30 data points) minus the average of the baseline plug (n = 30 data points).

4.5.1 Study of the Broadmeadow River

The Irish EPA monitor river quality throughout the country. The main parameters that are assessed are:

1. pH
2. Temperature
3. Conductivity
4. Dissolved Oxygen (DO)
5. Biological Oxygen Demand (BOD)
6. Chloride
7. Total Ammonia
8. Un-Ionised Ammonia
9. Oxidised Nitrogen
10. Ortho-Phosphate
11. Colour

These key parameters give an overall impression of the quality of the water and the results of which determine the classification a stretch of river gets. For each

parameter there are threshold levels based on a general classification [10]. The threshold values for orthophosphate along with their corresponding classification used by the Irish EPA reports are given in Table 4-4.

Table 4-4 Irish EPA water quality requirements [11-12]

Classification	Water Quality	Annual Median Conc. P [mgL ⁻¹]
A	unpolluted	0.015 - 0.03
B	slightly polluted	< 0.045
C	moderately polluted	< 0.07
D	seriously polluted	< 0.1

Orthophosphate concentrations are reported as mg P L⁻¹ for the median value derived from annual figures. In Table 4-5 the median values of orthophosphate are given for the period 1995 – 1997 [12]. There are approx. 20 points along the Broadmeadow River, which have been selected by the Irish EPA as sampling locations. However the list of water quality parameters are not given for each sampling location. In fact at the first two sites in Table 4-5 there was no available data exists for orthophosphate concentration. There doesn't appear to be a systematic sampling and testing protocol in place. The result is that the frequency of sampling varies from one location to the next. This means that no data from which an overall impression of the fluctuations in orthophosphate concentrations due to temporal / climatic changes and waste discharges can be gained.

Table 4-5 Irish EPA sampling locations and P concentrations for the 1995 – 1997 period

EPA Code	Sampling Location	Samples	Conc. P [mgL ⁻¹]		
			Min	Max	Median
0150	Ratoath Br.	0	?	?	?
0400	Br. 0.5 km o/s Ashbourne	0	?	?	?
0420	Ashbourne Br.	11	0.206	2.277	0.685
0500	Milltown Br.	11	0.310	4.450	0.881
0600	Fieldstown House	9	0.184	2.000	0.448
0700	Lispopple Br.	9	0.185	1.975	0.384
1000	Lissenhall Br.	9	0.192	1.029	0.346
1300	Malahide Estuary	8	0.192	2.000	0.387

From Table 4-5, P [mgL⁻¹] equals PO₄³⁻ [mgL⁻¹] divided by a factor of ca. 3.1. Also the median values are all well above the 0.1 mg P L⁻¹ (see Table 4-4) for a D

classification signifying serious pollution. However in the water quality report most of the sampling locations have been given only a C classification [12]. So there appears to also be an inconsistency in how the figures are reported. The sampling locations were not only chosen to highlight the high levels of orthophosphate concentration, but also to show the inconsistent sampling protocol that is currently employed across the country.

Prior to sample collection a new calibration was carried out over the concentration range 0 – 5 mgL^{-1} PO_4^{3-} - P at a wavelength of 380 nm. This smaller linear range was chosen because for river water samples an orthophosphate concentration in excess of 5 mgL^{-1} PO_4^{3-} - P would result in Eutrophication and large-scale fish kills.

Each standard was mixed on-chip under stopped flow with the reagent and analysed in triplicate resulting in highly reproducible values with a relative standard deviation of less than 3.2 % for each data point, consequently masking the error bars in Figure 4-4.

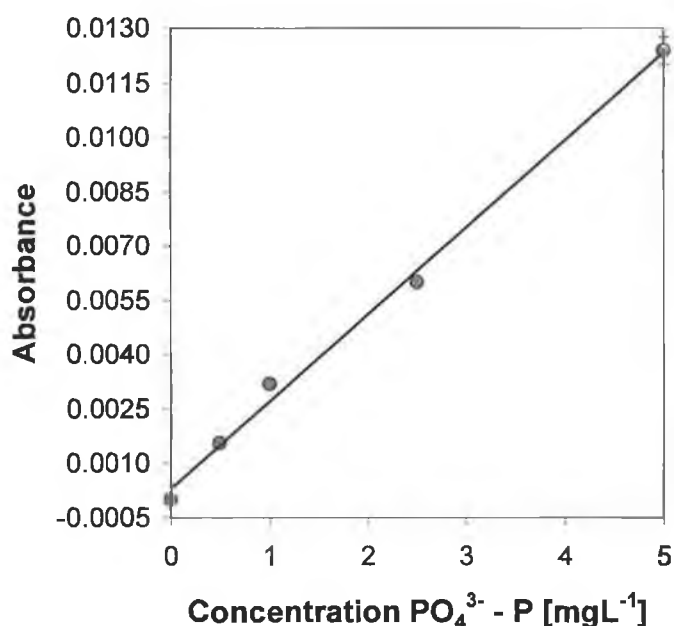


Figure 4-4 Linear plot of absorbance versus concentration over the range 0 – 5 mgL^{-1} PO_4^{3-} - P at a working wavelength of 380 nm in the microfluidic manifold

The absorbance for each of the eight Broadmeadow samples was analysed in triplicate with the average value being converted to a PO_4^{3-} - P concentration by equation of the line for the linear plot as given in Equation 5-1, where y is the average absorbance and x is the PO_4^{3-} - P concentration in mgL^{-1} .

$$y = 0.0024x + 0.0003$$

Equation 4-2

The results are shown in Table 4-6, where the relative standard deviation was calculated as less than 4.7 % for each of the samples. However the concentration values calculated for the river samples are only a snapshot of the orthophosphate levels present at a specific time on a specific day.

Table 4-6 Average absorbance measurements for the 8 samples taken from the Broadmeadow River analysed at a wavelength of 380 nm*

EPA Code	Sampling Location	$\text{PO}_4^{3-}\text{-P}[\text{mgL}^{-1}]$	Std. Dev.	% RSD
0150	Ratoath Br.	0.7874	0.0083	1.0540
0400	Br. 0.5 km o/s Ashbourne	0.8224	0.0108	1.3176
0420	Ashbourne Br.	0.4638	0.0185	3.9797
0500	Milltown Br.	0.9593	0.0447	4.6550
0600	Fieldstown House	0.0062	0.0002	3.4538
0700	Lispopple Br.	4.0509	0.1239	3.0584
1000	Lissenhall Br.	1.2181	0.0212	1.7406
1300	Malahide Estuary	3.2949	0.0801	2.4300
*IC measurement at Lissenhall Br.		1.1421	0.0360	3.1529

Because a river is constantly in flux the orthophosphate concentration fluctuates too, therefore making a direct comparison with the EPA values unwise. The results presented in Table 4-6 were recorded in mid-July 2002, when phosphate concentrations are at their highest due to temporal factors. Therefore a comparison with the Irish EPA data (see Table 4-5) will not be of great relevance. It is more important to stress that, with this microfluidic system, real sample analysis is not only possible but also comparable with other methods of determination including IC, e.g. Lissenhall Br. sample. Also the EPA's approach to compiling analytical information with regards to orthophosphate concentrations is flawed for a number of reasons including:

* The Lissenhall Br. Measurement made with the IC was taken from Table 4-3

1. In any 24-hour period the orthophosphate concentration fluctuates an infinitesimal number of times
2. Quoting annual figures based on less than 15 analyses / year is not an accurate measurement of the orthophosphate concentration of any water body
3. Manual sampling by filtration on-site followed by in-laboratory testing increases the error associated with the measurement

4.5.2 Weekly study of the Clonshaugh Bridge on the Santry River

The Clonshaugh Bridge sampling location was chosen for two reasons, its proximity to the laboratory for post-sampling analysis and the high concentrations of phosphorus found there, which were documented by the Irish EPA [12].

The study varied from the Broadmeadow analysis in that the phosphorus concentration was monitored on a weekly basis at the same sampling point to investigate the fluctuations in concentration attributed to variables such as temperature, climate and variation in discharges to the river. For example, the functions of the land, which the river runs through, i.e. agricultural, industrial, residential, can influence the phosphorus content of the soil. If there is heavy rainfall the volume of the river increases, increasing the flow-rate causing the river to pick up more suspended and dissolved solids as it flows.

Each week a sample was taken, filtered on-site and analysed in triplicate in the laboratory with the microfluidic system. An example of the triplicate measurements superimposed on top of each other is plotted in Figure 4-5. Each data set is treated by a moving average for $n = 25$ data points shown as treated data in the plot. The absorbance of the sample is estimated as the average of the stable maximum signal ($n = 30$ data points) minus the stable baseline ($n = 30$ data points).

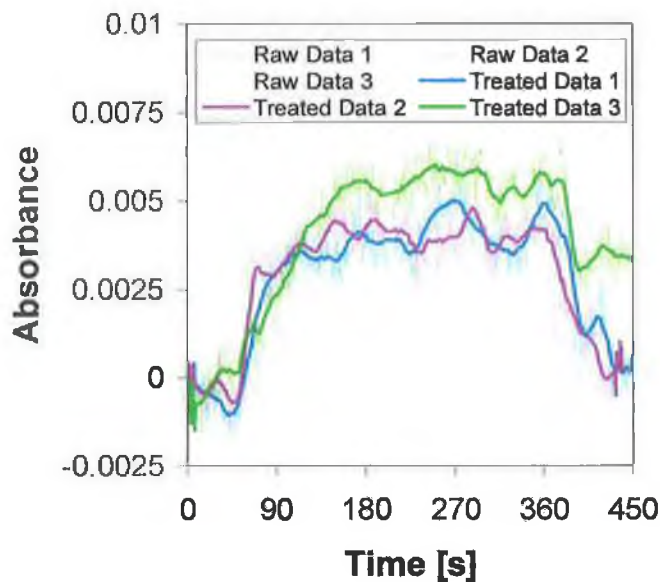


Figure 4-5 Example of the triplicate sample plugs taken at the Clonshaugh Bridge site

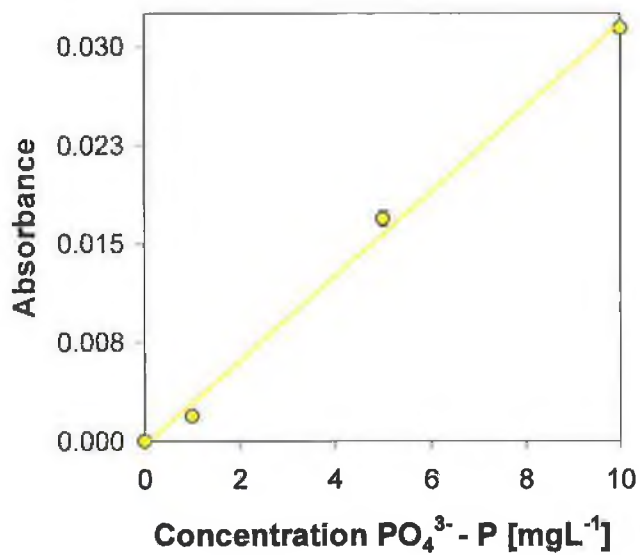


Figure 4-6 Linear plot of absorbance versus $\text{PO}_4^{3-} - \text{P}$ concentration performed in the microfluidic manifold over the range 0 – 10 mgL^{-1} at the working wavelength of 380 nm

A calibration plot was carried out prior to sample collection over the concentration range 0 – 10 mgL⁻¹ PO₄³⁻ - P at a working wavelength of 380 nm. The calibration was made in triplicate and the linear plot of the average absorbance versus the PO₄³⁻ - P concentration is plotted in Figure 4-6, where the R² value was calculated as 0.9955 ± 0.0021 (RSD: 0.2132 %).

The equation of the line, as shown in Equation 5-3, was utilised to convert the absorbance values to experimental concentrations.

$$y = 0.0025x + 0.0023$$

Equation 4-3

Table 4-7 Weekly absorbance measurements and corresponding concentrations from samples taken from the Clonshaugh Bridge site at a wavelength of 380 nm

Date	Absorbance			Exp. Conc. PO ₄ ³⁻ - P [mgL ⁻¹]		
	Average	Std. Dev.	% RSD	Average	Std. Dev.	% RSD
19-Jul-01	0.0055	0.0003	4.4000	1.6250	0.0387	2.3840
31-Jul-01	0.0051	0.0002	4.8644	1.5055	0.0778	5.1673
2-Aug-01	0.0044	0.0001	1.7682	1.2688	0.0241	1.8988
3-Aug-01	0.0050	0.0001	2.7087	1.4567	0.0420	2.8831
9-Aug-01	0.0040	0.0002	4.6036	1.1704	0.0582	4.9723

The data in Table 4-7 has been treated by a moving average for n = 25 data points. The average values of absorbance and concentration are the result of triplicate measurements (n = 30 data points / experiment). The weekly values of absorbance and concentration were averaged and calculated as 0.0048 ± 0.0006 (RSD: 12.2454 %) and 1.4053 mgL⁻¹ PO₄³⁻ - P ± 0.0186 mgL⁻¹ PO₄³⁻ - P (RSD: 13.0623 %) respectively.

The values were expected to vary due to the fact that a river is constantly under flux. However the values were all high compared to the recommended values quoted in Table 4-4. The high concentrations of phosphorus can be attributed to two principle factors namely:

A Population Density: Kilmore – Coolock suburbs means large quantities of domestic waste

Industry: Clonshaugh Industrial Estate

The Irish EPA quotes threshold P concentrations [mgL^{-1}] on an annual basis, so it has to be clarified that the concentrations calculated in this study are only a snapshot at a specific time on one particular day. Over a one-year period phosphorus concentrations are constantly under flux and are affected by temporal change, as well as the volume of discharge for domestic and agricultural waste. A follow-up study, whereby samples are taken each quarterly at a number of sampling locations along the Santry River would give a better trend, which could then be compared to the annual median values quoted by the EPA.

4.5.3 Real Sample Analysis of the River Ward

Repeatability studies were carried out on a sample taken from the Chapel Midway Bridge sampling location on the River Ward. Six repeat measurements were made on the same sample over a 60 min period post-filtration. Sample were filtered on-site and analysed back in the laboratory. Each measurement was made in triplicate and the whole process was repeated six times. The data treatment was the same as before, whereby the average values ($n = 30$ data points) were calculated from the treated data set (moving average for $n = 25$ data points) quoted in Table 4-8. The calibration data and its corresponding equation of the line for the Santry River analysis was used here, as the analysis was carried out at the same time on the microsystem (see Figure 4-6 and Equation 5-3).

For every absorbance data point a corresponding concentration data point was calculated. The concentration data was treated by a moving average for $n = 25$ data points and was plotted versus time as shown in the example in Figure 4-7. From the sample plug the baseline was calculated as the average of the stable portion of the baseline signal ($n = 30$ data points) for the raw and treated data as $0.3377 \text{ mgL}^{-1} \pm 0.1256 \text{ mgL}^{-1}$ (RSD: 37.2010 %) and $0.3027 \text{ mgL}^{-1} \pm 0.0153 \text{ mgL}^{-1}$ (RSD: 5.0629 %) respectively. The average of the plug maximum was calculated as $1.6764 \text{ mgL}^{-1} \pm 0.1279 \text{ mgL}^{-1}$ (RSD: 7.6317 %) and $1.6579 \text{ mgL}^{-1} \pm 0.0183 \text{ mgL}^{-1}$ (RSD: 1.1014 %) for the raw and treated data respectively. The results showed that when the raw data was treated with a moving average for $n = 25$ data points, where the data set has greater than 500 data points, there is a 7-fold reduction in the signal noise, thus improving the sensitivity of the measurement.

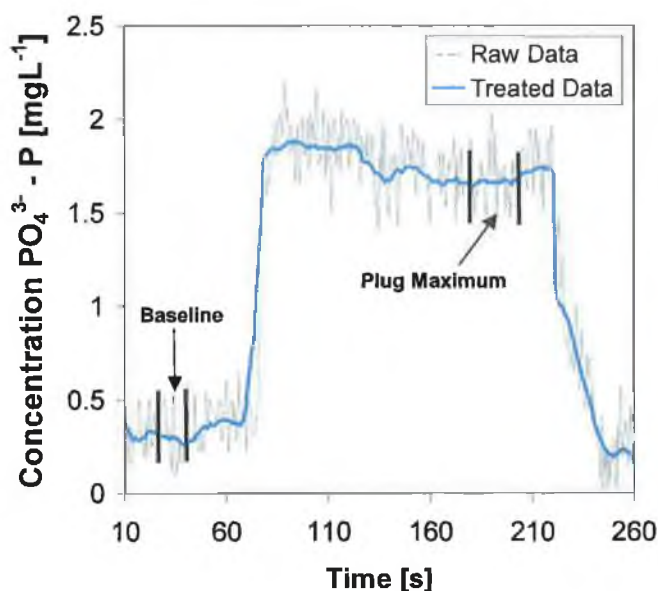


Figure 4-7 Example of a sample plug of $\text{PO}_4^{3-} - \text{P}$ concentration versus time at a working wavelength of 380 nm

The average absorbance and experimental concentration were calculated to be 0.004 ± 0.0002 (RSD: 5.5459 %) and $1.2434 \text{ mgL}^{-1} \pm 0.0690 \text{ mgL}^{-1}$ (RSD: 5.5458 %). The results showed a good reproducibility in the absorbance measurements made in the microfluidic manifold.

Table 4-8 Average absorbance and corresponding experimental concentrations calculated for the river sample taken at Chapel Midway Bridge

Run	Absorbance			Exp. Conc. $\text{PO}_4^{3-} - \text{P}$ [mgL^{-1}]		
	Average	Std. Dev.	% RSD	Average	Std. Dev.	% RSD
1	0.0043	0.0003	6.6620	1.3526	0.0003	0.0222
2	0.0038	0.0002	6.5006	1.1902	0.0002	0.0200
3	0.0038	0.0001	2.1148	1.1864	0.0001	0.0061
4	0.0039	0.0001	2.4969	1.2044	0.0001	0.0085
5	0.0042	0.0000	1.0408	1.3049	0.0000	0.0037
6	0.0039	0.0002	5.4770	1.2217	0.0002	0.0195

The biggest challenge encountered in real sample analysis of any river water body is the need for an increase in the frequency of sampling without being overly

labour-intensive. Without autonomous monitoring techniques, a true picture of phosphorus concentrations in water bodies cannot be determined.

The development of a simple testing device based on microfluidic analysis with the yellow method is a good alternative. The stopped flow regime means that the reagent consumption and waste production can be as little as 50 ml / year, which is an environmentally friendly approach. The stopped flow approach means that measurements are taken at set intervals, for example 2 measurements / hr with each measurement requiring 1 μL of reagent. The total volume for each measurement would then be 2 μL (combined volume of sample and reagent).

From this the yearly reagent and waste consumption can be estimated as 17.5 ml and 35 ml respectively. The yellow method reaction is fast, reaching completion within 3 min at room temperature, making sample turnaround quick. The yellow method has been validated in the microfluidic system and the results presented in this section have demonstrated that the microfluidic measurements are also comparable with bench-scale techniques such as Ion Chromatography.

4.6 Application of the Yellow Method in an Industrial Prototype Integrated Microfluidic System (MicroChem Project)

The yellow method is straightforward (one-reagent), and fast, enabling a relatively simple microfluidic manifold to be adopted. As has been demonstrated previously the method was first optimised on a bench scale, and then implemented in the lab demonstrator set up (Chapter 2, Section 2.4 – 2.9 and Chapter 3, Section 3.4.3 respectively). The next stage was its transferral to an industrial prototype (IP) designed under the MicroChem initiative (EU 5th Framework, No. BRPR - CT98-0787). The result section documents the initial experiments undertaken to implement a phosphate-monitoring method into the industrial prototype.

The MicroChem Project initially concerned itself with the determination of ammonia in wastewater, but the chemistry associated with the Berthelot reaction for

ammonia detection was far more complex than the yellow method for phosphate. Consequently the emphasis was switched to the determination of phosphorus with the IP. Preliminary trials were performed with the IP system and set of microfluidic chips were specifically designed for phosphorus determination.

4.7 Industrial Prototype

The industrial prototype was developed by the MicroChem project partners and took three years from inception to industrial prototype. The IP was contained within a leak-free solid shell to protect the electronics. The membrane dialysis filter of the sampling unit was the only component that was in contact with the external environment. The same principle components for the laboratory microfluidic system were applied here. However the complete integrated system is more complex to enable it to be used on-site at a riverbank or wastewater treatment facility. The sampling unit was already developed and operating in wastewater treatment plants as part of the Evita® sensor (Danfoss A/S, Nordborg, Denmark). It utilised a dialysis membrane filter with a diameter of 45 μm , which hasn't show any signs of biofouling in excess of one year. The sample passes through the membrane into a micro-channel before being introduced onto the microfluidic chip as the carrier solution. It was the remarkable anti-biofouling properties of the membrane that made this simple unit so effective for sampling and ensured that it could be used for long periods of time without being replaced.

The optical detection was achieved with a UV-LED and a photodetector, whereby optical fibres connected to either end of the microfluidic chip holder are aligned over the 200 μm -diameter optical cuvette. The microfluidic chip and holder have kept the same design as described in Chapter 3. However the chip layout has been altered and is described in more detail in Section 5.7. Again the fluidic interconnects were made with PEEK tubing for fluid transfer and o-rings for leak-free flow in the microfluidic chip. The reservoir solutions were stored in plastic leak-free pouches in the top part of the shell with the waste reservoir being kept separate.

The pumping was carried out by gas pressure, whereby when a small pressure was applied to the system the fluid flows at a corresponding flow-rate. The flow-rate and gas pressure were monitored with a flowmeter and a pressure sensor respectively and can be observed in real-time with the IP software.

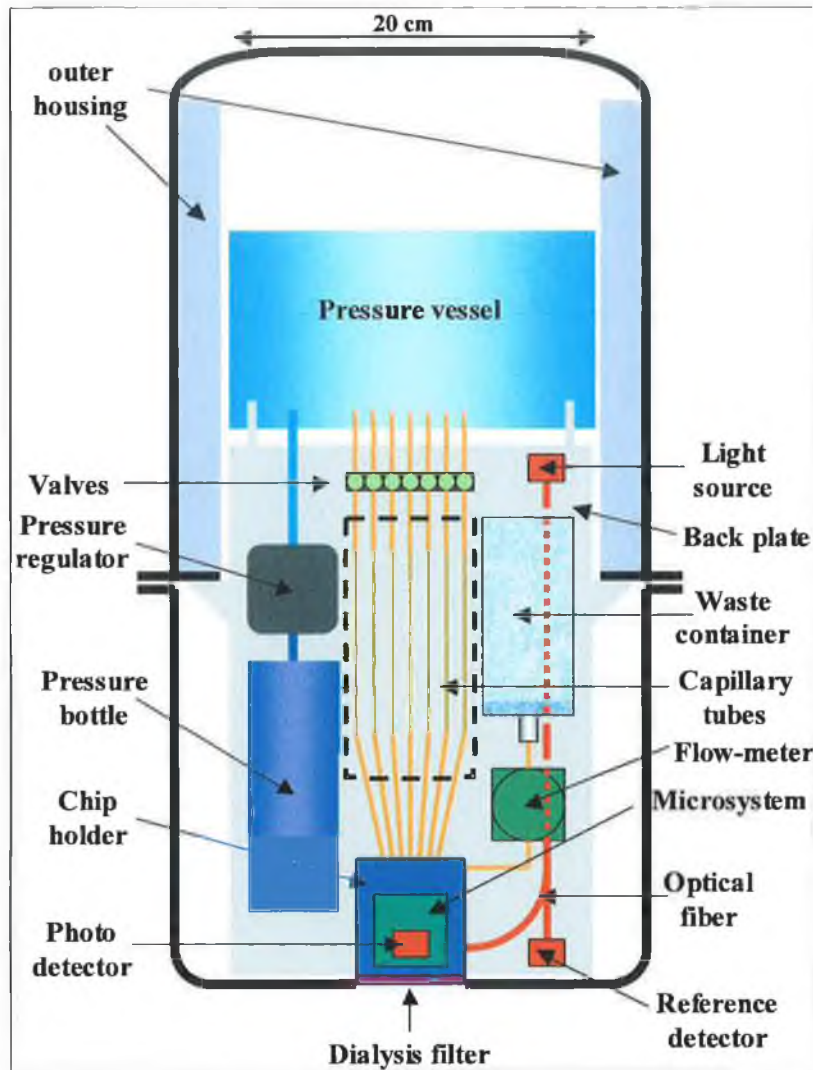


Figure 4-8 Schematic of the internal components of the industrial prototype, including the gas pressure pumping, microfluidic manifold, optical detection and sampling unit

The valves controlling the multiple channels were automated, as was the pumping and the light detection. All the components were connected to the back-plate as shown in Figure 4-8, which is the complex electronics board, which automates the whole process. The back-plate was connected to a PC and from the IP software the different components were individually controlled.

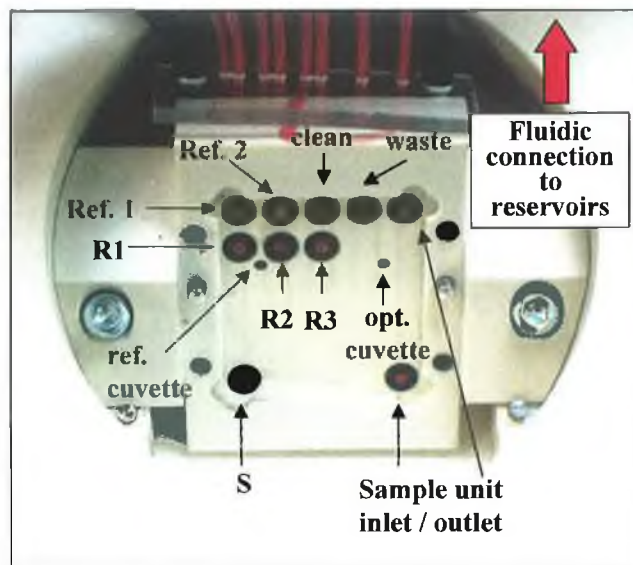


Figure 4-9 Photograph of the IP microfluidic chip holder

In Figure 4-9 the microchip holder is shown. The inlets / outlets are labelled to show where the respective solutions are introduced onto the chip. At each inlet / outlet the o-rings lie flush with the surface of the holder and the PEEK tubing. In the case of the sampling unit, prior to each analysis the solution upon filtration was introduced onto a micro-channel and passed out the other end to PEEK tubing where it was transported to the inlet marked S for sample. The components are labelled as follows:

1. S: the sample or carrier inlet
2. R1: the reagent inlet
3. Ref. 1: the 0 mgL^{-1} P standard solution inlet
4. Ref. 2.: the 50 mgL^{-1} P standard solution inlet
5. Clean: the 0.1 M HCl cleaning solution inlet
6. Waste: the waste outlet
7. Ref. Cuvette: the reference cuvette for referencing the light from the LED
8. Opt. Cuvette: the optical cuvette for the analytical measurement

The microfluidic chip was embedded into the holder and attached to the sampling unit and secured to the IP with four screws.

4.8 IP Chip Layout

Ultimately the phosphate chip was more simplistic in design due to the simple colorimetric chemistry employed for the reaction. The microfluidic chip designed for the phosphorus determination required two inlets, one for the reagent and one for the sample.

The phosphate chip layout is shown in Figure 4-10. There are a number of integrated components on the microfluidic chip. There were eight key components of the microfluidic chip, which are labeled 1 – 8 as follows:

1. The inlet for the combined yellow method reagent
2. The sample inlet
3. Disused reagent channel (Milli-q water)
4. Disused reagent channel (Milli-q water)
5. The mixing coil
6. The long reaction coil
7. The optical cuvette
8. The waste channel

The microfluidic channels had an etch depth of 120 μm with the exception of the waste channel, which had a 200 μm depth. The channel dimensions varied from 80 – 120 μm in width. The smaller width was for the mixing channel (5) and the larger for the reaction coil (6). All inlet holes were of 100 μm diameter with the exception of the waste channel, which was again bigger at 200 μm . The reference and optical cuvette were both 200 μm in diameter and had a path length of 400 μm , which is the thickness of the silicon wafer substrate upon which the microsystem was etched. All inlet holes are spaced 4.6 mm apart from each other on a 5 \times 6 hole grid to facilitate fluidic interconnects via PEEK tubing through the microchip holder.

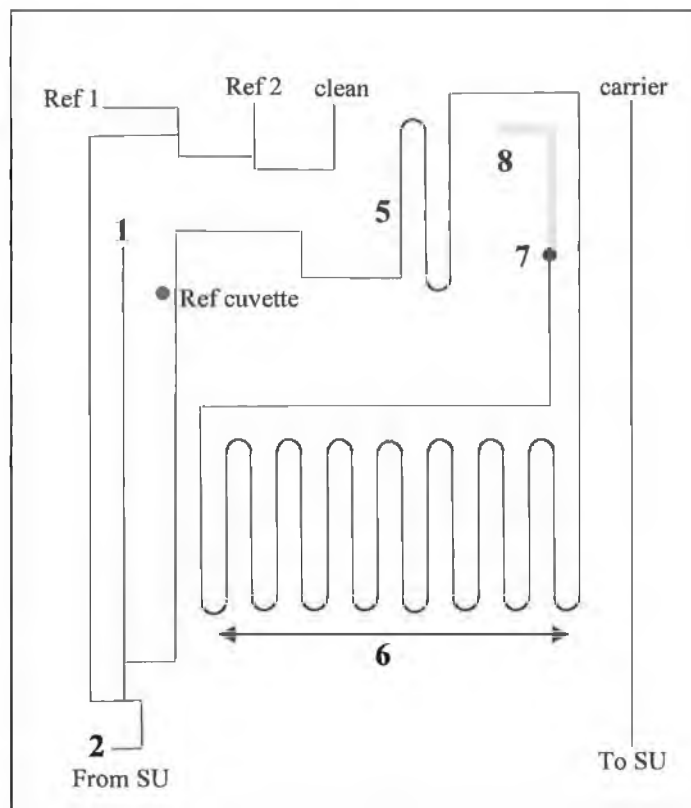


Figure 4-10 Schematic of the IP microfluidic chip

There were a number of additional components integrated onto the microfluidic platform including connection to the sampling unit, two reference channels and a cleaning channel. The sampling channel aided the transfer of the carrier solution, i.e. the sample, to the sampling unit from which it is passed to the sample inlet. The carrier was firstly passed through a polymer microdialysis membrane of 45 μm pore-size.

The IP software was designed so that an autocalibration would automatically be performed prior to any real measurement. Consequently the two reference solutions were chosen as 0 and 50 mgL^{-1} PO_4^{3-} -P standards. It was recommended for this test stage in the development that the system was autocalibrated on a daily basis. With respect to the cleaning solution for the yellow method, a 0.1 M HCl solution was used to flush the micro-channels, also on a daily basis.

The IP chip was designed for the yellow method reaction at elevated temperatures between 30 – 40 $^{\circ}\text{C}$ (similar to that of waste water, which was the target water body

for the IP). The reaction is complete between 20 – 30 s in this temperature range. The total flow-rate envisaged for the system was 1 μL / min to minimise the reagent consumption and waste generation under continuous flow conditions. The dead volume of the microfluidic chip therefore depended upon three parameters:

1. The temperature at which the reaction takes place ($< 40\text{ }^{\circ}\text{C}$)
2. The time required for the reaction to reach completion before the sample plug passes over the optical cuvette (40 s \approx 0.6667 min)
3. The dimensions and shape of the microfluidic channels for quick, efficient mixing by diffusion and full reaction development.

From the parameters given and the channel dimensions for the mixing and reacting coil the volume should theoretically be a minimum 0.6667 μL allowing for a 10% deviation after mixing was complete. The dead volume, from the intersection of the reagent channel and the sample channel to the optical cuvette, was calculated as 1.3 μL .

4.9 Experimental Procedure

A number of procedural steps had to be carried out before the analysis was started including the:

1. Stabilisation of the pressure
2. Optimisation of the optical signal
3. Realisation of a constant from all contributing channels
4. Cleaning of the microfluidic chip with deionised water

In order to optimise the conditions for the yellow method all the channels were switched on and the entire system was flushed to eliminate or at least minimise air bubble formation in the channels and to flush out only the reagent / sample residues of on the chip. Air bubbles commonly occur when the reservoir pouches are replaced because the accompanying PEEK tubing has to be detached from the old and reattached to the new pouch. Often minute amounts of air can get into the

tubing, which results in a poor and unstable optical signal. However, as long as fluid is flowing through the system continuously, the bubbles will pass through slowly. There were a number of ways the formation of air bubbles and their subsequent removal was dealt with. The number of air bubbles that form, either in the tubing or on the microfluidic channels, cannot be minimised. However the movement of these air bubbles through the system can be addressed. Air bubbles are only a major problem if, after they are introduced into any system, they become trapped or lodged in the system, resulting in rendering the measurement useless. The widening of channels at orifices, i.e. inlets, and at the optical cuvette, which is known as channel tapering, was used. The problem with the air bubbles was their size, in particular, in the optical cuvette. The dimensions of the optical cuvette were ideal for bubble lodgement. However with the inclusion of a taper leading up to and after the optical cuvette, the bubble settles for awhile, but eventually under pressure is pushed out and into the wide and deep waste channel. The waste channel dimensions ensured that once the bubbles had passed through the microfluidic chip, they were quickly removed to a waste reservoir.

The system was initially run with all channels open for 10 min to allow the system to begin to stabilise, at which point the software was started and under continuous flow with three channels running the system's stability was assessed for ca. 1 hour. During that time the flow-rate, pressure and optical signal were monitored continuously by the IP software. Three measurements were taken at time, $t = 0$, 30 and 60 min and the average value for each calculated demonstrating the systems stability. The average flow-rate, pressure and optical signal were estimated as $5.6667 \mu\text{L} / \text{min} \pm 0.1801 \mu\text{L} / \text{min}$ (RSD: 3.1781 %), $1019.3334 \text{ mbar} \pm 18.4752 \text{ mbar}$ (RSD: 1.8125 %) and $27986.3334 \text{ AU} \pm 15.1767 \text{ AU}$ (RSD: 0.0542 %) respectively (AU = arbitrary unit). The three channels used in the stabilisation of the IP were reference 1, the carrier and the cleaning solution. The flow-rate for each was set as approx. $2 \mu\text{L} / \text{min}$. However, the overall contribution, i.e. the Q_{TOTAL} was less than $6 \mu\text{L} / \text{min}$, which meant that either the flow from one channel was lower than the other or that the flow from each although equal was too low. The valves were switched to measure the flow-rate from each channel individually resulting in a relative deviation of less than 2 % for the the three channels. The average flow-rate was calculated as $1.8889 \mu\text{L} / \text{min} \pm 0.0388 \mu\text{L} / \text{min}$, which was down on the set value of $2 \mu\text{L} / \text{min}$. The relative error was calculated as 5.5550 %

for the experimental flow-rate compared to the set flow-rate. In this case because the channels were running at the same rate, the fact that the total flow-rate was lower than the set value did not interfere with the measurement.

When the system was flushed and ready for analysis the software program was restarted, which triggered the pump and the UV-LED, whilst continuously monitoring the flow-rate, optical signal, temperature and pressure via small sensors incorporated into the system. At the software interface the channels used for the analysis were selected as the reagent and the carrier. In order to make a measurement a sample solution was placed in the carrier reservoir, where the sampling membrane is submerged. For the laboratory experiments the carrier reservoir was a flat petrie dish for ease of change. In the harsher, real wastewater environment the system would be submerged or partly submerged in the activated sludge tank.

Five standard solutions were prepared from a $50 \text{ mgL}^{-1} \text{ PO}_4^{3-} - \text{P}$ stock by dilution. Calibration data was collected beginning with the lowest concentration of 0 mgL^{-1} and plotted against the $\text{PO}_4^{3-} - \text{P}$ concentration over the range $0 - 50 \text{ mgL}^{-1}$. Initially a single calibration was undertaken followed by a repeatability study, whereby the calibration was carried out in triplicate.

4.10 Preliminary analytical measurements

The optical signal was converted to an absorbance value from Equation 4-4, where A is the absorbance, I_{ref} is the averaged optical signal of the baseline or blank and I_{sample} the averaged optical signal of the sample for $n = 30$ data points.

$$A = \log\left(\frac{I_{ref}}{I_{sample}}\right)$$

Equation 4-4

The IP chip for the yellow method was designed for use in a wastewater treatment facility at a temperature of $30 - 40 \text{ }^\circ\text{C}$ at a total flow-rate (Q_{TOTAL}) of $1 \text{ } \mu\text{L} / \text{min}$. The highest chip temperature achievable in the system was $37 \text{ }^\circ\text{C}$ and the Q_{TOTAL}

fluctuated between 2.5 – 3.25 $\mu\text{L} / \text{min}$. The dead volume of the chip was calculated as 1.15 μL , and from Table 4-9 the time required for the sample plug to pass over the optical cuvette at three different flow-rates is given based on the Equation 5-5, where T is time, V is volume, μL and Q is total flow-rate, $\mu\text{L} / \text{min}$.

$$T = V/Q$$

Equation 4-5

Table 4-9 Time taken for a typical sample plug to pass through the optical cuvette at three different flow-rates

Q_{TOTAL} [$\mu\text{L}/\text{min}$]	Time [s]
2.5	31.25
3	25.99
3.25	24

From kinetic experiments carried out in the microfluidic system estimates of total reaction time were individually calculated over the temperature range 20 – 45 $^{\circ}\text{C}$ (Chapter 3, Section 3.5.2). The maximum temperature possible in the IP (using the heating unit) was approx. 37 $^{\circ}\text{C}$. From the reaction kinetics at 35 $^{\circ}\text{C}$ the reaction needed 30 – 35 s to reach completion, and at 40 $^{\circ}\text{C}$ required 10 – 15 s. There is no exact figure estimated for a temperature of 37 $^{\circ}\text{C}$. However, it can be estimated to be somewhere between 20 - 25 s. From Table 4-9 it is clear that if the reaction is to reach completion before it reaches the optical cuvette for detection the flow-rate cannot be any faster than 3.25 $\mu\text{L} / \text{min}$, if we assume the temperature is 37 $^{\circ}\text{C}$.

Initially when the experiments were started a blue colour was noted at the waste outlet. The chip was flushed for approx. 15 hours with the cleaning solution and the carrier (in this instance, H_2O). The system was flushed until the tubing and the waste running was clear in colour. Then the reagent valve was flushed out to ensure that the reagent channel was completely clear.

The software triggered the IP to perform an automatic calibration of two standards, 0 and 50 $\text{mgL}^{-1} \text{PO}_4^{3-}$, respectively. The manual calibration was then performed, whereby each standard passed through the sample unit to the carrier channel and onto the chip, where it mixed and reacted with the reagent.

Firstly an autocalibration was performed with the two standards (or autocal 1 and 2 as labelled in Figure 4-11), which were stored in reservoir bags within the IP. The process was automated by the IP software, whereby both standards were individually analysed by reacting each with the reagent on-chip under continuous flow. The absorbance plugs for autocal 1 and 2 are shown in Figure 4-11 and the average absorbance values were calculated from the treated data (moving average for $n = 30$ data points) as 0.3854 ± 0.0013 (RSD: 0.3240 %) and 0.0010 ± 2.1300 (RSD: 20.3721 %) for autocal 1 and 2 respectively.

A calibration was then manually performed for the concentration standards 0,5,10,25 and 50 $\text{mgL}^{-1} \text{PO}_4^{3-}$. From Figure 4-11 it was evident that sample plugs with a concentration less than 5 $\text{mgL}^{-1} \text{PO}_4^{3-} - \text{P}$ would be very difficult to decipher from the noisy baseline signal. It was obvious that the lower limits of detection were poor in this particular set up and have been shown to be significantly better in the laboratory microfluidic system (Chapter 3, Section 3.1).

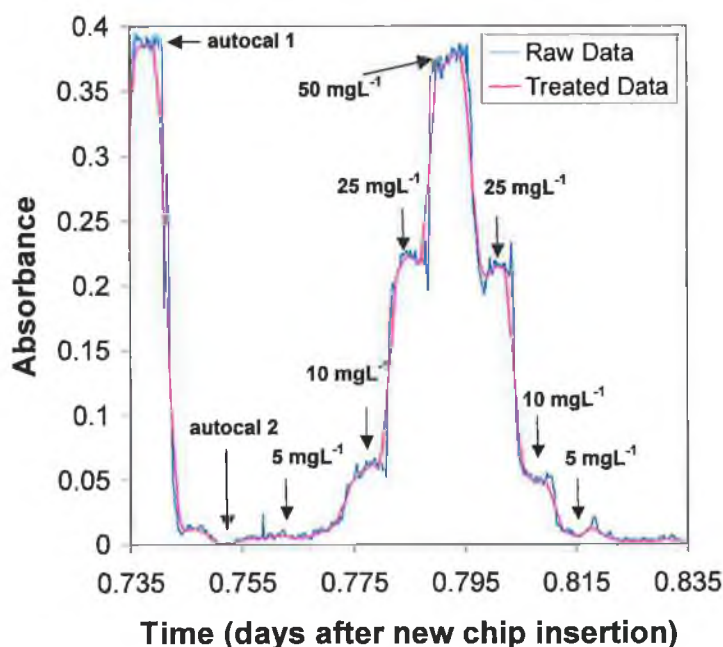


Figure 4-11 Automatic and manual calibration carried out on the IP

Average values for each sample were calculated from $n = 30$ data points on the stable portion of the plug. The absorbance values are shown in Table 4-10, where

the repeatable results meant the relative deviation of each standard over the linear range was less than 1.3 % with the exception of the 5 mgL⁻¹ concentration sample, which was considerably less repeatable with a relative deviation of 11.8 %. All absorbance values, presented in the table, were calculated by subtracting the absorbance of "autocal 2" (0 mgL⁻¹ PO₄³⁻ - P) from each average plug maximum.

Table 4-10 Absorbance measurements made for the initial calibration with the phosphate microfluidic chip layout

Conc. PO ₄ ³⁻ -P [mgL ⁻¹]	Abs. (treated)	Std. Dev.	% RSD
0	0.0000	0.0000	0.0000
5	0.0036	0.0004	11.8214
10	0.0588	0.0007	1.2285
25	0.1829	0.0014	0.7855
50	0.3735	0.0022	0.5973

The linear plot of absorbance versus PO₄³⁻ - P concentration over the range 0 – 50 mgL⁻¹ at a working wavelength of 380 nm is given in Figure 4-12. The linearity was good with an R² value of 0.9984.

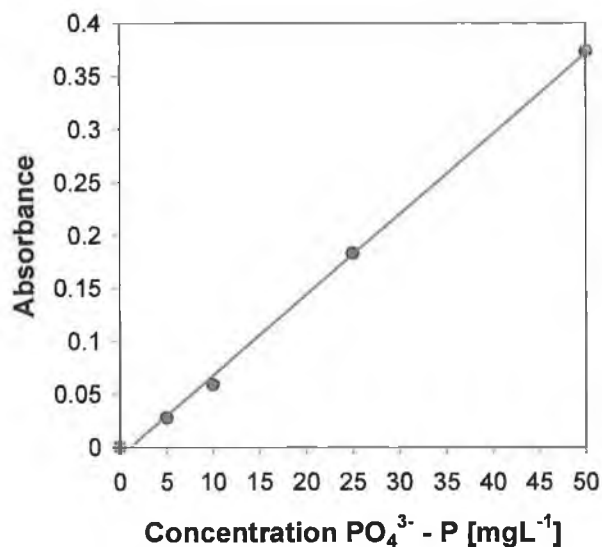


Figure 4-12 Calibration plot with the phosphate chip configuration over the concentration range 0 – 50 mgL⁻¹ PO₄³⁻ - P at a wavelength of 380 nm

The absorbance of autocal 1 (50 mgL⁻¹ PO₄³⁻ - P) was compared with the experimentally determined absorbance given in Table 4-10. A relative error of

3.0907 % was calculated, which showed that calibrations, which were carried out manually were very similar to the automated calibration values.

4.11 Calibration

Triplicate measurements were carried out with five different concentration standards, namely 0, 5, 10, 25 and 50 mgL⁻¹ P. The sample plugs were labelled 1 – 15 as shown in Figure 4-13. The absorbance values were calculated as the average of the baseline signal of deionised water ($9.9 \times 10^{-4} \pm 1.23 \times 10^{-5}$, RSD of 1.25 %) subtracted from the average plug maximum. In Figure 4-13 the fifteen the real time plot of absorbance is shown.

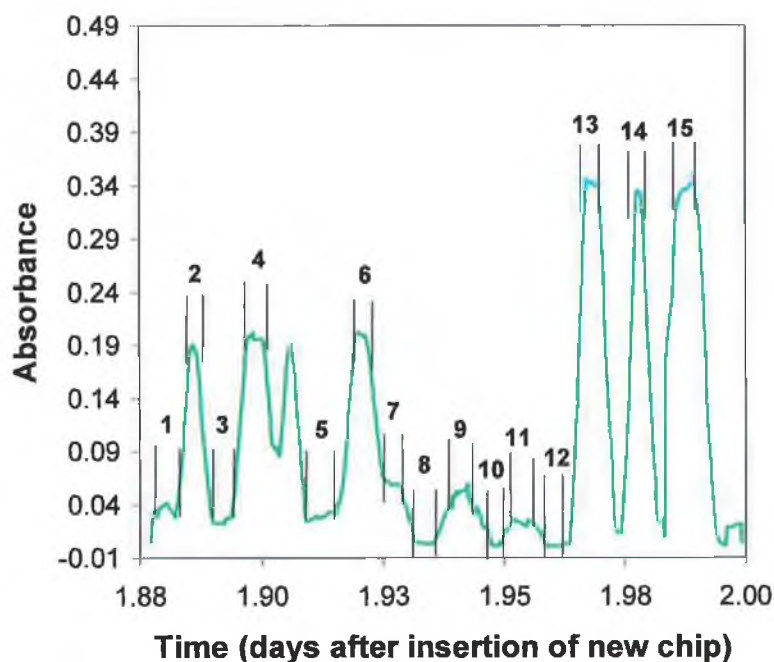


Figure 4-13 Triplicate measurements with the phosphate chip in the IP

The average, standard deviation and % relative standard deviation were calculated for each concentration and from the results presented in Table 4-11 there are

errors associated with all the results obtained, which can be directly attributed to the instability of the optical signal.

Table 4-11 Calibration data over the concentration range 0 – 50 mgL⁻¹ PO₄³⁻ - P for the IP

Conc. PO ₄ ³⁻ -P [mgL ⁻¹]	1	2	3	Average	Std. Dev.	% RSD
0	0.0000	0.0000	0.0000	0.0000	0.0000	0.0000
5	0.0228	0.0207	0.0207	0.0214	0.0012	5.7526
10	0.0435	0.0387	0.0452	0.0425	0.0034	7.9747
25	0.1599	0.1787	0.1872	0.1753	0.0140	7.9804
50	0.3332	0.3246	0.3282	0.3286	0.0043	1.3012

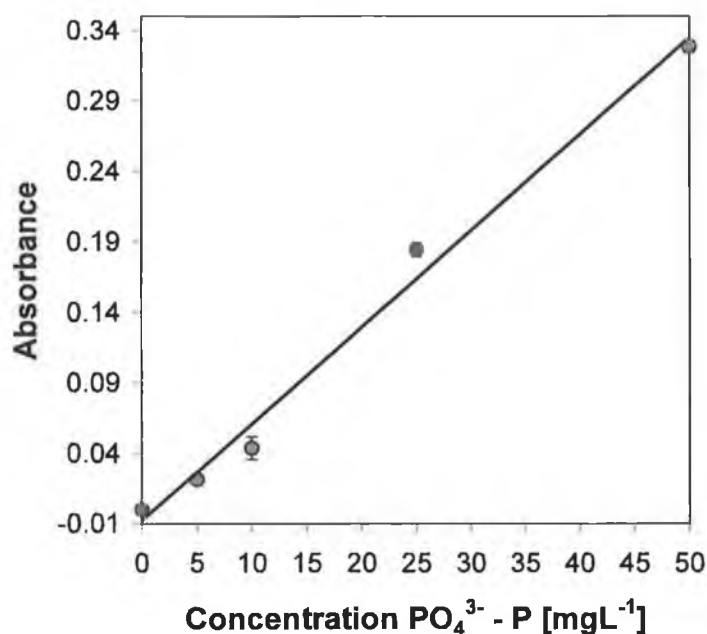


Figure 4-14 Linear plot of absorbance versus PO₄³⁻ - P concentration over the range 0 – 50 mgL⁻¹ in the industrial prototype with the phosphate configured microfluidic chip

In Figure 4-14 the linear plot of absorbance versus PO₄³⁻ - P concentration over the range 0 – 50 mgL⁻¹ at a working wavelength of 380 nm is plotted. Error bars are included in the plot and a relative standard deviation of less than 8 % for each standard in the calibration study was calculated.

The calibration was linear over the range with an R^2 value of 0.9907 ± 0.0044 (RSD: 0.4447 %).

4.12 Unknown analysis

The unknown solutions were prepared from the $50 \text{ mgL}^{-1} \text{ PO}_4^{3-}$ - P stock solution, and the dilution ratio is given in Table 4-12. 50 ml samples were prepared in volumetric flasks and mixed on-chip with the reagent.

Table 4-12 Dilutions made to 50 mgL^{-1} P stock solution resulting in five samples of "unknown" concentration [†].

Unknown	Vol. H ₂ O [ml]	Vol. PO ₄ ³⁻ -P stock [ml]
1	2	48
2	9	41
3	42.5	7.5
4	17	33
5	27.5	22.5

In Figure 4-15 the sample plugs of unknown concentration are shown, labelled 1 – 5. The plot represents the data, which has been treated with a moving average for $n = 25$ data points and the average absorbance of each sample was calculated for $n = 30$ data points.

There was an obvious absorbance change to coincide with the change of sample as each unknown was analysed, but accurate analytical results were not really possible.

† "unknown" concentration can theoretically be calculated, but is experimentally determined

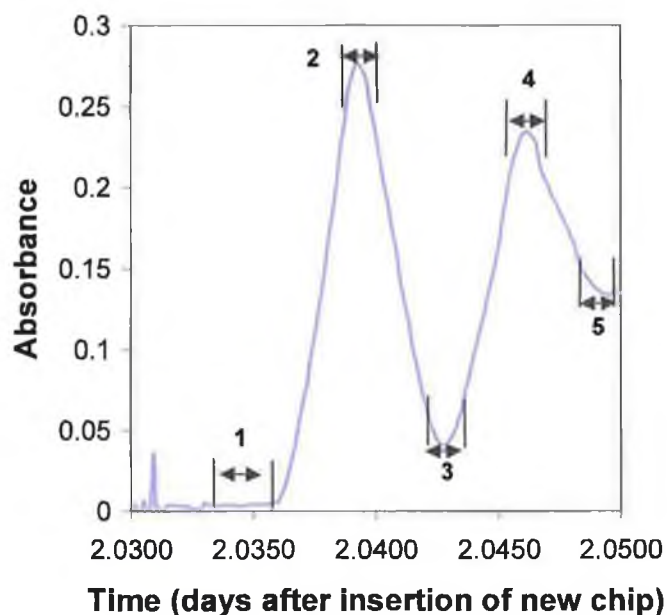


Figure 4-15 Injection plugs obtained for the 5 orthophosphate-containing samples of unknown concentration

Table 4-13 Absorbance measurements for the 5 unknowns analysed

Unknown	Absorbance (n = 20)	Std. Dev.	% RSD
1	0.0035	0.0004	10.1654
2	0.2651	0.0105	3.9714
3	0.0494	0.0081	16.3308
4	0.2267	0.0087	3.8216
5	0.1356	0.0020	1.4378

The experimental concentration of PO_4^{3-} - P was determined from the absorbance data in Table 4-13 and the equation of the line for the linear plot of Figure 4-14. The theoretical concentrations were calculated for the dilution factors given in Table 4-14 and compared with the experimental values in Table 4-14, where the relative deviation was less than 7.8 % for each unknown in the study.

Table 4-14 Comparison of actual concentration and experimental concentrations of the 5 unknowns

Actual Conc. [mgL ⁻¹]	Experimental Conc. [mgL ⁻¹]	% Relative Error
2	2.1543	7.7152
41	39.5515	3.5328
7.5	7.3757	1.6570
33	33.9869	2.9907
22.5	20.7890	5.5045

4.13 Conclusion

The analyses undertaken with various river water samples emphasised that when the yellow method is implemented in a microfluidic manifold real samples can be assessed with accuracy. This shows that both the method and the system are flexible and robust enough to be developed for in-situ analysis compared to many techniques and instruments can only be used under strict controls in a laboratory set up. The yellow method is very simple and when the microfluidic manifold is fully integrated concept is that will the system will require little or no maintenance for long periods of time (> 1 year).

The results obtained with the industrial prototype (IP) were carried out over a one-week period and serve as a precursor to precise analytical measurements. The IP performed reasonably well considering the number of parameters to be assessed and the limited analysis time period (1 week). If the optical signal had been more stable, the noise level would have been reduced and improved analytical measurements in terms of lower limits of detection could have been achieved. The yellow method was adapted to the IP instrument and promising results were obtained.

From the initial experiments it was determined that a more extensive study of the yellow method in the IP was possible and that with more time the system could be optimised and validated to produce reproducible analytical measurements comparable to those achieved with the laboratory microfluidic system (Chapter 3, Section 3.7). The primary benefit of optimising the yellow method in the IP was to demonstrate the flexibility of the colorimetric method in a new, field-deployable, prototype instrument that can be placed directly into a rigorous wastewater

environment to make real measurements. It was estimated that the labour time required to optimise the system and to prepare the IP for the real environment would be ca. 3 months. This short turnaround time is partly due to the simple chemistry of the yellow method and the ease of its adaptation to any instrument and the fact that the IP has been previously tested and optimised in a real wastewater treatment facility for the determination of ammonia.

Further improvements to the system in terms of materials used, fully integrated components and autonomous function in the environment are all currently under development. In Chapter 6 the use of polymer materials to fabricate the microfluidic manifold is described. Polymer materials not only provide a cheap alternative to silicon, but flexibility in terms of design and a fast turnover of devices. In Chapter 7 the use of hot embossing as a new polymer fabrication technique is described, along with a discussion relating to new polymer materials, miniaturised pumping designs, integrated sampling techniques and general strategies for remote monitoring of environmental water bodies.

4.14 References

- 1 I.D. Mv Kelvie, D.M.W. Peat, P.J. Worsfold, *Anal. Proc.*, 1995, **32**, 437-445.
- 2 EU publication, "*Council Directive on Urban Wastewater*", 91/271/EEC, document 391L0271, (official journal of the European Communities, L135, 30/05/91), 1991, p. 0040-0052.
- 3 DELG (Department of Environment and Local Government), "*Urban wastewater treatment regulations*", 2001b, 2001, S.I. no. 254, Govt. Supp. Agency.
- 4 L. Stapleton, M. Lehane, P.F. Toner, "*Ireland's Environment: A Millennium Report*", Irish EPA publ., 5, 2000, 41-54.
- 5 J. Brogan, M. Crowe, G. Carthy, "*Developing a national phosphorus balance for agriculture in Ireland*", Discussion document, EPA publ., 2001, **3**, 13-15.
- 6 C. Clenaghan, C. Collins, M. Crowe, "*Phosphorus regulations national implementation report*", Environment Protection Agency, Waterford, Ireland, 2001.

-
- 7 M.L. Mc Garrigle, J.J. Bowman, K.J. Clabby, J. Lucey, P. Cunningham, M. MacCárthigh, M. Keegan, B. Cantrell, M. Lehane, C. Clenaghan, P. F. Toner, "*Water Quality in Ireland 1998-2000*", Irish EPA publ., 2001, 2, 3-31.
 - 8 DELG (Department of Environment and Local Government), "Water quality (dangerous substances) regulations", S.I. no. 12, Dublin, Ireland, Government Supplies Agency, 2001.
 - 9 A.E. Greenberg, A.D.Eaton, L.S Cleseri, "*Standard Methods for the Examination of Water and Wastewater*", 4500-P Phosphorus, 18th Edit., 1994, ASPH, Washington, DC, USA, 166-181.
 - 10 K.J. Clabby, J.J. Bowman, J. Lucey, M.L. McCarrigle, P.F. Toner, "*Water quality in Ireland 1991-1994*", 1996, Envir. Res. Unit publi.
 - 11 J.J. Bowman, K.J. Klabby, J. Lucey, M.L. Mc Garrigle, P.F. Toner, "*Water quality in Ireland 1987-1990*", 1992, EPA publi.
 - 12 J. Lucey, M. J.J. Bowman, K.J. Klabby, P. Cunningham, M. Lehane, L. Mc Garrigle, P.F. Toner, "*Water quality in Ireland 1995-1997*", 1999, Environ. Res. Unit publi.

**5 The Design, Fabrication and Application of a Polymer
Microfluidic Manifold**

Many microfluidic systems have been designed and fabricated in silicon and applied to a variety of different analyses in silicon [1]. However in recent years the attention has turned to polymer-based fabrication as this offers rapid prototyping, low costs and a wide variety of materials for specific applications. There are a number of techniques that can be used to fabricate polymeric micro-devices including, micromilling, injection molding, laser ablation and hot embossing.

The yellow method has already been optimised on a standard bench scale instrument in Chapter 2 and implemented in the Si-microfluidic manifold as described in Chapter 3. The method is simple requiring one reagent and an orthophosphate-containing sample mixed in a 1:1 ratio to form a yellow heteropoly acid complex, which absorbs strongly below 400 nm. The kinetic information about the yellow method reaction was very useful when designing the layout and choosing the dimensions of the polymer microfluidic chip and during the overall analytical approach. Under stopped flow the reaction manifold was simplified and the reagent consumption and waste generation was minimised (< 50 ml / year).

The polymer microfluidic chip design is based upon a T-junction mixing channel to facilitate the simple colorimetric analysis for the determination of phosphorus that takes place in the optical cuvette. The optical detection was integrated into the microchip holder with the UV-LED embedded in the upper part and the detector connected to the bottom section and aligned above and below the optical cuvette in the microfluidic chip. Previously a portable spectrometer has been used as the detector, which is too big to be integrated into the microchip holder. Hence an optical fibre was aligned with the holder and transmitted the signal to the spectrometer. In this chapter the replacement of this bulky component with a smaller optical device, a photodiode is investigated. The photodiode can be easily embedded in the bottom section with the UV-LED integrated into the top part; a compact instrument can be envisaged.

Laser ablation techniques are fast and are often used to fabricate prototype systems. A CO₂ laser was used in the fabrication of the first generation chip presented here based on polymethyl methacrylate (PMMA), as the polymer substrate. The channels were sealed with a simple thermal bonding process and leak-free fluidic interconnects were designed. The polymer microfluidic chip was

used to analyse a number of water samples and the results were validated against two reference methods, a conventional spectrometric method and an FIA method.

5.1 Microfluidic Chip and Holder Design

The microfluidic chip was designed for the application of the yellow method in the determination of phosphorus. Taking from the design of the Pyrex / Silicon / Pyrex 3D stack from the previous silicon chips, a simplified concept was put forward. The new chip design was completely fabricated in a polymer material. With this in mind the simplest design possible was chosen. Polymeric microfabrication techniques are not as advanced as that of silicon due to the relatively short time polymer materials have been applied to microfluidic technology. There are so many classes of polymer materials with a vast array of properties that choosing the right one can be a lengthy process.

The microfluidic design had to have a minimum of three layers to ensure leak-free optical detection was achieved and fluidic interconnects for the sample, reagent and waste were established. The concept of a three-layered structure raised a number of issues including the alignment of each layer in terms of detection at the optical cuvette, the even bonding of multiple layers of varying thickness and leak-free transfer of fluid from the external environment onto the microfluidic channels.

The first chip design consisted of the most basic microfluidic structure to allow the yellow method reaction to take place on-chip under stopped flow conditions (see Figure 5-1).

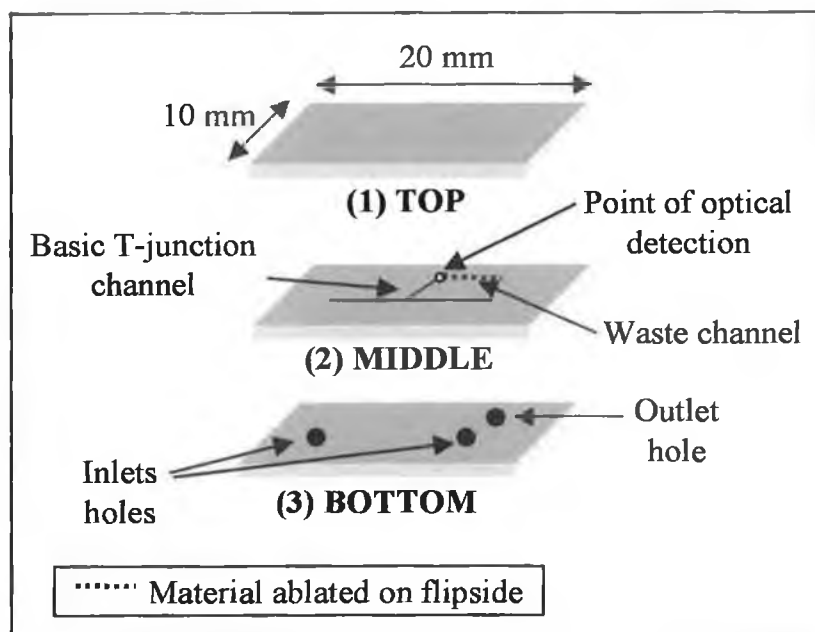


Figure 5-1 Schematic of the 3-D microfluidic chip with the three layers labelled (1) cover lid, (2) microfluidic features and (3) interconnects

The simple concept of a three-layered design is given, whereby the layers are labelled (1), (2) and (3). Layer (1) was a coverlid. Initially the only requirement of the coverlid was that it was of an optically clear grade polymer material. Layer (2) contained the microfluidic channels, where the sample and the reagent were mixed and reacted. The resulting coloured complex was detected and flushed to waste through an outlet to waste. Layer (3) contained three through holes (2 inlets for the sample and the reagent, the third, an outlet for the waste), which facilitated the introduction of fluid to the microfluidic channels and the removal of waste solution after detection.

In Figure 5-2 the basic design of the casing for the microfluidic chip is shown. The design incorporated components for the optical detection, and fluidic interconnects.

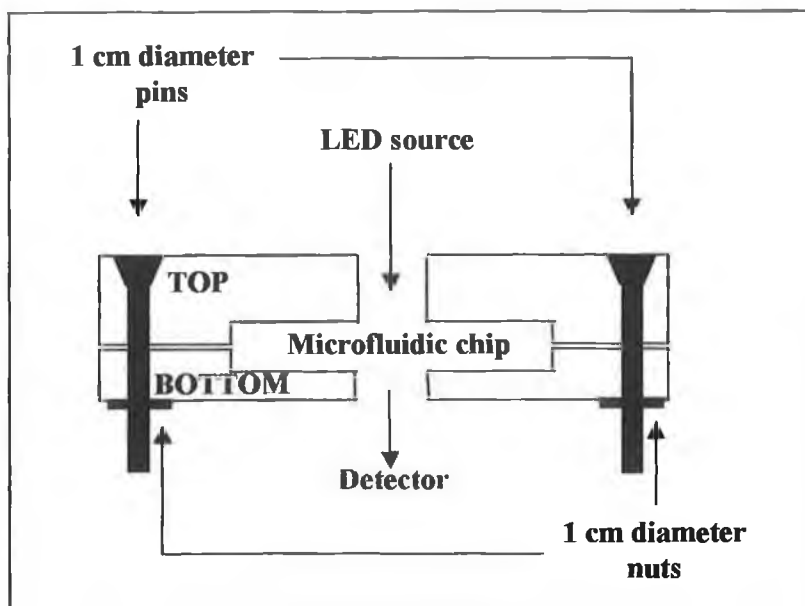


Figure 5-2 Side profile schematic of the microfluidic holder

The microfluidic chip is placed in the centre of the holder. The dual function of the holder is to protect the chip from the external environment and to align and integrate optical components, the light source and the detector, with the optical cuvette located on the microfluidic chip.

5.2 CO₂ Laser Technique

The CO₂ laser was manufactured by Synrad Inc. (Model: FH Series marking head 2, Mukilteo, WA, USA). A schematic of the process by which the laser cuts a surface is shown in Figure 5-3. The Winmark Pro software sends a series of commands, based on the design made in the drawing window of the software program, to the marking head. Basically the marking head was designed to mark stationary parts on a moveable platform. It positions and focuses the laser beam onto the surface to be ablated. The beam was first collimated, and then deflected onto two x, and y mirrors, which are mounted on scanners. When the exact position is reached the beam is passed through a single-element focusing lens onto the marking surface. This type of set up is known as vector micromachining [2].

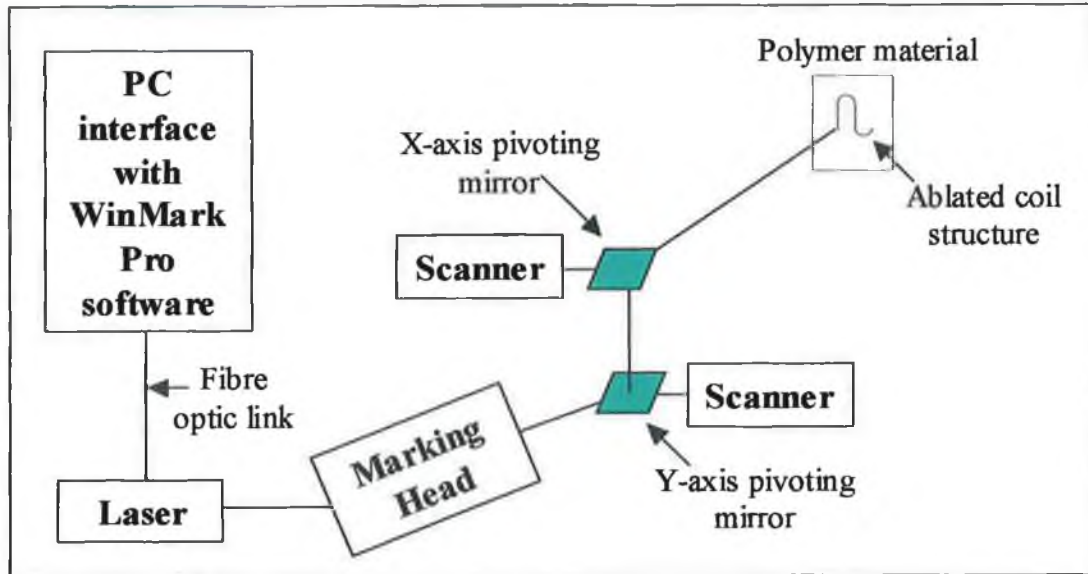


Figure 5-3 Vector micromachining with two pivoting mirrors

5.2.1 Laser Ablation

The CO₂ laser emits light in the infrared range at a wavelength of 10.6 μm. Because of this the material is always ablated photothermally. A number of factors influence the dimensions of structures in laser-ablated pieces including:

1. Choice of lens for the laser
2. Distance between the surface of the material to be ablated and the working lens
3. Specific properties of the material for ablation
4. Laser parameters

The minimum channel width is dependent on the choice of lens and each lens has a specific focal length. When that focal length is equal to the lens-surface distance the minimum spot size for that particular lens is achieved. The channel width is always greater than the spot size. From Table 5-1 the various settings for a particular lens are given [2]. For each lens there are six categories, which can be used as a guideline to optimise the performance of the CO₂ laser.

Table 5-1 Laser and marking head specifications according to the choice of lens

Lens Focal Length [mm]	80	125	200	370
<u>Marking Specifications</u>				
Nominal Field Size [mm]	27 × 27	74 × 74	110 × 110	198 × 198
Maximum Field Size [mm]	33.5 × 41.2	85.7 × 105.6	134 × 165	241 × 297
Working Distance [mm]	74 ± 1	128 ± 2	190 ± 3	350 ± 5
Spot Size [μm]	116	180	290	540
Depth of Field [mm]	± 0.4	± 1.5	± 2.5	± 10
Maximum Incident Angle [degrees]	5	11	16	19
<u>Marking System Parameters</u>				
Position Accuracy [mm]	0.01	0.02	0.03	0.05
Position Resolution [μm]	< 3	< 6	< 9	< 15
Repeatability [mm]	0.015	0.025	0.038	0.063

These include:

1. The focal length (F.L.): The distance required to ensure the laser beam is focused on the ablation surface
2. The nominal field: The surface area of the surface to be ablated by the laser
3. The maximum field: The maximum possible surface area that can be ablated
4. The working distance: The distance of the lens from the surface of the material to be ablated
5. The spot size: The diameter of the focused laser beam that ablates the material
6. The depth of field: The depth of the material at which the laser beam is still focused and able to form proper structures
7. The incident angle: The maximum deviation from 0° permissible, where there is still a satisfactory accuracy in the structures being ablated.

The cut of the laser as it ablates produces a distinctive shape in the material. The channel profile is Gaussian in form as is shown in Figure 5-4. The laser beam moves across the surface melting the polymer as it goes. Heated gases are given off whilst the polymer vaporises, which disperses the pool of molten polymer away from the beams spot, where it is sufficiently cool enough to solidify. The process of ablation allows structures such as channels, through holes etc. to be formed.

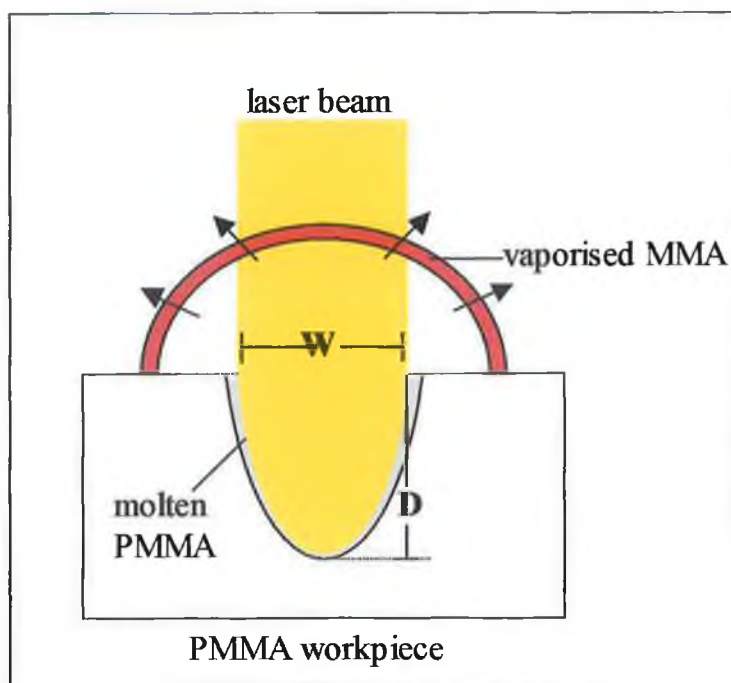


Figure 5-4 Schematic of the laser ablation process [3]

Polymethyl methacrylate (PMMA) is one of the most suitable polymers for CO₂ laser ablation. PMMA has many common names and is often referred to as acrylic and / or Plexiglas. Acrylic is a general term used to describe a large family of polymers. PMMA is an amorphous, transparent and colourless thermoplastic with a glass transition temperature, T_g of 105 °C. It has good abrasion and UV resistance, excellent optical clarity and good solvent resistance. Thin films of PMMA are normally made from impact-modified grades, which incorporate a small amount of elastomer, in order to improve their flexibility. PMMA is ideal for laser ablation because it is not easily melted and it has a high absorptivity at the laser's operating wavelength of 10.6 μm .

CO₂ lasers emit light continuously. In the case of PMMA this causes a rapid increase in the temperature of the polymer material when the focused laser beam hits the surface. The rapid elevation in temperature causes the material to decompose resulting in a cavity. At the boiling point of PMMA, the polymer chain vaporises in the form of monomers. The rate of decomposition depends on the strength of the chemical bonds and the structure of PMMA. When PMMA is ablated with a CO₂ laser it forms clean structures, which are not contaminated by degradation components [3-5].

Commercial black PMMA has virtually the same composition as the optically clear grade PMMA, the difference being purely the addition of a black dye to the composite mixture. This subtle difference in composition resulted in notable differences in the surface characteristics between the clear and black PMMA. This can be seen when the exact same structure, a reaction loop coil, was fabricated with the CO₂ laser using the same laser settings on both polymers.

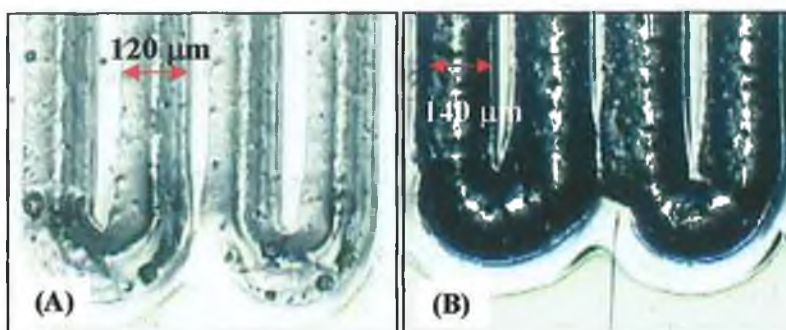


Figure 5-5 Photograph taken with a CCD camera under the microscope (magnification 10x) of two sets of micro-channels fabricated in (A) optically clear PMMA and (B) black PMMA

In Figure 5-5 (A) and Figure 5-5 (B) the reaction loop coil of each chip was compared. From Figure 5-5 (A) the channel is clearly defined with a width of 120 μm, compared with the channel in Figure 5-5 (B), which is slightly misshapen and wider at 140 μm. The optically transparent PMMA was shown to be more suited to the laser marking approach than the black PMMA. During the ablation process the black PMMA melted and deformed to cause a prominent ridge on the rim of the channel. However, even though the clear PMMA was better for fabrication with the CO₂ laser, in terms of optical detection the black PMMA was far superior. The sensitivity of the measurement was drastically improved due to minimal loss of light intensity compared to the transparent counterpart.

5.2.2 Fabrication of Micron-sized Structures

The laser parameters, which have been mentioned, are instrumental in terms of the dimensions of the ablated structures. Here the three laser control parameters are explained. By varying each parameter the ablation depth can be altered. The three parameters are:

1. No. of passes: The repetition of the same structure in the polymer material
2. Velocity [mm / s]: The speed at which the laser ablates a specific structure
3. Power [%]: The intensity of the laser beam as a percentage of the maximum intensity possible

The 3-D graph plotted in Figure 5-6 shows the interconnected relationship the three parameters had on the depth of ablation.

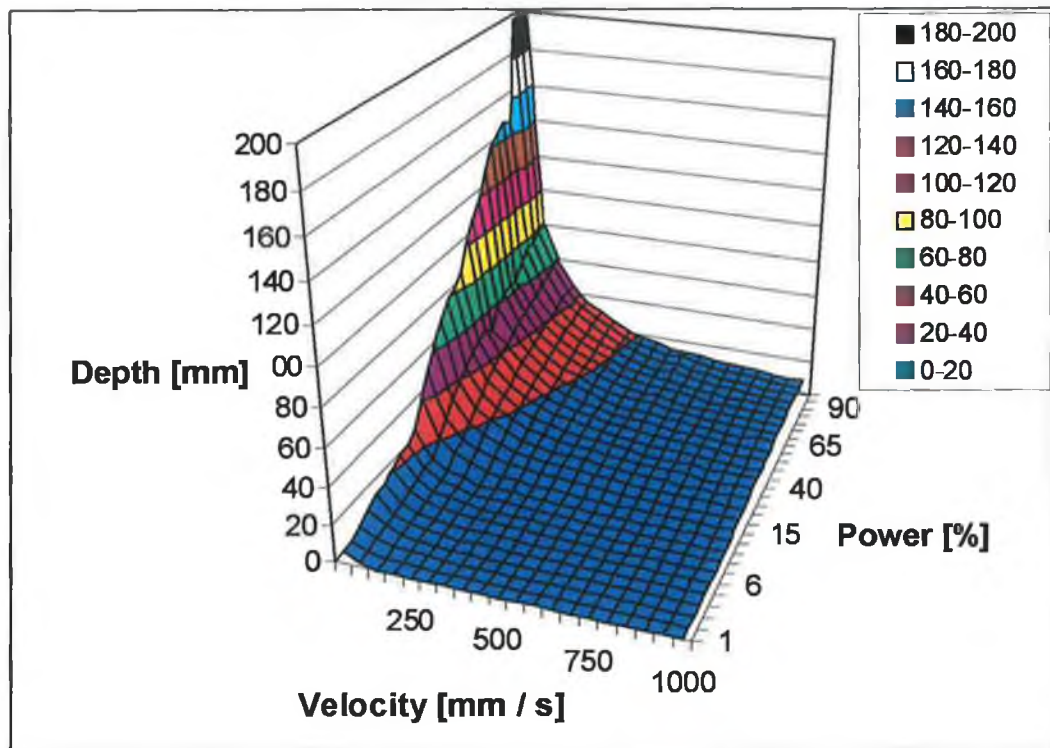


Figure 5-6 Relationship of velocity, depth and laser power with a focal lens of 200 mm

A general trend observed was as the power [%] increased and the velocity [mm / s] decreased the depth of ablation increased. This was caused by the longer time the laser beam took to ablate the surface at a higher intensity.

An experiment was designed to show that if two of the laser parameters were set as constant values and the third was varied the depth would change, but the width would remain as a constant. A 1.5 mm thick piece of PMMA was used for the experiment. The velocity was fixed as 120 mm / s and the number of passes made

was 1. The power range was maintained within 1 – 20 % because depths greater than 300 μm were not necessary. The structure ablated was a straight channel of 1 cm length. 5 power settings, within the range, were chosen as 1, 5, 10, 15 and 20 % and three 1 cm channels of each were ablated, which resulted in a polymer piece with 15 micro channels configured in a 3 \times 5 array as shown in Figure 5-7. The experiment was carried out with a 200 mm lens and the area of the ablated polymer piece had dimensions 75 (l) \times 25 (w) mm.

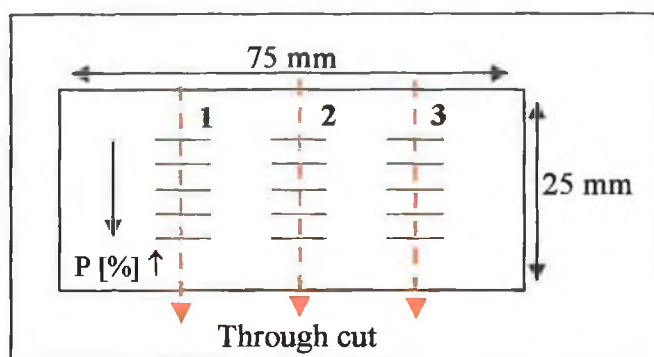


Figure 5-7 Channel layout on PMMA piece after ablation has taken place where rows, 2 and 3 represent the repeated structures of row 1

A microscope with an x, y scale on the objective was used to measure the width and depth of each channel using the scale given in Table 5-2.

Table 5-2 Scale based on magnification in the microscope for measuring micro-structure dimensions

Objective Magnification	Scale [μm / mark]
4x	26
10x	10
40x	2.5

Dimensions of the channel width were measured under the microscope at a magnification of 40x. For depth measurements the polymer piece was divided in three pieces down the middle of each channel as shown in Figure 5-7. The cross-section cut resulted in a depth profile for each channel. Each piece was milled to remove any surface deposition from the laser cutting process. The depth was then measured from the polymer surface to the apex of the Gaussian-type profile. For

both the width and depth the average value ($n = 3$) was plotted versus the Power [%] as illustrated in Figure 5-8.

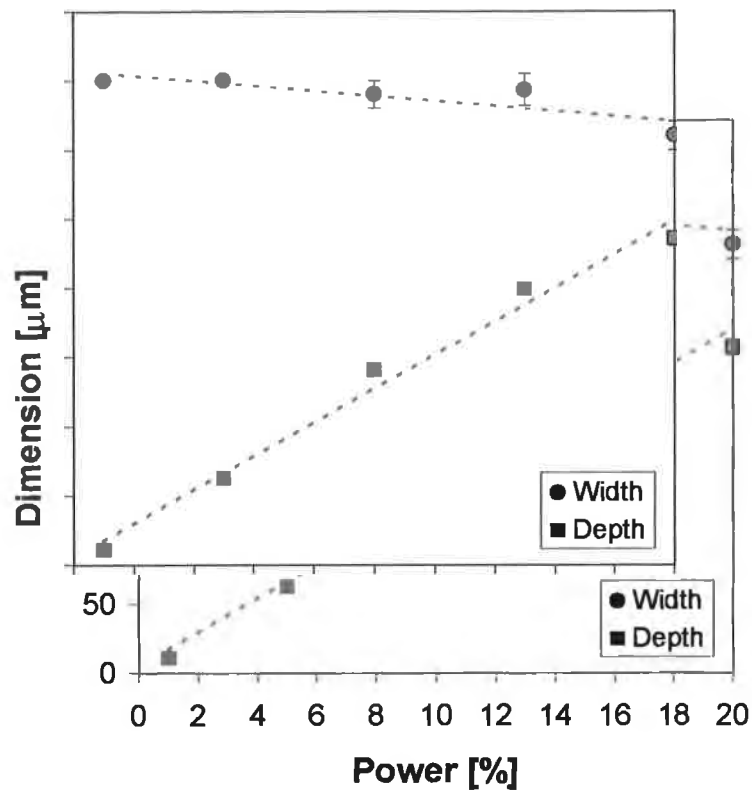


Figure 5-8 The dependence of the depth on the intensity of the laser beam (power [%]), where the velocity and the no. of passes are constant (120 mm / s and 1 , respectively)

The depth had a linear relationship with the power, i.e. an increase in power corresponded to an increase in the depth. Error bars were included for the triplicate measurements of depth and due to the good reproducibility a relative standard deviation of less than 4 % was calculated. The width remained constant as the power was increased. An average width for the 15 micro channels was calculated as 338.7 ± 16.9 (RSD: 5.0 %).

5.2.3 Order of Ablation

As a design is drawn with the software, the order, in which each part of the design is drawn, is recorded. The order has huge effects on the landscape of the ablated polymer, which is addressed in Figure 5-9. There are two sequences of ablation

presented, where a micro-channel and a through hole are cut in the middle of the channel.

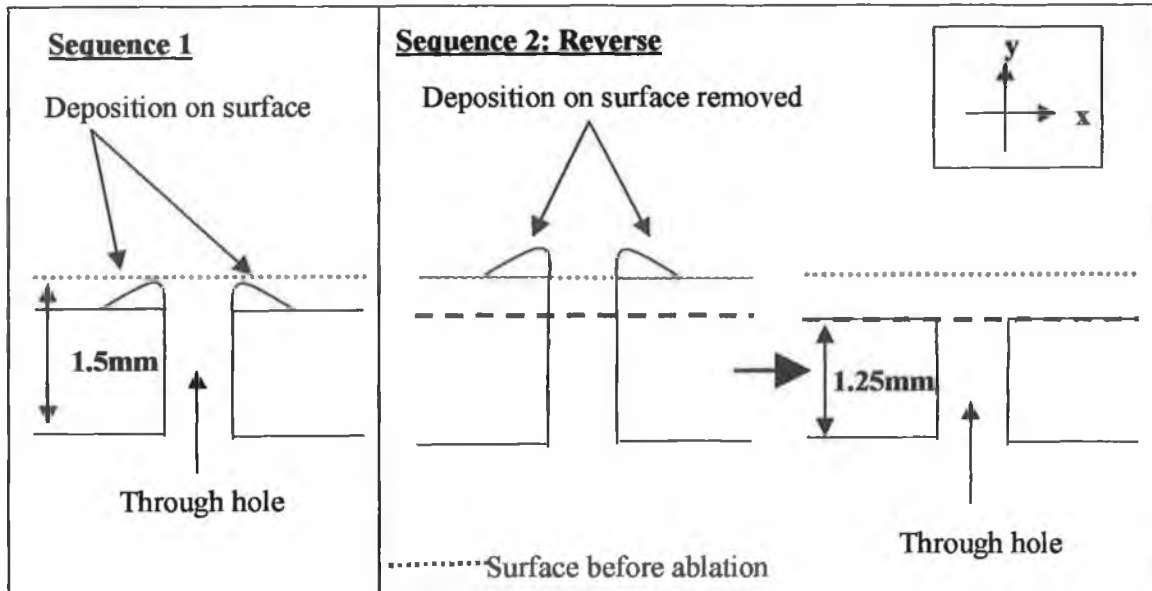


Figure 5-9 Schematic of the laser ablation of a through hole for the inlet, outlet and / or optical cuvette

Sequence 1 showed the resulting structure formed when the micro-channel was ablated before the through hole. The channel wasn't flat with ridges forming where the through hole was ablated, caused by the molten polymer material as it cooled down. These ridges impeded the uniform, controlled flow resulting in bubble formation. When the reverse sequence was implemented the through hole was ablated first. The ridges were removed when the micro-channel was ablated, which resulted in a flat, smooth flow surface.

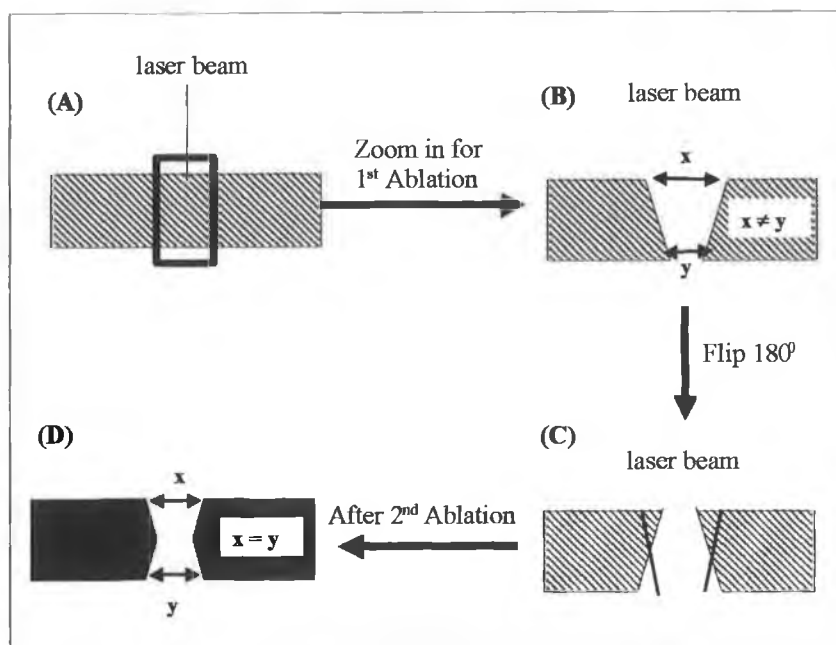


Figure 5-10 Schematic of the 1st approach to the fabrication of the optical cuvette in PMMA with the CO₂ laser

A uniform diameter of the optical cuvette through the polymer piece was extremely important, i.e. the diameter on the ablated and flipside (underside) of the polymer piece should be equal. The alignment of optical components was affected when the optical cuvette was not of uniform shape (cylindrical) and diameter. From Table 5-1 the depth of field for the 200 mm lens was ± 1.5 mm. For the microfluidic channels black PMMA of 2 mm thickness was utilised, which meant that when a through hole was ablated the diameter decreased with depth as shown in Figure 5-10 (B), where the diameter at the point $x > y$. The first suggestion to maintain a uniform shape was to ablate the hole from one side then the flip the chip 180° and repeat the same ablation step on the opposite side as shown in Figure 5-10 (C). However there were two major challenges posed by this approach. The first involved the difficulty in aligning the chip after it had been flipped 180°. The second is shown in Figure 5-10 (D), where the diameter of $x = y$, but that the diameter of the optical cuvette was not uniform through the whole piece.

The second suggestion for creating a through hole for the optical cuvette was to carry out the ablation in two steps as shown in Figure 5-11.

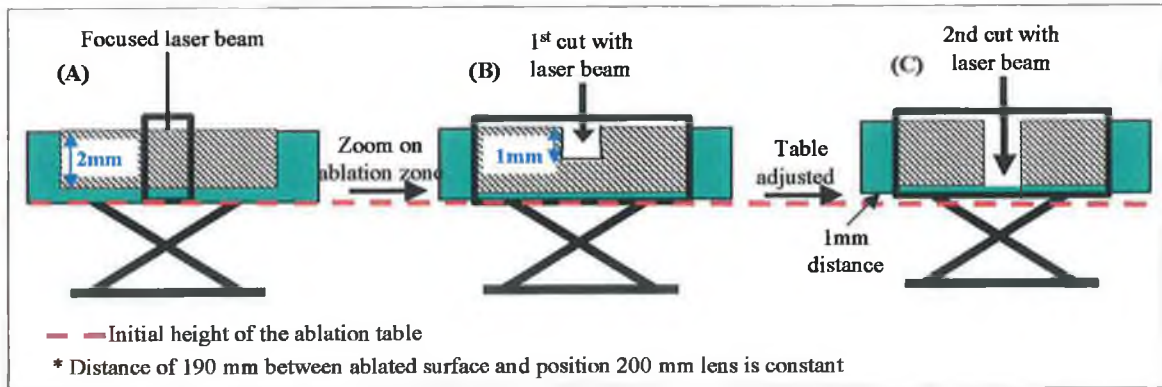


Figure 5-11 Schematic of the 2nd approach to the fabrication of the optical cuvette in PMMA with the CO₂ laser

The first cut only penetrated approx. 1 mm through the piece (Figure 5-11 (B)). The table upon which the ablation of the polymer material took place was adjusted, i.e. the distance was adjusted by 1 mm to accommodate the change in the depth, where the through hole was cut. The second cut was made at the same point and with the same laser settings resulting in a through hole of uniform diameter as shown in Figure 5-11 (C). This was achieved by always maintaining a constant distance between the lens and the ablation surface.

5.3 Scanning Electron Microscope (SEM) Analysis

A scanning electron microscope (SEM) was also used to measure channel and through hole dimensions and to establish that the microscope was a quick and accurate method of estimating width and / or depth. The polymer pieces were initially placed inside the SEM, but the intensity of the beam caused rapid changes in the surface morphology of the material. This was primarily due to the low glass transition, T_g , temperature of PMMA of 105 °C. Each surface that was analysed under the SEM had to be pre-coated in a fine layer of gold to protect the integrity of the structures. The gold was applied with a sputter coater instrument (Model: S150B, Edwards Sputter Coater, BOC Edwards, Sussex, old model discontinued). The process is very quick and the pieces were ready in less than 5 min for analysis.

For Scanning Electron Microscopy (SEM) analysis the surface to be examined is coated in order to make it conductive. The SEM instrument used was manufactured by Hitachi (Model: S-3000, SEM 50E5107, Hitachi Europe, Maidenhead, Berkshire, UK). The SEM uses electrons rather than light to form an image. The large depth of field associated with SEM allows a large surface area of the sample to be in focus at one time. SEM instruments produce images of high resolution, which means closely spaced features can be examined at high magnification.

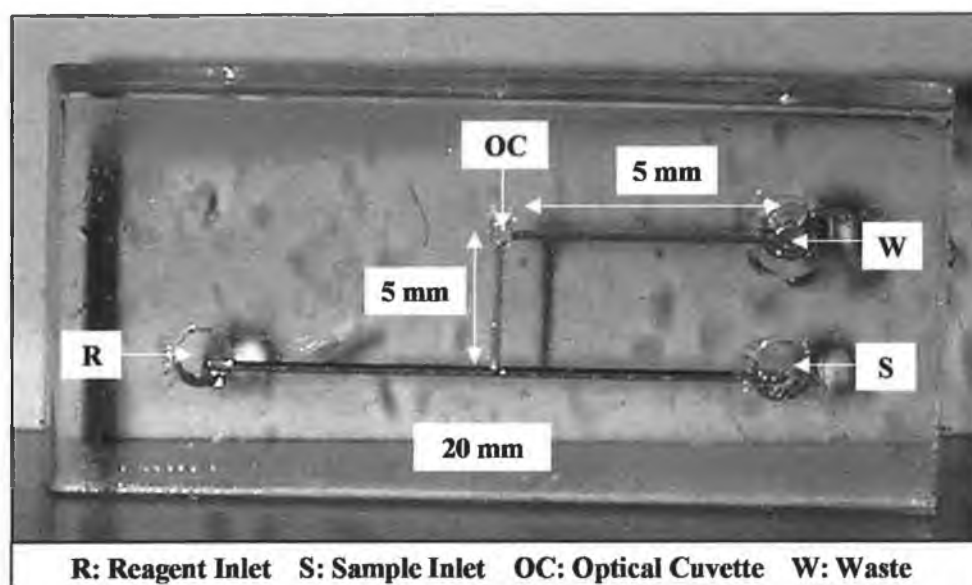


Figure 5-12 Photograph of the reaction micro-channel including dimension measurements

A photograph of the first three-layered polymer chip that was fabricated with the CO₂ laser is shown in Figure 5-12. The middle layer containing the microfluidic structures was analysed with the SEM prior to bonding the chip. The microfluidic chip is labelled R for reagent, S for sample, W for waste and OC for the optical cuvette. The micro channels were laser ablated at a velocity of 120 mm / s, with the number of passes made set as 1 and the power at 20 %. From Figure 5-8 the depth and width at 20 % power were calculated as 235.8 $\mu\text{m} \pm 5.2 \mu\text{m}$ (RSD: 2.2 %) and 310 $\mu\text{m} \pm 10 \mu\text{m}$ (RSD: 3.2 %) respectively with the microscope set-up.

In Figure 5-13 the width of the T-junction of the micro channel was measured at five points on the chip. The average width of the channel was calculated as 354.92 $\mu\text{m} \pm 3.50 \mu\text{m}$ (RSD: 0.99 %). The average width calculated with the SEM was

compared with the average width calculated with the microscope ($338.7 \mu\text{m} \pm 16.9 \mu\text{m}$ (RSD: 5.0 % for $n = 3$)). The relative error was calculated for the microscope values as 4.58 %, which was a good comparison and showed that the microscope was a satisfactory way to estimate the channel dimensions.

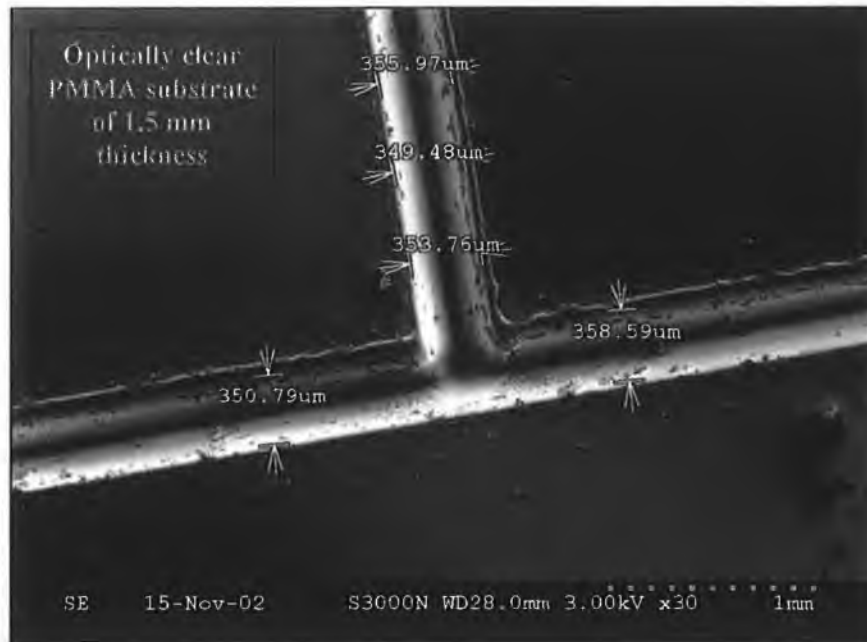


Figure 5-13 SEM image of a T-junction at a magnification of x30

For the depth measurements the channel was cut with the CO₂ laser across the micro channel to give the side-profile Gaussian, shape. The depth of the channel was measured from the flat surface of the polymer material to the apex of the peak as shown in Figure 5-14. The photograph also shows the small ridges, which formed after ablation, as previously discussed.

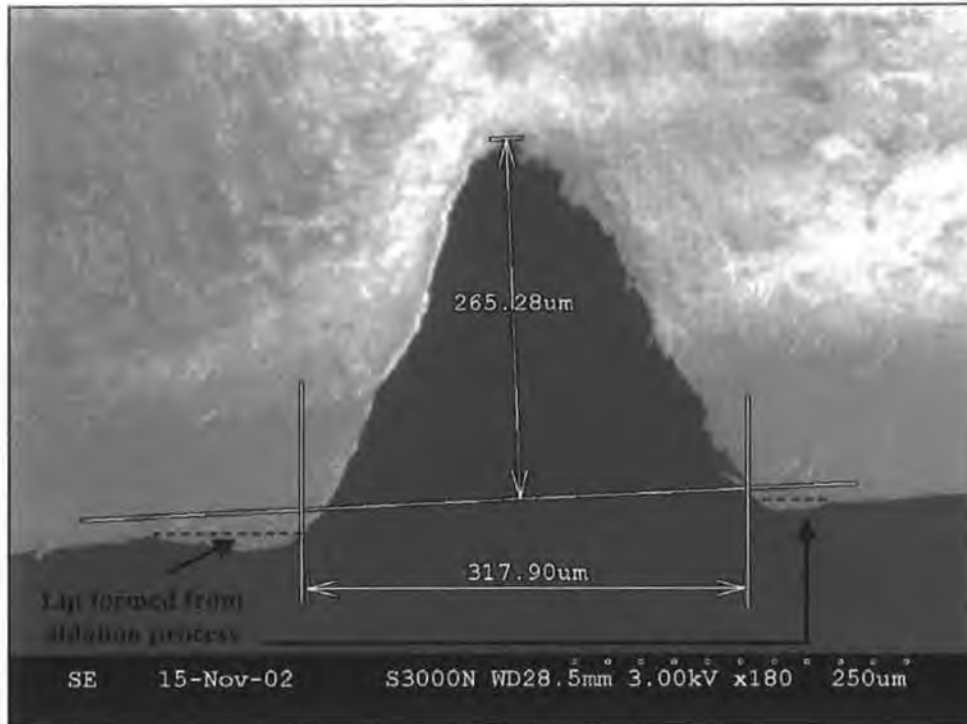


Figure 5-14 SEM image of the cross-section of a micro-channel depth at a magnification of x180

The depth was compared to the average depth calculated with the microscope at 20 % power. The relative error for the microscope measurements was calculated as 11.1 %. This was a larger error than that of the width measurements. The width was a direct measurement, whereas for the depth measurement the micro channel had to be cut resulting in polymer deposition after ablation on the surface, followed by a micromilling process, which can interfere with the accuracy of the measurement.



Figure 5-15 SEM image of the optical cuvette at a magnification of x30

The optical cuvette was analysed under the SEM as shown in Figure 5-15. The cut appeared to be fairly clean and the shape was symmetrical, however, it was noted, that the cracked rim could cause potential problems in terms of bonding. The diameter of the optical cuvette was significantly larger than that found in the silicon system, but again by varying the laser settings the diameter was reduced. The minimum diameter made with the 200 mm lens was calculated to be $340 \mu\text{m} \pm 10 \mu\text{m}$ (RSD: 2.9 %). This can be reduced to less than $200 \mu\text{m}$ when an 80 mm lens is used with the CO_2 laser.

5.4 Chip Integration

The final design of the three layers is shown in Figure 5-16. Layer 1 represents the coverlid that seals the microfluidic channels. It required no preparation, except cutting the piece to fit the microfluidic layer and was made from 0.125 mm thick optically clear PMMA. Layer 2 shows the simple T-junction design suitable for the yellow method. It consists of a T-junction channel, where the reagent and sample were introduced onto the chip at the points, R1 and S1 respectively, an optical cuvette labelled OC and a waste channel ablated on the flipside, which runs to an external waste reservoir at the point, W1.

The T-junction channel has dimensions 10 mm (l) × 200 μm (w) × 120 μm (d), where l represents the length, w the width and d the depth. The waste channel has dimensions 5 mm (l) × 200 μm (w) × 200 μm (d). And finally the optical cuvette has a diameter of 350 μm and a depth equal to the thickness of layer 2, which is 2 mm.

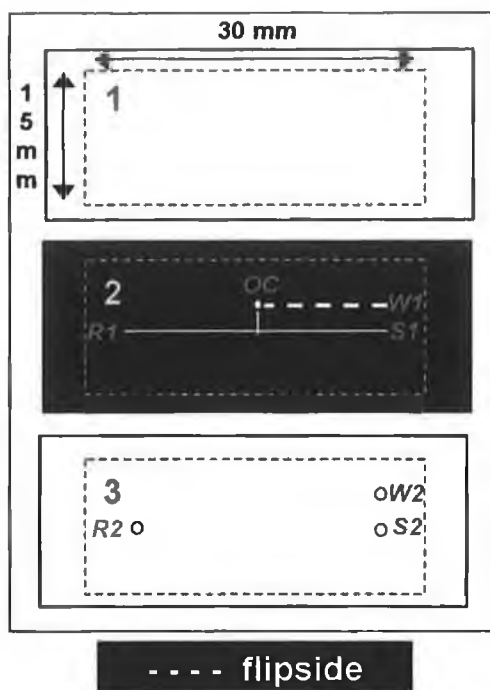


Figure 5-16 Layout and design of the three layers of the microfluidic chip

Layer 3 aids fluidic interconnection of the sample and reagent onto the chip and the removal of waste from the chip. There are three through holes in the 1.5 mm thick optically clear PMMA layer. 2 of the holes, labelled R2 and S2, act as inlets for the reagent and sample respectively, and 1 the final outlet hole for waste is labelled W2. The three holes have a diameter of 1.6 mm, to facilitate yellow PEEK tubing of inner and outer diameter 1.6 mm and 175 μm respectively (Model: Yellow PEEK, Anachem Ltd., Luton, Bedfordshire, UK), carrying fluids from the reservoirs onto the micro channels, and a depth of 1.5 mm (equal to the thickness of layer 3).

5.5 Bonding

When the microfluidic chip design was optimised and then fabricated, the three layers had to be bonded together. The Mikroelektronik Centret (MIC) at the Danish Technical University (DTU) in Copenhagen developed a thermal bonding process [3]. Prior to bonding the three layers were annealed, which involved placing the PMMA in an oven and ramping the temperature up to just above its glass transition temperature, T_g . The optimum temperature was maintained for 2 hrs and then the temperature was decreased slowly at a rate of 1.25 °C / min. PMMA is an acrylic polymer and depending on the thickness of the three layers a corresponding annealing program can be implemented (see Table 5-3). The three layers each have a different thickness. Therefore they had to be annealed separately. Layer 1 of 0.125 mm thickness was not annealed because there was an elasticiser included in the polymer batch cocktail and the properties of this thin sheet differed from the sheets with a thickness greater than 1mm. Layer 2 of 2 mm thickness and layer 3 of 1.5 mm thickness had total annealing times of 5.4 hrs and 4.9 hrs respectively as taken from Table 5-3.

Table 5-3 *The relationship of PMMA thickness and annealing time*

Time at Max. Temp. [min]	PMMA Thickness [mm]	Total Annealing Time [hrs]
30	0.5	3.9
60	1	4.4
90	1.5	4.9
120	2 - 3	5.4
150	3 - 4	5.9
180	4 - 6	6.4

The three major benefits of annealing were:

1. Minimum warping of the material
2. Reduction in stress cracking
3. Improvement in dimensional stability [6].

In Figure 5-17 a photograph of the bonding equipment is shown. The clamp, used to hold the bonded pieces in place, was manufactured by Scangrip (Model: 7, Optiko A/S, DK-5700, Svendborg, Denmark).

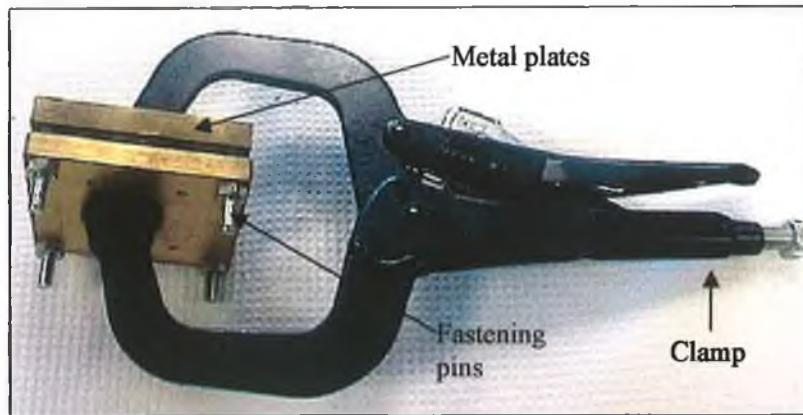


Figure 5-17 Photograph of the apparatus utilised to bond the polymer sheets under temperature and applied force

The three chip layers were wedged between two metal blocks and secured with 4 nuts and bolts (6 mm). The block was then placed in the clamp and the tightness adjusted to ensure no movement could take place and that just enough pressure was applied to facilitate bonding. The clamp was positioned in the centre of the block to evenly distribute the applied force across the three layers. It was important that the bonding was uniform for the whole chip.

In Figure 5-18 the bonding apparatus is illustrated. The three layers are centred within the metal blocks, which were sandwiched between the grips of the clamp. The two blocks of metal, labelled top and bottom, showed the four alignment holes and the positioning of the microfluidic layers.

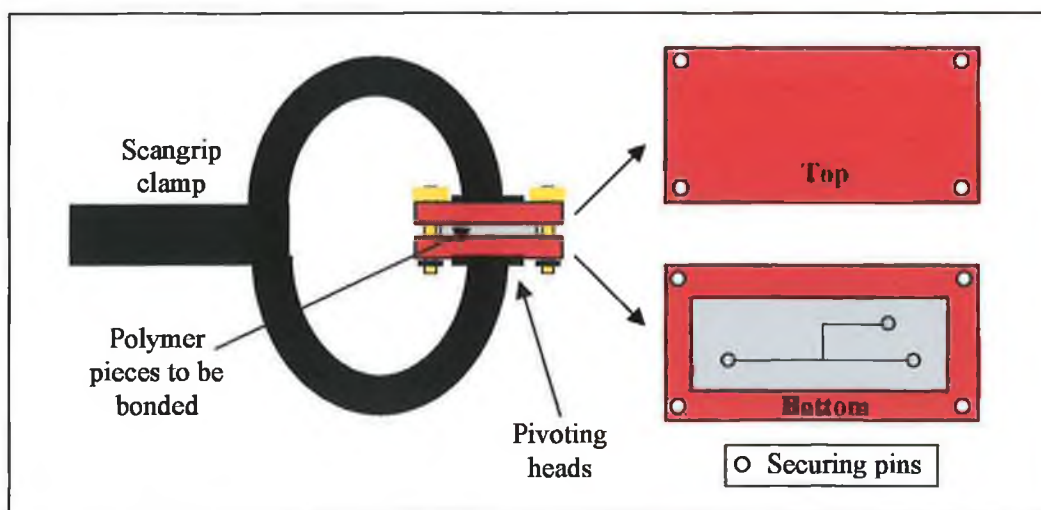


Figure 5-18 Schematic showing the bonding process

The bonding process was very straightforward. The three layers of PMMA were placed in an ethanol bath for 10 min to improve the adhesion properties of the polymer material. The pieces were then cleaned with lint-free, cleanroom-quality tissue to remove any excess ethanol. The locator pins were put in place to maintain the alignment and the pieces were sandwiched between two Pyrex plates of 25 mm (l) × 75 mm (w) × 1 mm (d) dimensions and pressed between two metal blocks, each of 3 cm thickness. The piece was then clamped and placed in the oven, when the temperature was still below 80 °C. The temperature was ramped up to 110 °C and maintained for 2 hrs. After which the program was stopped and the bonded piece was left to cool until the temperature had dropped to below 60 °C.

The top layer (or layer 1) has previously been described as the coverlid, which sealed the microfluidic channels resulting in leak-free flow. In Figure 5-19 a cross-sectional drawing of the bonding between layer 1 and layer 2 is shown.

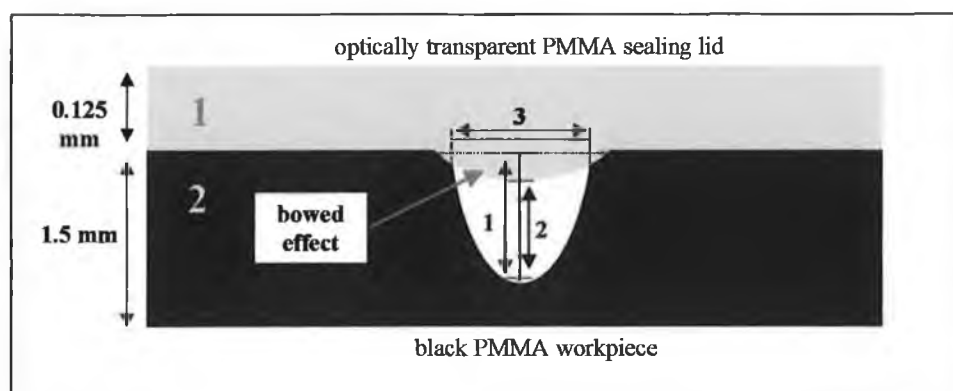


Figure 5-19 Schematic showing the effect bonding had on the three-layered microfluidic manifold

The force applied on the three layers during bonding can cause a bow effect in layer 1, which occurs over cavities (channel, optical cuvette etc.) in layer 2. This bowing alters the channel geometry, changing the total chip volume. When the chip volume is very small to begin with, the extent of the change in channel geometry after bonding can hinder the proposed analytical measurement.

With this bonding method there was no definitive applied force that could be set. The optimum conditions were discovered by trial and error.

5.6 Leak-free Microfluidic Interconnects

In Figure 5-20 the complex interconnection network is shown from two angles (A) the top view and (B) the side profile. In Figure 5-20 (A) the three components that facilitated leak-free flow were PEEK tubing (yellow), o-rings (black) and “polymer bricks” (red and white striped). In Figure 5-20 (B) the order and alignment of the three components is shown with respect to the microfluidic chip.

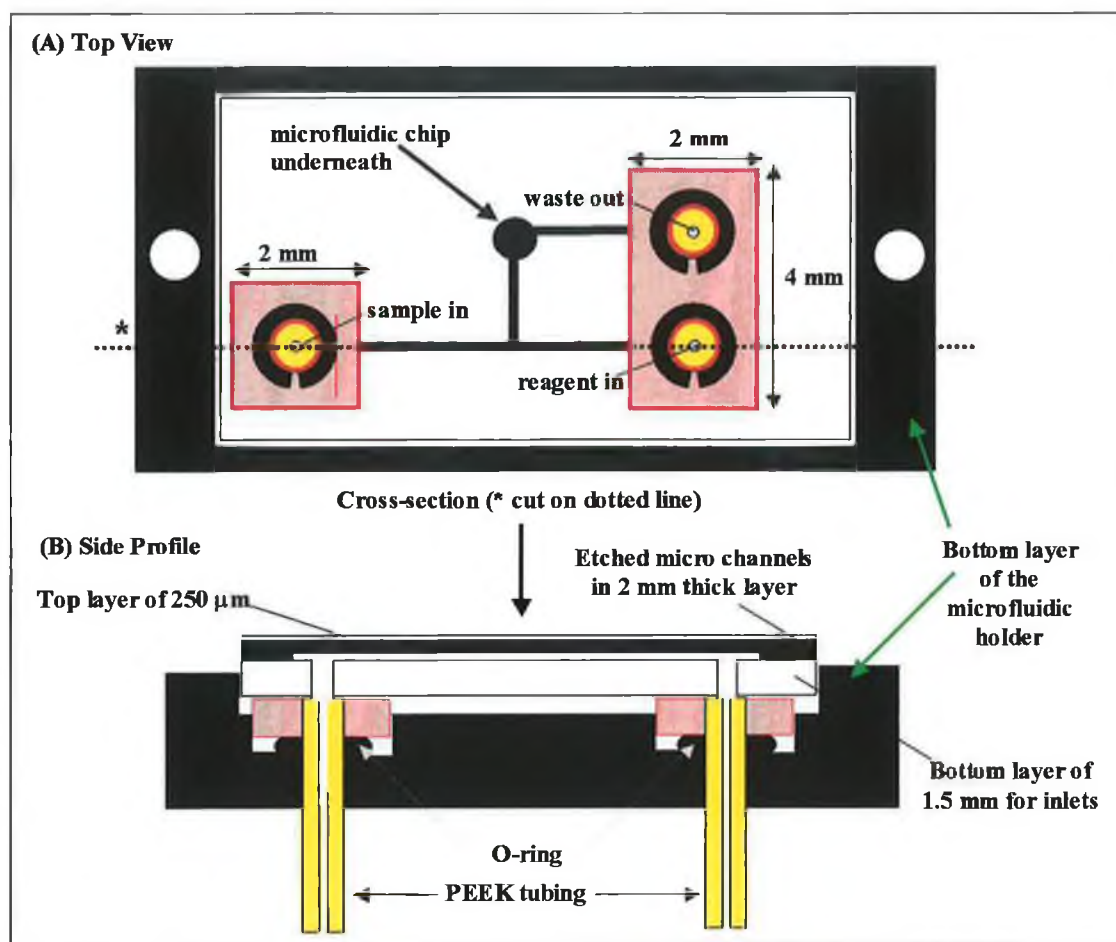


Figure 5-20 Schematic of interconnects used in polymeric microfluidic manifold

The interconnection of the micro-fabricated fluidic device and the external environment was initially made with yellow PEEK tubing, which was chosen because it coincided best with the through hole dimensions (outer diameter) and the micro-channel dimensions (inner diameter) made with the CO₂ laser. The bottom layer of the chip holder had sunken crevices, where the fluidic connections were made, to accommodate rubber o-rings of inner and outer diameter of 1 mm

and 2 mm respectively (Apple Rubber Products Inc., Florida, USA). The o-rings were selected based on three criteria, size, hardness and chemical compatibility of the material with the yellow method reagents. A sunken depth of 0.5 mm was required to ensure the o-rings lay flush with the surface of the chip holder. The CO₂ laser was used to make the o-ring holes in the chip holder.

The polymer bricks were made to further ensure that leak-free flow was maintained in the microfluidic manifold. These bricks had a through hole in the centre, which the PEEK tubing was fed through. They were fabricated in 1mm thick PMMA using the CO₂ laser and sat on top of the o-rings.

When the entire system was assembled and tightened with the alignment pins the polymer blocks were an extra protection for the transfer of fluid from reservoir onto the chip and from the chip to a waste container.

5.7 Experimental

In this section the final integrated microfluidic system is discussed. Two detectors, a silicon photodiode detector and a portable spectrometer (Ocean Optics S2000) were used and the results from both were compared. The portable spectrometer is the same detector that has been used throughout this research. The Si-photodiode was used because it is a small compact, cheap, low-powered alternative to the spectrometer. The overall goal of the project was to scale down each component of the system whilst maintaining good analytical data. Replacing the spectrometer with a suitable photodiode is the next obvious step.

5.7.1 Microfluidic System

In Figure 5-21 the microfluidic system is shown for the two modes of optical detection and are labelled **(A)** for the portable spectrometer and **(B)** the silicon photodiode detector. The system in Figure 5-21 **(A)** has previously been described in chapter 3, Figure 3-1. On the other hand the system in Figure 5-21 **(B)** is new design.

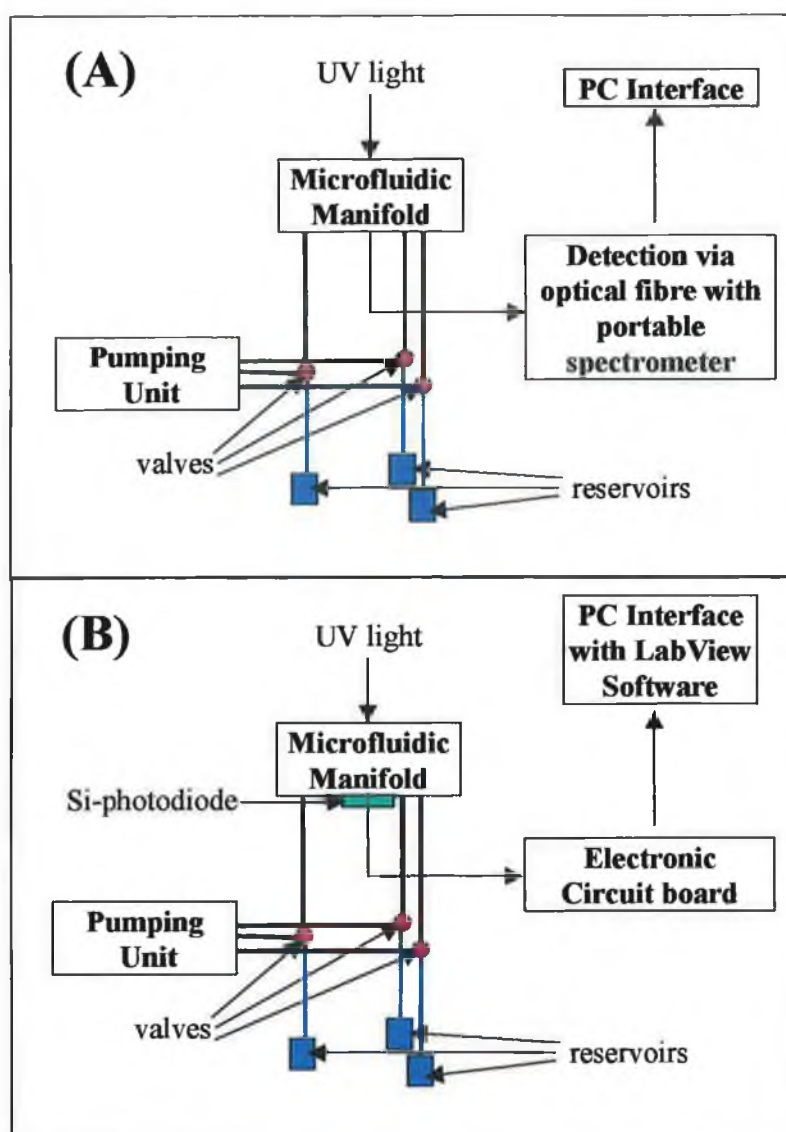


Figure 5-21 Schematic of the integrated microfluidic system

In Figure 5-21(B) the optical detection is integrated into the microfluidic manifold with the Si-photodiode embedded in the bottom layer of the chip holder. When the yellow heteropoly complex is formed under stopped flow conditions in the optical cuvette of the microfluidic chip an electronic signal is captured from the Si-photodiode into the LabView program in the form of a voltage change, which is visually displayed on the PC screen. The electronic circuit board is used to power and control the UV-LED and the Si-photodiode.

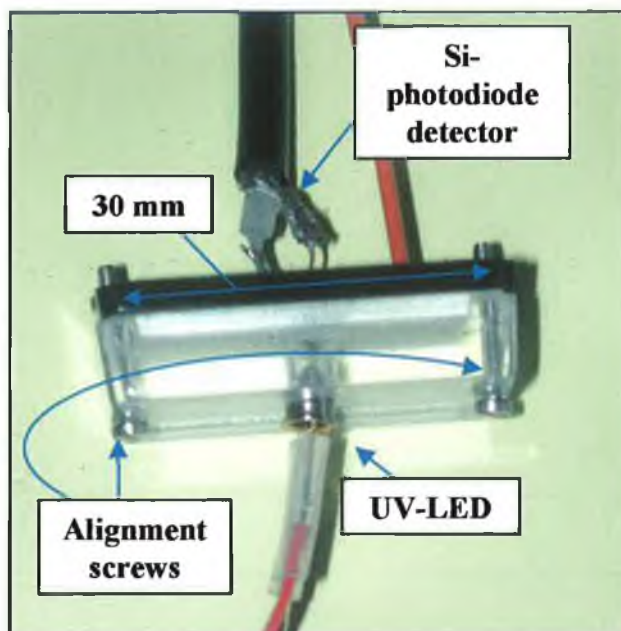


Figure 5-22 Photograph of the microfluidic chip holder

In Figure 5-22 a photograph of the polymeric microfluidic manifold is shown. The optical alignment involved the positioning of the UV-LED and the Si-photodiode over the optical cuvette ensuring that the maximum light intensity was detected in the system. Screws (3 mm diameter \times 14 mm length) with washers and bolts were used for aligning and the securing the holder in position. The alignment holes were made with a micro-milling machine and located on opposite ends of the holder.

5.7.2 Optical Detection

The optical cuvette was designed as shown in Figure 5-23, whereby three laser cuts were made. The first labelled, 1, was ablation of the through hole, the second was ablation of the reaction channel and the third was ablation of the waste channel. In that way the fluid flows down through the optical cuvette, where detection occurs and out to waste. The top and bottom layers act as cover plates for the channels and the optical cuvette.

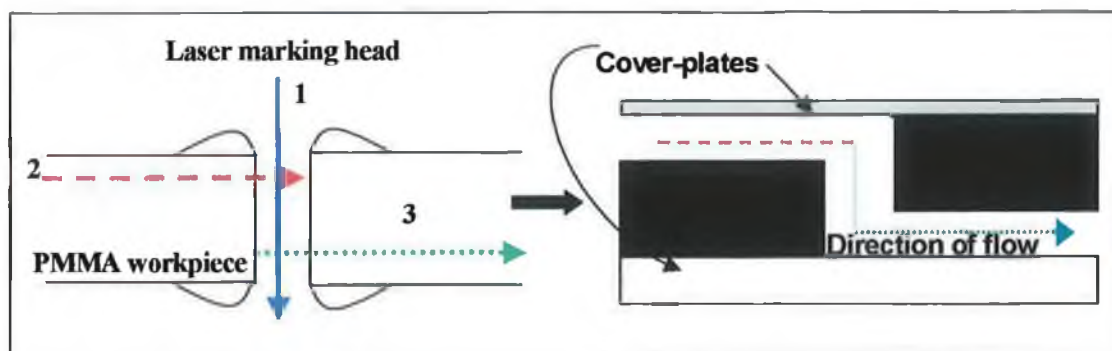


Figure 5-23 Ablation sequence for the fabrication of the optical cuvette

Photodetector

The use of a UV-LED as the light source has been elaborated upon in Chapter 2, Section 2.3. The silicon photodiode detector was manufactured by Hamamatsu (Model: S1227-33BR, Hamamatsu Photonics UK Limited, Hertfordshire, UK) and was powered by 2×5 V batteries in series. The photodiode was attached to an electronic PC-board and controlled by a simple LabView program. The optical signal was recorded in LabView and exported to Microsoft Excel for post-run data analysis.

In Figure 5-24 the alignment of the UV-LED and the Si-photodiode with respect to the rest of the microfluidic manifold is schematically shown. The chip holder was fabricated to house and align the optical components over the optical cuvette in the microfluidic chip for optimum detection. The side profile shows the optical alignment with respect to the inlet channels.

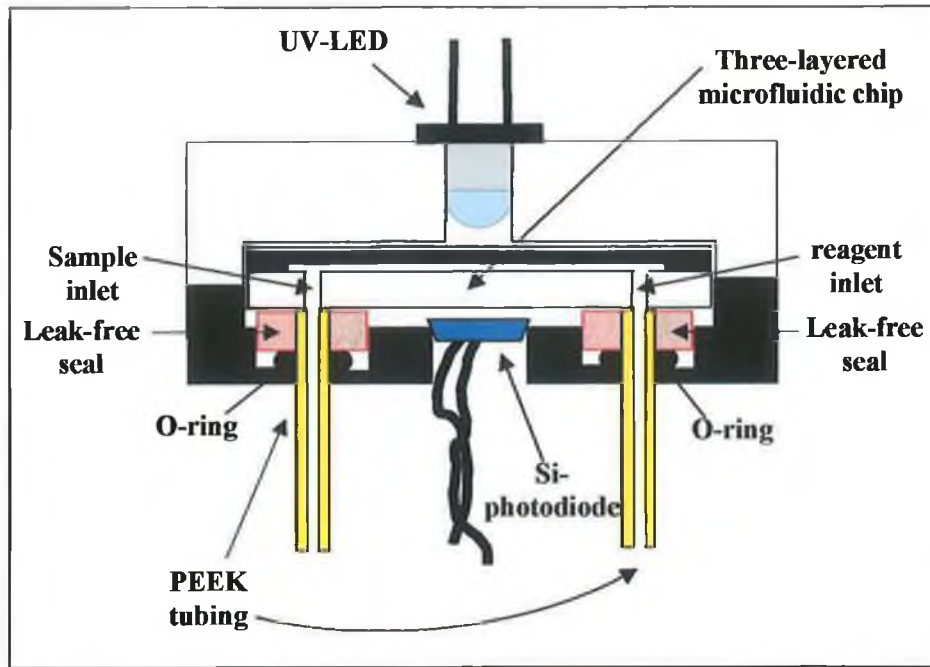


Figure 5-24 Schematic of the integration of optical components, the UV-LED and Si-photodiode in the microfluidic manifold

In Figure 5-25 the side profile shows the alignment of the optical components over the optical cuvette and with respect to the waste channel.

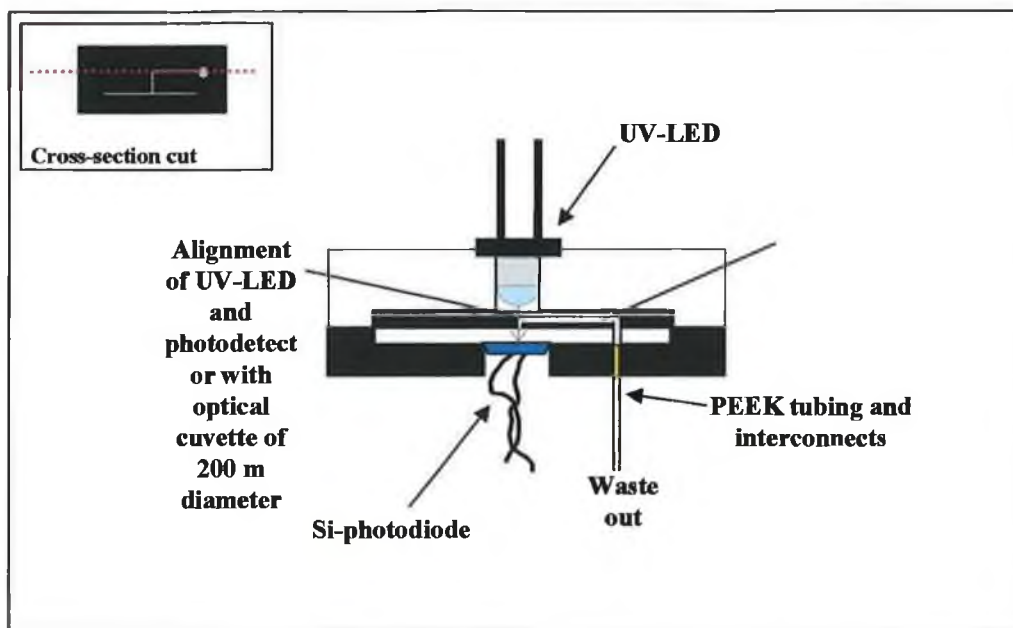


Figure 5-25 Schematic of the optical alignment within the microfluidic manifold

The optical detection was best when both the UV-LED and silicon photodiode were precisely aligned as shown in the illustration. The schematic also highlights how

waste fluid was removed from the chip through the waste outlet and back through the bottom layer of the chip and holder.

5.8 Analytical Results

The first analytical measurements taken with the polymer microfluidic system are presented here. This included a linearity study with both optical detectors, namely the silicon photodiode and the portable spectrometer. The results from the study were also validated against conventional measurements in a 1-cm cuvette spectrophotometric system and a flow analysis system. Real samples were collected and analysed on-chip under stopped flow demonstrating the versatility of the yellow method in the determination of phosphorus.

5.8.1 Validation of Polymer Microfluidic Chip

A five-point calibration was performed with the two detector systems. Both microfluidic systems were identical, the only difference being the detector used. The analyses were carried out under the same experimental conditions over the concentration range 0 – 50 mgL⁻¹ PO₄³⁻ - P as all previous calibrations described in this thesis and the standards were prepared from the same 50 mgL⁻¹ P stock solution as prepared in Chapter 2, Section 2.1.

The Silicon Photodiode as a Detector

The UV-LED is a narrowband light source, which emits in over the wavelength range ~ 370 – 385 nm. Consequently the Si-photodiode receives light within the same wavelength range and transmits an averaged signal for the entire range. For the purpose of calibration a baseline optical signal was recorded for distilled water and then the optical signal of the sample was taken. The signal was converted to an absorbance value using Equation 6-1.

$$A = \log \left(\frac{I_{ref}}{I_{sample}} \right)$$

Equation 5-1

Where A was absorbance, I_{ref} was the optical signal of the blank (distilled water) and I_{sample} was the optical signal of the product (heteropoly acid complex). When the reaction had reached completion and a stable signal had been achieved, data points were acquired at a rate of six measurements / min. Five repeats were taken for each standard and the average absorbance was plotted against the PO_4^{3-} - P concentration over the range 0 – 50 mgL^{-1} at a working wavelength of 380 nm as shown in Figure 5-26. The raw data recorded is shown in Table 5-4.

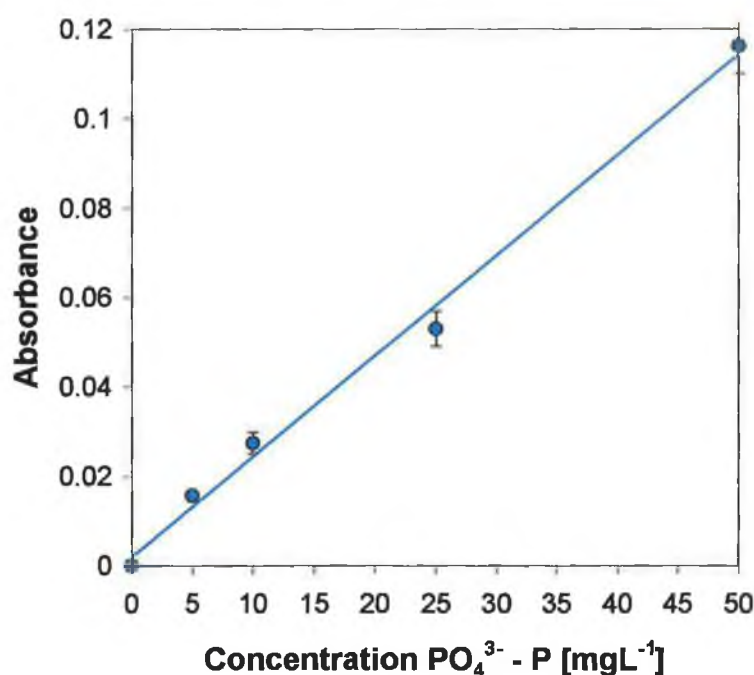


Figure 5-26 Calibration plot of absorbance against PO_4^{3-} - P concentration over the range 0 – 50 mgL^{-1} with the Si-photodiode as the detector

The calibration plot gives an R^2 value of 0.9940 ± 0.0037 (RSD: 0.3767 % for $n = 5$) that indicates good linearity. The reproducibility was reasonably good for each calibration point, which is evident from the RSD less than 8.8 % determined for each set of repeat values, where $n = 5$.

Table 5-4 Repeat absorbance measurements of standard samples for the determination of $\text{PO}_4^{3-} - \text{P}$ made with Si-photodiode

Conc. $\text{PO}_4^{3-} - \text{P}$ [mgL^{-1}]	1	2	3	4	5	Aver. Abs.	Std. Dev.	% RSD
0	0.0000	0.0000	0.0000	0.0000	0.0000	0.0000	0.0000	0.0000
5	0.0154	0.0157	0.0170	0.0149	0.0148	0.0156	0.0008	5.1473
10	0.0291	0.0242	0.0288	0.0248	0.0301	0.0274	0.0024	8.7894
25	0.0497	0.0517	0.0586	0.0482	0.0563	0.0529	0.0040	7.4759
50	0.1200	0.1207	0.1083	0.1095	0.1230	0.1163	0.0061	5.2742

The Portable Spectrometer as a Detector

The calibration was performed in triplicate and the sample plugs obtained under stopped flow for the first set of calibration standards are shown in Figure 5-27.

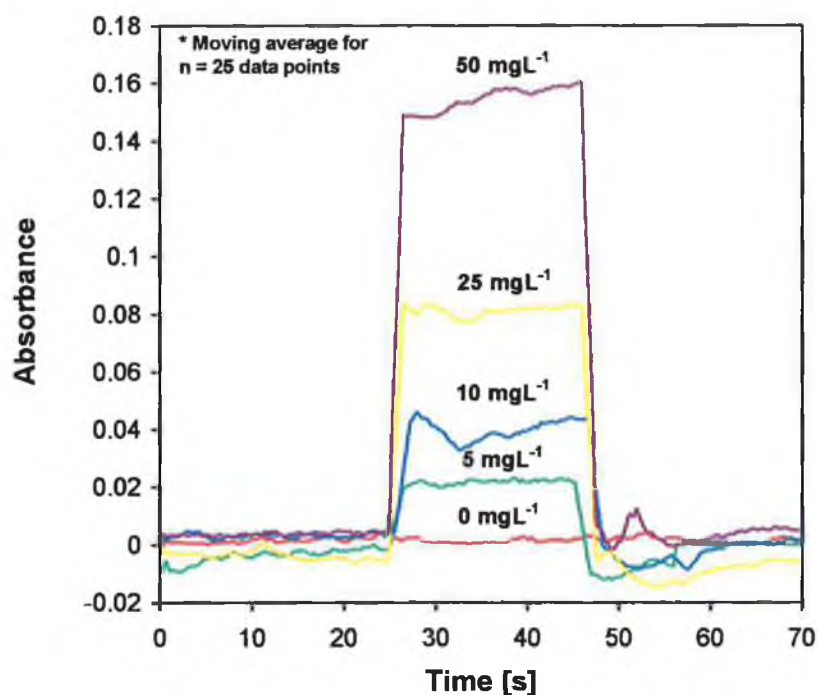


Figure 5-27 Real-time plot of absorbance for a series of calibration standards at a wavelength of 380 nm using the Ocean Optics spectrometer

The real-time data shown in Figure 5-27 have been processed (moving average for $n = 25$) to give a smoother response profile. Absorbance values were then calculated by subtracting the baseline signal from the plug maximum at steady state. An average of 25 data points was used. Each standard was analysed in triplicate and the average absorbance was then plotted against $\text{PO}_4^{3-} - \text{P}$ concentration. An R^2 value of 0.9938 ± 0.0040 (RSD: 0.4020 % for $n = 3$) was calculated indicating a good linear response over the range 0 – 50 mgL^{-1} .

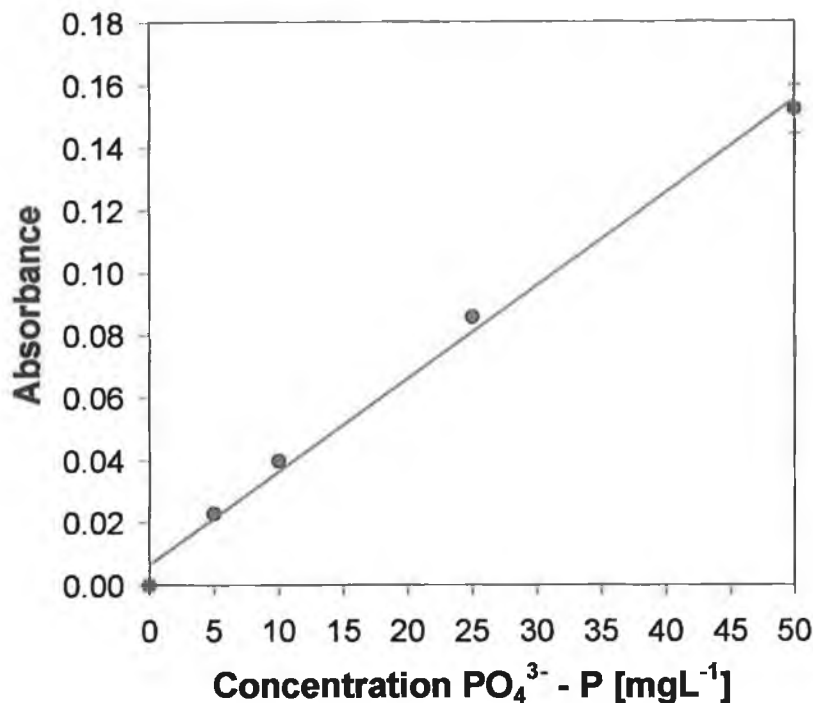


Figure 5-28 Calibration plot of absorbance against $PO_4^{3-} - P$ concentration over the range $0 - 50 \text{ mgL}^{-1}$ with the portable spectrometer as the detector at a wavelength of 380 nm

Error bars were included for each data point and the reproducibility of the calibration was shown to be good with an RSD less than 5.2 % ($n = 3$), which was calculated from the data represented in Table 5-5.

Table 5-5 Repeat absorbance measurements for the determination of $PO_4^{3-} - P$ over the concentration range $0 - 50 \text{ mgL}^{-1}$ $PO_4^{3-} - P$ with the portable spectrometer at a working wavelength of 380 nm

Conc. $PO_4^{3-} - P$ [mgL^{-1}]	1	2	3	Aver. Abs.	Std. Dev.	% RSD
0	0.0000	0.0000	0.0000	0.0000	0.0000	0.0000
5	0.0222	0.0215	0.0221	0.0219	0.0003	1.5204
10	0.0398	0.0393	0.0371	0.0387	0.0014	3.6297
25	0.0847	0.0848	0.0849	0.0848	0.0001	0.1488
50	0.1568	0.1543	0.1423	0.1511	0.0077	5.1262

The calibrations from the two detectors were plotted on the same graph to compare the performance of the Si-photodiode against that of the portable spectrometer. The calibration comparison is shown in Figure 5-29.

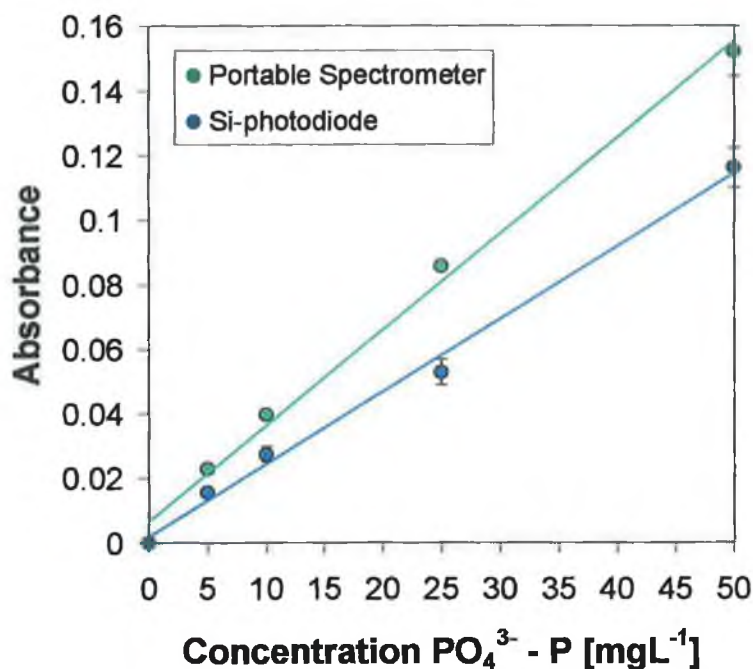


Figure 5-29 Comparison plot of the calibrations with the Si-photodiode and the portable spectrometer over the concentration range 0 – 50 mgL^{-1} $\text{PO}_4^{3-} - \text{P}$ at a wavelength of 380 nm

A linear relationship between absorbance and $\text{PO}_4^{3-} - \text{P}$ concentration over the range 0 – 50 mgL^{-1} was observed with both detectors. The sensitivity of the measurement was a magnitude of approx. 1.3 better with the portable spectrometer, which was established by the ratio of the respective slopes. The Si-photodiode was an inexpensive, small device compared with the more robust and powerful portable spectrometer, which can explain the obvious difference in sensitivity between the two detectors.

The main reason for using a photodiode as the detector was to develop a fully integrated microfluidic system capable of performing as well, if not better than a bench-size instrument. The results achieved with the Si-photodiode could be improved, if the optical set up was fully optimised. A narrow bandpass filter would limit the wavelength range (10 nm range), which would mean that the averaged signal from the Si-photodiode would be nearer the chosen working wavelength of 380 nm. Then a better comparison could be made between both detectors.

5.8.2 Real Sample Analysis

Real samples were analysed in the polymer microfluidic manifold utilising the portable spectrometer. The portable spectrometer was easier to set up, calibrate and apply to the determination of PO_4^{3-} - P in real samples. In Chapter 4 river samples were exclusively analysed. In this chapter a range of different water samples were collected. In Table 5-6 a list of the samples collected and analysed is given.

Table 5-6 *List of water samples, type and location*

Sample No.	Water Type	Source
1	River	Santry River: Clonshaugh Bridge
2	Pond	St. Anne's Park
3	Sea / Estuary	Bull Island Estuary, Dollymount
4	Wastewater	Swords Water Treatment Facility
5	Tap	Leixlip Drinking Water Facility

Again the samples were filtered on-site through single use disposable 0.22 μm membrane filters. The samples were stored in acid-washed brown glass (24 hrs in 2 M HCl) and transported back to the laboratory. The analysis of each sample was performed in triplicate in less than 2 hrs (Post-filtration).

Validation Methods

Two simple analytical methods were chosen to establish the validity of the microfluidic measurements. They were a conventional 1 cm cuvette measurement with a spectrometer and a HPLC instrument re-configured as a simple direct injection flow analyser. Two calibrations were performed in triplicate over the concentration range 0 – 50 mgL^{-1} PO_4^{3-} - P at a working wavelength of 380 nm. Firstly the calibrations performed with both instruments are described in the section, followed by the results of the real sample analysis for both systems compared with the results from the polymer microfluidic manifold.

Flow Injection Analysis with a Modified HPLC Instrument

The separation column of a standard HPLC instrument (Model: Varian ProStar, JVA Analytical Ltd., Dublin, Ireland) was removed and replaced with a stainless steel union. This allowed direct sample injection. The instrument was run at a flow-rate of 2 ml / min and all injections were made at a fixed wavelength of 380 nm. 5 ml pre-mixed samples of the reagent and sample were prepared in a 1:1 ratio prior to injection. 1 μL aliquots of the sample were injected via the injection port (in the load position). The Varian Star software (Version 5.3) plotted the corresponding real-time peak as absorbance against time [s]. Because there was no column used the elution time response was quick (< 20 s / injection). In Figure 5-30 the averaged data from the triplicate runs was plotted against time [s] over the concentration range 0 – 50 mgL^{-1} PO_4^{3-} - P at a working wavelength of 380 nm.

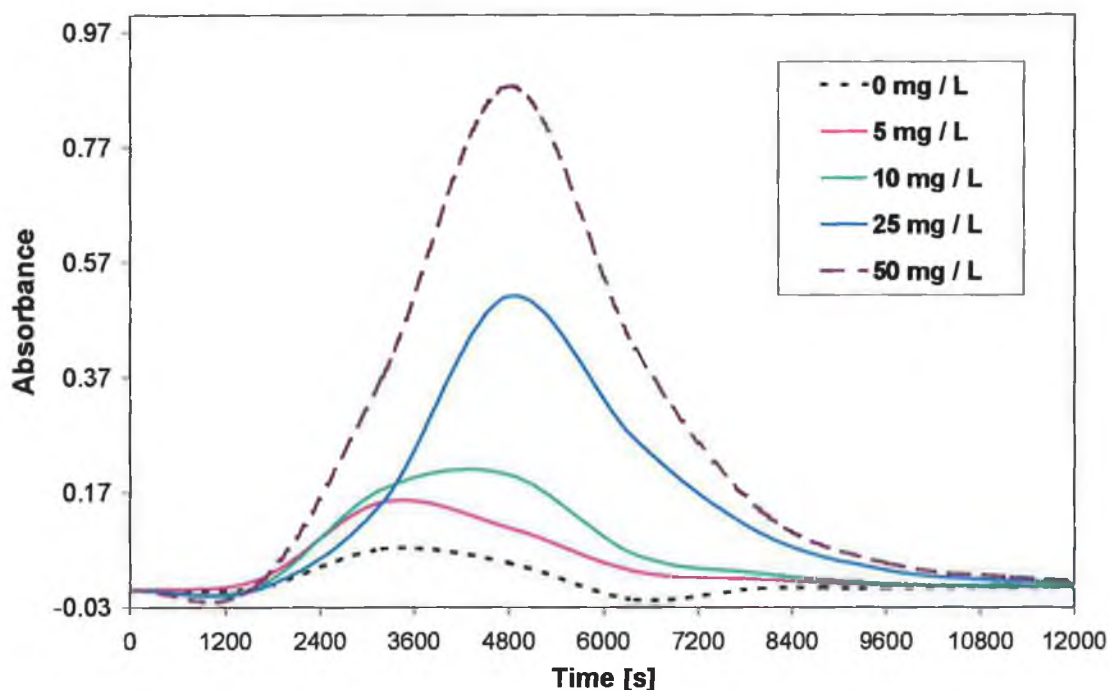


Figure 5-30 Elution peaks of each calibration standard plot as absorbance versus time over the concentration range 0 – 50 mgL^{-1} PO_4^{3-} - P

From the triplicate measurements the peak maximum at $t = 4.8$ s for each standard was averaged and plotted versus PO_4^{3-} - P concentration over the range 0 – 50 mgL^{-1} at a working wavelength of 380 nm as shown in Figure 5-31. The

relationship was linear and an R^2 value of 0.9942 ± 0.0063 (RSD: 0.6392 % for $n = 3$) was calculated.

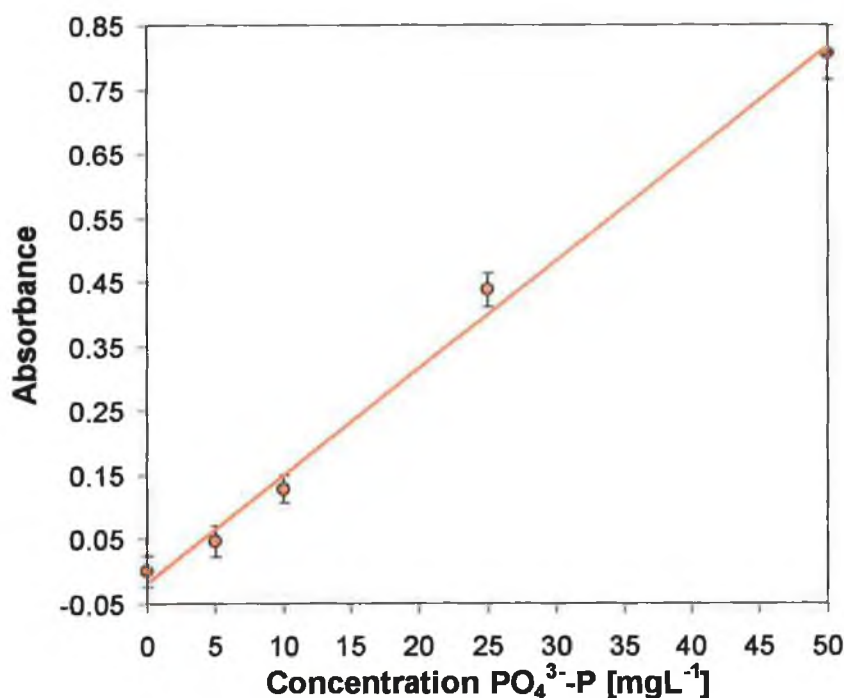


Figure 5-31 Linear plot of absorbance versus $PO_4^{3-} - P$ concentration over the range $0 - 50 \text{ mgL}^{-1}$ at a wavelength of 380 nm with the FIA analyser

Error bars were included ($n = 3$) and the data was reproducible with a relative standard deviation of less than 4.7 % over the entire calibration.

Conventional Spectrometer with 1 cm Cuvette

The conventional system was documented in Chapter 2 and the same system was utilised here. The calibration was carried out over the concentration range $0 - 50 \text{ mgL}^{-1} PO_4^{3-} - P$ at the working wavelength of 380 nm. A series of standards were prepared from the $50 \text{ mgL}^{-1} P$ stock solution and each standard was mixed with the reagent in 1:1 ratio and the absorbance of the resulting yellow heteropoly solution was measured at 380 nm. Each sample was analysed in triplicate and the average absorbance was plotted against $PO_4^{3-} - P$ concentration as shown in Figure 5-32.

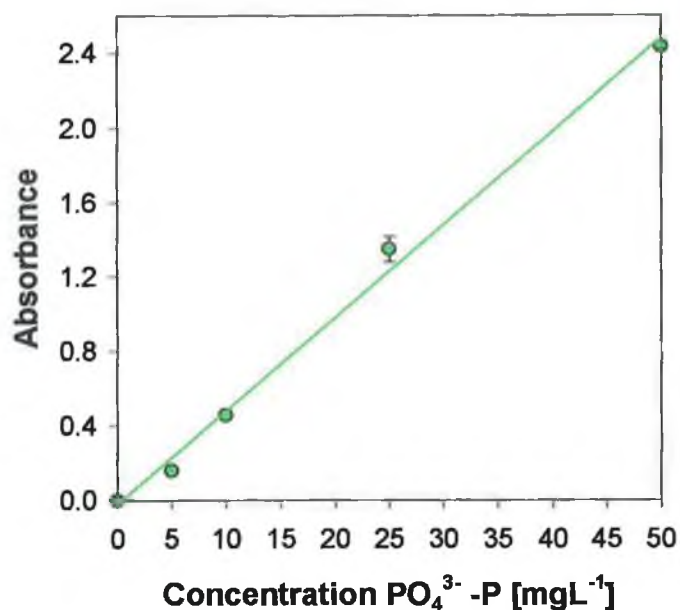


Figure 5-32 Linear plot of absorbance versus $\text{PO}_4^{3-} - \text{P}$ over the range 0 – 50 mgL^{-1} at a wavelength of 380 nm in a conventional 1 cm cuvette

The linear relationship was reflected in an R^2 value of 0.9947 ± 0.0041 (RSD: 0.4091 %). The reproducibility was good as the RSD of less than 5 % ($n = 3$) showed.

Polymer Chip Calibration

A second calibration was made with the portable spectrometer prior to the analysis of the real samples. The method is as described previously. The calibration has been demonstrated to be linear and the equation of the line was given as in Equation 6-2.

$$y = 0.0031x + 0.0058$$

Equation 5-2

In Table 5-7 the average absorbance values were calculated from the triplicate measurements highlighting the accuracy of the measurement with a RSD of less than 5 % ($n = 3$).

Table 5-7 Average absorbance values calculated from the triplicate measurements made for the real sample analysis at a wavelength of 380 nm

Sample No.	1	2	3	Aver. Abs.	Std. Dev.	% RSD
1	0.0134	0.0131	0.0126	0.0130	0.0004	3.0956
2	0.0184	0.0192	0.0191	0.0189	0.0004	2.3063
3	0.0276	0.0302	0.0279	0.0286	0.0014	4.9794
4	0.008	0.0084	0.0083	0.0082	0.0002	2.5283
5	0.0072	0.0071	0.007	0.0071	0.0001	1.4085

There were five real samples, labelled 1 – 5 as shown in Table 5-6. Each sample was analysed on the three systems, the conventional 1 cm cuvette, the microfluidic chip and the FIA system. On each system the samples were analysed in triplicate. From the three calibrations carried out Equation 5-2 was used to determine the PO_4^{3-} - P concentration of the unknown samples. This was done to consolidate the microfluidic results with those obtained with the instrumental methods. The results obtained for each sample are tabulated in Table 5-8.

Table 5-8 Comparison of the concentrations calculated for the real samples from the three methods at a wavelength of 380 nm

Experimental PO_4^{3-} - P Concentration [mgL^{-1}]						
Label	Sample No.	1	2	3	4	5
A	Microfluidic	2.3323	4.2258	7.3441	0.7849	0.4194
B	1 cm Cuvette	2.4313	4.0627	7.0613	0.8780	0.4573
C	Flow Injection	2.5309	4.0459	7.0978	0.8822	0.4571
A to B	% RE	4.2480	3.8606	3.8501	11.8548	9.0564
A to C	% RE	8.5188	4.2571	3.3535	12.3944	8.9974

Previous analyses of the Santry River showed that the PO_4^{3-} - P concentrations determined here (Sample No. 1) was slightly higher than the trend in the measurements made at the Clonsaugh Bridge location (Aver. conc. of $\sim 1.4 \text{ mgL}^{-1}$ PO_4^{3-} - P) as shown in Chapter 5, Section 4.5.2. The relatively high PO_4^{3-} - P concentration determined in the pond water (Sample No. 2) can be attributed to the stagnant nature of the water and the obvious signs of Eutrophication at this location. The seawater (Sample No. 4) had a considerably lower PO_4^{3-} - P concentration than expected. However the seawater content is very different from that of fresh water and the high concentration of various salts may have influenced the measurement. The PO_4^{3-} - P concentration of the wastewater (Sample No. 3) was within the criteria outlined by the Irish EPA and documented in a EU directive

[7]. Finally the tap water (Sample No. 5) had an acceptable concentration within the EU requirements for drinking water [8].

The experimental concentration of each sample calculated for the polymer microfluidic system was compared with results from the 1 cm cuvette and FI systems by calculating the RE [%] (see Table 5-8). From the results the microfluidic measurements compared favourably with the other methods for Sample No. 1, 2 and 3. However, for the seawater and tap water samples, which were in the lower concentration range, the RE [%] was not as good. This validation study showed that the first microfluidic chip fabricated with the CO₂ laser in PMMA was successfully used to determine PO₄³⁻ - P concentrations in real samples with the yellow method.

In this chapter the initial goal was to fabricate a microfluidic chip, similar to the Si chip used in previous chapters, in a polymeric material. In order to bring the concept to fruition many challenges were presented. The CO₂ laser was chosen as the micro-fabrication technique because structures could be fabricated rapidly and many designs could be tested in a short period of time. PMMA was chosen as the polymer material because it was the most suitable for CO₂ laser ablation. The thermal bonding procedure was optimised for PMMA and the design of the microchip holder facilitated optical integration and alignment and a tight, leak-free environment for the microfluidic chip.

The system described in this chapter is the first polymer microfluidic system with integrated optical detection that was utilised to analyse real samples. There are a number of changes that could be made to improve the performance of the system. The laser ablation technique can be changed to a more accurate method of fabricating micron-sized structures, for example, hot embossing. Nearly all polymers can be hot embossed, which means that the material that suits the methods chemical and optical requirements can be selected, rather than the material that suits the micro-fabrication technique. The optical path length can also be optimised and the alignment of the optical components be improved upon.

The main advantages of developing the polymer microfluidic system were rapid prototyping, low cost (when compared with silicon chip fabrication costs), range of material properties (in contrast to silicon), including mechanical, electrical, thermal

and optical, robustness, integration of optical components and a simple bonding process. Sampling strategies can be developed and sampling components can either be fabricated in polymer materials as a separate unit or a more complex microfluidic manifold can be designed to integrate the sampling. Finally by utilising either small-sized pumps with microlitre flow-rates or fabricating smart on-chip flow components, an integrated miniaturised system can be realised.

5.9 Conclusion

In conclusion a simple microfluidic system was designed and fabricated in the polymer material, PMMA. The CO₂ laser was used to fabricate the microfluidic structures and a thermal bonding process was used to seal the channels. The optical components were integrated into the microfluidic manifold. Real samples were collected, filtered and analysed under stopped flow in the new polymer system. The PO₄³⁻ - P concentration of each sample was determined and the results were validated against two reference methods. The polymer microfluidic chip was successfully fabricated and applied to the analysis of "unknowns".

5.10 References

- 1 J.C. Cooper, G.M. Whitesides, *Acc. Chem. Res.*, 2002, **35(7)**, 491-499.
- 2 "FH Series Marking Head: Operators Manual for Index and Tracker Models", 2000, Version 2, Synrad, Washington, USA, **4**, 1-13.
- 3 H. Klank, J.P. Kutter, O. Geschke, *Lab on a Chip*, 2002, **2(4)**, 242-246.
- 4 J. Powell, *CO₂ Laser Cutting*, 1998, Springer-Verlag, Berlin.
- 5 P.G. Berrie, F.N. Birkett, *Opt. Lasers Eng.*, 1980, **1**, 107-129.

6 "*Annealing*", Technical data provided by Laird Plastics, 2000, West Palm Beach, Florida, <http://www.lairdplastics.com/techdata/anneal.htm>

7 EU publication "*Council Directive on Urban Wastewater*", 1991, 91/271/EEC, document 391L0271, (official journal of the European Communities, L135, 30/05/91), p. 0040-0052.

8 EU publication "*Drinking Water Directive*", 1998, 98/83/EC, http://europa.eu.int/comm/environment/water/water-drink/index_en.html

6 Current Status and Future Work

6.1 Polymer Microfluidic Manifold Fabrication

The initial results with the polymer microfluidic manifold were promising. The technique employed in the fabrication of the device was CO₂ laser ablation. CO₂ ablation is a reasonably crude method, which is noted more for its ability to rapidly reproduce simple designs than its pinpoint accuracy for small-scale dimensions. However there are other micro-fabrication techniques available that could be used to improve the system described in this chapter. One such method was hot embossing. A combination of hot embossing and micromilling is a possible alternative to CO₂ laser ablation. At present fabrication of a new microfluidic manifold has begun. The goal of this research is to develop the second-generation prototype. From which point the basic research emphasis would turn to other challenges such as sampling, total component integration, power consumption, remote monitoring and new pumping initiatives.

6.1.1 Hot Embossing

The technique of hot embossing has been briefly discussed in the literature survey (Chapter 1, Section 1.4.5). However to recap, hot embossing involves the stamping of a pattern into a polymer softened to just below its glass transition temperature. A tool / stamp / mold, upon which the design is inverted, is used to make the micron-scale size features. Once the various conditions such as touch and applied force, temperature and time at T_g have been optimised the process the cycle time can be less than 10 min. The particular instrument we used was manufactured by Jenoptik (Model: Hex 02, Jenoptik Mikrotechnik, Jena, Germany).

With this system there are four main parameters to be optimised in order to produce micron-scale size features in polymer materials and these are force, temperature, position and time. The four parameters are all inter-dependent, for example if the temperature is increased; a decrease in the time and the applied is usually necessary. The optimisation process is governed by a trial and error approach. There are two types of force, a touch and an applied mode. The touch force is used to bring the tool and substrate into contact. The applied force is an additional exerted pressure applied to the tool and substrate. The applied force depends on the aspect ratio of the structures to be fabricated, whereas sometimes

the touch force can be enough to fabricate microstructures, when the temperature and time at temperature have been extended. There are 4 temperatures to consider. These are the temperature of the tool, the substrate, i.e. the polymer material, the top plate upon which the tool is affixed and the bottom plate upon which the polymer sheet sits. An optimised hot embossing program would have an even temperature distribution from the time the tool comes into contact with the substrate until the microstructures are formed and the plates are moved. An example of a typical temperature profile is shown in Figure 6-1. Initially all four components are heated. Then when the touch force is reached, the temperature begins to balance out. At time, $t = 500$ s, all four components have reached the same temperature. When this occurs the polymer sheet is ready for embossing and the applied force is exerted.

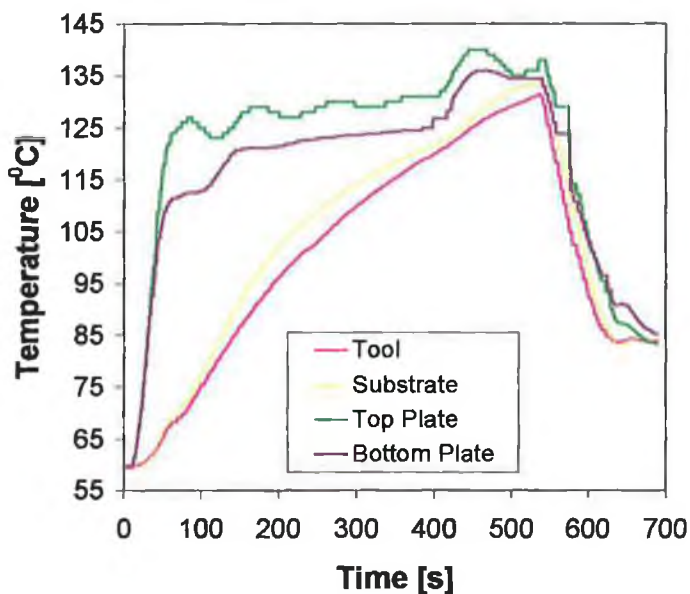


Figure 6-1 Example of the plot of the change in temperature as a function of time for the process of hot embossing

Another important rule is that the glass transition temperature should never be exceeded; otherwise the structures will not be completely formed. The next parameter is position. This refers to the position of the top and bottom plates. When the plates are moved towards each other they use micro-sensors to align themselves with each other and to bring both into contact. If the sensors are not

functioning correctly the microstructures formed are not always representative of the tool being used. Finally the timing is vital. Every step of the process is timed. The time taken to bring the tool and substrate into contact, the time required to ramp the temperature up to near its glass transition temperature, the time taken at the applied force, the time taken for the tool and substrate to cool down etc.. The timing of each of these steps has an overall effect on the embossing of the microstructures.

Master Fabrication

The tool used for the fabrication of microfluidic structures suitable for the determination of phosphorus with the yellow method was designed with Tanner EDA software (Package: L-Edit, EDA Solutions Ltd., Southampton, UK). A mask template was set up in L-Edit, whereby a total of 12 chip layouts could be designed. In this case 4 chips were designed and repeated in triplicate as shown in Figure 6-2. The tool / stamp used to fabricate the micro-channels in the polymer material was fabricated on a silicon 4" wafer with an inverted surface topography with respect to a normal silicon etched mask, i.e. the micro structures are raised on the surface of the silicon. The inverted mask was coated in Teflon to protect the integrity of the structures. The mask was designed by Steffen Horowitz (Gesellschaft für Silizium Mikrosysteme (GeSim) mbH, Dresden, Germany).

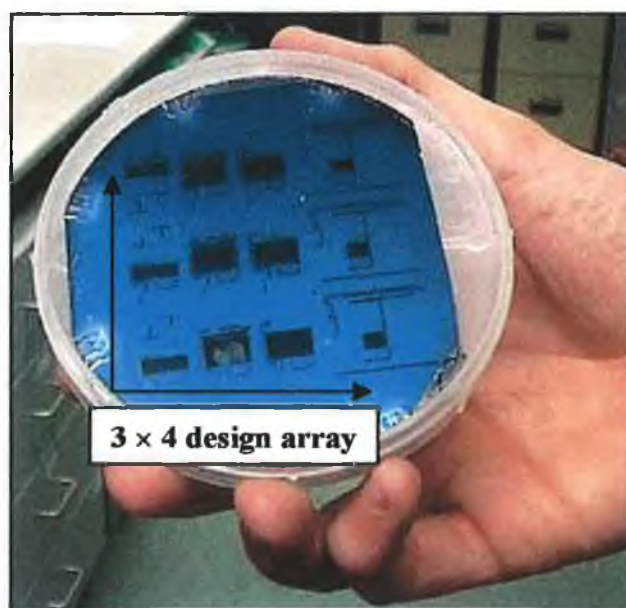


Figure 6-2 *Handheld photograph of the inverted Silicon mask with a 3 × 4 chip design layout*

The tool was affixed to an aluminium plate with an epoxy resin (Model: EPO-TEK 377, Epoxy Technologies, Promatech Ltd., Gloucestershire, England), which was a two-component adhesive that was applied thinly and cured at 150 °C for 1 hr.

In Figure 6-3 a micro-channel fabricated with the CO₂ laser is compared with one that was made with the hot embosser. The photographs were taken with the SEM at a magnification of 70x and 350x for (A) and (B) respectively. Not only is the micron-scale width of the channel far smaller in Figure 6-3 (B) but also the definition, i.e. channel walls, and the surrounding surface are clearer than in Figure 6-3 (A). In (A) the surface of the polymer, which wasn't ablated is covered in debris from the process. The amount of debris is much less in photograph (B).

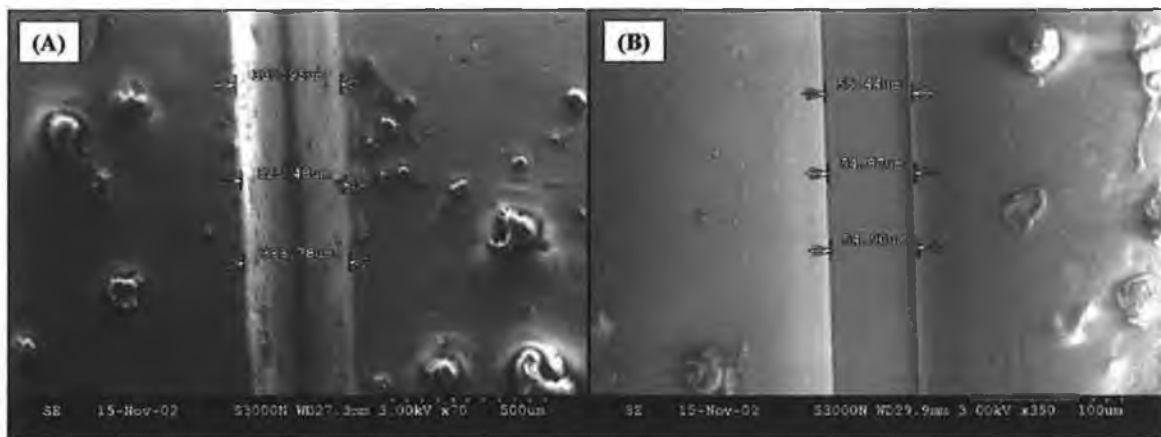


Figure 6-3 Photograph of a microfluidic channel in a 1.5 mm thick PMMA sheet made by (A) CO₂ laser ablation and (B) hot embossing

In Figure 6-4 the first PMMA sheet, to be hot embossed with the optimised parameters, containing the microfluidic structures from the inverted mask is shown.

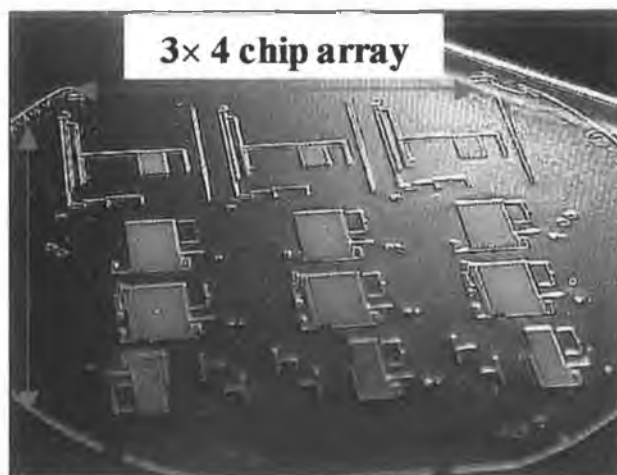


Figure 6-4 Photograph of the hot embossed PMMA sheet of 1.5 mm thickness fabricated from the inverted mask tool

The PMMA sheet has a thickness of 1.5 mm and the embossed wafer contained the microfluidic channels for all 12 chips from the mask. The total time required to produce 1 wafer was 15 min, which computes to 50 microfluidic test pieces / hour.

Hot embossing is a powerful tool that when optimised can produce highly reproducible micron-scale sized dimensions and can be used for rapid prototyping. The next stage in the design is to cut the chips to size and source a reliable way to make the through holes of the inlets, outlet and optical cuvette. After that, other issues such as the bonding, alignment and preliminary analytical testing of the microfluidic chip have to be addressed. Ultimately the hot embosser has so far proven a useful micro-fabrication instrument.

6.1.2 Choice of Polymer

Of the abundance of polymer materials currently commercially available, polymethyl methacrylate (PMMA) is one of the most frequently used in micro-fabrication (Röhm GmbH, KG, Darmstadt, Germany). At present PMMA has been the most adaptable material to both CO₂ laser ablation and hot embossing, but PMMA is not, in the long-term, the most chemically compatible material for the yellow method reagent and end product, which are both extremely acidic. In an effort to design a microfluidic system, which can function, maintenance-free for 1 year in the environment a PMMA-based chip would show signs of acidic erosion. PMMA chips can be used for several months without any signs of erosion. After

this time the surface characteristics of the polymer will be compromised and subsequently interfere with the analytical measurement in several ways including, erosion of channel walls, wall coating by reagent solutions in channel and optical cuvette and dissolution of polymer surface molecules in acidic yellow method reagent.

In order to pre-empt this problem becoming the limiting factor in this research, preliminary investigation of a number of alternative polymer materials has begun. There are an ever-growing number of polymer composites coming onto the market, which offer limitless opportunities to researchers to find the ideal polymer for a specific application. Two such polymer materials are polydimethyl siloxane (PDMS) and Topas®, which stands for a thermoplastic olefin polymer of amorphous structure. PDMS is more hydrophobic than glass, which makes it difficult to wet with aqueous solvents, however it has excellent bonding properties without the need to chemically alter its surface, which could make it more desirable than PMMA (Sylgard 184 Kit, Silicon Elastomer, Dow Corning GmbH, Wiesbaden, Germany). Topas® comes from a strand of polymers known as the cycloolefin copolymers (COC's), which consists of amorphous, transparent copolymers based on cyclo- / linear- olefins. There are many advantages to this new polymer material including its low density, high transparency, extremely low water absorption, good electrical heating, high rigidity, strength and harness and its good resistance to acids and bases. The most interesting property of Topas® is probably its optical transparency. It has a 95 % transmission for a 2 mm thick sheet, surpassing that of both PMMA and PDMS. The major drawback in using Topas® is that it is only commercially available as a resin, which means that the sheets have to be fabricated in the laboratory. This can be done with a "mini" injection molder (Model: Babyplast, Cronoplast S.L., Barcelona, Spain). The resin is annealed in the oven just below its glass transition temperature (~ 115 - 118 °C depending on batch and supplier). A copper tool has to be micro-milled and polished, which can take hours to get the smoothest possible finish.

In silicon-based microfluidic systems Perspex or glass has primarily been used as the cover and seal microfluidic channels. There are numerous reasons for this, but for colorimetric analysis glass has been proven to have excellent optical properties in terms of % transmission. The yellow method complex absorbs strongly below

400 nm and throughout this research a working wavelength of 380 nm has been selected as the λ_{max} for yellow method analysis, which coincidentally coincides with the emission spectrum of the UV-LED (λ_{max} : 375 nm).

The absorbance spectra of the three polymer materials of 1 mm thickness were measured to assess their optical transparency, with comparisons being made at a wavelength of 380 nm as shown in Figure 6-5. The absorbance spectrum of glass was also plotted on the same graph as a reference spectrum. From Figure 6-5 it was clear that at 380 nm there were no two materials with the same optical properties. For optical detection systems the ideal polymer would mimic the optical properties of glass.

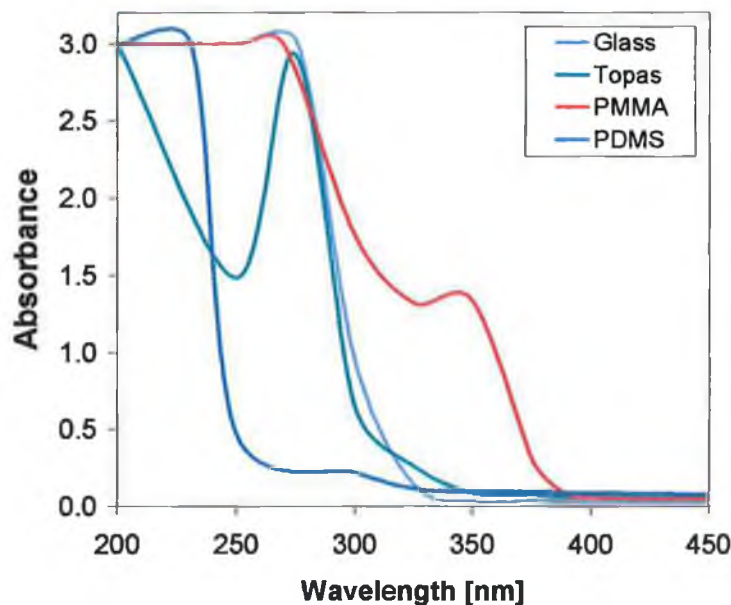


Figure 6-5 UV spectra for a range of polymer materials compared with glass over the wavelength range 200 – 450 nm

A wavelength of 380 nm has been used throughout this research. So in order to compare the polymer materials the wavelength range in Figure 6-5 has been made smaller to focus on the range of interest, 375 – 385 nm.

A surprising outcome from Figure 6-6 was the relatively high absorbance of PMMA with respect to the two other polymers and to glass. It is well known that the composition of any polymer can vary greatly from supplier to supplier, which could in fact be the cause of this phenomenon. A further study of polymer material suppliers would confirm this.

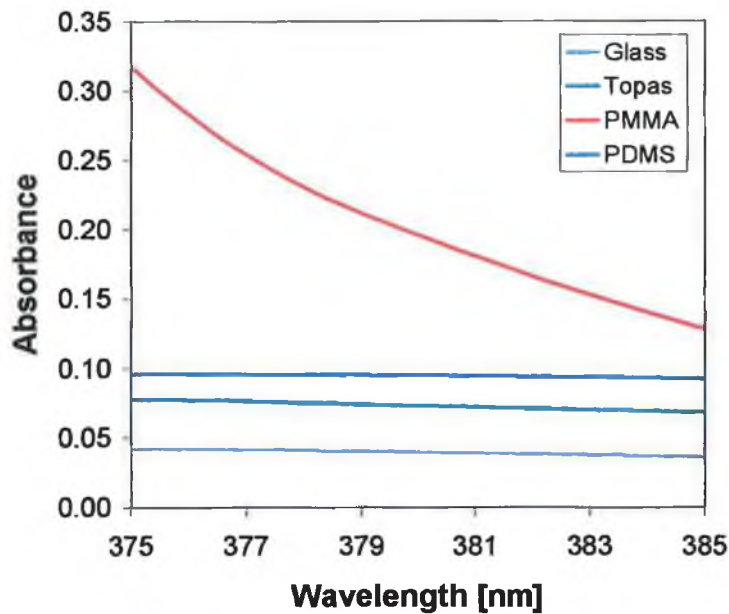


Figure 6-6 UV spectra of the same materials over the range of interest 375 – 485 nm w.r.t. the yellow method

PDMS and Topas® were initially investigated in terms of fabricating microstructures, chemical compatibility with the reagents of the yellow method and bonding possibilities. Neither PDMS nor Topas® can be ablated with the CO₂ laser. The former has a very hydrophobic surface, a low T_g and is very elastic, which mean it can't be ablated with the CO₂ laser because it melts before any structures can be formed. The T_g of the latter's, on the other hand, is too high, which results in pinhole markings, but again no structures being formed. The bonding capabilities of PDMS and Topas® were both assessed. Because of its hydrophobicity PDMS exhibits good bonding qualities and can be bonded to most polymer surfaces, including PMMA, without the need for a chemical pre-treatment, an applied force and / or a temperature increase. Topas® can at extremely high

temperatures be bonded to another sheet of Topas®, but under no conditions to PMMA.

6.2 Pumping

In order to power the microfluidic device over long periods of time, the pumps, which will be programmed to switch in and out, periodically delivering sample and reagent, will have to have very low power requirements. Initially to test the feasibility of a pumping system for use in the device, Bio-Chem Valve pumps (Bio-Chem Valve Inc., New Jersey, USA) were tested. However these pumps, while robust and capable of dispensing the samples required in addition to high purity or aggressive fluid samples with discrete outputs of 8 μL per solenoid actuation, have very high current requirements, 0.22 amps at 70° F (21° C), with a 12V DC supply, and this therefore eliminated the possibility of using these pumps for long-term battery powered field work.

A second set of pumps, shown in Figure 6-7, recently purchased from Fraunhofer Verbund Mikroelektronik are currently under evaluation.

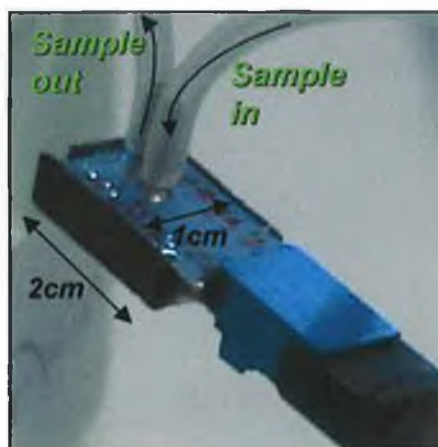


Figure 6-7 Photograph of the piezoelectric pump and driver taken with a Canon MV1 digital video camcorder

These piezoelectrically actuated micropumps have a maximum flow rate of 2 ml / min with self-priming and bubble tolerance. Pump delivery is controlled using a tiny potentiometer in the controller interface and can be set from 2 Hz to 650 Hz, thus allowing an adequate flow-rate range to suit the application. Due to its very low

current requirements, this pump is also ideally suited to use in portable battery powered devices. Currently, software to allow the switching on / off of the pump has been developed using a LabView program (Model: DAQ-700 Card, LabView, Version 5, National Instruments Corp. (UK) Ltd., Hambridge Rd., Newbury, Berkshire, RG14 5SJ, UK). However the micropumps and the optical detection will eventually be on one integrated platform with a remote web-based control of the various components (see Section 6.2.3).

6.2.1 Preliminary Flow-rate Measurements

Preliminary lab tests were undertaken to ascertain the smallest flow-rate possible with the micropumps. These experiments were conducted by manually adjusting the frequency of the pumps. The pumps are connected to a driver, which is shown in Figure 6-8. The driver connects the pump to a power supply and also facilitates the pumps manual or external control. The driver can be connected to a software program, which can trigger the pumps to start / stop and to set / change the frequency at which the pump works. Manually the pumps can be turned on and (see "ein / aus" switch in Figure 6-8) and the frequency can be adjusted with a small flat-head screw-driver, i.e. clockwise to increase the flow-rate, anti-clockwise to decrease the flow-rate.

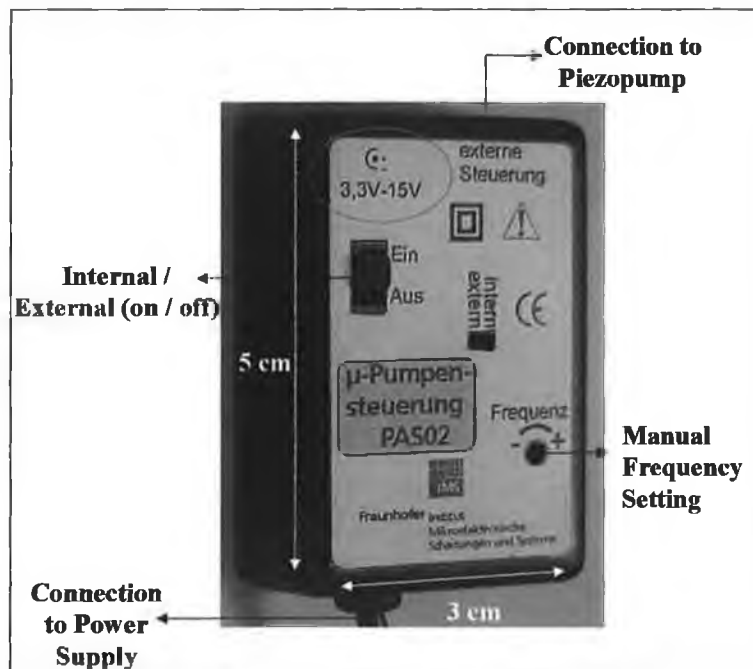


Figure 6-8 Piezoelectric pump driver to control the flow-rate

The preliminary tests to ascertain the lowest repeatable flow-rate were carried out by manual adjustment of the frequency. The frequency was turned off completely and then tweaked to allow a minimum flow to be transported through the pump. The pump was connected via FIA tubing of 0.6 mm internal diameter and an external diameter of 10 mm to a glass capillary of 0.6 mm inner diameter. The glass capillary was affixed to scientific paper, where each square has an area of 1 cm². The volume of the glass capillary was calculated using the formula for the volume of a cylinder.

The volume of the glass capillary was calculated as 0.0141 cm³, where the capillary length was 5 cm. A schematic of the experimental set up is shown in Figure 6-9.

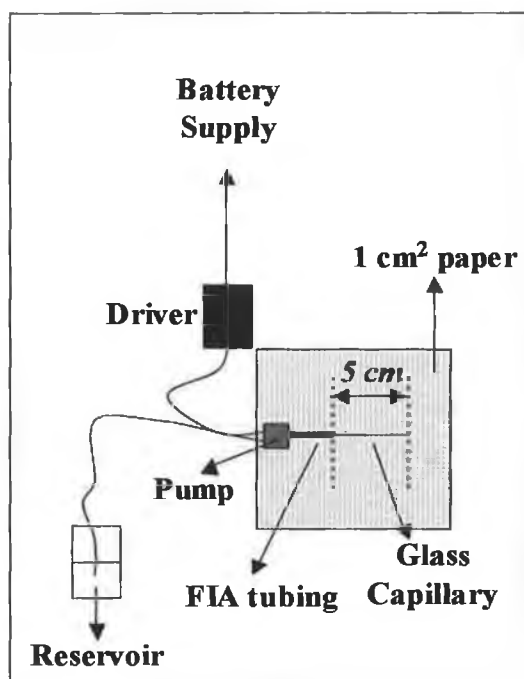


Figure 6-9 Schematic of the flow-rate experimental set up

The pump was turned on and the water from the reservoir passed through the tubing into the glass capillary. A bubble was generated along the tubing by removing the reservoir tubing from the solution of water. The time taken for the bubble to pass through the glass capillary (5 cm length) was recorded and used to calculate the flow-rate [$\mu\text{l} / \text{min}$] by applying the results to Equation 6.2, where T is the time [s], V is the volume [μl] and Q is the total volume [$\mu\text{l} / \text{min}$].

$$T = V/Q$$

Equation 6-1

The simple experiment was repeated ten times and the results are shown in Table 6-1. The results showed that even at a very flow-rate the repeatability was good with a relative standard deviation of less than 3.8 % for the ten measurements.

Table 6-1 Flow-rate measurements by manual manipulation of the frequency (Hz)

Measurement	T [s]	T [min]	Flow-rate [ml / min]
1	100.9	1.6817	8.4024
2	92.0	1.5333	9.2152
3	91.4	1.5233	9.2757
4	97.6	1.6267	8.6865
5	94.6	1.5767	8.9619
6	92.3	1.5383	9.1853
7	100.1	1.6683	8.4695
8	99.8	1.6633	8.4950
9	95.5	1.5917	8.8775
10	93.4	1.5567	9.0771
Average	95.8	1.5960	8.8646
Std. Dev.	3.6	0.0601	0.3313
% RSD	3.8	3.7662	3.7369

It has been established that the pumps can operate reproducibly at flow-rates below 10 $\mu\text{l} / \text{min}$, the next step is to have two pumps working in tandem at identical flow-rates. Two pumps are required to introduce the orthophosphate-containing sample and the yellow method reagent onto the microfluidic chip, whereby a determination is made under stopped flow conditions. The sample and reagent react in a 1:1 volume ratio, which means that the pumps must both have the same flow-rate.

There are two ways to approach this. The first involves setting each pump driver to the same frequency and establishing whether the flow-rate is the same from both pumps. If it isn't the same then it can be assumed that the difference will be the same every time and the difference can be accounted for in the data analysis. The second approach involves running both pumps off one driver. If one driver can be used to control both pumps the flow-rate from both pumps can be made equal. The investigation of both procedures is on-going.

6.2.2 Sampling

Sampling is of major importance to most environmental monitoring systems and is nearly always the limiting factor in water analysis. The development of sampling techniques, which can be integrated into the microfluidic system, and function long-term, maintenance-free in an external environment, has been the main goal. Initially the decision to use membrane filtration was made from previous experience in the MicroChem Project^{*}. In orthophosphate determinations water samples must be filtered through membranes of 0.45 μm pore size to ensure all organic phosphates are removed [1].

Two-week field trials were performed with four different membrane materials as shown in Figure 6-10. The membranes were polyvinylidene fluoride (PVDF), polyether sulfone (PES), Nafion, Teflon (PTFE) with pore sizes of between 0.2 and 0.5 μm and were labelled 1 to 4 respectively. The membranes were incorporated into the top lid of 5 \times 5 cm leak-free plastic containers. Each sampling unit was placed in pre-filtration bags to ensure large particulate matter didn't damage the membrane surface.

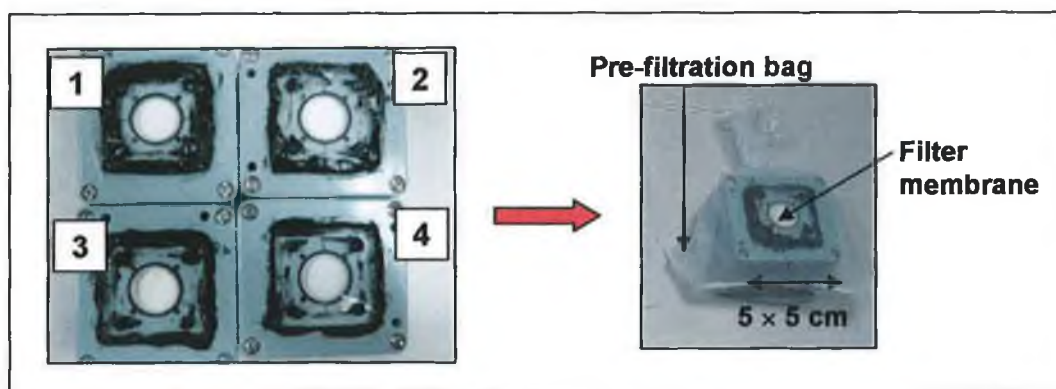


Figure 6-10 Photograph comparing 4 filter membranes after two week field trials[†]

The sampling units were left for two weeks in a river untouched. After which the sampling units were retrieved and brought back to the laboratory for assessment. The purpose of this trial was to identify the membrane materials with the best anti-

^{*} EU 5th Framework (BRPR-CT98-0787), www.microchem.dk

[†] Field trials carried out by Dr. Edel Minogue, NCSR, Dublin City University.

biofouling properties that would be capable of operating long-term maintenance-free.

The second issue associated with sampling was the design, fabrication and integration of the sampling unit / component with respect to the microfluidic manifold. Currently a number of ways to achieve this are being examined. There are two ways to approach this issue. The first involves developing a sampling unit as a separate component, which is attached to the microfluidic manifold via PEEK tubing and can be replaced with ease, if biofouling should occur. The second incorporates a sampling channel into the microfluidic chip adopting a fully integrated approach, which is the most desirable development provided that a suitable membrane material can be found.

6.2.3 Remote Sensing

The development of a device capable of functioning autonomously in an external environment, with reliable data capture and retrieval, is the next hurdle to be overcome. Now that the chemistry and the microfluidic design are optimised the focus turned towards how the data will be captured, stored and then transmitted without having to go to the actual location of the device. There were many complex and long-term ideas put forward, but in order to develop a prototype that can be tested on a river body easiest approach was to take one measurement per day and store the information in a simple data logger. Routinely the logger transmits the raw data via GSM to a web-based program, where the data is treated and a graphical display of the results is plotted.

In Figure 6-11 a photograph of the small data logger is shown along with the modem for GSM transmission.



Figure 6-11 Photograph of remote data logger[‡]

In Figure 6-12 the sequence in which data is recorded and transmitted is shown. The data is initially transmitted to a base station with a GSM modem phone connection. The PC is programmed to update the web site at specific time interval. The PC has a modem installed and calls up the remote GSM phone attached to the base station. The data is transmitted across the connection and the web page automatically updates.

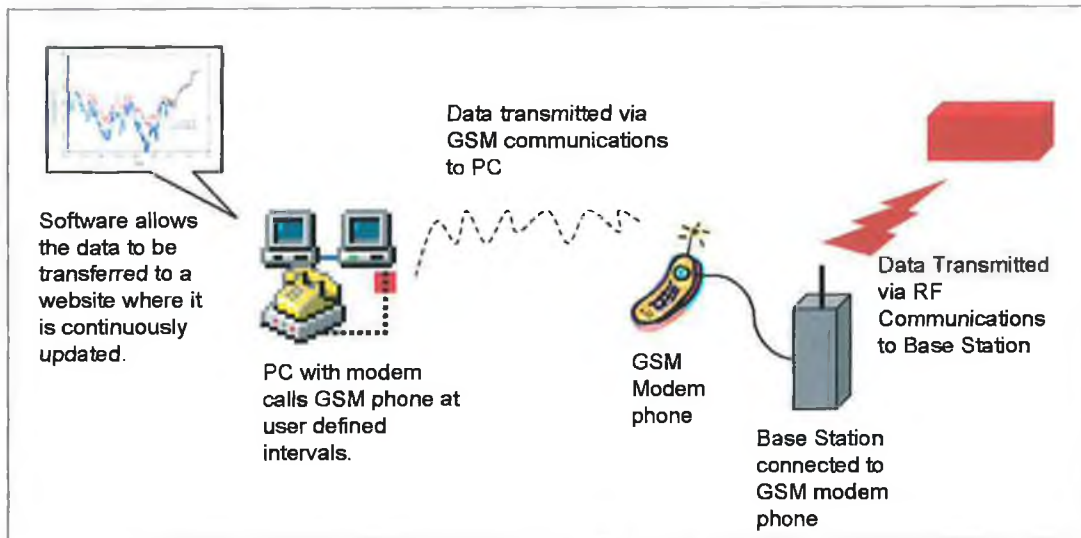


Figure 6-12 Operation of GSM-data logger[§]

The schematic gives an impression of the type of system we are currently developing with Whistonbrook Technologies. Our system will be slightly larger than the one shown in Figure 6-11 because it has additional components included within the packaging. The other components include four input switches to

[‡] Fabricated by Steve Edwards of Whistonbrook Technologies, Luton, UK.

automate the operation of the two pumps, the UV-LED and the Si-photodiode detector and a bulky battery that will power the entire system for a minimum of six months.

6.2.4 Packaging

The dimensions of the components are tabulated to give an indication of the scale of the entire system. The electronic parameters and power usage are given in the technical data sheets attached.

- Light Source: UV-LED (Model: NSHU590E, Nichia Europe B.V., Hornweg 18, 1045 AR Amsterdam, The Netherlands). A more detailed description of the UV-LED is given in Chapter 3, Section 3.2.1.
- Photodiode detector: Si photodiode (Model: S1227-33BR Series, Hamamatsu Photonics UK Ltd., 2 Howard Court, 10 Tewin Road, Welwyn Garden City, Hertfordshire, AL7 1BW, UK). Another more detailed description of the Si-photodiode detector is given in Chapter 5, Section 5.7.2.
- Pumps: piezo-electric pumps (Micro pump driver module PAS 002, Fraunhofer Institut IZM, Micro-Mechatronic Centre (MMZ), Argelsrieder, Feld 6, D-82234 Oberpfaffen-Weßling, Germany, see Fraunhofer Institut)
- Packaging: Polycarbonate (Model: IP67 piccolo series, RS components, Radionics Ltd., Glenview Industrial Estate, Herberton Road, Rialto, Dublin 12)

The polycarbonate packaging was chosen because it is airtight in water under pressure to depths of approx. 1 m, which is suitable for our application. The container has dimensions 17 cm (l) × 14 cm (w) × 9.5 cm (d) to house all the system components. In a list of all the components dimensions was used as a rough estimate for the packaging size required.

[§] Figure 6-11 courtesy of June Frisby, NCSR, Dublin City University.

Table 6-2 List of components spatial dimensions

Component	length [cm]	width [cm]	thickness [cm]
Chip	1	1	0.12
Holder	2	2	1.2
Pump	1	3.5	0.5
Pump driver	4	4.5	2
UV-LED	5.6	4.7 (diam.)	N/A
Photodiode	7.6	6	2
Active Area	2.4	2.4	N/A
Leak-free box	17	14	9.5

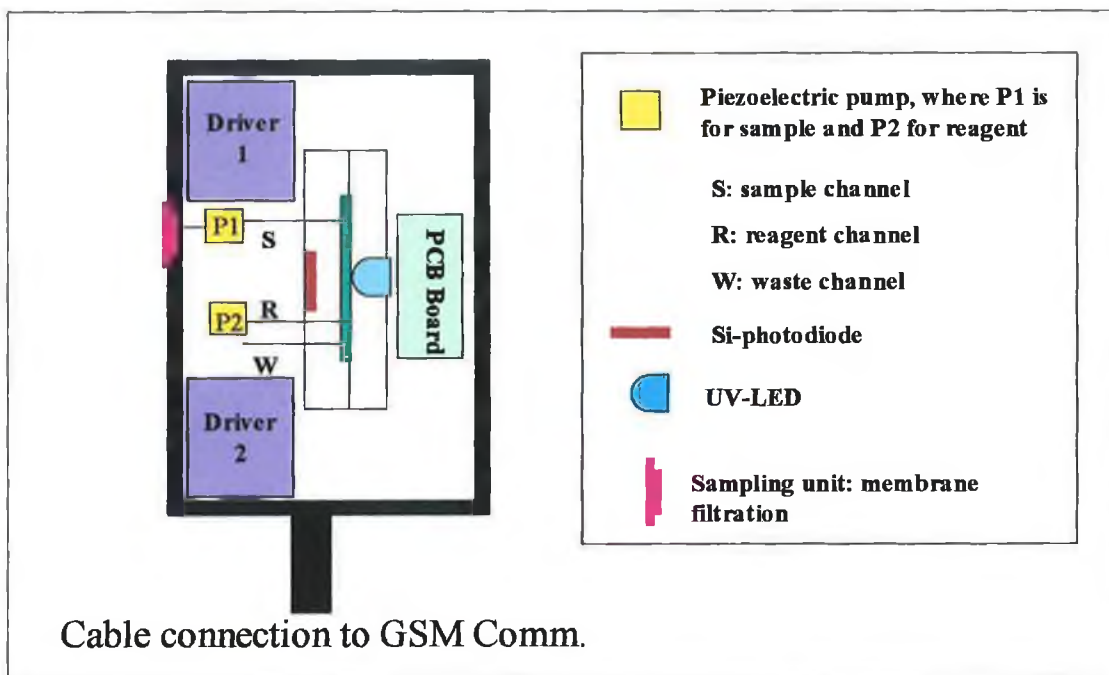


Figure 6-13 Schematic of proposed design for the packaged microfluidic system with integrated sampling, pumping and optical detection

In the prototype system shown in Figure 6-13 the chip holder has dimensions 2 × cm × 2 cm × 1.1 cm. The UV-LED and Si-photodiode have to be positioned opposite each other at about a distance of 1 cm. The system is connected to the data logger via the cable in the schematic. The data logger also contains the battery supply, which can power the system for a minimum of six months when operated in "sleep mode".

6.3 Conclusion

The microfluidic manifold has been fabricated by a number of techniques with the best results, to date, being found with the hot embosser. The microchip holder has been fabricated to house the chip, to facilitate leak-free fluidic interconnects and to integrate the optical components. Small-sized piezoelectric pumps have been assessed and will be incorporated in the final packaged device. The sampling will initially be a separate component for the first prototype system, but will eventually be incorporated in the microfluidic design. The data retrieval and transmission will be established by GSM communications and the data uploaded to a web-based program periodically. The power requirements will be kept to a minimum by limiting the number of measurements to be made and the "sleep mode" operation of the system. The waste production and reagent consumption, which have already minimised by adopting a stopped flow microfluidic measurement, are further reduced by the periodic measurement strategy.

The project is moving towards integration and autonomous function. It is envisaged that a fully automated autonomous laboratory demonstrator will be complete by end of March 2003 with the first set of field trials to take place in early May. At this point it is hoped that further funding can be acquired with the scope for development of a commercial product.

6.4 References

-
- 1 A.E. Greenberg, A.D. Eaton, L.S. Cleseri, *Standard Methods for the Examination of Water and Wastewater*, 4500-P Phosphorus, 18th Edit., 1994, ASPH, Washington DC, USA, 166-181.

Conclusion

Clearly it can be seen that some of the major issues relating to the use of the yellow method in the determination of phosphorus have been resolved. The yellow method was an excellent choice, in terms of long reagent lifetimes, stability of the reaction, adaptability to the microfluidic manifold and the availability of a low power UV-LED light source.

A validation study of the yellow method has been carried out in the microfluidic manifold to include parameters such as linearity, reaction rate, pH, Fe^{2+} interference, repeatability, reproducibility and limits of detection. The analysis of river water samples has been carried out in the microfluidic manifold with the yellow method and compared to analyses performed with conventional techniques, such as spectrometry and ion chromatography (IC).

The adoption of this simple method, and the use of a stopped flow regime, enabled a very simple fluidic manifold to be employed, with considerably smaller reagent consumption than equivalent continuous flow. It was clearly established that the kinetics of the method were very rapid, even at room temperature (~ 3 min), enabling sample turnaround in less than 5 min.

A novel microfluidic manifold solely consisting of PMMA was successfully designed and fabricated using CO_2 laser ablation. Most of the challenges faced have now been overcome including channel sealing / bonding, optical alignment and leak-free fluidic interconnects. The polymer device has since been applied to real sample analysis. The initial use of the CO_2 laser was a good platform upon which to begin this part of the project with and knowledge gained there is now being applied to the fabrication of a new and improved prototype device with a hot embossing instrument and an Excimer laser. This research also raised awareness of other issues such as the choice of polymer material, the range of micro-fabrication techniques available and the integration of multiple components into one device.

The concept of a fully integrated analytical instrument has now become the main emphasis of the research with a whole new set of considerations including the design and integration of a sampling unit, the pumping unit, the power consumption

of the system, the choice of location for preliminary *in-situ* testing and the transmission of raw data to a base station via GSM or radio frequency communications (RF). Cosmetic decisions such as the frequency with which a measurement should be made and the number of times / day data is retrieved and downloaded to a base station or web site have also been discussed.

The development of a remote, compact, *in-situ* micro-device is the next major stepping stone in the realisation of our goal of the development of an extended environmental "digital nervous system". The outcome of developing such a device will be reduced costs, efficient energy usage, lower consumption of reagents (10 μL / min flow rate \approx 50 ml / year reagent consumption using stopped flow pumping) coupled with less waste production, compact design, reliable analytical data and higher sample throughput.

In conclusion the yellow method has been optimised and implemented in both silicon and polymeric microfluidic manifolds. The polymer microfluidic manifold was designed and fabricated using a CO_2 laser and real samples were analysed and validated against more conventional analytical techniques. The yellow method itself is very simple, the reagent is stable for time periods in excess of one year and the reagent consumption and waste generation is minimised by utilising a microfluidic system in the determination. Bulky conventional optical components have been replaced with LED's and photodiodes and syringe pumps with piezo-electric micro-devices. Overall the project has been successful and it is envisaged that within the next six months a field-deployable prototype will be completed and field trials begun.